اثر فلسفة العلم المعاصرة على العمارة

د.أريج كريم مجيد السدخان–أستاذ مساعد القسم المعماري–كلية الهندسة–جامعة بغداد
علاء عبد الرزاق كريم بكالوريوس هندسة معمارية

ملخص البحث

يتناول هذا البحث المواقف الفكرية العامة للعلاقة بين فلسفة العلم المعاصرة و العمارة،و مناقشتها ضمن طروحات كل من K .Popper ، والتي تم بلورتها ضمن مفردات أساسية و فرعية شملت ما يأتي:

الموقف من النظرية النفسية، الموقف من نظرية المعرفة،الموقف من المجتمع،الموقف من التاريخ.

وقد تم تعريف جوانبها بضوء المعرفة المرتبطة بها و المطروحة في الدراسات الفلسفية العلمية المعاصرة و المعمارية. و بيان القيم الممكنة و المرتبطة بمفردتي الموقف من المجتمع و الموقف من التاريخ لبعض الجوانب المشتركة بين طروحات Popper و الواقعية الجديدة و طروحات Kuhn و العقلانية الجديدة ، فقد تم التوصل إلى بعض الجوانب المشتركة بين طروحات Popper و طروحات الواقعية الجديدة و طروحات Kuhn و العقلانية الجديدة ، شملت الأسس الفلسفية و موقفهما من التقاليد ، فضلا عن طبيعة المراجع المعتمدة و طبيعة التعامل مع التقاليد وفي ضوء ذلك تم بلورة مفردة ، عرفت (بالموقف من التيارات المعمارية) ارتبطت بمفردات فرعية عرفت بضوء جوانب اكثر تفصيلية و المتعلقة بالموقف من العمارة و أهدافها و التقاليد و طبيعة المراجع التي يتم محاكاتها و موقفهما تجاه نظريات العمارة و ماهية المعاني و الأفكار التي يعبر عنها المصمم .

الكلمات الرئيسية: العمارة ، فلسفة العلم ، المجتمع و العمارة ، تاريخ العمارة .

Research abstract

THE EFFECT OF CONTEMPORARY SCIENCE PHILOSOPHY ON ARCHITECTURE

Ass.Prof. Dr.Areage Karim Al-Sadkhan
University of Baghdad - Engineering College- Architectural Department.
Alaa Abdul-Razzaq Karim

ABSTRACT

The research tries to investigate the effects of Contemporary Science Philosophy on Architecture. The research depends on contemporary Science Philosophy of K.Popper and T.Kuhn. The procedures of the research contain the construction of comprehensive theoretical framework that includes the influence of contemporary of Philosophy of Science on Architecture in the following level which contains the general thought position, which includes (The position of Psychological Theory, knowledge Theory, the society, the history and the position of Architecture views). The conclusions of the research focus on the theoretical framework that depends on the previous views of K.Popper and T.Kuhn which reflected on Architectural views.

KEY WORDS
Architecture, philosophy of science, society and architecture, history of architecture.

المقدمة

يتناول البحث وصف المواقف الفكرية العامة لفلسفة العلم وانعكاس تأثيرها على العمارة.وقد تطلب وصفها التوجه نحو الدراسات الفلسفية العلمية والمعمارية بغية استكشاف الأطر النظرية الكامنة فيها ،ثم بلورة الطروحات ضمن مفردات ثانوية اكثر وضوحا فضلا عن استخلاص قيمها الممكنة.

وقد تم مناقشة المفردات الأساسية للإطار النظري من خلال استكشافها في الدراسات الفلسفية العلمية أولا،ثم معماريا من خلال تقصي المواقف العامة في الطروحات المعمارية ،ولغرض تعزيز القاعدة النظرية وبناء إطارا نظريا شاملا ،كما توجه البحث إلى الدراسات المعمارية المتخصصة لاستكشاف خصوصية الأفكار والمفاهيم التي تعكس الجوانب المشتركة والمتباينة بين فلسفة العلم والعمارة.

سيقتصر البحث على تناول الطروحات الفلسفية العلمية لكل من T.Kuhn&K.Popper،لأهميتها على المستوى الفلسفي العلمي ،فلو استقصينا تاريخ فلسفة العلم المعاصر وعدنا إلى ستينات القرن العشرين لوجدناهما من أهم فلاسفة العلم المعاصرين الذين تمكنوا من خلال طروحاتهم ،من قلب نظرية المعرفة العلمية رأسا على عقب فضلا عن حل معضلات وخصومات فلسفية كانت قائمة،فقد جاءPopper بمشروع(الفرضي–الاستدلالي Hypothetico-Deduction)الذي يمكن أن يستوعب العلم،واقترح Kuhn نموذجا معرفيا يعمل العلم من خلاله كنشاط لحل الألغاز إلى حين حدوث الانقلاب في النموذج (حمدي،ص15). طرحت فلسفتيهما صراعا فلسفيا علميا ألقى بضلاله على مبحث فلسفة العلم المعاصر ،من خلال بروز طروحا ت تقف إما موقف المؤيد لا حدهما متأثرا ومستلهما لمبادئي طروحاته،أو موقف الضد من مواقف أخرى (السابق،ص18).

معماريا،فقد بدأت ملامح التأثر في هذه الطروحات الفلسفية العلمية من خلال تبني بعض المنظرين والمصممين المعماريين لهذه الطروحات .

فلسفة العلم

يعرف (د. احمد فؤاد باشا) فلسفة العلم :بالمبحث الجديد الذي أضافه المحدثون إلى مباحث التفكير الفلسفي العلمي على حد سواء، يشمل البحث في تحليل لغة العلوم المختلفة واستخلاص ما يساعدنا على تكوين نظرة شاملة إلى الكون من خلال الربط بين سلوك الظواهر التي يتعامل معها الإنسان (باشا،ص 63) ،ويعرف (د.مهران) فلسفة العلوم بأنها ذلك النسق المترابط من المفاهيم والقوانين الذي يشمل العلوم الطبيعية والفلسفية والإنسانية ويهدف إلى فهم مكانة العلوم في حضارتنا (د.مهران ,ص 10)،ويعرفها (د.الجابري) في كتابه (مدخل إلى فلسفة العلوم) بأنها المبحث الذي يهتم باستقصاء الحقيقة وتكوين الأحكام الشاملة و تبني النماذج الفكرية وخلق الصور الذهنية عن العالم المحيط (الجابري،ص20).

ويمكن التفلسف في العلم من وجوه أربع حسب ما تطرحه أدبيات العلم المعاصر وهي:

- دراسة علاقة العلم لكل من العالم والمجتمع (العلم من حيث هو ظاهرة اجتماعية).
- محاولة وضع العلم في المكان الخاص به ضمن مجموع القيم الإنسانية.

- الرغبة في تشيد فلسفة للطبيعة انطلاقا من نتائج العلم.
- التحليل المنطقي للغة العلمية.(محمود،ص38).

كما تطرح أدبيات العلم المعاصر توجهين رئيسين في فلسفة العلم هما:

- **فلسفة العلم الخاصة**

ينطلق أصحاب هذا التوجه من كون القضايا والمشاكل المبدئية أو المنهجية التي تخص علم من العلوم قد لا تخص بالضرورة علما أخر بل العكس في نظرهم هو الصحيح، فمشاكل الرياضيات ليست هي مشاكل العلوم الإنسانية وهكذا،وان محاولة الجمع بين قضايا العلوم المختلفة في إطار أو نسق فلسفي علمي واحد هو في نظرهم – عمل فلسفي –لا يمكن الاستفادة منه في حل المشاكل الدقيقة الخاصة، لذا فهم يحرصون على أن تحتفظ الفلسفة العلمية بطابعها العلمي الخاص و عدم التقيد بأي نظرة فلسفية عامة ، فكان فلسفة العلم في نظرهم لا تختلف عن الميثودولوجيا ألا بقدر ما يكون التحليل اكثر عمقا والنقد اكثر صرامة .(الجابري ،ص 50).

- **فلسفة العلم العامة**

يرى أصحاب هذا التوجه ، أن فلسفة العلم الخاصة ذات نزعة ضيقة , ويطرحون نظرة مغايرة أخرى فالمشاكل التي تعترض علم من العلوم كثيرا ما تكون هي نفسها التي تعترض علما أخر، علاوة على أن العلوم نفسها متداخلة وبينها علاقة لا يمكن تجاهلها .لذا فالتوجه السائد والذي اصبح حقيقة واقعية هو التركيز على (وحدة العلوم) وتوقف بعضها على بعض هذا من جهة، من جهة أخرى فان معالجة القضايا والمشاكل الفلسفية العلمية الخاصة لكل علم ،لن تكون مثمرة، إلا إذ تم تحليلها والنظر أليها من عدة زوايا، فالمعالجة المنطقية لا تكفي بل لابد من اللجوء إلى علم النفس وتاريخ العلوم وعلم الاجتماع .(السابق ، ص 50).

يتبنى البحث دراسة تأثير طروحات أصحاب هذا التوجه على العمارة.

فلسفة العلم وطبيعة موضوعاتها

يطرح Feigl & Brubeck في كتاب(Readings in Philosophy of Science)الجوانب التي تشتملها فلسفة العلم والتي تتعدى نطاق تحليل لغة العلم لتشمل :

- **انطولوجيا العلم** : البحث في كشف طبيعة الوجود اللامادي في القضايا الميتافيزيقية المرتبطة بالتطورات والمفاهيم العلمية.
- **ابستيمولوجيا العلم** : البحث في نظرية المعرفة العلمية بجوانبها الثلاث (إمكان المعرفة ومصادرها وطبيعتها).
- **اكسيولوجيا العلم** : البحث في القيم والمثل العليا ومدى ارتباطها بالعلم وخصائص التفكير العلمي.
- **سايكولوجيا العلم** :تبحث في العمليات النفسية والعقلية التي تتعلق بالكشف العلمي وما يقترن بها من القدرات الإبداعية والخيالية لحل المشكلات العلمية .
- **سوسيولوجيا العلم** : تبحث في التفسير الاجتماعي لتطور النظريات العلمية ومدى تقبل المجتمع لها بالإشارة إلى أسلوب التنظير العلمي ونمطه الذي يعكس الصيغة السائدة في مجتمع ما ،وتلعب المعايير الثقافية والقيم السلوكية في التأثير على تحديد الاتجاهات العقلية و منهاالتفكير العلمي والفلسفي .(Feigl & Brodbeck,p47).

ويقول Laland في معجمه الفلسفي أن فلسفة العلم ترتبط بالدراسة النقدية لمختلف العلوم، لتحديد اصلها المنطقي (موضوع الابستمولوجيا) ودراسة المناهج العلمية (موضوع الميثودولوجيا) والتي تشكل جزء من المنطق (الجابري ،ص 18) .كما أن المنهج العلمي هو جملة العمليات العقلية والخطوات العملية التي يقوم بها العالم من بداية بحثه حتى نهايته من اجل الكشف عن الحقيقة والبرهنة عليها وهي دراسة وصفية تحليلية لبيان مراحل عملية الكشف العلمي وطبيعة العلاقة بين الفكر والواقع خلال هذه العملية.(السابق ،ص 20).ويرىPierre Bont أن تاريخ العلم هو المقدمة الطبيعية لفلسفة العلم وميز أربع أنواع منه وهي (التاريخ الوثائقي , تاريخ الأخطاء , التاريخ المكاني , التاريخ الفلسفي للعلم) (الجابري،ص28-40).

مما سبق يمكن استخلاص المواقف الفكرية العامة والتي تصوغها أشكال الارتباط الأنفة الذكر وهي كالأتي :

- **الموقف من نظرية الوجود العلمية (انطولوجيا العلم).**
- **الموقف من نظرية المعرفة العلمية (ايستمولوجيا العلم) .**
- **الموقف من نظرية القيم العلمية (اكسيولوجيا العلم).**
- **الموقف من النظرية النفسية العلمية (سايكولوجيا العلم).**
- **الموقف من النظرية الاجتماعية العلمية (سوسيولوجيا العلم) .**
- **الموقف من المنهجية العلمية (ميثودولوجيا العلم).**
- **الموقف من تاريخ العلم.**

وسيتم مناقشة كل من الموقف من النظرية النفسية العلمية والموقف من نظرية المعرفة العلمية و الموقف من النظرية الاجتماعية العلمية و الموقف من تاريخ العلم ، لارتباطها بتوجه البحث و على مستوى الطروحات الفلسفية العلمية ومن ثم استكشافها على مستوى العمارة.

- فلسفة العلم والعمارة (المواقف الفكرية العامة)

- <u>الموقف من النظرية النفسية</u>

يرى Fiagl & Broadbeck أن فلسفة العلم تبحث في سايكولوجيا العلم، أي العمليات النفسية و العقلية التي تتعلق بالكشف العلمي و ما يقترن بها من القدرات الإبداعية و الخيالية الموجهة لحل المشكلات العلمية (Fiagl&Broadbeck,p47) ،فبالنسبة لفلسفة Popper تنطلق من سايكولوجيا Piaget التوليدية أما Kuhn فيصف في كتابه(The Structure of Scientific Revolutions) فلسفته بأنها جشتالتية (Gestalt) (Kuhn,p78) ، و على مستوى البحث في العمليات النفسية و العقلية التي تتعلق بالكشف العلمي و ما يقترن بها ، يطرح Able في بحثه(The Case for Anarchy in Design Research) مقارنة بين نمط التغيير في النظرية العلمية عند كل من Popper وKuhn ، فعند الأول نمط التغير عقلاني أو على الأقل قابل لاعادة الإنشاء عقلانيا و يقع ضمن عوالم منطق الاكتشاف العلمي ، أما Kuhn فانه لا يوجد أي تفسير عقلاني معين لظهور الأزمة في النظرية الأساس و هي عنده (أي الأزمة) حدث سايكولوجي و هو نوع من الذعر الجمعي (Able,p20)

ويرى Kuhn أن التغير العلمي من نموذج إلى آخر ليس حسب قواعد التعقل إنما يقع ضمن عالم السايكولوجي الاجتماعي للاستكشاف، لذا فان التغير العلمي نوع من التغير الديني الخاضع لقوى الإقناع للذين لا يسعون إلى معاكسات جديدة (Ibid,p209).

يرتبط نموذج Popper للعلم و على المستوى السايكولوجي بالنظرية التفاعلية (علم النفس الترابطي) و الذي يؤكد على دور الخبرة في الإدراك و التركيز على العلاقة الديناميكية بين الفرد و بيئته ، تأخذ هذه النظرية من مجالات علمية أخرى مثل (الفلسفة التفاعلية (Transactional Philosophy)لـDewey و مفاهيم علم الاجتماع التي جاء بها G. meed و يعتمد علم النفس التفاعلي على بعض الافتراضات منها :-

- علاقة الفرد-البيئة هي علاقة ديناميكية .
- أن الخيال الذي يحمله الشخص عن البيئة يعتمد على التجربة فضلا عن التوجهات و الدوافع الآنية الحاضرة و أن الخبرة السابقة تحضر للفرد في الحالة الآنية لموضوع معين.
- التغير الادراكي محكوم بالتوقعات و التفضيلات و بالتالي فان المعلومات التي يكتسبها الفرد تكون ذات طبيعة احتمالية يتم اختبارها و تفضلها ثم تأكيدها خلال الفعل و المعلومات تكون ذات خصائص رمزية و معنوية (Lang,p76).

أما بالنسبةلـKuhn فيرتبط (بعلم النفس الجشتالتي) وهو على النقيض من علم النفس التفاعلي، يعد أن ما يصفه بالبناءات النفسية هي كليات منظمة أو (جشتالت) ،كما أن الأحاسيس ليست أساسية و أولية في وظائف العقل ، و يخضع تكون الكليات إلى الملكات الغريزية للأفراد، و التي تمكن من خلق أشكال بسيطة و متعامدة و مقفلة أو متكاملة (Lang,p80) و تفترض نظرية (الجشتالت) انعزال الفرد عن بيئته و عن نشاطه العملي، إذا أنها تعزو البناءات النفسية إلى قوانين ذاتية داخلية و ضمن التوجه المثالي ، فهي تفترض أن الفرد يتمكن من أدراك البيئة بوصفه بنياناً مكوناً من عناصر تتشكل مع بعض ضمن ستة قوانين لانتاج الهيئات البصرية و هي (قانون التقارب ،التماثل ، الهيئات المغلقة ، التدرج ، الحركة العام ،و قانون الخبرة) (Ibid,p84) .

يتبين مما سبق ، أن النظرية النفسية التي يعتمدها Popper في تحليله لمنطق الاكتشاف العلمي و الجانب الإبداعي فيه هي ذات نزعة فردية براغماتية قائمة على أن الذات هي المؤثرة في الموضوع و المحدثة فيه التغيير نتيجة الجدة المتنامية في الإبداع المعرفي عند الذات ، أما Kuhn فالنظرية التي يعتمدها ذات نزعة جمعية استقلالية ، فالموضوع هو المؤثر في الذات ، فتتغير و تنمو المفاهيم الذاتية بتغير رؤيتها للموضوع الثابت (النموذج عند Kuhn) و في حالة تغير النموذج (الموضوع) يحدث نوع من الذعر الجمعي ، و الذي يمهد لاكتشاف نموذج جديد .

إما على مستوى استخلاص المفردات الفرعية المتعلقة بالموقف من النظرية النفسية فيمكن أن نصوغها كالآتي :

- **الموقف من حيث الأسس الفلسفية للنظرية النفسية :أما علم النفس التفاعلي أو علم النفس الجشتالتي.**

- **من حيث نوع التغير في الاكتشاف العلمي :أما التغير عقلاني:يقع ضمن عوالم منطــق الاكتــشاف العلمي.أو التغير الديني : ضمن عالم السايكولوجي الاجتماعي.**

- <u>الموقف من نظرية المعرفة</u>

تناولت الزنكة في بحثها الموسوم (الفلسفة الوضعية – تاريخ نظريات العلم) أفكارPopper و علاقتهــا بالتجريبية المنطقية ، كون الأخيرة حاولت ردم الهوة بين العقلانية و التجريبية على أسس مثالية ذاتية ، توحد بين الطريقتين المتنافستين بإيجاد الفلسفة العلمية (الزنكــة ، ص 166) ،وتقول الزنكة أن Popper هو أحد الذين طوروا المبدأ التجريبي المنطقي ، خصوصا الجانب النقدي منه ، من خلال (الحدس و الــدحض) وهمــا الموضــوعين المركزيين في فلسفته ، فالفرضية عبارة عن حدس ، وفي الدحض يتجلى الوجه الأخر للمسالة فالفرض وحــده لا يكفي ، و إنما يجب دحضه و الذي يقابل ما يسمى بالتحقق التجريبي عند الفلاسفة (الــسابق ، ص 168) ،تنــاقش الزنكة الحركة من التطبيق إلى النظرية و العودة ثانية إلى التطبيق و بهذه الحركة ذهابا و إيابا تتحقــق الوحــدة بينها ، مركزا على ظهور انطباعات جديدة في التطبيق ومن ثم إلى الخطوة التي تقرر فيها فكرة نظرية موثــوق بها بسبب الاستخدام لها في خطة عمل أو في تجربة(السابق ، ص 168) , ينعكس ذلك ضمن منهجية (فرضــية – استدلالية) يطرحها Popper ضمن منهجه الذي يتخذ من مبدا اطراد الحوادث مصادرة منهجية ، هذا المنهج لا يفسر حوادث أو ظواهر بقدر ما يفسر قوانين و يكتشف ظواهر جديدة ، يقوم هذا المنهج على ثلاث خطوات :-

- البدء بتعميمات استقرائية.
- افتراض فرضٍ مفسرٍ (غالبا ما يكون مشحون بصيغ رياضية مجردة لا تقبل التحقيق التجريبي المباشر).
- محاولة استنباط ما يلزم عن تلك الصيغ من نتائج و استنتاج ما يلزم عن هذه من نتائج أخرى حتى نصل إلى نمط من النتائج يمكن التحقق من عدم صحتها بالتجربة (زيدان ، ص127)، وقد شبه أحد المنطقيين الفرنسيين هذه المنهجية بالصعود من مجال التجربة إلى عالم العقل ثم العودة إلى عالم الواقع ، لكي نضمن الصلة بين المعقول و الواقع (السابق ،ص 130).

أما بالنسبة إلى موقف Kuhn فتناقش الزنكة طروحات الأخير في كتابه (تركيب الثورات العلمية،1962) ، موضحا أن الفكرة الأساسية فيه هي (ميزان التصريف) المبنية على أساس أن العمل التجريبي في العلم مليء بالتفكير النظري ، و إن العمل النظري توجهه الأفكار العامة ، طارحا مكونات أربعة لميزان التصريف:

- التعميمات الرمزية :- بديهيات و مبادئ نظرية علمية معينة.
- العنصر ألميتا فيزيقي الموجه :- صورة عامة عن الكون (وجهة النظرية الفكرية).
- الجانب الطرائقي :- مكونات القيم (يرتبط بالنواميس الإجرائية في سياق البحث).
- مجموعة الأمثلة و العمليات الاجتماعية في المجتمع العلمي :- ساهمت في إدامة ميــزان التــصريف مثل (كتاب القواعد) لنيوتن و(اصل الأصناف) لدارون (الزنكة ، ص 192 ،1981).

نتيجة موازيين التصريف هي إنتاج النماذج الفكريةParadigms و يعتمد على التحقيق الفلسفي في تأكيــد هذه النماذج الفكرية.

الاختلاف بين Popper و Kuhn هو في منهج الاختبار و مصدرية الفرض ، فعند Popperالاختبار يعتمد (التكذيب)، أما عند Kuhn فانه يقدم نقده لهذا المبدأ و يستخدم منهج (التحقيق) و يصفه كونه انتصار للنماذج الجديدة على حساب النماذج القديمة ، وان فكرة المقارنة بين النظريات تمكننا من تفسير الموافقة وعدم الموافقة عن طريق الربط بين الوقائع و النظرية ، و يخلق (التحقيق) التوافق بين النظرية و الواقع (Kuhn,p206) ،أما بالنسبة للفرض فانه عندPopper ينشا بالحدس، أما عندKuhn فانه ينشا (بالتركيب) . أذن ينطلقKuhn من الجانب التنظيري لعالم التجربة عن طريق الفرض التركيبي ثم إلى عالم العقل فتجري عملية الإسناد (ضمن مجموعة الأمثلة حسب موازيين التصريف وضمن مرحلة توسيع نطاق الفرض) ،وهكذا يتم صياغة (النماذج الفكرية) و التي يصنفهاKuhn إلى ثلاثة أشكال هي :-

نماذج فكرية اعتيادية ، نماذج فكرية تفصيلية ، نماذج فكرية ثورية.

النموذجيين الأولين يحدثان ضمن ما يسميهKuhn (بالعلم السوي)، أما النموذج الثالث فيحدث ضمن (العلم الشاذ) (Ibid ,p209) .

يتبين مما سبق ما يأتي :-

- أن نموذج Popper ينطلق بالمشكلة من العالم التجريبي بصياغة نظرية ثم يتحقق من صحتها عقلانيا ومنطقيا في عالم الفكر ضمن نموذجه التكذيبي (صياغة التخمينات ، الحلول المفترضة) وبالتالي اختبار مدى صحتها و ملاءمتها لتصوغ الناتج النهائي ذا الصفة التحويرية لغرض إزاحة الفكرة ، أما Kuhn فانه ينطلق بالمشكلة من الجانب النظري ضمن (التوجه العام) من العالم التجريبي و يتم اختبارها تجريبيا من خلال الإسناد النظري و التجريبي خلال مرحلة توسيع نطاق الفرض (مجموعة الأمثلة ضمن موازيين التصريف) المؤكد للحل المبداي و الذي يطرحه ضمنيا النموذج ،أما في حالة الاختلاف فيتم عزل القرينة ويتم معا لجتها مستقبلا ضمن العلم الشاذ، ليطرح النتاج مؤكدا للنمط العام (الجو الفكري السائد) و مطورا لتفاصليه على مستوى التنظير و التطبيق .
- في نموذجPopper التغير الجديد تظهر نتائجه في الواقع و الذي يثير معرفة جديدة تؤسس فيما بعد المفاهيم ألما بعدية، تنتج لحظة التقاء النتاج بالسياق ، و من الوسائل لتحقيق ذلك استخدام ما هو تقليدي في موقف معين جديد وهكذا تنمو المعرفة الفلسفية العلمية .
- التغير في نموذج Popper ثوري ضمن نظام معرفي عام، أماKuhn فالجانب الثوري في فلسفته يتمثل في العلم الشاذ أي الحقائق التي لا تتفق مع النموذج السائد و التي تبدا بالظهور في اللحظة التي يعاني منها النموذج السائد من العجز في وضع الحلول للموقف الجديد أو مجموعة المواقف التي تطرح نفسها مشاكل تريد من النموذج وضع حلا و تفسيرا لها فتظهر أزمة براغماتية يعجز فيها التنظير و التجريب السائد في التخلص من تفاقم ملامحها و بشكل متعاقب يتم الاستعانة بالقضايا الشاذة و تركيب بعضا منها ملائمة للموقف الجديد ، بالتالي سيكون الموقف ذا صفة ثورية في التغيير على اعتبار أن أساس صياغة النماذج وفقا لموازيين التصريف هو المبدأ العام و النواميس الكونية

السائدة مرورا بالنظريات المفسرة و التقاليد و القواعد الجزئية، فتنقلب الأفكار رأسا على عقب، أذن فالتغير ثوري ضمن نظام معرفي متخصص و هو تعاقبي بين العالم السوي و الشاذ.

-العمارة و نظرية المعرفة

معماريا و ضمن الطرح الفكري للتجريبية الجديدة ، نشر G.Cullen طروحاته القائمة على تبني مبادئ تجريبية تستند على فهم العلاقة بين الأجراء كفن مواز لفن العمارة ، و كانت وسيلته إلى ذلك التتابع البصري ضمن البيئة لانتاج الكل من خلال المفاهيم الآتية:-

- **التتابع البصري** :- الذي يتم تحفيزه بوجود قيم فيزيائية أساسية و قيم حسية ثانوية ناتجة من تجاوز العناصر المتناقضة مع بعض .
- **المكان:** الذي يعني الشعور بين الوجود في مكان محدد و بين الشعور بالوجود في مكان أخر مقارب و مساوي له بالقيمة خارجه.
- **المحتوى** :الذي يمثل الطراز و عناصره والذي يمكن بواسطته ربط نوعين من العوامل :العوامل الإنسانية التي تتضمن شروط المشاعر و الأحاسيس الناتجة من العلاقات الإنسانية،و العوامل الفيزيائية التي تتضمن الشكل الحقيقي و ترتيب بنية المكان الذي يقطن فيه الإنسان (Norris,p45).

انعكست هذه الأفكار وتم تبنيها من قبل الكثير من المصممين مثل (Sporry,Alexander,Gosling و غيرهم) ، فضلا عن المعماريين ضمن نتاجا تهم المعمارية مثل (R.VENTURI, F. Spoerry). فعلى سبيل المثال قام F. Spoerry بمحاولة تجريبية تصورية مميزة لتصميم (Port Grenond) اعتمادا على المنهج الفرضي ببناء نموذج مصغر للاختبار و التعديل بأجراء التغيرات التدريجية عليه و تعرضه لتجربة الصح و الخطا،فضلا عن محاولات إجرائية براغماتية أخرى من خلال تغيير الاتجاهات و إعادة ترتيب الأجزاء ضمن الفرضية واختبارها شيئا فشيئا لحين الوصول إلى المقترح النهائي ،متجاوزا اعتبارات المركزية و النظام و معتمدا على ما تضيف إليه نتائج التجربة التي لعبت فيها الخبرة الذاتية و المشاعر الحسية و البصرية الدور الأساسي في تحديدها (O.Connor,p150). وقد سار Alexander على النهج التجريبي البراغماتي ذاته للبحث في المدن و البيئات الحضرية و تمكن من استقراء مئتان وثلاث وخمسون نسقا من العلاقة بين الأجزاء و الكل ،لتشتمل المستويات التصميمية كافة (Ibid,p152).

أن المقدمات الشكلية للتجريبية الجديدة هي احتمالية تعرض للتساؤل والتمحيص و التجربة على اعتبار أن المعرفة الإنسانية الحقيقية ، حتى أن وجدت فهي معرضة للتعديل و التغيير حتى في اكثر القضايا الرياضية دقة و موضوعية ، لذا فالمبدأ الغائي لا يكون في البحث عن المعرفة المطلقة بل في تعدد و تنوع و تناقض أوجهها المختلفة ذات الحقائق النسبية المتغيرة كنوع من الحقيقة(العزاوي ، ص 42) .

أما بالنسبة للطروحات الفكرية للعقلانية الجديدة و التي بدأت بالظهور خلال الخمسينات و الستينات من القرن العشرين و تبلورت في السبعينات على يد Rossi و الأخوان Krier و آخرين ممن دعوا إلى إعادة أحياء المفاهيم العقلانية (العزاوي ، ص 47) ، فقد كانت اغلب توجهاتهم تعيد إثارة الجدل حول القيم الإنسانية و أن طريقة التفكير العقلانية و التي تجسدت بالحلول الهندسية ، أنتجت بناء ا على افتراضات تؤخذ كبديهيات قبلية مسلم بها،

تمثل بالتالي حقائق واضحة بذاتها و غير قابلة للتحليل و الاستفسار ، فتولد منظومة من الافتراضات تعود إلى نتائج معينة بالاستدلال العقلي تعطي حقائق عن الواقع الموجود ، فيكون بالتالي معيارا للحقيقة ليس الخبرة الذاتية و لكن الثبات المنطقي في البناء الفكري .

و كانت الأشكال الأساسية المعمارية العقلانية تمثل بديهيات لا يمكن الاستغناء عنها كما لا يمكن إهمال النتائج المستخلصة منها بالاستدلال المنطقي ، وهي نتائج لا تخضع لمقياس التجربة و لكن بالكيفية التي يتم استدلالها من المقدمات ، و قد حاولت العقلانية الجديدة في طروحاتها إعادة الإشارة إلى المبادئ الأساسية للرواد العقلانيين باعتبار الأشكال الأساسية الكاملة و تركيباتها تعكس بوضوح ذاتي غير قابل للبحث و السؤال ، الحقيقة الموضوعية لماهية العمارة المطلقة (العزاوي ص 176).

يتبين مما سبق التوافق من خلال بعض الجوانب المشتركة بين موقفPopper وطروحات التجريبية الجديدة و موقفKuhn وطروحات العقلانية الجديدة في العمارة من نظرية المعرفة ،خصوصا من حيث طبيعة البناء الفكري والمقدمات الشكلية للمعرفة ،فضلا عن طبيعتها ومنهجيتها المعرفية .

كما يمكن أن نصوغ المفردة المتعلقة بنظرية المعرفة العلمية (ضمن فلسفة العلم) وبالتوافق مع الطروحات الفكرية المعمارية كالأتي :-

المفردة الأساسية (الموقف من نظرية المعرفة):تشتمل على المفردات الفرعية الآتية :-

- **من حيث طريقة البناء الفكري : أما (معرفة تجريبية –ثم حسية و نظرية عقلانية –ثم معرفة تجريبية جديدة) أو (معرفة عقلانية نظرية – ثم تجريبية (اختبار)–ثم معرفة عقلانية جديدة).**
- **من حيث المقدمات الشكلية للمعرفة: أما (معرفة احتمالية: معرضة للتعديل و التغيير) أو(يقينية مطلقة، تعكس الحقيقة الموضوعية لماهية العمارة).**
- **من حيث جزئية وكلية المعرفة: أما معرفة جزئية :أهمية للجزء ضمن الكل معتمدة على التأثيرات العاطفية النفسية. أو كلية: التركيز على الكل من خلال الأشكال الأساسية الكاملة التي تعكس ماهية العمارة.**
- **من حيث المنهجية المعرفية : أما (تخمين – تحليل تكذيبي – تخمين جديد متغاير)،أو(تركيب –تحليل إسنادي–تثبيت التركيب المعدل).**

– الموقف من المجتمع

تصف الزنكة اقتران فلسفة العلم بثلاثة حقول هي (منطق العلم – نظرية نمو المعرفة العلمية ، نظرية العلم في المجتمع) ، وترى أن هنالك توجهين في نمو العلم (داخلي و خارجي) و هما من ابرز سمات التوجه المعاصر في العلم ، الحقلين الأخيرين اصبحا مركز الاهتمام منذ ستينات القرن العشرين و خصوصا ما قدمه Kuhn&Popper من نماذج تعتمد أساليب وصفية تستخدم تاريخ العلم ،فضلا عن سوسيولوجيا العلم و حتى الآن (الزنكة،ص 181).

وتناقش الزنكة في بحثها الموسوم (فكرة الثورات العلمية) التوجهين السابقين موضحة أن هنالك جانبين في فلسفة العلم هما :

- **خارجي:** يتعلق بعملية النمو في المجتمع و يرتبط ارتباطا وثيقا بالتكنولوجيا و الإنتاج و التحول الاجتماعي .
- **داخلي:** يتعلق بنمو المعرفة العلمية ضمن مجالها المعرفي.

وعلى هذا الأساس يصنف توجهين لفلسفة العلم إحداهما خارجي يصف نمو العلم كإحدى العمليات الموجودة في المجتمع ،و الآخر يركز على المنطق الداخلي للتطور العلمي فهو توجه داخلي(السابق ،ص188).

تعتمد الفكرة الرئيسية في نموذج Popper على التخمين المتعدد القائم على الحدس الذاتي و تصف الزنكة فلسفته الاجتماعية بأنها (مفتوحة) تؤمن بالتحول الاجتماعي ومواكبة التطورات و التغيرات الآنية(السابق ،ص 190). **و بالتالي فأنها تشجع على التنامي المعرفي وفقا للمؤثرات الخارجية ، لذا يمكن القول أن توجه Popper هو ذاتي خارجي .**

أما بالنسبة لـ Kuhn فان الفكرة الرئيسية في نموذجه هي إن المعرفة العلمية تعتمد على الإجماع في الرأي ضمن ما يصفه ب (العمليات الاجتماعية في المجتمع العلمي) في ميزان التصريف ، و تتطور هذه الموازيين تبعا لعمليات اجتماعية يتحاور و يتجادل فيها الباحثون حتى الإجماع(السابق ،ص 193). **لذا فتوجهKuhnموضوعي داخلي يتميز بكونه محافظ و عقلاني و يؤكد على التنامي المعرفي المستقل(المؤثرات داخلية في نمو المعرفة العلمية).**

– العمارة و المجتمع

توالت الكتابات النقدية في مجال العمارة منذ الخمسينات مطالبة بالرجوع إلى المقياس الإنساني و حقوق الفرد على اثر ما خلفته الفلسفة الاجتماعية التي انطلقت من الحركة الحديثة وأسلوبها الذي وصفه Kaufman (فرض وجهة نظر الحكومة الجديدة للمجتمع على كافة المجالات ،لأعادة هيكلة المجتمع بشكل موحد منظم و سهل الإدارة ، وعدم اخذ اللغة المحلية بنظر الاعتبار ،و معارضة كافة التنظيمات التقليدية)(Kaufman,p75). و يعزوKaufman السبب الأساسي لظهور حالة ما بعد الحداثة إلى تغيير في الأبعاد التكوينية لمجتمع ما بعد الصناعة الغربي، مما دعى المعماريين و المنظرين إلى تقسيم المجتمع إلى عدة أذواق عامة و ثقافات ذوقية ثانوية ، كما دعوا إلى تفضيل التعددية واستعمال العناصر الشكلية المرتبطة بالعمارة المحلية والتي حسب رأي Kaufman تعزز التلاحم الاجتماعي وتجلب الاستقرار للمجتمع (Ibid,p155) .

وفي بداية الستينات حدث ثوران فكري و ضغوط لخلق عمارة تعدل الصفة المنفردة للعمارة الحديثة فوجدت عدة طرق لتحقيق ذلك منها (Schulz,p8):

- إدخال العلوم الاجتماعية في العمارة : إذ ظهر تأثيرها على فكرة الفضاء و المكان فيها،فضلا عن أن ناقدي الاجتماع في الخمسينات انتقدوا فكرة سيطرة المعماري و دعوا إلى المشاركة في التصميم (Scott,p42).
- البحث عن لغة تعبيرية تستجيب للمتطلبات الاجتماعية و تطلّع على الثقافات الذوقية و التي تبنى من اجلها العمارة ورائدها R.VENTURI).
- محاولات الأسلوبية العلمية و لظهور مبادئ أساليب التصميم ورائدها C.Alexander .

كما ظهرت العديد من النزعات ذات التوجهات الاجتماعية الجديدة منها :

- **التكاملية** في اليابان التي طورها Kara Kawaو التي تقوم على التعايش بين التكنولوجيا و التقاليد و الإنسان ,و كان من خصائصها و من وجهة نظر فلسفية هي تساوي الثقافات و العمل بعيد عن الانتقائية.
- **العقلانية الجديدة** : القائمة على فكرة النمط Type و النظرة المثالية للأشكال و المحلية و التي تبلورت بالضد من الوظيفية و الواقع الاجتماعي .(Jencks,p130)
- **الإقليمية** : في بداية السبعينات وهي تحترم الثقافات المحلية و المناخ و في بعض الأحيان التكنولوجيا (Ibid,p8) .

يتبين ما سبق التوافق بين الأسس الفكرية لتوجهات ما بعد الحداثة و الأسس الفكرية العامة لفلسفة العلم ، من منطلق اجتماعي ، وتبعا لذلك ووفقا لما طرحه المنظرون المعماريون أمثال (Stern,Jencks) ومن خلال المحاولات النقدية المستمرة و نتيجة للتحليلات الأساسية ، طرح تصنيف للتوجهات المعمارية المعاصرة وفقا لاستحقاقات النظرة المعاصرة إلى المجتمع وهي كالأتي(kaufman,1982,p8) :-

الواقعية الاجتماعية ، التخطيط الاجتماعي و معارضة النظام، الانتقائية الراديكالية و السميولوجية، العفوية و مدينة التعارضات ، التراثية الراديكالية و التفكير المتدرج، الحفاظية و إعادة التأهيل والأحياء.

ومما سبق يمكن أن نستخلص الفقرات الفرعية المرتبطة بمفردة الموقف من المجتمع ، التي يمكن تبويبها وفقا لما يأتي :-

- من حيث طبيعة التوجه الاجتماعي : أما خارجي يتعلق بعملية النمو في المجتمع و يرتبط ارتباطا وثيقا بالتحول الاجتماعي و التغير التكنولوجي أو داخلي : يتعلق بالنمو المعرفي ضمن المجال الواحد .

- من حيث الأسس الفلسفية الفكرية :-أما اجتماعي واقعي: يعكس الطروحات الفلسفية الواقعية .

أو اجتماعي عقلاني : يعكس الطروحات الفلسفية العقلانية.

-الموقف من التاريخ

تعددت معاني التاريخ المرتبطة بفلسفة العلم إذ تمايزت أربعة أنواع شملت حسبPierre Bont :

- التاريخ الوثائقي :جميع النصوص المتعلقة بمنهجية العلماء.
- تاريخ الأخطاء: جمع سلسلة النظريات و الفروض العلمية التي تم وصفها خلال مختلف العصور .
- التاريخ المكاني :البحث عن وطن للاكتشافات العلمية الكبرى ، لتتبع التيارات الجديدة التي تنشا عنها و الذي يشكل الخصوصية العلمية أو الأصالة الفكرية لشعب ما الكامنة في طرائق العمل التي يعتمدونها و العادات و الميول العقلية السائدة.
- التاريخ الفلسفي للعلم : التاريخ الذي يربط الاكتشافات أو التيارات العلمية لا بمختلف الفلسفات الميتافيزيقية التي استندت عليها ، بل بالفكر العلمي و بتطور العلم ذاته (الجابري،ص40).

هذه المستويات من تاريخية الفلسفة العلمية تعكس الكيفية التي نتصور بها تطور المفاهيم و طرق التفكير العلمية . هل هو (تطور متصل) أي بناء يشيد باستمرار لبنة فوق لبنة . أم هو تطور متقطع (منفصل) بناء يشيد ويعاد تشيده باستمرار ، يعلق د.الجابري على أن وجهة النظر السائدة اليوم قائمة على (الانفصال) وهي ترى أن تطور المعرفة العلمية لا يستند دوما على نفس المضامين التي تحملها المفاهيم و التطورات العلمية في عصر من

العصور أو فترة من فترات تطور العلم بل انه تطور يستند على إعادة بناء المفاهيم و التصورات و النظريات العلمية و إعادة تعريفها و إعطاءها مضمونا جديدا، أن تاريخ العلم ليس تاريخا استاتيكيا ، بل هو تاريخ ديناميكي ثوري يمتاز بخاصية نوعية . (الجابري ،ص 44).

و قد أكد كل من Popper و Kuhn على الاهتمام بالمسار الديناميكي الذي اكتسبت به المعرفة العلمية ،اكثر من التركيب المنطقي لنتائج البحث العلمي مؤكدين على الأهمية المركزية في الرجوع إلى تاريخ العلم بمستوياته المختلفة ، وقد أكد كل منها على التقدم الثوري للعلم بدلا من التقدم بالنمو (Kuhn,p18) و التساؤل ما هو الفرق بين موقفيهما من التقاليد ؟

تناقش الزنكة في بحثها الموسوم (النظريات الأخرى في العالم) المقارنة بين Popper و Kuhn واصفا مبدا الأول بالتخلص من الأخطاء و المرتبط بنموذج يصف نمو العلم على انه تحويرات متفرقة لاجزاء المعرفة (الزنكة،ص 228) إذ ترفض نظرية Popper التبدلات الواسعة النطاق (الثورات في العلم) فلا يؤمن ألا بالتحوير و النمو من خلال التطور ، و يصف (الزنكة) الفرق بينهما من خلال تأكيد Kuhn على الدور الإيجابي للتقاليد في نمو العلم ، بينما يؤكد الأخر على أفكار التقاليد (السابق،ص 233).

أي أن Kuhn ينظر إلى التاريخ من وجهة نظر صورية تجسيدية (وهي نظرة مقيدة بالتقاليد و بالمستوى الفيزيائي الوجودي) ، أما Popper فيركز على وجهة نظر التمثيل المعنوي للتقاليد (المستوى الفكري المعنوي) وهي نظرة منفتحة.

-العمارة و التاريخ

برز التباين على مستوى العمارة بشكل واضح خصوصا على مستوى التوجهات المعمارية و المتعلقة بموقفها من التقاليد ، إذ برز توجهين مختلفين في وجهات النظر المفسرة للتقاليد و بالتالي إفرازها لصيغ مختلفة للتعامل معها و التي يمكن تبويبها كالأتي :

- التوجه المحافظ : يتقيد بالتقاليد رافضا تغييرها و متبنياً صيغة الاستنساخ .
- التوجه التحرري: نادى بضرورة التحرر من قيود التقاليد و أيد تغييرها و تعديلها ،إذ تبنى صيغة (المحاكاة) .هذا التوجه الثاني برزت فيه على مستوى العمارة و جهات نظر مختلفة تمثلت بموقفي تياري الواقعية الجديدة والعقلانية الجديدة،والتي عكست في مواقفها بعض الجوانب المشتركة بينها وبين موقف طروحات فلاسفة العلم Popper و Kuhn من التاريخ ، كما سيتضح من الآتي :-

يرى Rowe في ضوء الطروحات النقدية المكثفة للعمارة الحديثة التي استهدفت طرح حلول بديلة اكثر تكاملا و شمولية ، تصدي التيارات لا براز مشاكل العمارة الحديثة المتمثلة باستبعاد الماضي و تقاليده و مطورين نظريات و صيغا للتعامل معه, مستحضرين نظريات العلوم الإنسانية و خاصة علم التاريخ و اللغة و الاجتماع لتطوير نظرياتهم الخاصة في تفسير العمارة و تحديد أهدافها (Rowe,p170) ،و يرى Broadbent أن التيارين طرحا أسساً فكريةً فسرت العمارة بمنظور جديد، فكلاهما لم يرفض فكرة التبرير العقلاني المنطقي لأشكال العمارة و إنما اوصى تضمينها جوانب أخرى معنوية و إنسانية ، فتيار الواقعية الجديدة فسر العمارة بمنظور واقعي جديد متأثرا بمبادئ الفلسفة الواقعية السائدة في المجتمع الأمريكي و التي من وجهة نظر البحث كما سبق

تعكس طروحات الفلسفة الاجتماعية التي نادى بها Popper في فلسفته حول المجتمع المفتوح في كتابه (المجتمع المفتوح و أعداءه) و المرتبطة بنظريته الفلسفية العلمية (الزنكة ،ص 230) . و تيار العقلانية الجديدة الذي فسر العمارة بمنظور عقلاني جديد (حسب البحث عكس طروحات Kuhn الفلسفة العلمية) و التي يمتد جذورها حسب Broadbent إلى Descrates ،(Broadbent,p81) .

ويمكن توضيح ابرز الأسس الفكرية التي طرحها التيارين و المرتبطة بمفردة (التاريخ) و المتوافقة مع الطروحات الفلسفية العلمية بما يأتي (Rowe,p159):

- محاكاة و تمثيل عمارة الماضي و تقاليده لتوليد الأعمال الجديدة.
- العمارة بوصفها نتاجا حضاريا يشبه اللغة.
- العمارة بوصفها ظاهرة مستقلة ، لغة تعبر عن ذاتها مبررين ذلك (كون لغة الأشكال السابقة تمثل عوالم قائمة بحد ذاتها عبر الإنسان من خلالها عن عالمه) لذا فان إعادة تشكيل هذه اللغات السابقة يمكن من توليد لغات جديدة .
- خلق عمارة تخاطب الإنسان بلغة بليغة معبرة تحقق الانتماء والتواصل الحضاري ، عمارة تتفاعل مع التقاليد لتجادل و تناقش ، عمارة تقارن، عمارة تفسح مجالا للتعليق عن الإنسان و عالمه.
- استثمار الستراتيجيات النقدية في التعامل مع التقاليد كالاستعارة و إعادة التعريف و المقارنة الجدلية.

مما سبق يمكن أن نتبين ما يأتي :

أن الطروحات الفكرية المعمارية تعكس التوافق مع الطروحات الفلسفية العلمية فمثلا :

محاكاة عمارة الماضي و خلق عمارة تعبر عن الانتماء و التواصل الحضاري ترتبط بالمعنى المكاني للتاريخ (ضمن فلسفة العلم) ، و اعتبار العمارة نتاجاً حضارياً يشبه اللغة و أن العمارة ظاهرة مستقلة تعبر عن ذاتها . ترتبط بالمعنى الوثائقي للتاريخ الفلسفي العلمي ، أما المستويات النقدية السابقة سواء في الاستراتيجيات أو في خلق العمارة التي تخاطب الإنسان و تفسح مجالات النقد والتغير فأنها ترتبط بالمعنى الفلسفي العلمي للتاريخ).

أما على مستوى استخلاص المفردات الفرعية والمرتبطة بمفردة الموقف من التاريخ فيمكن بلورتها كما يأتي :

المفردة الرئيسة : الموقف من التاريخ

المفردات الفرعية:

- **الموقف من حيث أسلوب التعامل مع التقاليد:أما وثائقيا أو أخطاءيا أو مكانيا أو فلسفيا.**
- **الموقف من حيث العودة إلى التقاليد(يستثمر التقاليد و انظمتها التعبيرية في توليد أعمال جديدة) . و يشمل:**

1- الموقف من حيث خصائص المراجع المعتمدة : أما فكرية معنوية أو فيزيائية مادية.

2- الموقف من حيث نوعية (طبيعة) المراجع المعتمدة :أما مرجعية داخلية : تركز على المصادر المرجعية من داخل الحقل العرفي أو مرجعية خارجية : تركز على المصادر المرجعية من خارج الحقل المعرفي.

تم في الفقرات السابقة استكشاف الأطر النظرية الكامنة في الطروحات الفلسفية العلمية والمعمارية واستخلاص بعض الجوانب التفصيلية المتعلقة بالمواقف الفكرية العامة ،مشيرة في بعض قيمها إلى الجوانب المشتركة بين الأسس الفكرية لفلسفتي العلم عند Popper و Kuhn والأسس الفكرية لتياري الواقعية الجديدة والعقلانية الجديدة

من خلال مرجعيتهما خصوصا ما يتعلق بموقفهما من النظريات الاجتماعية أو موقفهما من التقاليد،مما دفع البحث للتوجه نحو الدراسات المعمارية المتخصصة لاستكشاف المواقف الفكرية للتيارين.

- المواقف الفكرية للواقعية الجديدة و العقلانية الجديدة في العمارة

- طروحات Scott /1984

ناقشت هذه الدراسة مجموعة من المفاهيم بعضها عام والآخر خاص وفيما يخص المفاهيم العامة ، قارنت الدراسة بين تياريي الواقعية الجديدة و العقلانية الجديدة موضحة اشتراكهما بمبدأ موحد (العودة إلى التقاليد) ، واختلافهما في طبيعة تلك العودة. (Harvard ,p6) وكالأتي:-

تنظر الواقعية الجديدة إلى التاريخ بوصفه مستودعاً للصور الشكلية ويدمج تقاليد العمارة مع تقاليد أخرى مستمدة من مصادر خارج حقل العمارة ، بينما تميل العقلانية الجديدة في نظرتها إلى التاريخ بوصفه سلسلة متصلة من النتاجات تستنبط من خلالها قواعد و مبادئ العمارة (Harvard,p7) .أوضحت الدراسة خصوصية تيار العقلانية الجديدة في عودته إلى التقاليد بإبراز مفهوم النمط (Type) ومفهوم التحولات النمطية مؤكدة على استثمار هذا المفهوم في التعامل مع التقاليد معتمدة على استثمار قواعد التجميع و التركيب التي تميز أنماط الأبنية السابقة باعتبرها أسسا كلية تخلق بموجبها الأشكال الجديدة (Ibid,p7) فضلاً على اعتماده على الإسناد والإشارة والتلميح إلى أشكال مسبقة ذات طابع فكري، ومن خلال ذلك التلميح إلى التصورات الفكرية عن الأشكال يكمن ارتباط هذا المفهوم بالجوهر ويسمو فوق الممارسات الفردية (Ibid,p7) .

كما أشارت الدراسة إلى أن العقلانية الجديدة تستثمر فكرة النمط الفعال في توليد نتاجا ته الحالية مبيناً أنها تكون مستمدة من نظريات معمارية سابقة ؛ تستثمر القدرة العالية للنمط على التحول وتوليد أنماط جديدة. **ويتضح مما سبق أن ابرز الجوانب التي ركزت عليها الدراسة تمحورت حول جانبين رئيسيين هما مبدا العودة إلى التقاليد وطبيعة تلك العودة التي عرفت في ضوء جوانب اكثر تفصيلية.**

- طروحاتColquhoun /1985

اهتمت هذه الدراسة بمناقشة التغير الحاصل في أنظمة التعبير، واوضحت خصوصية الحقبة المعاصرة مقارنة بالحقب السابقة (الكلاسيكية و الحديثة) ،فقد برزت من خلال المناقشة مجموعة مفاهيم : استثمرت في توضيح التباين في أنظمة التعبير التي شملت (طبيعة الأشكال المستخدمة،طبيعة المعاني المرتبطة بها ، كيف تدرك تلك المعاني) وفي ضوءها طرحت خصوصية الحقبة المعاصرة وكما يأتي :

تعمقت هذه الدراسة في توضيح الاختلاف بين العقلانية الجديدة والواقعية الجديدة مستندة إلى جانبين أساسيين هما : **الجانب الأول**،شمل كيفية استثمار الأنظمة التعبيرية السابقة ، ومميزات النظام التعبيري الجديد ، وفي ضوءه ، وصف تيار الواقعية الجديدة ، كونه يستثمر الأنظمة التعبيرية السابقة كرموز مجزأة كالسقوف و النوافذ والأعمدة ، أما تيار العقلانية الجديدة فقد عرف كونه سيستثمر الأنماط السابقة ويركز على الأنماط العامة . و**الجانب الثاني** اوضحت الدراسة من خلاله خصوصية تيار الواقعية الجديدة مبينة بان نظامه التعبيري الجديد لا يتقيد بحقل العمارة بل أن رموزه متنوعة معمارية وغير معمارية ،اذ تحددها العوامل والظروف الخاصة بكل مشروع . في حين نجد اقتصار أنظمة التعبير في العقلانية الجديدة على حقل العمارة المستقل ذاتياً وباستثماره

لرموز تفهم معانيها ضمن إطار فكري يهدف إلى استرجاع العمارة باعتبارها تجربة جماعية (Colquhoun,pp195-199) .

يتضح ما سبق أن أهم الجوانب التي وردت في وصف صيغ التيارين تمحورت حول جانبين هما : كيفية استثمار الأنظمة التعبيرية السابقة (التقاليد) ومميزات النظام التعبيري الجديد ، وقد وضح كل منهما في ضوء جوانبه التفصيلية .

- طروحات Rowe /1988

ناقشت هذه الدراسة المفاهيم المرتبطة بالواقعية الجديدة و العقلانية الجديدة على مستويين ،تبنى **المستوى الأول** مناقشة المفاهيم المشتركة التي اعتمدوها شملت مواقفهم تجاه النواحي التالية :

(نوعية المراجع التي تعتمد في خلق التصاميم ، ماهية العمارة وأهدافها ، نوعية المناهج المستثمرة في خلق التصاميم) ؛ في حين اعتمد **المستوى الثاني** على مقارنة صيغ التعامل مع التقاليد في كل منهما وتناول صيغتين رئيسيتين هما :(صيغة المعالجة اللغوية و التي تستثمرها الواقعية الجديدة ، وصيغة النمط التي تستثمرها العقلانية الجديدة) .

ومن خلال مناقشة المواقف المشتركة لهما ، بينت طروحاتRowe بأنهما يعتبران العمارة وتقاليدها كمرجع أساسي لتوليد التصاميم ، ويشتركان في تفسير العمارة وتحديد أهدافها لكونها لغة بليغة للتعبير و التخاطب ، تجادل وتناقش وتطرح وجهات نظر متعددة عن الإنسان وعالمه ،فضلاً عن استخدام مناهج نقدية في توليد نتاجاتهم كالاقتباس و إعادة التعريف والجدل والمناظرة (ROWE,P.P.150-155)، أما بالنسبة للمستوى الخاص و المتعلقة بالمعالجة اللغوية و النمط حيث وضحت الدراسة صيغة المعالجة اللغوية من خلال ممارسة المعماريR.VENTURI بالشكل آلاتي : استعارة و اقتباس عناصر رمزية مستقلة خارجة عن نطاق العمل ، تقحم فيه بقصد معين ، أما لتعديله وتأهيله أو لطرح تعليقات إضافية (Ibid,p181)، أما بالنسبة لصيغة النمط فقد بينت الدراسة ابرز مميزات هذه الصيغة من خلال ممارسات المعمار A. ROSSI من خلال استثماره مفهوم النمط بوصفه تصوراً فكرياً للعلاقات التي تربط بين أجزاء الشكل من جهة وبين تلك الأجزاء و الكلمن جهة اخرى، مشيرة إلى قدرته العالية على الظهور في عدة نماذج، وبينت بان استثمار الأنماط السابقة يعتمد على المعاني المرتبطة بتلك الأنماط والتي تنقسم إلى ثلاث أنواع هي (معاني مرتبطة بالأجزاء من الأشكال السابقة ، معاني مفترضة ومقترحة تنتج من خلال إعادة تجميع الأجزاء في سياق جديد) . (Ibid,p191) .

ويتضح مما سبق أن طروحات Rowe تركز على جانبين أحدهما مرتبط بصيغ التصميم فيهما ، فبعض الجوانب ارتبطت بمواقف مشتركة يؤمن بها معماريو التيارين شملت ثلاث أمور رئيسية هي: (نوعية المصادر المعتمدة في خلق التصاميم . ماهية العمارة وأهدافها ، وماهية الستراتيجيات المعتمدة)، أما الجانب الأخر، فارتبط بعمليات أساسية يعتمدها المصمم كالاقتباس و الاستعارة و الإقحام في حالة المعمار VENTURI ، و النمط وقواعد استثماره في حالةA. ROSSI .

- طروحات KLOTS/1988

ناقشت ابرز مميزات التيارين وعلى مستوى عام و تفصيلي : ففي المستوى الأول برزت مميزات الواقعية الجديدة من خلال ما يأتي : (استثمار العالم الواقعي مصدرا للأشكال و الأفكار ، التوجه الواقعي الذي يستند على عناصر موجودة في الواقع ، معالجة الأشكال بمنظور نسبي ، التحويل و التغريب و التهكم على الأشكال السابقة) ،أما العقلانية الجديدة فوضحت مميزاتها من خلال استثمار مفهوم النمط واسترجاع الدور المهم للأنماط التاريخية (KLOTZ,PP210-212) أما على المستوى التفصيلي ، فقد وضحت من خلال مميزات ابرز مؤسسي التيارين ، فقد وضح KLOTZ خصوصية المعماري R. VENTURI بإبراز الجوانب الآتية :(النظرة الواقعية للعمارة واستثمار ما موجود مسبقاً وتعديله وتطويره ، استثمار نتاجات حضارية مختلفة كمصادر للأفكار ، اعتماده على أسلوب التلميح و التداعي الفكري، استثماره لمفهوم البناية كسقيفة مزخرفة ، التخاطب بالصور المجازية ، دعوته لاستثمار مفاهيم التنوع و التعددية و التناقض و الغموض . كما وضحت خصوصية المعمار A. ROSSI من خلال ما يأتي :(استر جاع الأنماط الأولية و البدائية للأبنية ، البحث عن قواعد عامة تلائم عدة مشاريع، تقبل الأشكال البسيطة و الاعتراض على تجريدها من المعاني و الرموز التاريخية).(KLOTZ,P214).

يتضح من هذه الطروحات ، بأنها تضمنت جوانب مختلفة في توضيح صيغ التباين ؛ فبالنسبة للواقعية الجديدة ، برزت مفاهيم متنوعة ارتبطت بمصادر الأشكال و الأفكار ومفاهيم مثل النسبية الواقعية والاتصال من خلال العمارة والتخاطب بالصور المجازية ؛ أما العقلانية الجديدة فبرزفيها التاكيدعلى فكرة النمط واستثمار الأنماط الأولية .

طروحات JENCKS/1988

وضحت طروحات **JENCKS** ممارسات مؤسسي التيارين من خلال جانبين رئيسيين هما :مفاهيمهم وخصائص نتاجاتهم كما يأتي :

بالنسبة للمفاهيم ، وضحJENKS مفاهيم المعماري R.VENTURI ممثل تيار الواقعية الجديدة بالشكل الآتي: (الدعوة إلى استثمار النتاجات التاريخية مصدر أساسي في خلق الأعمال الجديدة ، استثمار الأفكار المتاصلة في التقاليد السابقة كالغموض والتوتر ، ضرورة تضمين الأعمال المعمارية شفرات مختلفة تخاطب عامة الناس فضلاً عن خاصتهم) . (JENKS,P115) .

أما العقلانية الجديدة فشملت المفاهيم الآتية: (استثمار نظرية الذكريات المتراكمة الجماعية والتي تقوم على تذكر الأبنية المهمة من خلال الخبرة و تراكم المعرفة). (Ibid,p 116) ،ويوضح JENKS خصائص نتاجاتهم ، من خلال التركيز على الخصائص المميزة لأعمال VENTURI و المتمثلة بـــ (امتلاكها خاصية الإشارة المزدوجة ، استثمارها لخاصية المحاور المنحرفة وخاصية اللاتناظر ، و التوازن الديناميكي للعناصر وخاصة الإدغام ،وخاصية التزيين والتشويه للأشكال البسيطة (Ibid,p 117) ،فضلا عن الإشارة إلى الخصائص المميزة لنتاجات A. ROSSI و المتمثلة بـــ (الإشارة إلى معالم المدينة التقليدية الكلاسيكية وتبسيطها ،استرجاع التنظيمات الكلاسيكية المحدثة بأسلوب معماريّ الثورة الفرنسية أمثال LEDOUX). (Ibid,p118) .

– مناقشة نقدية

تبين من تحليل الطروحات السابقة ، للكشف عن ابرز الجوانب التي وصفت في ضوءها التيارين ، بأنها طرحت جوانب كثيرة ومتنوعة شملت : المفاهيم و المبادئ التي يتبناها معماريو التيارين ، مميزات أنظمتهم التعبيرية ، كيفية استثمارهم للتقاليد ، تعبيرهم عن معان معينة ، أسلوب إشارتهم إلى التقاليد ، وعمليات التحويل للأشكال السابقة . وبعد التعرف على هذه الجوانب التي اعتمدتها الطروحات السابقة يمكن تحديد مجموعة من الاستنتاجات حول طبيعة هذه الجوانب و المعرفة المرتبطة بها و كالأتي :

- أن الجوانب التي تطرحها الدراسات متباينة ومتنوعة .
- لم تتبلور هذه الجوانب في مفردات واضحة ومحددة يمكن اعتمادها مباشرة وبالتالي تشكيل الإطار في المرحلة الأخيرة .

فالتباين في نوعية الجوانب المعتمدة ، برز من خلال تكرار جوانب محددة في معظم الدراسات و اقتصار ذكر جوانب أخرى على بعض الدراسات فقط ، وعلى سبيل المثال فقد وصفت معظم الدراسات المفاهيم و المبادئ التي يتبناها التيارين وخاصة مبدا العودة إلى التقاليد ،أما الناحية الاخرى و المرتبطة بعدم تبلور هذه الجوانب في مفردات واضحة ومحددة فقد برزت بشكل واضح في جميع الطروحات حيث اتصفت بعمومية الطرح وتداخل المفاهيم .ويمكن استخلاص المواقف الفكرية للواقعية الجديدة و العقلانية الجديدة كما يأتي:

- استخلاص المواقف الفكرية للواقعية الجديدة و العقلانية الجديدة

المواقف الفكرية المشتركة

- **الموقف الفكري في تفسير العمارة وتحديد أهدافها :** وضحت الطروحات اشتراك التيارين في مبدا موحد يميز العمارة نتاجاً حضارياً كاللغة ، تعكس معاني وأفكار وتعبير عنها باستثمار قدرات اللغة التعبيرية و الجدلية ، فدراسة Colquhoun قارنت النظام التعبيري للتيارين وميزته عن نظام العمارة الحديثة مبينة استثمارهم لفكرة الشكل الرمز في التعبير عن معاني خاصة بينما يستثمر تيار العمارة الحديثة الشكل المجرد في التعبير عن معانٍ عامة، و دراسة Rowe بينت بان التيارين يستثمران قدرات اللغة التعبيرية البلاغية وفن المناظرة و الجدل لتحقيق أهداف أساسية للمجتمع كالتخاطب والتفاعل الإيصال ، يتضح من هذه الطروحات بان التيارين يشتركان في مبدا موحد يشبه العمارة باللغة ويستثمر قدراتها التعبيرية .

- **الموقف تجاه استثمار التقاليد :** عرفت معظم الطروحات صيغ التيارين ، بكونها تؤيد التقاليد السابقة وتستثمر أنظمتها الرمزية في توليد أعمال جديدة ، فطروحات (Klots,Jencks,Colquhoun،Scott) أشارت إلى استخدام معماري التيارين للتقاليد السابقة وأنظمتها التعبيرية (أشكالها ومعانيها) لتوليد أعمال جديدة منها ، أما طروحات Rowe فقد أضافت بان هذا المبدأ يستثمر لتحقيق أهداف مهمة كالتواصل و الاستمرارية الحضارية و الفهم العام المشترك .

- **الموقف تجاه المراجع المعتمدة :** عرفت الطروحات صيغ التيارين كونها تعتمد العمارة كمرجع أساسي تتولد منه الأعمال الجديدة فقد أشارت دراسة (Scott) إلى اشتراك التيارين في مبدا موحد يعتبر العمارة مرجعاً أساسيا ولكنها ميزت تيار الواقعية الجديدة بكونها تستثمر مصادر أخرى إضافية . أما Colquhoun فقد أكدت على تنوع الرموز في تيار الواقعية الجديدة بين رموز معمارية و غير معمارية واختصارها على الرموز المعمارية في تيار

العقلانية الجديدة ، من ناحية أخرى قارنت طروحاتRowe بين مراجع التيارين ومراجع العمارة الحديثة فالأخيرة تستثمر مصادر من خارج حقل العمارة كالطبيعة أو التكنولوجيا .

– **الموقف تجاه نوعية المناهج والستراتيجيات المعتمدة في خلق الأعمال** ؛ يستثمر التيارين وفقاً للطروحات السابقة سترتيجيات لغوية نقدية ، فقد وصف استراتيجيات التيارين بأنهما يستثمران سترتيجيات نقدية مثل (الاقتباس و إعادة التعريف و الجدل و المناظرة) .

– **المواقف الفكرية المتباينة :**

استند توضيح المواقف المتباينة إلى استخلاص القضايا التي نوقشت بصددها هذه المواقف وبشكل عام يمكن تحديد ابرز المواقف التي اختلف فيها التياران بالنقاط الآتية :

. **الموقف تجاه النظريات الفلسفية :** تبرز المواقف الخاصة للمصمم في تبنية نظريات فلسفية معنية دون غيرها تنعكس بالضرورة في نظرياته المعمارية فتيار الواقعية الجديدة يتأثر بمبادئ الفلسفة الواقعية و التجريبية وهي الفلسفة الأكثر شيوعاً في المجتمع الأمريكي ، أما تيار العقلانية الجديدة في إيطاليا فقد تأثر بمبادئ الفلسفة العقلانية ومؤسسها الفيلسوف و الفيزيائي الفرنسيDescarts .

. **الموقف تجاه نظريات العمارة :** تبرز المواقف الخاصة للتيارين في النظريات التي طرحها ابرز رواد التيار وخاصة المعماريان ROSSI& VENTURI ، فبرغم الاشتراك في قضايا محددة عكست نظرياتهم اختلافا في المفاهيم ، فقد استثمر VENTURI وجهة النظر النسبية في تفسير العمارة مؤكداً أهمية التفاصيل و الأجزاء وخاصة العناصر الزخرفية و التزيينية طارحاً وجهة النظر التي تفسر العمارة كونها ابنية مزخرفة، أما ROSSI فقد عكست طروحاته نظرة شمولية كلية ارتبطت بالمدينة وتراكيبها و بنيتها ،وبرز في طروحاته مفهوم النمط وتحولاته عبر الزمن كمفهوم أساسي .

– **طبيعة الأفكار و المعاني المقصودة في العمل :** وصفت بعض الطروحات السابقة صيغ التيارين بكونها تستثمر رموز التقاليد وتعبر من خلالها عن معان جديدة ، ويتضح من هذه الطروحات بان الهدف الرئيسي من هذه الصيغة هو توليد معان جديدة من معان سابقة فطروحات Colquhoun أوضحت بان رموز ومعان تيار الواقعية الجديدة لا تتحدد بحقل العمارة وتستثمر رموز معمارية وغير معمارية بينما تقتصر رموز تيار العقلانية الجديدة على حقل العمارة فقط ، لقد بينت هذه الطروحات بان تحديد هذه الرموز و المعان يعتمد على الظروف الخاصة بكل مشروع في تيار الواقعية الجديدة بينما يتجنب تيار العقلانية الجديدة هذا التحديد . أما طروحات Rowe فقد وصفت المعاني المنعكسة في أعمال تيار العقلانية الجديدة بكونها معان تخص العمارة و أنماطها البنائية ووضحت أنواعها في ثلاث هي : (معان سابقة وموروثة ومكتسبة ومنسوبة إلى تلك الأنماط ، معان مرتبطة بأجزاء تلك الأشكال السابقة ، معان جديدة يقترحها المصمم وتنتج من إعادة تجميع الأجزاء و العناصر في نسق جديد) .

وفي ضوء ما سبق، يمكن توضيح المفردات كما في الجدول(1) الآتي :

جدول (1) يوضح المفردات الرئيسية و الفرعية المرتبطة بالمواقف الفكرية للواقعية الجديدة و العقلانية الجديدة

المفردة الرئيسية	الفقرات الفرعية		القيم الممكنة	
الموقف الفكري للواقعية الجديدة و العقلانية الجديدة	1. تجاه العمارة وأهدافها		العمارة لغة تعبير و تخاطب ، أهدافها تلبي متطلبات معنوية ومادية أهمها التواصل و الاستمرارية الحضارية	
			العمارة هي المنفعة والمتانة ، أهدافها:تلبية حاجات الإنسان المادية	
	2.تجاه التقاليد		موقف مؤيد للتقاليد مزيحاً لها	
			موقف مؤيد للتقاليد مؤكداً لها	
	3.تجاه المراجع التي يتم محاكاتهم		مراجع داخلية (العمارة وتقاليدها هي المرجع الأساس)	
			مراجع خارجية (مراجع من خارج العمارة .الطبيعة / التكنولوجيا).	
	4. تجاه نوع المناهج و الاستراتيجيات		مناهج العلوم الإنسانية /مفاهيم النقد الأدبي / جدل ومقارنة	
			مناهج أخرى	
	5.تجاه النظريات الفلسفية		تتبنى مبادئ الفلسفة الواقعية	
			تتبنى مبادئ الفلسفة العقلانية	
	6.تجاه نظريات العمارة		التركيز على معاني الأجزاء (تزيين وزخارف)	
			التركيز على معاني الكل (أنماط)	
	7.المعاني والأفكار المقصودة في العمل	ماهية المعاني والأفكار المعبر عنها	التعقيد و التناقض في العمارة	
			العمارة واسطة لنقل المعلومات	
			العمارة تعني الحياة	
		ماهية العوامل المحددة للمعاني والأفكار	عوامل ذاتية تخص المصمم	
			عوامل موضوعية تخص المشروع	موقعه
				وظيفته
				الجهة المستفيدة منه

-الجوانب المتعلقة بفلسفة العلم عندPopper وKuhn والواقعية والعقلانيةالجديدة في العمارة:

تضمنت الفقرات السابقة بعض الجوانب المشتركة بين طروحات Popper والمواقف الفكرية للواقعية الجديدة،وبين طروحات Kuhn والمواقف الفكرية للعقلانية الجديدة،والتي يمكن توضيحها بالمناقشة الآتية:

من جانب الموقف من التاريخ : فقد بينت المعرفة المطروحة أن هنالك بعض الجوانب المشتركة بين طروحات Popper و الواقعية الجديدة و طروحات Kuhn و العقلانية الجديدة ،تتمثل في الموقف من العودة إلى التقاليد، خصوصا ما يتعلق بموقفهما من المراجع المعتمدة سواء على مستوى خصائصها أو طبيعتها،فضلا عن التوافق في

الأسس الفكرية لتوجهاتهما مع توجهات ما بعد الحداثة و من منطلق اجتماعي ، إذ ترتبط النظرية الاجتماعية الواقعية المنفتحة والتي تقترب من طروحات Popper الواقعية في كتابه (المجتمع المفتوح و اعدائه) مع الأسس الفلسفية للواقعية الجديدة في العمارة ، خصوصا ما طرحه S.Brawn في كتابه (Architecture Test in aPluralistic Socity) من خلال البحث عن لغة تعبيرية مستجيبة للمتطلبات الاجتماعية و مطلعة على الثقافات الذوقية و التي تتبنى من اجلها العمارة ،مشيرا إلى عمارة R.Venturi كونها رائدة في هذا المجال فضلاعن إدخال العلوم الاجتماعية في العمارة ضمن الفضاء والمكان،(Scott,pp42-50) .

أما بالنسبة إلى طروحات Kuhn وتطابقها مع طروحات العقلانية الجديدة في العمارة،فقد أشارت Scott إلى النزعات ذات التوجهات الاجتماعية الجديدة و التي احدثت ثوران فكري في الستينات من القرن العشرين ومنها العقلانية الجديدة القائمة على فكرة النمط و النظرة المثالية للأشكال المحلية ، فضلا عن ما قدمه Stern&Jencks من دراسة نقدية طرحا من خلالها بعض النزعات ذات التوجهات المحا فظة (التراثية الردايكالية ،الحفاظية ، إعادة التأهيل و الإحياء) و التي تعكس الأسس الفكرية للواقعية الجديدة في نظرتها المحافظة إلى المجتمع ،والتي تتطابق مع ما تطرحه (الزنكة) حول فكرة التوجه الداخلي في نمو العلم ، كونه متعلقا بنمو المعرفة العلمية ضمن مجالها المعرفي والتي تنعكس من خلال(ميزان التصريف)مما يضفي عليها الصفة المحافظةوالمستقلة عن المجتمع

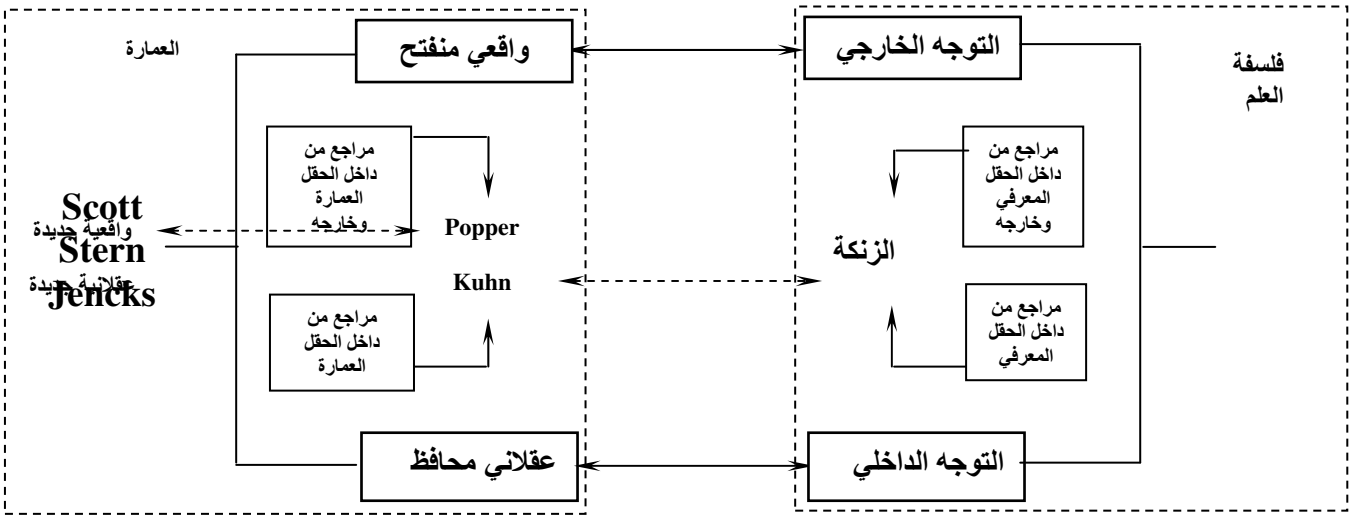

مخطط (1) يوضح الجوانب المشتركة بين طروحات Popper و الواقعية الجديدة و طروحات Kuhn و العقلانية الجديدة

ومما سبق يمكن أن نبلورمفردة تتعلق بالمواقف الفكريةالعامة تتمثل بـ(**الموقف من التيارات المعمارية**)كما يأتي:

الجدول(2) الفقرات الفرعية المتعلقة بالموقف من التيارات المعمارية

المفردة الرئيسية	الفقرات الفرعية	القيم الممكنة
الموقف من التيارات المعمارية	من حيث نوعها	تيار الواقعية الجديدة
		تيار العقلانية الجديدة
	من حيث موقفها من النظريات الفلسفية	تتبنى مبادئ الفلسفة الواقعية
		تتبنى مبادئ الفلسفة العقلانية
	من حيث موقفها من التقاليد	موقف مؤيد للتقاليد مزيحاً لها
		موقف مؤيد للتقاليد مؤكداً لها
	من حيث موقفها من نظريات العمارة	التركيز على معاني الأجزاء (تزيين وزخارف)
		التركيز على معاني الكل (أنماط)
	من حيث موقفها من المراجع التي يتم محاكاتهم	مراجع داخلية(العمارة وتقاليدها هي المرجع الأساس) و مراجع خارجية (مراجع من خارج العمارة .الطبيعة / التكنولوجيا)
		مراجع داخلية(العمارة وتقاليدها هي المرجع الأساس)
	من حيث ماهية العوامل المحددة للمعاني والأفكار	عوامل ذاتية تخص المصمم
		عوامل موضوعية تخص المشروع
		عوامل ذاتية وعوامل موضوعية

وبعد مناقشة الجوانب المشتركة بين الطروحات الفلسفية العلمية والمعمارية، يمكن أن نلخص المواقف الفكرية العامة كما في الجدول الآتي:

يوضح الجدول (3) المواقف الفكرية العامة والمفردات الفرعية المرتبطة بها والقيم الممكنة

المفردة الرئيسية	الفقرات الفرعية	القيم الممكنة	
المواقف الفكرية العامة	الموقف من النظرية النفسية	من حيث الأسس الفلسفية النفسية	علم النفس التفاعلي
			علم النفس الجشتالتي
		من حيث نوع التغير في الاكتشاف	تغير عقلاني يقع ضمن عوالم منطق الاكتشاف العلمي
			تغير ديني يقع ضمن عوالم السايكولوجي الاجتماعي
	الموقف من نظرية المعرفة	من حيث طريقة البناء الفكري	تجربة–حسية و نظرية عقلانية –تجربة جديدة
			عقلانية نظرية –تجريبية –نظرية جديدة
		من حيث المقدمات الشكلية للمعرفة	معرفة احتمالية
			معرفة يقينية مطلقة
		من حيث جزئية و كلية المعرفة	معرفة جزئية
			معرفة كلية

الموقف من المجتمع	من حيث طبيعة التوجه الاجتماعي	خارجي
		داخلي
	من حيث الأسس الفلسفية الفكرية	اجتماعي واقعي
		اجتماعي عقلاني
	من حيث طبيعة النزاعات المعمارية	نزعات واقعية اجتماعية
		نزعات عقلانية اجتماعية
الموقف من التاريخ	من حيث أسلوب التعامل مع التقاليد	الجانب الوثائقي
		الجانب الاخطائي
		الجانب المكاني
		الجانب الفلسفي
	من حيث العودة إلى التقاليد	الجانب الفكري(المعنوي) للتقاليد
		الجانب الفيزيائي (المادي) للتقاليد
	من حيث نوعية المراجع المعتمدة	مرجعية داخلية و خارجية
		مرجعية داخلية
	من حيث المنهجية المعرفية	تخمين – تحليل تكذيبي– تخمين مغاير
		تركيب– تحليل إسنادي– تركيب معدل

الموقف من التيارات المعمارية	من حيث نوعها	تيار الواقعية الجديدة
		تيار العقلانية الجديدة
	من حيث موقفها من النظريات الفلسفية	تتبنى مبادئ الفلسفة الواقعية
		تتبنى مبادئ الفلسفة العقلانية
	من حيث موقفها من التقاليد	موقف مؤيد للتقاليد مزيحاً لها
		موقف مؤيد للتقاليد مؤكداً لها
	من حيث موقفها من نظريات العمارة	التركيز على معاني الأجزاء (تزيين وزخارف)
		التركيز على معاني الكل (أنماط)
	من حيث موقفها من المراجع التي يتم محاكاتهم	مراجع داخلية(العمارة وتقاليدها هي المرجع الأساس)و خارجية (من خارج العمارة .الطبيعة / التكنولوجيا)
		مراجع داخلية(العمارة وتقاليدها هي المرجع الأساس
	من حيث ماهية العوامل المحددة للمعاني والأفكار	عوامل ذاتية تخص المصمم
		عوامل موضوعية تخص المشروع
		عوامل ذاتية وعوامل موضوعية

- الاستنتاجات

- ظهر للبحث أن فلسفة العلم المعاصر تهتم بتكوين الأحكام الشاملة المشتركة القائمة على التمايز النوعي الفردي لكل علم والذي يكسب النتاج المعرفي الوحدة والشمولية والجدة المتنامية، فضلا عن تبني النماذج الفكرية وخلق الصور الذهنية عن العالم المحيط واستشعار الجمال الحسي والمطلق في النفس والوجود.

- تبين للبحث أن فلسفة العلم المعاصر فلسفة مفتوحة تؤكد على التعدد في زوايا الرؤية للموضوع الذي تتركز دوافعه في إعادة البناء المنظم المتنامي، فضلا عن التداخل بين عالم العقل و معطيات التجربة و من ثم إعادة التفسير الظرفي (الآني) اعتمادا على التداخل بين المعرفة العقلية و المعرفة التجريبية.

- وفرت الطروحات والأدبيات السابقة قاعدة أساسية استثمرت لبناء إطار نظري اكثر شمولية ووضوحا ، يمكن من خلاله وصف تأثير فلسفة العلم المعاصر على العمارة بشكل عام ، و تأثير فلسفتي العلم عند Popper& Kuhn على العمارة بشكل خاص .

- توصل البحث إلى بلورة خمسة مفردات فرعية ارتبطت بطبيعة المواقف الفكرية العامة تمثلت ب(الموقف من نظرية المعرفة، الموقف من النظرية النفسية، الموقف من المجتمع، الموقف من التاريخ).

- توصل البحث إلى بلورة بعض الجوانب المشتركة بين المواقف الفكرية لفلسفة العلم عند Popper و المواقف الفكرية للواقعية الجديدة في العمارة و بين المواقف الفكرية لفلسفة العلم عند Kuhn و المواقف الفكرية للعقلانية الجديدة في العمارة، شملت الأسس الفلسفية (موقفهما من النظريات الفلسفية) و موقفهما من التقاليد (مؤيد للتقاليد ومزيحا لها أو مؤيد للتقاليد و مؤكد لها)، فضلا عن طبيعة المراجع المعتمدة (من داخل حقل العمارة و خارجه أو اختصارها على داخل حقل العمارة) و طبيعة التعامل مع التقاليد(التركيز على الجانب الفكري لها أو الشكلي).

المصادر العربية

- **الجابري** ، د. عابد ، (**مدخل إلى فلسفة العلوم ، العقلانية المعاصرة وتطور الفكر العلمي**) ، الطبعة الرابعة ، بيروت ، 1998.
- **الزنكة**،آنت ،(**الفلسفة الوضعية**) مؤتمر اتحاد مجالس البحث العلمي العربية،ترجمة :د.خليل إبراهيم الحماش،بغداد ،1981.
- **الزنكة**،آنت ،(**فكرة الثورات العلمية**) مؤتمر اتحاد مجالس البحث العلمي العربية،ترجمة :د.خليل إبراهيم الحماش،بغداد ،1981.
- **الزنكة**،آنت ،(**النظريات الأخرى في العلم**)،بحث مقدم في وقائع مؤتمر اتحاد مجالس البحث العلمي العربية،ترجمة :د.خليل إبراهيم الحماش،بغداد ،1981.
- العزاوي ، **هشام** ، (اثر تغيير البنية الفكرية على هيئة النسيج الحضري) ، أطروحة دكتوراه،كلية الهندسة ، جامعة بغداد 1998.
- **باشا** ، د. احمد فؤاد ، (**فلسفة العلوم بنظرة إسلامية**)،1984 .
- **حمدي** ،فاتنة ،(**الأسس النظرية للمناهج العلمية**) ،بحث مقبول للنشر ،كلية الآداب ،جامعة بغداد ،1997
- **زيدان**،د.محمود،(**مناهج البحث الفلسفي**)،الهيئة العامة للتأليف والنشر،مصر،1979.
- **محمود** ، زكي نجيب ، (**المنطق الوضعي**) ، مكتبة الانجلو المصرية ، ط4 ، 1986.
- **مهران**،د.محمد،(**فلسفة العلوم ومناهج البحث**)،مكتبة الانجلو المصرية،1986.

REFERENCES

-**Able** ,C.,(The Language Analogy In Architectural Theory and Criticism),Architecture association Quartery,1980.
- **Broadbent** ,G.,(Emerging Concepts in Urban Space Design). Van nosrand,N.Y.,1990 - **Colquhoun** ,Alan ;(Essays in Architectural Criticism Modern Architecture and Change Historical) .Appositions Books ;The M.I.T . press; Cambridge ;1985.
- **Feigl , H.& Brodbeek , M.; (**Readings In The Philosophy Of Science), Paris, 1972.
- **Harvard,** Architectural Review Editorial :Autonomous Architecture.No.3,M.I.T.;1984.
-**Jencks** ,Charles ;(Architecture Today); Academy Editions ;London ;1988.
-**Jencks** ,Charles ,(Late Modern Architecture ,and other essays)Academy Editions , **Kaufman,** Jacob ; (Post Modern Archecture ,An Ideology) , P .H .D Thesis ,University of California ,Los Angeles ,1982.
-**Klotz** , Heinrich . (The History of Postmodern Architecture); The M.I.T . press; Cambridge Mass. 1988.
-**Kuhn** ,T.,(The structure of Scientific Revolutions),Princeton University Press,1965.
-Lang, Jon ;(Creating Architecture Theory , The Role of Behavioral Sciences in Environmental Design), Van Norstand Reinhold Company,N,Y.,1987.
-**Norris ,**Christopher;(What is Deconstruction),St. Martins press ,N . Y.,1988.
-O' Connor ,D.J .;(A Critical History of Western Philosophy),The Free press ,N. Y., 1964.
-Rowe ,Peter G .(Design Thinking), The M.I.T . press; Cambridge;1988.
-Schluz ,C.N. ;(Existence Space and Architecture), praeger publisher ;N.Y 1971**.**
-Scott Brown . Denise;(Architectural Taste in a pluralistic Society), the Harvard Architecture Review Vol. 1,Spring 1980 , MIT press.

AN APPROACH IN IMPROVING THE PROPERTIES OF SAND DUNES

Dr. Saad F.I. AL-Abdullah,
Highways and Transportation Dept.
College of Engineering,
University of Al.Mustansiria,
IRAQ.

ABSTRACT

An experimental study to improve sand dunes to gain economic construction of highway using these locally available materials. The study was divided into two approaches; the first was by using different bituminous binder proportions from (2) to (10) percent, while the second was to use fine metals as reinforcement. The results show an increase in the degree of improvement as reinforcement layers and silt contents were increased. Also it was found that 8% 0f asphalt cement increase the stabilization of sand dunes.

الخلاصة

أجريت دراســات مختبرية لتحسين الكثبان الرملية للحصول على مادة إنشائية اقتصاديةلاستعماها كمادة انشلئية محلية في أعمـــال الطرق .قسمت الدراسة إلى اتجاهين الأول باستعمال المحتوى الإسفلتي بنسب من (2)% إلى(10)%بينما الاتجاه الثاني باستعمال شبكات التسليح

تبين من النتائج إن هناك زيادة في درجة التحسين كلما زادت طبقات التسليح مع زيادة نسب الغرين.كذلك وجد أن النسبة 8%من الإسفلت الأسمنتي قد سببت زيادة في تثبيت الكثبان الرملية.

KEYWORDS

Sand Dunes, Local, Reinforcement, Asphalt, Triaxial

INTRODUCTION

In south of Iraq, especially between Nasria and Basrah, sand dunes of uniform size are available in abundance and can be used for low- cost stabilizer constructions. Obviously these soils may be improved its properties and behavior in order to use it in project for strategic use as bridges, road, and building. Obviously, these roads should be constructed at much cheaper cost, using the locally available sand which are stabilized with bitumen and could be improved also by reinforced such types of soils which is one of considered methods in improvement for these in this study.

Reinforced Earth is a composite of material formed by the association of granular fill and tensile resisting elements (strips, grids or sheets) as reinforcement. This concept is totally based on the friction mobilized between the reinforcement and the soil grains surrounding it. Due to this interaction to a tensile normal load on the reinforcement mass will be transferred to a tensile force along the reinforcement. Consequently the reinforcing element will act as a tie between the particles of the fill material.

The modern technique was introduced by Vidal and earliest studied were dealt with retaining walls such as the work of Lee et al, AL-Hussainy and Perry and others. Then the advantage of reinforced earth as foundation material attracted many investigators

who studied the bearing capacity of reinforced earth slabs or subgrades, Binquet and Lee, Akinmusurg and Akinbolade.

Almost all types of sand and sandy soils have been successfully stabilized by the addition of bituminous materials like cutback emulsions or low viscosity straight run asphalt. Bituminous binders, when used as additive to non- plastic sand proved sufficient cohesion to develop resistance to displacements under wheel loads. The cementing process of sand – bitumen mixes is more effective when these are highly compacted at ambient temperature such stabilized and bitumen materials be used as sub-base or base courses for flexible pavements as studied by Singh et al (1979).

- DUNE SAND:

The sand dunes were obtained from the dunes area south of Iraq, between Nasria and Basrah with specific gravity of (2.69) and gray in color.

-GRAIN SIZE DISTURBUTION:

Fig. (1) gives the grain size distribution; it is mainly fine sand and has a sigmoid shape with a very well sorting.

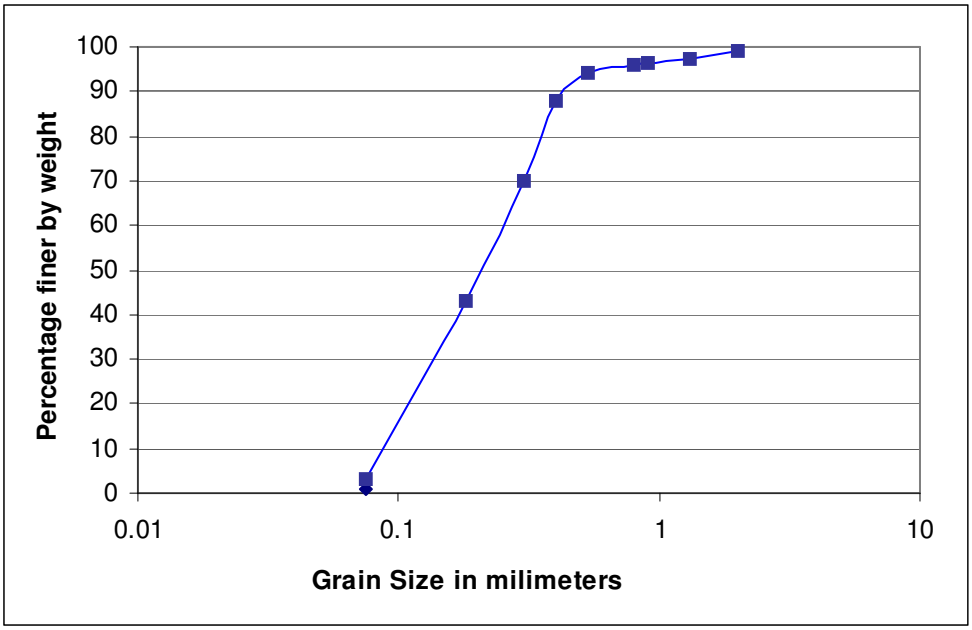

Fig (1). Grain size distribution of dune sand

-ATTERBERG LIMITS

Laboratory tests for liquid limit and plastic index determinations were conducted. The soil was found to be completely non- plastic in character.

-DRY DENSITY

The maximum dry density of the dune sand as determined is (1.7) gm/cm^3, while the minimum dry density was found to be (1.25) gm/cm$^{3.}$ The filling density used throughout the tests was (1.45) gm/cm^3 which gives a relative density of (51.9)%. The angle of internal friction of dune sand at this density is (29)$^\circ$ as determined from direct shear test.

-BITUMINOUS MATERIALS

The road paving bituminous materials, as asphalt cement (85/100), RC selected for stabilization, for various reasons including their commercial and availability in

large quantity and the ease of mixing with sand. These binders were tested according Iraqi standard specification.

REINFORCED TYPE:

The suggested type of reinforced used are fine metal wire mesh. The properties of this material are shown in table (1).

Table (1) properties of reinforcement used in the test

Type of reinforcement	Aperture size (mm)	Thickness (mm)	Tensile strength (kPa)
Fine wiremesh	1.7 x1.7	0.7	27.3

TEST PROCEDURE

STABILIZATION BY BITUMINOUS MATERIALS:

TEST PROCEDURE:

Marshall Stability or Hveen stabilometer tests are commonly used to determine stability of sands for sand bitumen mixes as mentioned by Klarkson (1965).

Sand dunes and the selected grade of bituminous materials were heated separately to (160 C°) and then mixed together in required proportion till a uniform color was obtained. Moulds of (4) cm in diameter (2.5) cm in height of Marshall stability apparatus were then prepared and tested at (60 C°). Different bituminous binders in percent age varying from (2) to (10) percent by weight of sand dunes were used.

. AGING AND CURING:

The half of specimens from each trial was subjected to aging in air at room temperature for (1), (7), and (15) days. The other half of sand – bitumen mix was subjected to curing in water for (1), (7), and (15) days. In both samples, A/C (85/100) and RC as a binder were used.

. IMPROVING BY REINFORCED TYPES:

The samples used in the triaxial tests were (38) mm in diameter and (76) mm in length. All the samples were prepared by pouring the sand inside the triaxial mold in three layers. Each layer was compacted (using wooden tamping rod) to the required density. The reinforcing layers placed at the specified spacing provided that the uppermost and lowermost of reinforcing layers are located at half of the spacing from the top and bottom of the sample.

The conventional triaxial testing techniques as suggested by Bishop and Henkle were used in the investigation. Also to study the improvement which could be obtained in adding fine soil passing #200? In the preparation of unreinforced and reinforced sand dune, different percentages of silt were added to the sand dune in order to investigate their effect on the strength of the reinforced soil. Table (2) is representing the main test program.

Table (2) Main test program

Series of tests	Type of reinforcement	No. of reinforcing layers (N)	Silt content %
1ST	Fine metal wiremesh	0,1,2,3	0
2nd	Fine metal wiremesh	0,2	10,25,50,60

The all round pressure (σ_3) was selected to be (100) kN/m^2 throughout the tests. A consolidated – Undrained Triaxial test were conducted. The rate of deformation was (0.6) mm/ min (chosen according to operation manual of W.Ferrance Company of Triaxial Test).

TEST RESULTS AND DISCUSSIONS:

Stabilization by bitumen:

The test results for marshal stability values for various sand- bitumen mixes tested reported in table (3) and represented graphically in figure (2), (3), (4), and (5).

A steady rise in the stability value is initially observed with increasing binder content up to an optimum binder content, beyond which it decrease. The fall in stability value is very sharp in the case of cutback (Rc). The maximum stability value is obtained at (8) percent for (A/C) (85/100) and (Rc), for one day aging (10.70 and 5.74 kN).

From the results it is also observed that (A/C 85/100) prove to be the best binder for (8) percent of sand- bitumen mixes.

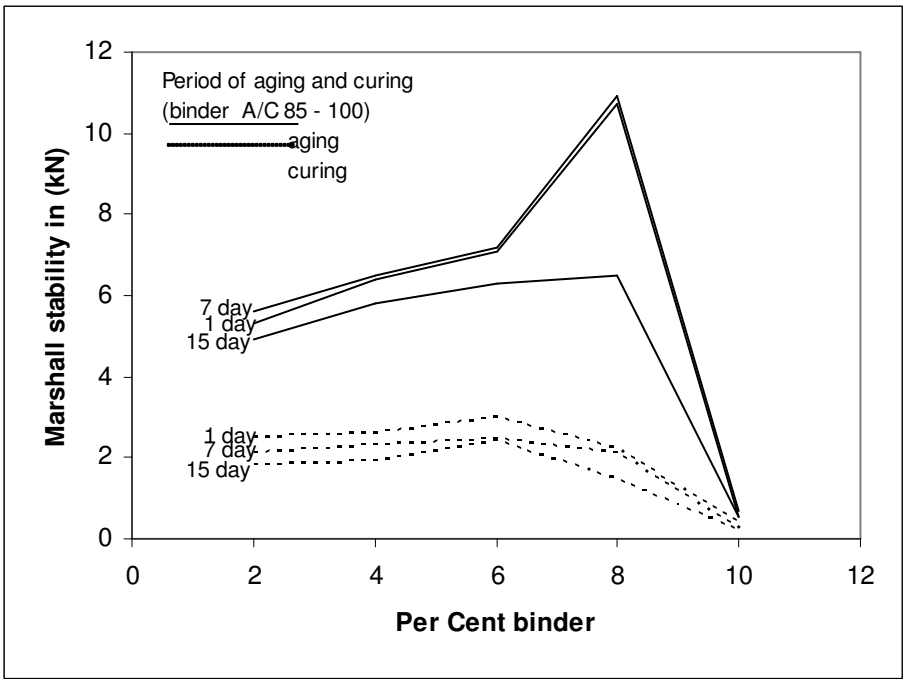

Fig (2). Marshall Stability vs. percent binder

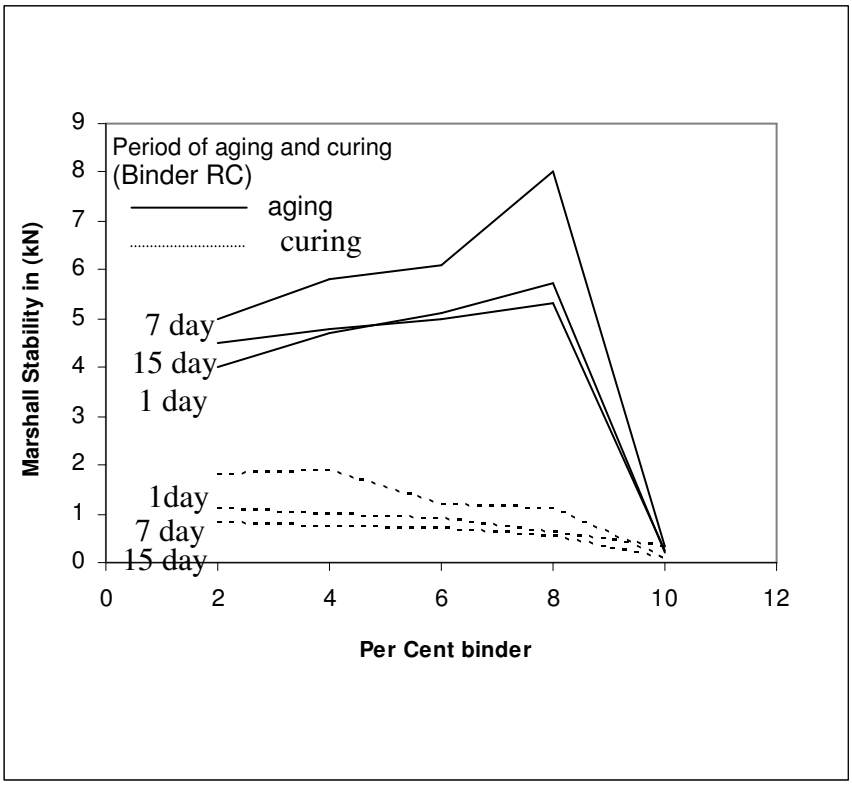

Fig (3). Marshall Stability vs. percent binder

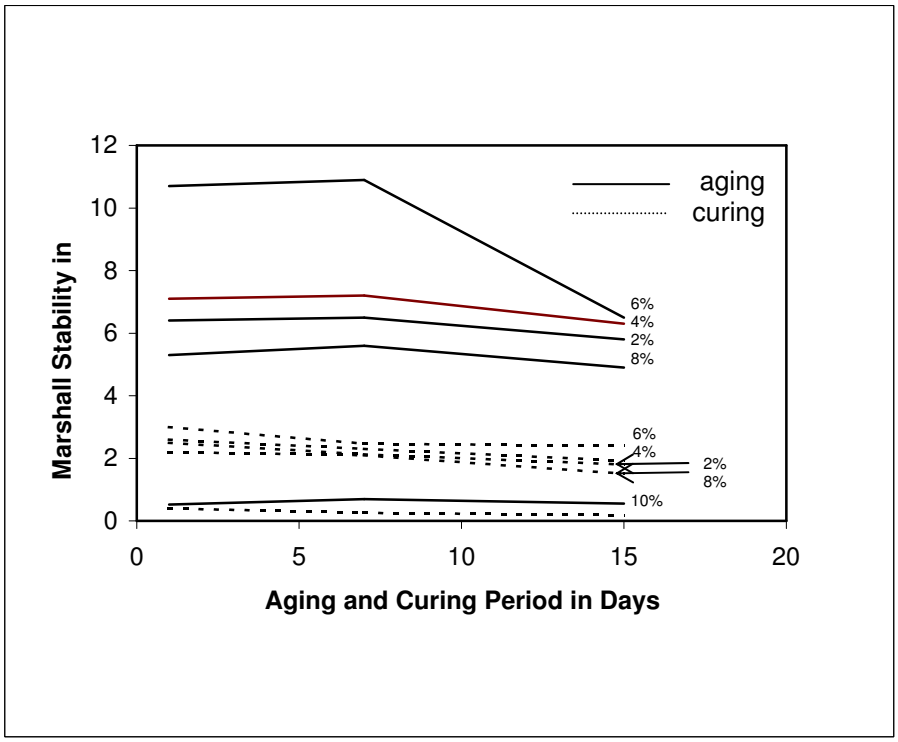

Fig (4). Marshall Stability vs. aging and curing of specimens (Binder A/C 85 – 100)

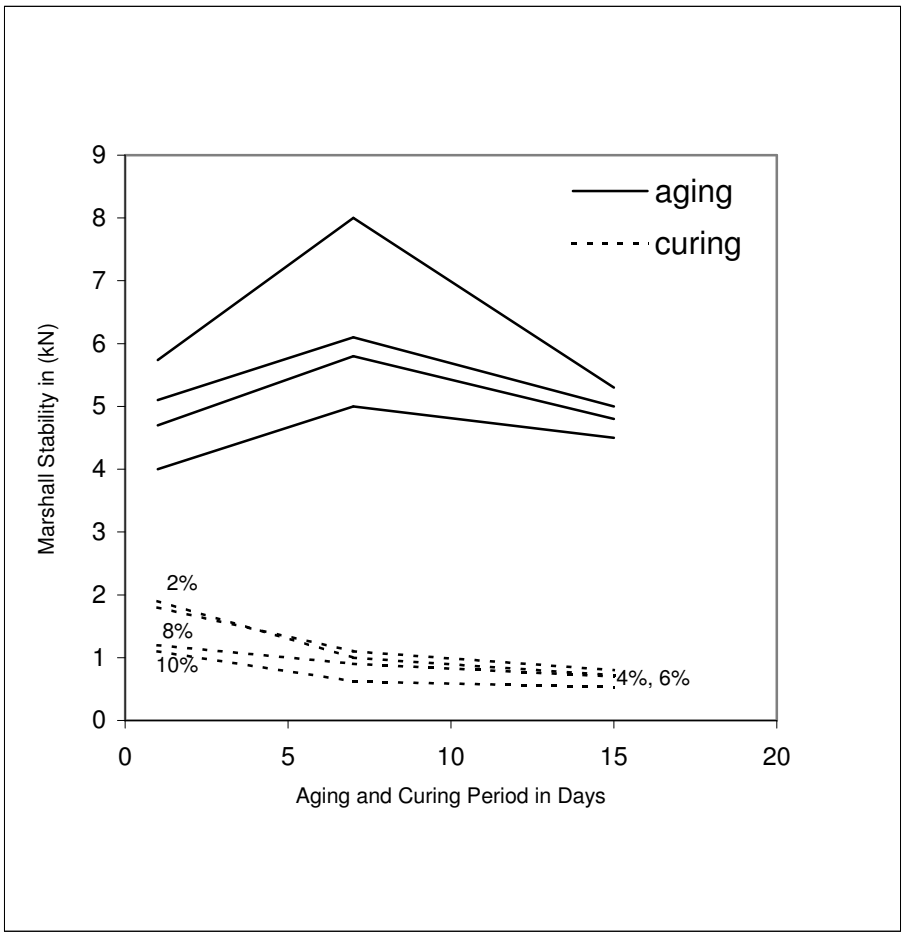

Fig (5). Marshall Stability vs. aging and curing of specimens (Binder R.C.)

Table (3) Effect of aging and curing Marshall stability (kN) 0f Sand-Bitumen at 60^0

Stabilize No.	Binder	% Binder	1Day aging and curing		7Day aging and curing		15Day aging and curing	
			aging	curing	aging	curing	aging	curing
1	A/C 85 - 100	Sand +2%Binder	5.30	2.50	5.60	2.13	4.90	1.80
2	A/C 85 - 100	Sand +4%Binder	6.40	2.60	6.50	2.30	5.80	1.92
3	A/C 85 - 100	Sand +6%Binder	7.10	3.00	7.20	2.47	6.30	2.40
4	A/C 85 - 100	Sand +8%Binder	10.7	2.20	10.9	2.10	6.50	1.50
5	A/C 85 - 100	Sand +10%Binder	0.52	0.40	0.70	0.26	0.55	0.18
6	RC	Sand +2%Binder	4.00	1.80	5.00	1.10	4.50	0.80
7	RC	Sand +4%Binder	4.70	1.90	5.80	1.00	4.80	0.72
8	RC	Sand +6%Binder	5.10	1.20	6.10	0.90	5.00	0.70
9	RC	Sand +8%Binder	5.74	1.10	8.00	0.62	5.30	0.53
10	RC	Sand +10%Binder	0.20	0.10	0.32	0.32	0.24	0.07

EFFECT OF AGING AND CURING ON STRENGTH:

Aging have been increased stability for (7) days for both binder (A/C) and (Rc) [figure (2), (3)], while the curing have been decreased stability for (7) and (15) days [Figure (4), (5)] and the results were tabulated in table (2). It could be noted that for both binder the stability value increases with increasing period of aging to (7) days and stability values begun to decrease after (7) days period. Sand- bitumen mixes having optimum binder contents have shown the least – improvement of strength.

Reinforcement OF Sand Dunes:

The relationships between stress- strain for dune sand and that provided with different layers of wire mesh reinforcement are plotted in fig. (6). It is obvious that the results of reinforced samples showed well-defined peak stress in contrary to the reinforced sand dunes, these results confirmed the results obtained by Al-Abdullah et al (1993), also it could be considered as identical with the failure criterion adopted by Akinmusuru and Akinbolade.

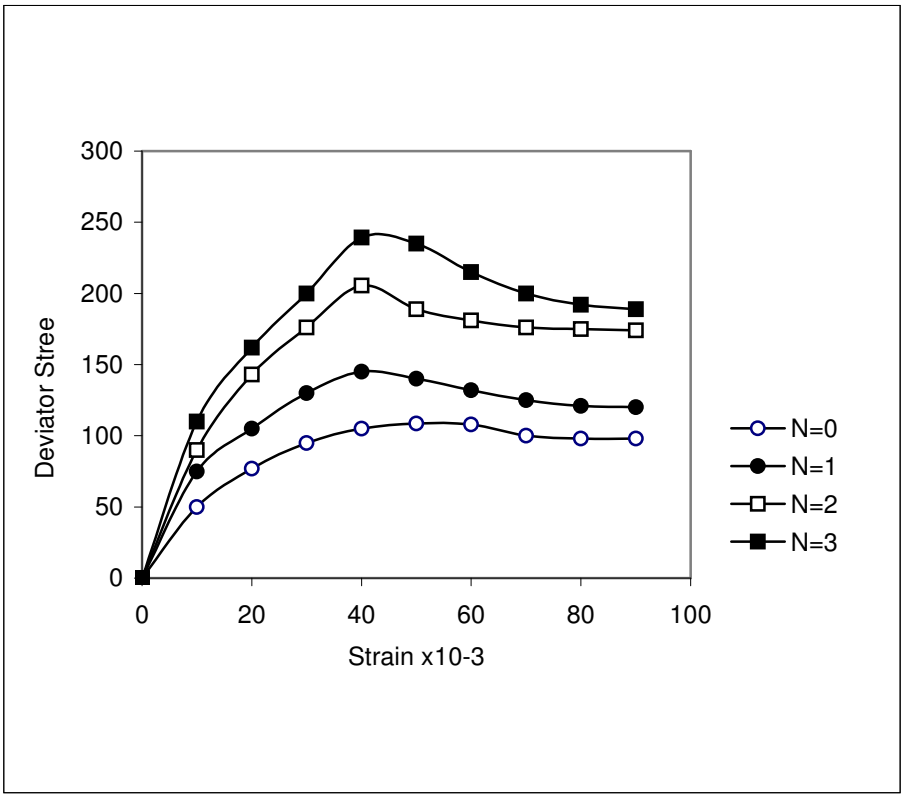

Fig (6). Stress-strain relationship of dune sand with different Layer of wire mesh reinforcement

The benefit of these results could be clearer if the results were expressed in term of Degree of Improvement (D.O.I.) which is the ratio of the peak deviator stress of reinforcement soil to the peak deviator stress of unreinforcement soil. It is clear that the deviator stress at failure increased with the increased of (D.O.I.), this also confirmed by AL-Omari (1989). The results shows that reinforcement of the three reinforcing layers (N=3) gave largest degree of improvement for silt content equal to (0)% as shown in Fig. (7). While the D.O.I. not much more than that for two reinforcing layers, these results could be attributed to the interaction between the soil particles and the wire mesh which helped to transmit the stress on a large area, much more that was from (N=3).

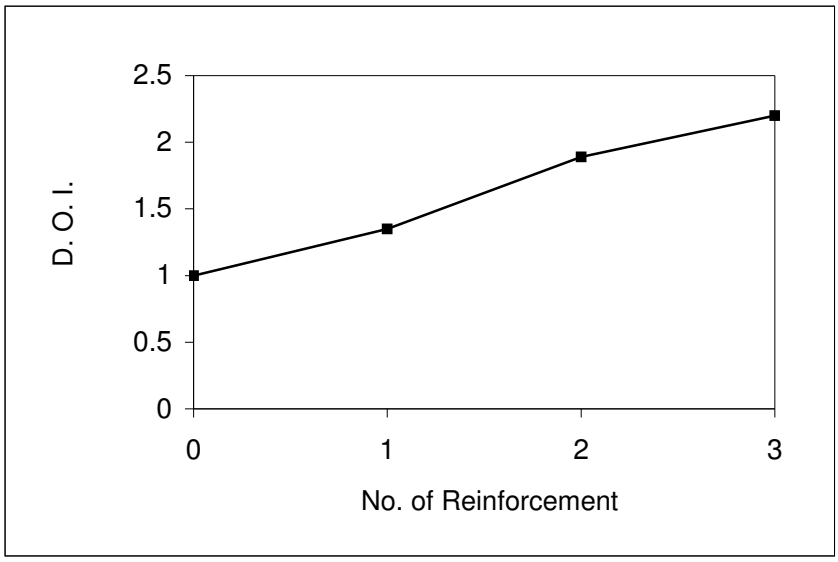

Fig (7). Degree of improvement against number of reinforcing layers (N)

The effect of adding variable percentage of silt (10, 25, 50, and 60)% on stress-strain relationship to the sand dunes could be shown in Fig. (8). Also the variation of peak deviator stress of unreinforced and reinforced for different percent of silt with degree of improvement were shown in table (4). The optimum silt content (that gives maximum deviator stress and degree of improvement) was found to be (25)% for unreinforced sand dunes.

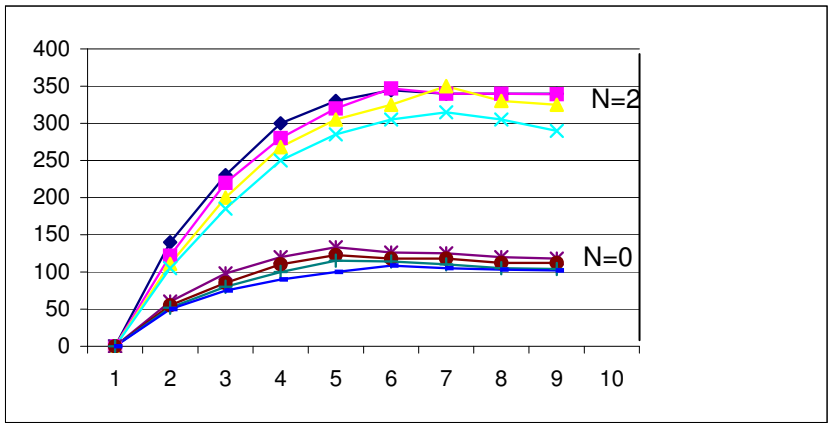

Fig (8). Stress-strain relationship of unreinforced and reinforced Dune sand with different percent of silt

They can be attributed to presence of fine particles surround the reinforcing in addition to the friction mobilized between the reinforcement and surrounding soil.

Table (4) Degree of improvement of dune Sand with different silt contents

Silt content %	Strength of non reinforced dune sand kPa	Strength of reinforced dune sand(N=2) kPa	D.O.I.
0	108.68	205.5	1.89
10	115.39	312.42	2.71
25	122.81	346.68	3.1
50	133.35	344.69	2.58
60	142.41	340.25	2.38

CONCULUSIONS:

From the basis of the last results and their discussions, the following conclusions are derived:

1. Sand dunes have no stability and could be not used for road construction purpose without stabilization and improvement and it could be improved by using fine wire mesh metal reinforcement.
2. Stability of stabilized sand dune increased as high as (10.70) kN when stabilized with bituminous materials.
3. Aging process for specimen increases the stability value over period of (7) days for both binders.
4. The degree of improvement shows an increase in shear strength at silt content of (25)% to the reinforced sand dunes.
5. Sand Dunes could be improved by using fine wire mesh metal reinforcement. The degree of improvement showed an increasing by addition of reinforcement and is proportional with the number of reinforcing lager.

REFERENCES:

1. AL-Azzawi, K. Y., AL-Abdullah, S.F. (1993) //Stabilization of dune sand with bituminous then user for highways in south of Iraq //, NCCL conference, 1st. Edition – Baghdad.
2. Akinmusuru, J., and Akinbolade, J. A. (1981) //Stability of loaded footing on reinforced soil// journal of Geot. Eng. Div. Proc. ASCE, Vol.107, No. GT6, pp. (819-828).
3. Al-Hussainy, M. and Perry, E.B. (1978) // Field Experiment of reinforced Earth wall //, Proc. ASCE Spring convention and Exhibition, Pittsburgh Pennsylvania, reprint No. 3131.
4. AL-Abdullah, S.F., Al-Ashou, M. O., and Salih, S.M. (1993) // Triaxial strength of reinforced soil //, Mutah Journal for research and studies Vol.7, No.3.pp. (209-222).
5. Al-Omari, R. R, Al-Doobassi, H.H., Nazhat, Y.N., and Al-Wadaad, B. A. (1989) // Shear strength of Geomesh reinforced clay// Geotextiles and Geomembarance Vol.8.
6. Binquet, J., and Lee K. (1975) // Bearing Capacity Tests on Reinforced Earth slabs//, J. O. Geot. Eng. –Div., Vol.101, No. GT12, pp. (1241 – 12852).
7. Bishop, A.W. and Henkel, D. J. (1962) // The Measurement of Soil Properties in Triaxial Test // Edward Arnold Ltd. London, 2nd edition.
8. Lame, T. W. and Whitman, R. V. //Soil mechanics//, John Wiley and Sons, New York, 1969.
9. Lee, K.L., Adams B. D., and Vagneron, J.M.J (1973) // Reinforced Earth Retaining Walls //.J. O. soil Mech., ASCE, SM 10.PP. (747-763).

10. Sing Alan, Nag., C.P. and Joshi, S.M.// Stabilization of Dune Sand With Bitumen//, Indian Highway, 1979.
11. // Standard Specification for Road and Bridge //, Republic of Iraq, Ministry of Housing and Construction, State Organization of Roads and Bridges.
12. Vidal H, (1969)// The principle of Reinforced Earth //, Thoroughfare Res., Rec., No.282, pp. (1-6).

AN IMPROVED NEWTON METHOD FOR RADIAL DISTRIBUTION SYSTEM LOAD ANALYSIS

Asst. Professor Hassan A. Kubba
Electrical Engineering Department
Baghdad University

ABSTRACT:

This paper presents a modified Newton method of load flow analysis for radial distribution systems. It is derived with the Jacobian matrix is in $\mathbf{UDU^T}$ form, where **U** is a constant upper triangular matrix depending solely on system topology and **D** is a block diagonal matrix. With this formulation, the conventional steps of forming the Jacobian matrix, LU factorization and forward/back substitution are replaced by back/forward sweeps on radial feeders with equivalent impedances. The method has advantages over Newton' s method in terms of speed of solution (no. of iterations), and reliability of convergence by inserting a minimization technique (Cubic Interpolation Technique). The algorithm exhibits a control of the convergence. As such the method converges for cases when conventional Newton' s method and some other popular methods diverge. Two large distribution systems of 490 nodes and 722 nodes with different r/x ratio in line impedance are used to examine the performance of the method. These tests have shown that the proposed method is as robust and efficient as the forward/back sweep method. The proposed method can be extended to the solution of three phase unbalanced representation.

الخلاصة:

يقدم البحث طريقة نيوتن-رفسن مطورة لتحليل انسيابية الاحمال الكهربائية لانظمة التوزيع الشعاعية. الطريقة المقترحة في البحث اعتمدت على ان مصفوفة الجاكوبين تكون بشكل (UDU^T) حيث ان مصفوفة [U] تمثل مصفوفة مثلثية علوية ثابتة تعتمد على طوباغرافية المنظومة بينما مصفوفة [D] تمثل مصفوفة قطرية. من خلال هذه الصيغة، فان الطريقة التقليدية لاعداد مصفوفة الجاكوبين وهي طريقة التحليل العلوي-السفلي (LU) والتعويض (forward/back) قد استبدلت بطريقة (back/forward sweeps) على المغذ يات الشعاعية بممانعات مكافئة.

الطريقة المقترحة في البحث لها افضلية وفوائد على طريقة نيوتن-رفسن التقليد ية في عدة معايير وهي سرعة الوصول الى الحل (عدد العمليات التكرارية), ووثوقية الوصول الى الحل من خلال استخدام تقنية التضئيل واستخدام عامل التصحيح (α) . ان خوارزمية الطريقة المقترحة تقدم سيطرة على عملية الوصول الى الحل الموثوق لانظمة مختلفة التعقيد بينما طريقة نيوتن-رفسن التقليد ية وطرق اخرى شائعة تفشل في الوصول الى الحل.

استخدم نظامان كبيران لتوزيع الطاقة الكهربائية وهما (490 عقدة و 722 عقدة) ذو نسب مختلفة مقاومة/محاثة لخطوط التوزيع لتقييم اداء الطريقة المقترحة. الدراسة اظهرت قوة وكفاءة الطريقة المقترحة في البحث, كما يمكن استخدامها في انظمة احادية الطور وانظمة ثلاثية الاطوار غير المتوازنة.

KEYWORDS

Load Flow, Radial Distribution System, Newton's Method, Cubic Interpolation Technique.

INTRODUCTION:

A load flow study involves the determination of voltages, currents, powers, and losses at various points in an electrical network under existing or contemplated condition of normal operation, subject to the regulating capability of generators, condensers, and tap changing under load transformers as well as specified net interchange between individual operating systems. In 1967, Tinney and Hart developed the Newton based power flow solution method [1]. Later work by Stott and Alsac [2] made the fast decoupled Newton method as well as its alternatives; a standard methods for load flow studies.

The Fast decoupled Newton method works well for transmission systems, though, its convergence performance is poor for most distribution systems due to their high r/x ratio which deteriorates the diagonal dominance of the Jacobian matrix. For this reason several non-Newton type methods have been proposed [3-5]. Their algorithms all consist of back/forward sweeps on a ladder system. The formulation and the algorithm of these methods are different from the Newton's power flow method, which makes these methods hard to be extended to other applications, such as the state estimation and the optimal power flow, in which the Newton method seems more appropriate.

Recently, a fast decoupled load flow method has been proposed in [6]. This method orders the laterals instead of busses into layers, thus reduces the problem size to the number of laterals, and then assumes initial end voltage for all laterals. The iteration starts from the first lateral using the method proposed in [4]. The voltage mismatch obtained from this lateral is applied to correct not only the end voltage of this lateral but also the end voltage of laterals of the next layer. The algorithm converges when all voltage mismatches are within a certain tolerance. Using lateral variables instead of bus variables makes this method efficient for a given system topology, but it may add some overhead if the system topology is changed regularly, which is common in distribution systems due to switching operations.

The purpose of this paper is to derive a modified Newton method for radial distribution systems without reducing the problem size, yet, capable of achieving robust convergence and high efficiency by inserting an accelerating and controlling factor using the cubic interpolation technique[7]. Specifically, this paper aim to derive a Newton algorithm in which the Jacobian matrix is in ($\mathbf{UDU^T}$) form, where **U** is a constant upper triangular matrix depending solely on system topology and **D** is a block diagonal matrix resulting from the radial structure and special properties of the distribution system. With this formulation, the conventional Newton algorithm of forming the Jacobian matrix, **LU** factorization and forward /back substitution can be replaced by back/forward sweeps on radial feeders with equivalent impedances. To assist in presenting the main difference between the proposed method and other methods, the following definitions are used:

(i) Conventional Newton method: a method in which the partial derivative of the power flow equation, i.e., the Jacobian matrix elements are used to determine the search direction, and forward/back substitutions on the **LU** factors of the Jacobian matrix are used to calculate the incremental correction of the state variables.

(ii) Back/forward sweep method: a method in which the derivative of the power flow equation is not used, instead, basic circuit laws, i.e. Ohm' s law, KVL, and KCL (or the generalized KCL for power summation) are used as basis for back/forward sweeps on a radial network to calculate the incremental correction of the state variables.

(iii) Improved Newton method: the proposed method in which an approximate Jacobian matrix in $\mathbf{UDU^T}$ form is used to determine the sereach direction, the linearized power flow equation based on this Jacobian matrix is used as basis for back/forward sweeps on a radial network to calculate the incremental correction of the state variables.

By means of cubic interpolation minimization technique, the algorithm exhibits an accelerating factor (α) to control the convergence process.

BASIC CIRCUIT THEORY IN DISTRIBUTION SYSTEMS[8]:

For a linear, time invariant RLC circuit with a sinusoidal voltage source, the basic circuit theory can be expressed as (see Appendix I for details):

Ohm's law: $I_b = Y_b V_b$ (1)

KCL: $A I_b = I_n$ (2)

KVL: $b V_b = 0$ (3)

For fundamental frequency power flow calculations, a distribution system is always modeled as a linear, time-invariant RLC circuit. Earth is always treated as a reference node. For a radial distribution system with (n) nodes and without shunt branches, the number of branches is (n-1). Therefore, the dimension of matrix A is nx(n-1).

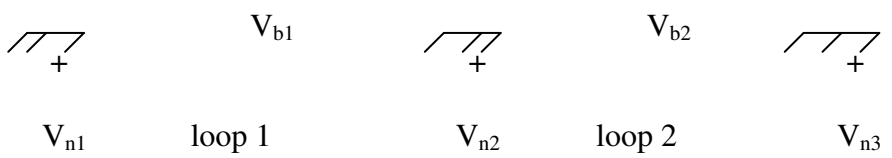

Fig (1)

The independent loop for radial distribution systems can always be formed by a branch with its two shunt branches. Since shunt branches are usually neglected in modeling distribution lines, a fictitious shunt branch can be placed with branch voltage to be the nodal voltage as shown in Figure (1), and eqn.(3) can be written as:

$$V_b = A^T V_n \quad (4)$$

Combining eqn's (1), (2), and (4), we have:

$$A\, Y_b\, A^T V_n = I_n \quad (5)$$

By knowing the nodal voltage at one node, assuming it is the first node(slack bus "s") for convenience, and nodal current injections at the other (n-1) nodes, eqn. (6) can be derived from eqn. (5) for solving the remaining (n-1) unknown nodal voltages:

$$A_{n-1}\, Y_b\, (A_s^T\, A_{n-1}^T) \begin{bmatrix} V_s \\ V_{n-1} \end{bmatrix} = I_{n-1} \quad (6)$$

where $A = \begin{bmatrix} A_s \\ A_{n-1} \end{bmatrix}$, $V_n = \begin{bmatrix} V_s \\ V_{n-1} \end{bmatrix}$, and $I_n = \begin{bmatrix} I_s \\ I_{n-1} \end{bmatrix}$

Note matrix A_{n-1} is a square matrix. Since every branch is always directed away from one node and towards the other node, we have:

$$A^T e_n = 0 \quad (7a)$$

or

$$A_s^T + A_{n-1}^T e_{n-1} = 0 \quad (7b)$$

where e_n and e_{n-1} are unity column vectors with dimensions n and n-1 respectively. Hence, eqn. (6) can be simplified as:

$$A_{n-1} Y_b A_{n-1}^T (V_{n-1} - V_s e_{n-1}) = I_{n-1} \quad (8)$$

$A_{n-1} Y_b A_{n-1}^T$ is the Nodal Admittance Matrix. In other words, for a radial system without shunt branches, the nodal admittance matrix is formed as the product of three square matrices. If we organize eqn. (8) as follows:

$$A_{n-1} I_L = I_{n-1} \quad (8a)$$

$$Y_b A_{n-1}^T (V_{n-1} - V_s e_{n-1}) = I_L \quad (8b)$$

Solving for I_L from (8a) is equivalent to the "Backward sweep", and solving for V_{n-1} from (8b) is equivalent to the "Forward sweep". This observation is very important as it motivated us to derive a Jacobian matrix in UDU^T form and a back/forward sweep algorithm for the Newton method.

THE IMPROVED NEWTON METHOD:

Under the following assumptions:

Small voltage difference between two adjacent nodes, no shunt branches, the Jacobian matrix for a radial system is formed as UDU^T, where U is a constant upper triangular matrix depending solely on system topology and D is a block diagonal matrix. The first assumption above is valid, since typical distribution lines are short and power flows are not high. The second assumption is not valid if there exist shunt capacitor banks, constant impedance loads, as well as non-negligible shunt admittance of distribution line models (π-model). However, all the shunt branches can be converted to node power injections using initial and updated node voltages. In the conventional Newton method[7,9,10], the power flow problem is to solve eqn.(9) for $\Delta\theta$ and ΔV :

$$\begin{matrix} H & N & \Delta\theta & \Delta P \\ J & L & \Delta V/V & \Delta Q \end{matrix} \quad (9)$$

where

$$H_{km} = -V_k V_m (G_{km}\sin\theta_{km} - B_{km}\cos\theta_{km}) \qquad m = k \quad (10)$$

$$H_{kk} = V_k \Sigma V_m (G_{km}\sin\theta_{km} - B_{km}\cos\theta_{km}) \qquad m=1,..n \ ,m\neq k \quad (11)$$

$$N_{km} = -V_k V_m (G_{km}\cos\theta_{km} + B_{km}\sin\theta_{km}) \qquad m = k \quad (12)$$

$$N_{km} = -V_k \Sigma V_m (G_{km}\cos\theta_{km} + B_{km}\sin\theta_{km}) - 2V_k^2 G_{kk} \qquad m=1,..n \ ,m\neq k \quad (13)$$

$$j_{km} = V_k V_m (G_{km}\cos\theta_{km} + B_{km}\sin\theta_{km}) \qquad m = k \qquad (14)$$

$$j_{kk} = -V_k \Sigma V_m (G_{km}\cos\theta_{km} + B_{km}\sin\theta_{km}) \qquad m=1,..n \ ,m\neq k \qquad (15)$$

$$L_{km} = -V_k V_m (G_{km}\sin\theta_{km} - B_{km}\cos\theta_{km}) \qquad m = k \qquad (16)$$

$$L_{kk} = -V_k \Sigma V_m (G_{km}\sin\theta_{km} - B_{km}\cos\theta_{km}) + 2V_k^2 B_{kk} \qquad m=1,..n \ ,m\neq k \qquad (17)$$

$G_{km} + jB_{km}$ is the entry of nodal admittance matrix. Since the voltage difference between two adjacent nodes is small as well as: $G_{kk}+jB_{kk} = -\Sigma (G_{km}+jB_{km})$,

for systems without shunt branches, the Jacobian matrix can be approximated as:

$$H_{km} = V_k V_m B_{km} \cos\theta_{km} \qquad m \neq k \qquad (18)$$

$$H_{kk} = -V_k \Sigma V_m B_{km} \cos\theta_{km} \qquad m=1,..n \ ,m\neq k \qquad (19)$$

$$N_{km} = -V_k V_m G_{km} \cos\theta_{km} \qquad m \neq k \qquad (20)$$

$$N_{kk} = V_k \Sigma V_m G_{km} \cos\theta_{km} \qquad m=1,..n \ ,m\neq k \qquad (21)$$

$$j_{km} = V_k V_m G_{km} \cos\theta_{km} \qquad m = k \qquad (22)$$

$$j_{kk} = -V_k \Sigma V_m G_{km} \cos\theta_{km} \qquad m=1,..n \ ,m\neq k \qquad (23)$$

$$L_{km} = V_k V_m B_{km} \cos\theta_{km} \qquad m \neq k \tag{24}$$

$$L_{kk} = - V_k \Sigma V_m B_{km} \cos\theta_{km} \qquad m=1,..n \ ,m\neq k \tag{25}$$

Equations (18) to (25) shows thath matrices H, N, j, L all have the same properties (symmetry, sparsity pattern) as those of the nodal admittance matrix, hence they can be formed as:

$$H = L = A_{n-1} D_B A_{n-1}^T \tag{26}$$

$$j = -N = A_{n-1} D_G A_{n-1}^T \tag{27}$$

where D_B, and D_G are diagonal matrices with diagonal entries to be $V_k V_m B_{km} \cos\theta_{km}$ and $V_k V_m G_{km} \cos\theta_{km}$ respectively. Therefore eqn. (9) can be rewritten as:

$$\begin{matrix} A_{n-1} & D_B & -D_G & A_{n-1}^T & \Delta\theta & \Delta P \\ A_{n-1} & D_G & D_B & A_{n-1}^T & \Delta V/V & \Delta Q \end{matrix} \tag{28}$$

It is also noted that if nodes and branches are ordered properly, A_{n-1} is an upper triangular matrix with all diagonal entries to be 1 and all non-zero off- diagonal entries to be -1. One way to achieve such an A_{n-1} is ordering branches by layers away from the root node (source bus)[3]. This ordering scheme is adopted here. The direction of each branch is towards the root node. The node ordering is proceeded simultaneously with the branch ordering. The branch "from side" node number is the same as the branch number, as illustrated in Fig (2). The node to branch incidence matrix of Fig (2) is given in eqn. (29).

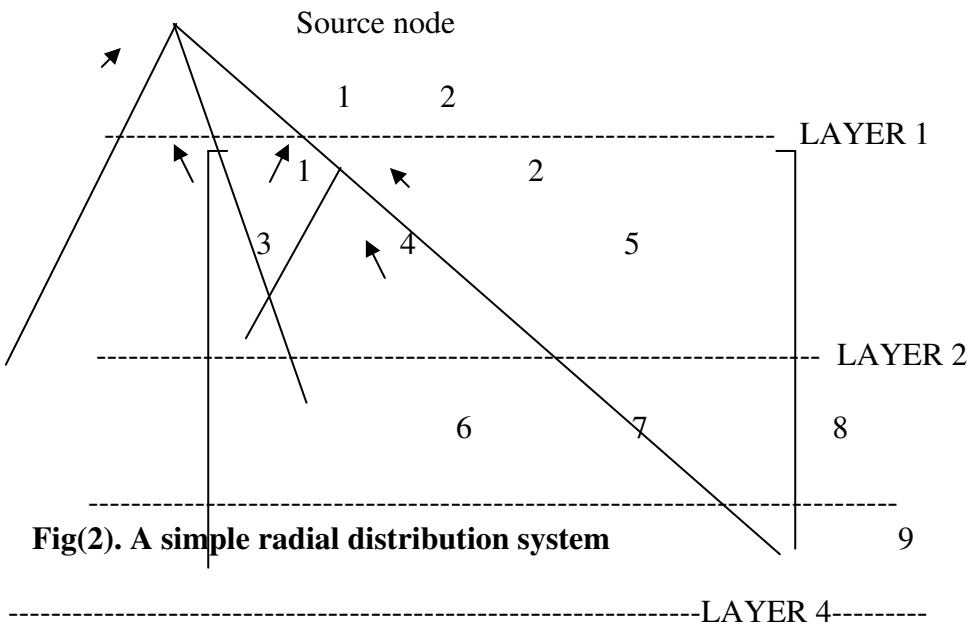

Fig(2). A simple radial distribution system

By now we have shown that the Jacobian matrix can be formed as the product of three square matrices eqn. (28), same as the nodal admittance matrix in eqn. (8). Next, we will show that eqn. (28) can be solved by back/forward sweeps as well. Let 's define:

$$E = \Delta\theta + j\,\Delta V/V \quad (30)$$

$$S = \Delta P + j\,\Delta Q \quad (31)$$

$$W = D_B + j\,D_G \quad (32)$$

then eqn. (28) can be written as:

$$W\,A_{n-1}^{T}\,E = S \quad (33)$$

$$A_{n-1}\,S_L = S \quad (34)$$

or:

$$W\,A_{n-1}^{T}\,E = S_L \quad (35)$$

Where eqn. (34) is the back sweep, the diagonal matrix W can be inverted for each line. The diagonal in W^{-1} is denoted as the equivalent line impedance:

$$Z_{eq} = R_{eq} + jX_{eq} \quad (36)$$

Where $R_{eq} = X_{km}/(V_k V_m \cos\theta_{km})$ (37)

$X_{eq} = R_{km}/(V_k V_m \cos\theta_{km})$ (38)

R_{km} and X_{km} are resistance and reactance of line k-m respectively. Note that matrix A_{n-1} of non-zero entries are either -1 or 1

4. CUBIC INTERPOLATION TECHNIQUE [7,9,10] :

It is well-known that the load flow calculation can be regarded as a nonlinear programming problem [7] , [9] , which determines the direction and magnitude of the solution so that a certain function F(x) may be minimized. The F(x) is the squares of the active and reactive mismatch power. By employing this formulation, the valuable property can be obtained that the solution never diverges. The value of the function F(x) becomes eventually zero if there is a solution from the initial estimate, and stays at a positive value if no solution exists. In nonlinear programming approach (Fletcher-Powell method), (Δx) is modified by a correction factor (α) which can be considered as an acceleration factor. The computation of (α)is made such that F(x) is minimized F(x). The function to be minimized is

$$F(V,\theta) = \sum_{k \in PQ,PV}^{n} \Delta P_k^2 + \sum_{k \in PQ}^{n} \Delta Q_k^2 \quad (39)$$

The minimization of F(x) with respect to (α) in the direction of (Δx) is a one-dimensional problem. The object is to determine the correction factor (α) given (Δx) and the point (x). The problem can be stated as that of finding a value of (α) that will minimize :

$$Z(\alpha) = F(x_o + \alpha \ \Delta x) \tag{40}$$

And therefore the derivative of (Z) with respect to (x) is :

$$Z'(\alpha) = 2 \sum f(y) \frac{\partial f(y)}{\partial y} \Delta x \tag{41}$$

Where ;

$Y = x_o + \alpha \ \Delta x$

A cubic interpolation technique is used to find (x) as follows :

1) A step "a" is chosen as :

$$a = \min (1, -2 (F_x - F_o)/z'_x) \tag{42}$$

Where (F_o) is an estimate of (F) at the problem optimum, (Fx) is the value of function (F) at point (X), and (Z_x') is the derivative of (Z) with respect to (X) evaluated at point (X).

2) A step of size (a) is taken to arrive at point (y), $y = X + \alpha \ \Delta X$, and (Z_y') is evaluated to determine whether a change of sign has occurred with respect to (Z_x'). Such a change of sign, from negative (Z_x') to positive (Z_y') would indicate that the minimum is enclosed within these two points . If there is no change of sign, successive steps of size (a) are taken until two adjacent points that enclose the minimum are found. Let these two adjacent point be called (w) and (y) which are located at distances (α_w) and (α_y) from the original point (x).

3) The distance (α) from (x) to the minimum point is :

$$\alpha = \alpha y - \frac{(\propto y - \propto w)(Zy' + r - s)}{Zy' - Zw' + 2r} \tag{43}$$

Where ;

$$r = (s^2 - Z_w' \, Z_y')^{1/2} \tag{44}$$

And $s = 3 \dfrac{(Z_w - Z_y)}{(\alpha_y - \alpha_w)} + Zw' + Zy'$

4) The point ($x_o + \alpha\Delta x$) is accepted as the minimum point if the function $F(x_o + \alpha\Delta x) = Z(x)$ is smaller than both (Z_w) and (Z_y). If this is not true, the interpolation is repeated using the point ($x_o + \alpha \ \Delta x$) and either (w) or (y), chosen so that the minimum is enclosed.

This decision is based on the sign of Z'(α). The cubic interpolation process is shown in fig (3).

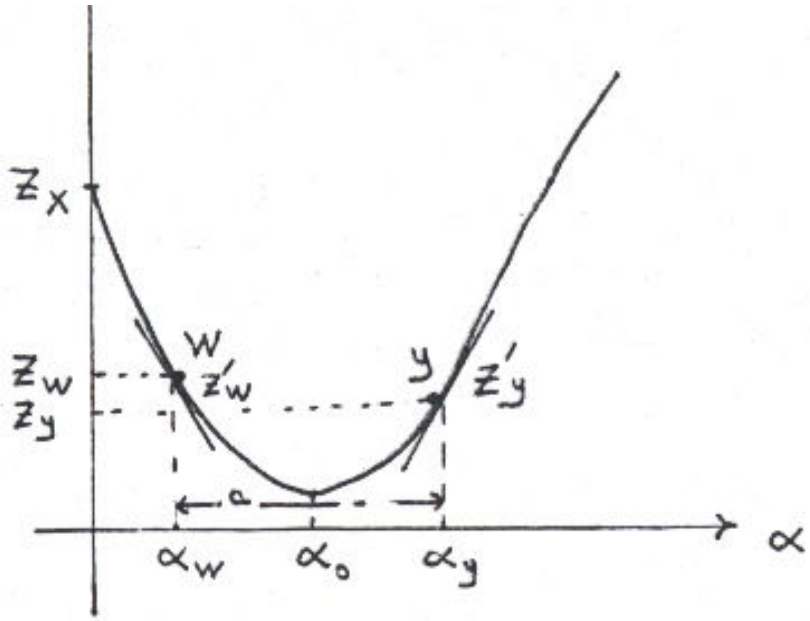

Fig.(3) Cubic interpolation to minimize F(x) with respect to (α) in the direction of (Δx)

The interpolation process can be simply implemented in Newton's program. Equation (41) must be evaluated for several values of (α).

When $\alpha = 0$,

$$f(y) = f(x) \tag{45}$$

and

$$\frac{\partial f(y)}{\partial y} = \frac{\partial f(x)}{\partial x} \tag{46}$$

Therefore ;

$$2\sum f(y)\frac{\partial f(y)}{\partial y}\Delta X = 2\sum f(x)\frac{\partial f(x)}{\partial x}\Delta X \tag{47}$$

from the equation $f(x) = -J\ \Delta x$

∴ Equation (46) becomes :

$$Z'(0) = -2\sum f(x)^2 = -2\,F(x) \tag{48}$$

The minus sign of equation (47) shows the direction of minimization (Δx) always points in a direction which reduces F(x) that the terms f(x), which represent the power mismatches , are calculated from the Newton algorithm, the optimum (α) and the new point ($x_1 = x_o + \alpha\,\Delta x$) is used for the start of the next iteration. The additional requirement

of this method is the re-evaluation of the Jacobian matrix which is small, using sparsity techniques. There is no need for extra Gauss – Eliminations and back substitutions, just addition evaluation of the Jacobian.

An algorithm based on eqns. (34), (35) and finding the optimal correction factor (α) following the cubic inlerpolation technique has been developed. Figure (4) is the flow chart of the proposed algorithm. The matrix A_{n-1} has never been formed in the program since its non-zero entries are either -1 or 1.

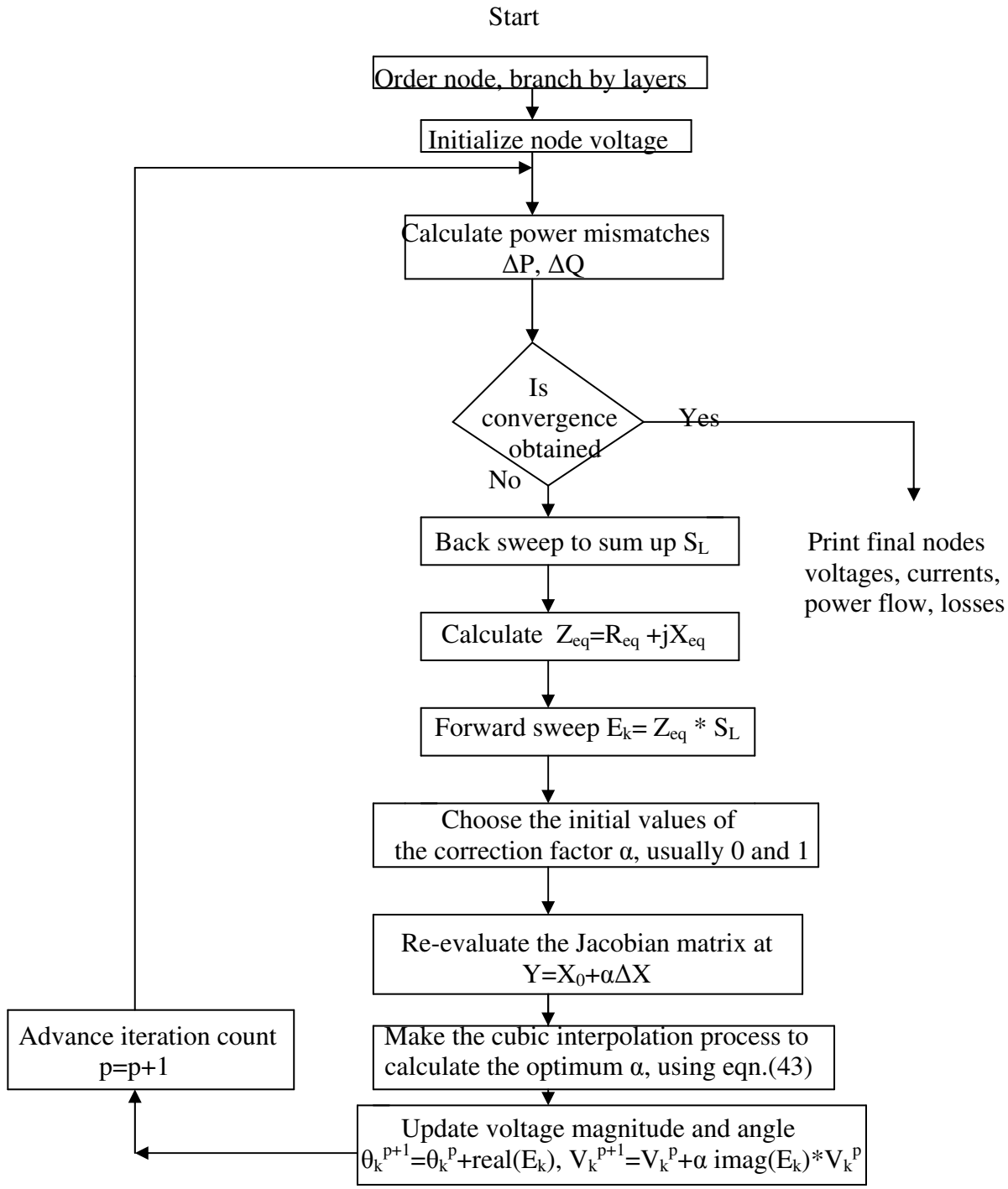

Fig(4) Flow chart of the proposed algorithm

5. ANALYSIS BASED ON NUMERICAL EXAMPLES:

A 490-node and 722--node typical distribution systems of various sizes taken the pacific Gas and Electric distribution system[5]. Both capacitors and regulators are included in the test systems, but the automatic controls for switching capacitors on/off, and the automatic tap adjustment function for regulators are not modeled in the test. All the loads are modeled as lumped constant power load. Table (1) lists the attributes of these test systems. It is seen that the two test systems have wide range of r/x ratio and line impedance.

Table(1) Attributes of Test systems

Test system	No. of nodes	Voltage level (Kv)	r/x ratio		$\lvert Z_{km} \rvert$ Ω	
			Max	Min	Max	Min
1	490	12	5.06	0.15	3.07	0.0012
2	722	12	5.06	0.26	2.43	0.0004

Table(2) shows that the load flow problem was solved by back/forward sweep conventional Newton's method in 4 iterations to an accuracy of 10^{-4} for each individual power mismatch (ΔP_k, ΔQ_k). In the proposed method 3 iterations were required with the same accuracy. The values of optimum (α) obtained for each iteration in the proposed method were close to one. My experience has shown that optimum (α) is either close to 1 or very close to 0. The cubic interpolation formula will produce an appropriate value of (α) even in the case where the optimum is near, but outside the interpolating limits. So optimum (α) may sometimes be slightly greater than one. If the interpolation is performed between zero and one, the correction (α) value would determined for all cases without any extra Jacobian calculation per iteration, thus saving computation time. From table (2), it is seen that the proposed method is as robust as the back/forward sweep method. All the cases tested have reached convergence regardless the wide range of r/x ratio and line impedance. The principal value of the proposed method lies in the control of the convergence process for both weakly Meshed networks and data error cases, whereas using the conventional Newton's method alone during the iterations of a load flow problem may result in poor solution or divergence.

Table (2) Comparison of the proposed method with back/forward sweep method with the value of optimum (α).

Test system of distribution sys.	No. of iterations Back/Forward sweep method	No. of iterations Proposed method	Optimum α/iteration Proposed method			
			1	2	3	4
Test sys. 1	4	3	1.02	1.01	1.001	
Test sys. 2	5	4	0.995	1.01	1.01	1.001

Table (3) Convergence pattern (power mismatches at each iteration) of the proposed method and the back/forward sweep method.

Iteration		Test sys. 1		Test sys. 2	
		Proposed	B/F sweep	Proposed	B/F sweep
1	ΔP_k	0.30000561	0.30000561	0.14006200	0.14006200
	ΔQ_k	0.14322091	0.14322091	0.05244800	0.05244800
2	ΔP_k	0.00989422	0.00643219	0.01709456	0.00982138
	ΔQ_k	0.00149278	0.01113158	0.01512962	0.02180936
3	ΔP_k	0.00009821	0.00057982	0.00012252	0.00415140
	ΔQ_k	0.00002741	0.00027818	0.00011821	0.00148164
4	ΔP_k		0.00001753	0.00004853	0.00034887
	ΔQ_k		0.00003554	0.00003041	0.00077424
5	ΔP_k				0.00015501
	ΔQ_k				0.00005526

Note: All algorithms programs were executed using MATLAB 5.3 .

CONCLUSIONS:

This paper presents an improved Newton method for solving the load flow problem of radial distribution systems. The derivation of this method has revealed that under certain assumptions, the Jacobian matrix of a radial system can be formed as UDU^T , with identical topology to that of the nodal admittance matrix. The attractive characteristic of such a Jacobian matrix is to allow a back/forward iteration algorithm instead of the conventional LU factorization. Thus, the proposed method is more reliable in convergence with ill-conditioned radial distribution systems. Also, a more rapid convergence and a non-divergent characteristic for both well-conditioned and ill-conditioned systems by using the optimum correction factor (α) through the cubic interpolation technique. Tests of the proposed method on large distribution feeders have shown that it is as robust and efficient as the back/forward sweep method.

References:

[1] W.F. Tinney and C. E. Hart, "Power Flow solution by Newton's method", IEEE Trans. Power App. System, Vol.PAS-86, Nov. 1967, pp. 1449-1460.

[2] B. Stott and O. Alsac, "Fast Decoupled Load Flow", IEEE Trans. Power App. System, Vol.PAS-93, May-June 1974, pp. 859-869.

[3] D. Shirmohammadi, H.W. Hang, A.semlyen, and G. X. Luo, "A compensation-based power flow method for weakly Meshed distribution networks", IEEE Trans. on power systems, Vol.3,No.2, May 1988, pp. 753-762.

[4] G. X. Luo and A. Semlyen, "Efficient load flow for large weakly meshed networks", IEEE Trans. on power systems, Vol.5, No.4, Nov. 1990, pp. 1309-1316.

[5] C. S. Cheng and D. Shirmohammadi, "A three-phase power flow method for real-time distribution system analysis", IEEE Trans. on power systems, Vol.10, No.2, May 1995, pp. 671-679.

[6] R. D. Zimmerman and H. D. Chiang,"Fast decoupled power flow for unbalanced radial distribution system", 1995, IEEE PES Winter meeting, New York, Paper No. 95 WM 219-6 PWRS.

[7] H. A. Kubba, "A rapid and more reliable load flow solution method for ill-conditioned power system", Eng. And Technology. Vol.17, No.5, 1998, pp. 550-568.

[8] H. N. Dhar, "Computer aided power system operation and analysis", 1982, McGraw-Hill company.

[9] H. A. Kubba, "An efficient and more reliable second order load flow solution method", Fifth-scientific meeting, 25-27 Feb. 2003, Engineering College, Baghdad University.

[10] H. A. Kubba,"An improved method of automatic adjustment of transformer and phase shifter taps for constrained load flow", AL-Muhandis, No.4, Dec.2001, pp. 34-50.

APPENDIX I:

For a linear, time-invariant RLC circuit with sinusoidal voltage, which a typical distribution system is modeled as, Ohm's law has the following familiar form[8]:

$$I_b = Y_b V_b \qquad (A.1)$$

where I_b : a vector of complex branch current,
Y_b: a diagonal matrix with diagonal element to be branch admittance,
V_b: a vector of complex branch voltage.
The directions of I_b and V_b must be consistent. For KCL, we have:

$$A\, I_b = I_n \qquad (A.2)$$

where I_n : vector of nodal injection current,
A : node to branch incidence matrix, defined as:

$$A_{km} = \begin{cases} 1, & \text{if branch m is directed away from node k} \\ -1, & \text{if branch m is directed towards node k} \\ 0, & \text{if branch m is not incident to node k} \end{cases}$$

Each row of (A.2) corresponds to KCL for a node. Since each branch is always directed away

from one node and towards one other node, the summation of all rows will end with zero. Hence, for a system with n nodes, only (n-1) rows in (A.2) are independent. An arbitrary row can be removed from (A.2) so that the remaining (n-1) rows are independent. The node corresponding to the removed row is usually called the reference node. To express KVL in matrix form, a loop matrix B is defined as:

$$b_{km} = \begin{cases} 1, & \text{if branch m is in loop k, and their direction agree} \\ -1, & \text{if branch m is in loop k, and their direction oppose} \\ 0, & \text{if branch m is not in loop k} \end{cases}$$

Then KVL can be expressed as:

$$b\, V_b = 0 \qquad \text{(A.3)}$$

Each row of (A.3) corresponds to KVL for a loop. It is not necessary to include all loops in (A.3) since independent loops are sufficient for V_b to obey. The independent loop is defined as that not all the branches of the independent loop can be found in other independent loops.

CURVATURE DUCTILITYOF REINFORCED CONCRETE BEAM SECTIONS STIFFENED WITH STEEL PLATES

Prof. Dr. Thamir K. Al-Azzawi
Dept. of Civil/ College of Engineering University of Baghdad

Assist. Prof. Raad K. Al Azzawi
Dept. of Civil/ College of Engineering University of Baghdad

Teghreed H. Ibrahim
Dept. of Civil/ College of Engineering University of Baghdad

ABSTRCUT

This paper presents theoretical parametric study of the curvature ductility capacity for reinforced concrete beam sections stiffened with steel plates. The study considers the behavior of concrete and reinforcing steel under different strain rates. A computer program has been written to compute the curvature ductility taking into account the spalling in concrete cover. Strain rate sensitive constitutive models of steel and concrete were used for predicting the moment-curvature relationship of reinforced concrete beams at different rate of straining. The study parameters are the yield strength of main reinforcement, yield strength of transverse reinforcement, compressive strength of concrete, spacing of stirrups and steel plate thickness. The results indicated that higher strain rates improve both the curvature ductility and the moment capacity of reinforced concrete beam sections. Moreover the section curvature ductility increases as the thickness of the stiffening plates decreases.

الخلاصة

قدم هذا البحث دراسة نظريه لقابلية مطيلية التقوس لمقاطع الاعتاب الخرسانية المسلحه والمقواة بالصفائح الحديدية. تم في هذه الدراسه الأخذ بنظر الأعتبار تصرف كل من الخرسانة وفولاذ التسليح تحت تأثير نسب قيم زمنية مختلفة للأنفعال. لحساب مطيلية التقوس تم كتابة برنامج كومبيوتر واخذ بنظر الأعتبار الانفصال الحاصل في غطاء الكونكريت. لقد تم استعمال مخططات متحسسه للمعدل الزمني للأنفعال لكل من الفولاذ والخرسانة وذلك لتوقع علاقة العزم مع التقوس لمقاطع الاعتاب. المتغيرات التي استخدمت في هذه الدراسة هي مقاومة الخضوع لفولاذ التسليح الرئيسي، مقاومة الخضوع لفولاذ التسليح الثانوي، مقاومة الانضغاط للكونكريت، مسافات روابط الاعتاب و سمك صفائح الفولاذ المقواة. النتائج المستحصلة من الدراسه أشارت الى أن زيادة المعدلات الزمنية للأنفعال تحسن من المقاومة و قابلية العزم لمقاطع أعتاب الكونكريت المسلح. اضافة الى ذلك ازدادت مطيلية التقوس بنقصان سمك صفائح الفولاذ المقواة.

KEYWORDS

Curvature Ductility, Beams, Reinforced Concrete, Steel Plates, Strain Rate.

INTRODUCTION

The philosophy of seismic design for moment resisting reinforced concrete frames is based on the formation of plastic hinges at the critical sections of the frame under the effect of substantial load

reversals in the inelastic range. The ability of the plastic hinge to undergo several cycles of inelastic deformation without significant loss in its strength capacity is usually assessed in terms of the available ductility of the particular reinforced concrete section.

The ductility capacity of reinforced concrete sections is usually expressed in terms of the curvature ductility ratio ($\mu_\phi=\phi_u/\phi_y$) where ϕ_y is the curvature of the section at first yield of the tensile reinforcement and ϕ_u is the maximum curvature corresponding to a specific ultimate concrete compression strain.

The moment-curvature analysis of the section is usually performed under monotonically increasing load which represents the first quarter-cycle of the actual hysteretic behavior of the plastic hinge rotation under the earthquake loading. Therefore, μ_ϕ of a section calculated under such assumption is a theoretical estimate of the actual inherent ductility of the section when subjected to an actual earthquake loading. However, the theoretical estimation of μ_ϕ under monotonic loading is widely used as an appropriate indicator of the adequacy of earthquake resistant design for reinforced concrete members.

Steel plates have been used for many years due to their simplicity in applying and their effectiveness for strengthening and stiffening. The high tensile strength and stiffness lead to an increase in bending capacity and a reduction of the deformations. Hussain et. al (1995)[4] tested eight beams of (0.15*0.15*1.25m) with a steel ratio (ρ=0.0096), the concrete cylinder strength was (f_c'=31 MPa) and the average yield strength of the main steel and stirrups was (414 and 275 MPa). The effect of plate thickness and plate end anchorage on ductility and mode of failure of beams were studied and concluded that increasing the plate thickness than 1mm caused a premature failure due to tearing of concrete in the shear span at loads lower than that calculated according to the ACI code shear strength formula.

Soroushian and Sim (1986)[9] used strain rate sensitive constitutive models for steel and concrete to predict the axial load-axial strain relationship of reinforced concrete rectangular columns at different rates of strain. The analysis parameters were the yield strength of reinforcement (f_y =276, 414, 552 MPa), the concrete strength (f_c'=20.7, 27.6 MPa), the steel ratio (ρ=0.026, 0.032, 0.04) and the amounts of hoop reinforcement (ρ_s=0.01388, 0.02082, 0.04164). The results indicated that for the range of analysis parameters considered and for the range of strain rates of (0.00005/sec - 0.5/sec) the secant axial stiffness increases in the range of (16%-36%). Al-Haddad (1995)[1] studied the curvature ductility for reinforced concrete beams under strain rates in a range of (static, 0.05 and 0.1/sec) for values of (f_y =414, 440, 483, 518 MPa) and reinforcement ratio (ρ=0.003, 0.3). He assumed that only the steel reinforcement is a strain rate sensitive. The results indicated that for a strain rate of (0.05/sec) the curvature ductility ratio was decreased by about (12%) for an increase of (34.5 MPa) in f_y compared with that under static loading.

MATERIAL MODELS OF THE PRESENT STUDY

Constitutive Concrete Model

The concrete constitutive model adopted in the present study is that of Razvi & Saatcioglu (1999)[6] which takes into account the cross sectional shape and reinforcement arrangements, **Fig.(1)**. The effect of the strain rate had been accounted for in this model by using the two coefficients (k_f, k_ε) as had been derived by Soroushian (1986)[9] on the test results basis.

The ascending part of the proposed curve is represented by:

$$f_c = \frac{f_{cc}'.k_f.(\frac{\varepsilon_c}{\varepsilon_1.k_\varepsilon}).r}{r-1+(\frac{\varepsilon_c}{\varepsilon_1.k_\varepsilon})^r} \qquad (1)$$

Where:

$$r = \frac{E_c}{E_c - E_{sec}} \quad , \quad E_{sec} = \frac{f_{cc'}.k_f}{\varepsilon_1.k_\varepsilon} \quad , \quad E_c = 4730\sqrt{f_{c'}} \quad , \quad \varepsilon_1 = \varepsilon_{01}(1+5k_3K)$$

The descending part assumes a slope that changes with confinement reinforcement and as follows:-

$$\varepsilon_{85} = 260k_3.\rho_c.\varepsilon_1[1+0.5k_2(k_4-1)]+\varepsilon_{085} \qquad (2)$$

$$k_1 = 6.7(f_{le})^{-0.17} \quad , \quad k_2 = 0.15\sqrt{\left(\frac{b_c}{S}\right)\left(\frac{b_c}{SL}\right)} \le 1 \quad , \quad k_3 = \frac{40}{f_{c'o}} \le 1$$

$$k_4 = \frac{f_{Le}}{500} > 1 \quad , \quad K = \frac{k_1.f_{Le}}{f_{c'o}}$$

$$\varepsilon_{01} = 0.0028 - 0.008k_3 \qquad \varepsilon_{085} = \varepsilon_{01} + 0.0018k_3^2$$

$$\rho_c = \frac{\sum_{i=1}^{n}(A_{sx})_i + \sum_{j=1}^{m}(A_{sy})_j}{S(b_{cx}+b_{cy})}$$

$$f_{Le} = k_2 f_L$$

$$k_f = 1.48 + 0.16\log_{10}\varepsilon^{\bullet} + 0.0127(\log_{10}\varepsilon^{\bullet})^2$$

$$k_\varepsilon = 1.08 + 0.112\log_{10}\varepsilon^{\bullet} + 0.0193(\log_{10}\varepsilon^{\bullet})^2$$

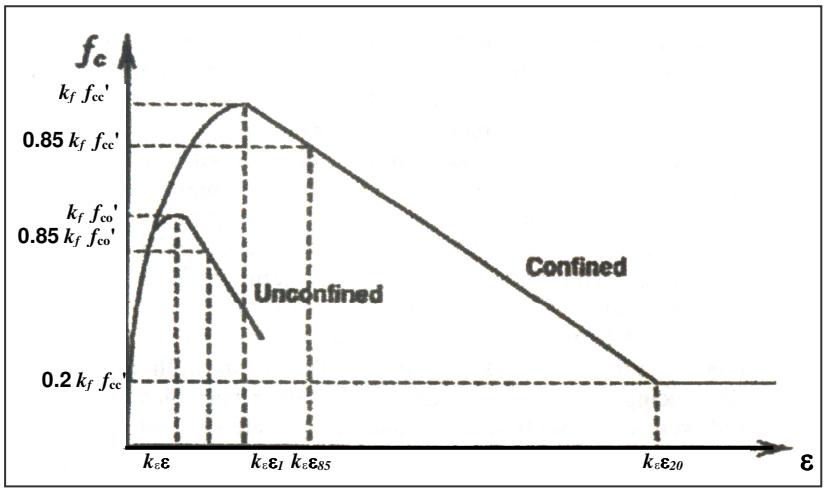

Fig.(1). Strain rate modified stress-strain relationship for concrete[6]

Constitutive Steel Model

Several models were proposed to represent the stress-strain relationship of steel reinforcement by using many dynamic tests results[7]. The following constitutive model of steel has been empirically derived by Parvis Soroushian (1987)[8] from dynamic test results on structural steel, reinforcing bars and deformed wires for different wires and for different types of steel**, Fig.(2)**.

$$f_s = \begin{cases} E_s \varepsilon_s \cdots\cdots\cdots\cdots\cdots\cdots\cdots\cdots\cdots\cdots\cdots\cdots\cdots\cdots if \quad \varepsilon_s < \dfrac{f_y'}{E_s} \\ f_y' \cdots\cdots\cdots\cdots\cdots\cdots\cdots\cdots\cdots\cdots\cdots\cdots\cdots\cdots if \quad \dfrac{f_y'}{E_s} < \varepsilon_s < \varepsilon_h' \\ f_y' \left[\dfrac{112(\varepsilon_s - \varepsilon_h') + 2}{60(\varepsilon_s - \varepsilon_h') + 2} + \dfrac{(\varepsilon_s - \varepsilon_h')}{(\varepsilon_u' - \varepsilon_h')} (\dfrac{f_u'}{f_y'} - 1.7) \right] if \quad \varepsilon_h' < \varepsilon_s < \varepsilon_u' \\ 0.0 \cdots\cdots\cdots\cdots\cdots\cdots\cdots\cdots\cdots\cdots\cdots\cdots\cdots\cdots if \quad \varepsilon_s \geq \varepsilon_u' \end{cases} \quad (3)$$

Where:

$$f_y' = f_y[(-6.54*10^{-8} f_y + 1.46) + (-1.334*10^{-7} f_y + 0.0927)\log_{10} \varepsilon^{\cdot}] \quad (4)$$

$$f_u' = f_u[(-1.118*10^{-7} f_y + 1.15) + (-0.354*10^{-7} f_y + 0.04969)\log_{10} \varepsilon^{\cdot}] \quad (5)$$

$$\varepsilon_h' = \varepsilon_h[(-6.105*10^{-6} f_y + 4.46) + (-1.22*10^{-6} f_y + 0.693)\log_{10} \varepsilon^{\cdot}] \quad (6)$$

$$\varepsilon_u' = \varepsilon_u[(-1.295*10^{-6} f_y + 1.4) + (-2.596*10^{-7} f_y + 0.0827)\log_{10} \varepsilon^{\cdot}] \quad (7)$$

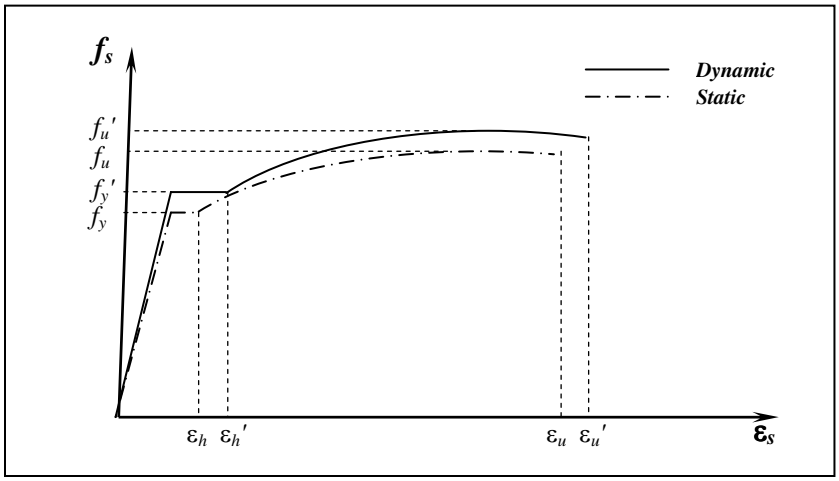

Fig. (2). Comparison of Static and Dynamic Constitutive Model of Steel [8]

The comparison between the experimental (*f*-ε) curve and Parvis Soroushian (1987)[8] constitutive model for two different strain rates for steel specimens with yield strength of (235 MPa) as shown in **Fig.(3).**

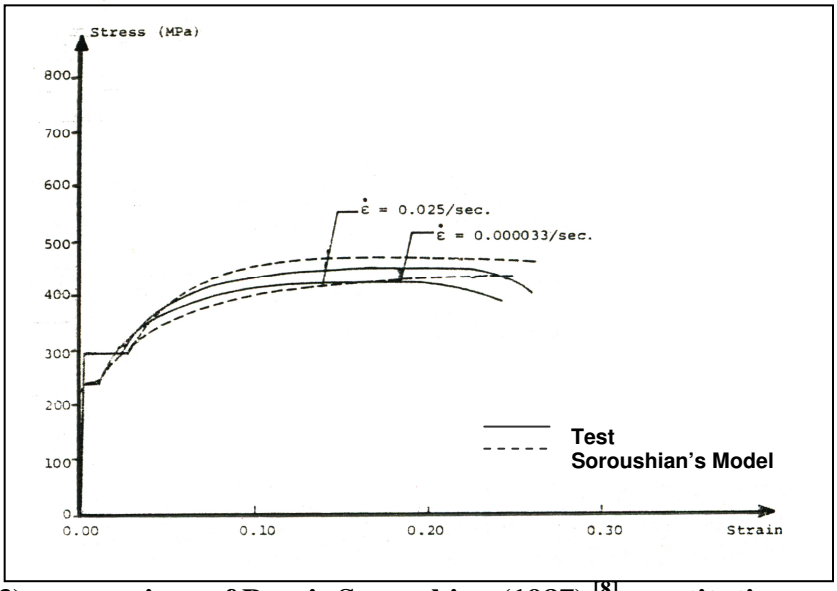

Fig.(3). comparison of Parvis Soroushian (1987) [8] constitutive model of steel with test results for f_y=235 MPa

MOMENT-CURVATURE RELATIONSHIP FOR CONCRETE SECTION

The response of reinforced concrete cross section to an applied bending moment and an axial force may be adequately described by the relation between moment and curvature referred to moment-curvature relationship. This relation depends on the material and geometrical properties of cross section as well as the level of the applied axial force.

This relationship is established using the following procedure:

1. The ultimate concrete compressive strain is first computed using Bing, Park and Tanka (2001)[2] equation and as follows:

$$\varepsilon_{cu} = \varepsilon_{co}[2 + (122.5 - 0.92 f_{co})\sqrt{\frac{f_l}{f_{co}}}] \qquad (8)$$

Where:

f_l =lateral confining stress of transverse reinforcing steel

f_{co} =compressive strength of unconfined concrete

ε_{co}=strain at peak stress of unconfined concrete

The concrete spalling strain is limited by (0.004) as reported in Ref.[5].

2. For a given concrete strain in the extreme compression fiber ε_{cm} and neutral axis depth *kd*, the analysis is performed as follows:
   a) The steel strains (ε_{s1}, ε_{s2}…) can be determined from similar triangles of the strain diagram. For example, for bar *i* at depth d_i the steel strain is:

$$\varepsilon_{si} = \varepsilon_{cm}(\frac{kd - di}{kd}) \qquad (9)$$

The steel stresses (f_{s1}, f_{s2}…) corresponding to strains (ε_{s1}, ε_{s2}…) may be found from the stress-strain curve for the steel using equations (3). Then the steel forces (S_{s1}, S_{s2}…) may be found from the steel stresses and the areas of steel, **Fig.(4)**. For example for bar *i* the force equation is:

$$S_i = f_{si} \cdot A_{si} \qquad (10)$$

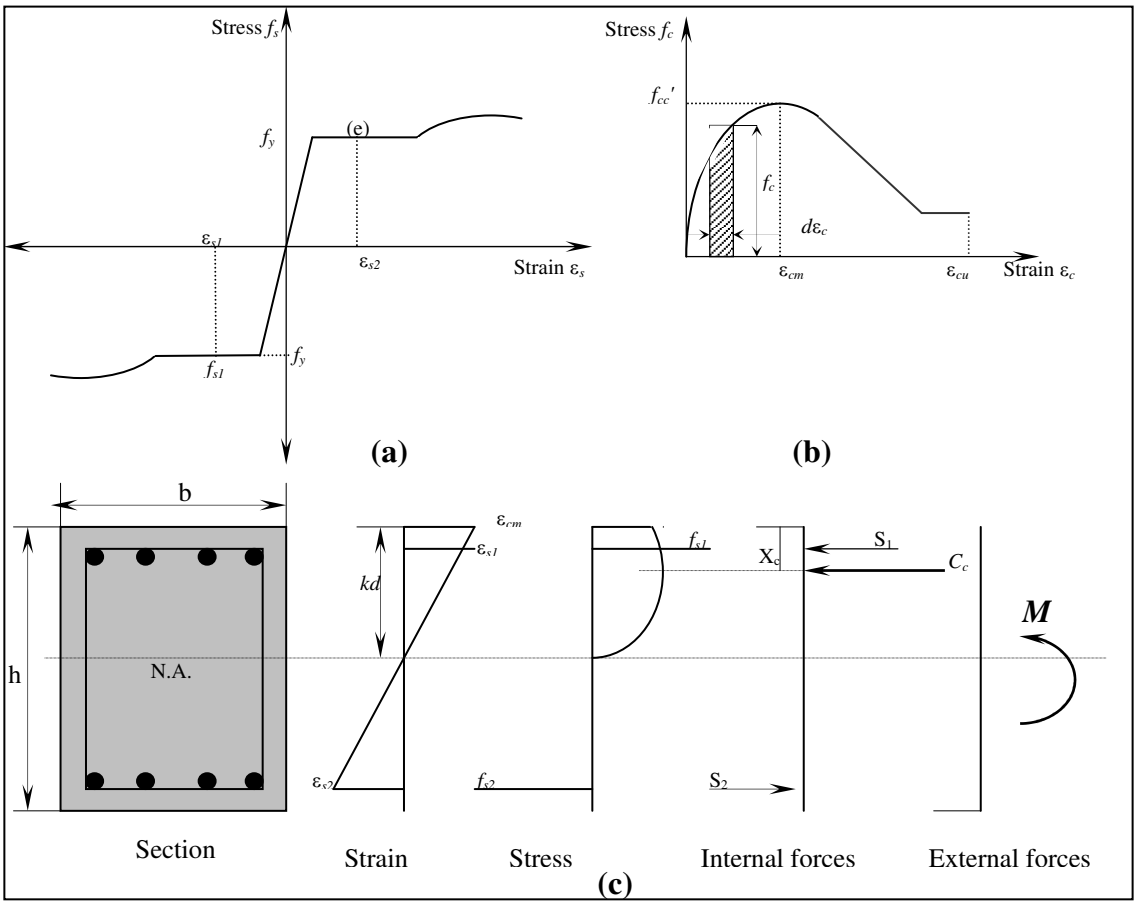

Fig.(4). theoretical moment curvature analysis (a) steel in tension and compression.

b) The concrete compressive force C_c is made up of two parts, a confined part coming from the core concrete confined by the stirrups, and the unconfined part coming from the cover concrete. Each part is analyzed separately and both are added to make up the total concrete compressive force, **Fig.(5)**.

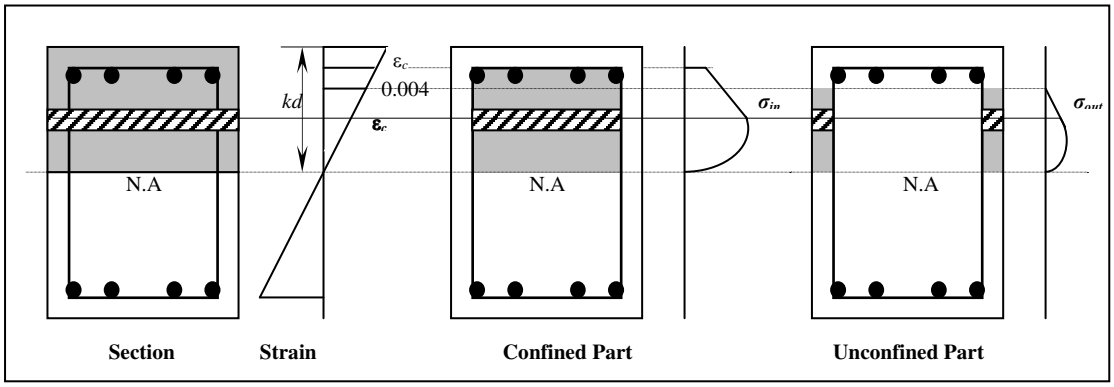

Fig.(5). concrete section analysis.

3. The force equilibrium equation is:

$$C_c = \sum_{i=1}^{n} f_{si} \; A_{si} \qquad (11)$$

and the moment equilibrium equation:

$$M = C_c(\frac{h}{2} - X_c) + \sum_{i=1}^{n} f_{si} \; A_{si}(\frac{h}{2} - d_i) \qquad (12)$$

Where:

X_c=the moment arm of concrete compressive force (C_c).

The curvature is given by

$$\phi = \frac{\varepsilon_{cm}}{kd} \qquad (13)$$

4. The method of establishing these relations is based on equilibrium of internal and external forces assuming a linear distribution of strain across the depth of section. Concrete spalling outside the ties has no contribution in internal force calculation at strains more than the maximum unconfined value of (0.004). The moment-curvature curve exhibits a discontinuity at first yield of tension steel and has been terminated when external fiber compressive concrete strain ε_{cm} reaches the maximum compressive strain ε_{cu}, **Fig.(5)**.

Fig.(6) shows a comparison between experimental results and the present study results. It is obvious that there is a good agreement between the analytical model and the test results.

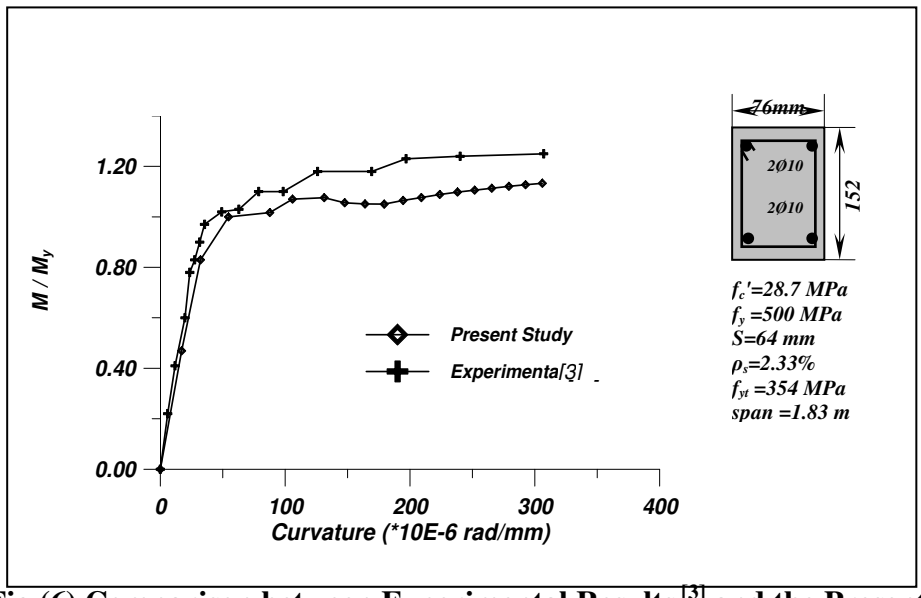

Fig.(6) Comparison between Experimental Results [3] and the Present Study Results for Confined Beam Section

Effects of Strain Rate on the Curvature Ductility

Any increase in the rate of loading usually increases both the compressive strength of concrete and the yield strength of steel. Hence it may be expected that the moment capacity of reinforced concrete beams increases with increasing in the loading rate.

The reinforced concrete beam shown in **Fig.(7)** is analyzed the results are presented in **Figs.(8)** to **(12)**. In each Figure five curves of moment-curvature relationships are shown for four different strain rates of 0.0001/sec (a typical quasi-static value), 0.001/sec,0.01/sec and 0.1/sec in addition to the static load condition for different parameters of (f_y, f_{yt}, f_c', S and steel plate thickness). The steel plates stiffening the top and the bottom face of the reinforced concrete section.

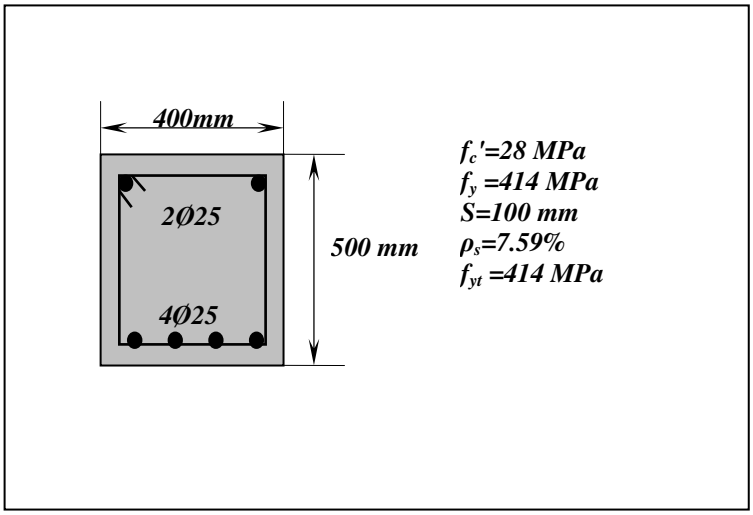

Fig.(7) Details of Beam

Table (1) summarizes the results of the curvature ductility for different parameters (f_y, f_{yt}, f_c' and S). The effects of the above parameters on μ_ϕ for reinforced concrete beam sections are as follows:

1. μ_ϕ is increased by about 10% for f_y =414 MPa and by about 30 % for both f_y =345 and 276 MPa under the strain rate of (0.1/sec) as compared to the static loading, **Fig.(13-a).**
2. For different yield strengths of the transverse reinforcement the curvature ductility factor under the strain rate of (0.1/sec) increased an average by about (14%) as compared to the static loading, **Fig.(13-b)**.
3. For different concrete compressive strengths the average increase in curvature ductility under the strain rate of (0.1/sec) is about (10%) as compared to the static loading, **Fig.(13-c)**.
4. For different values of spacing of stirrups the average increase in μ_ϕ under strain rate of 0.1/sec is about 12% as compared to the static loading**, Fig.(13-d)**.
5. for different f_y, f_c', f_{yt} and S the average increase in moment capacity at strain rate of (0.1/sec) as compared to the static rate is about 20%, **Figs.(8)** to **(11)**.

Effects of Strengthening by Steel Plates:

For different strain rates the beam section of **Fig.(7)** has been strengthened by using steel plates of 1mm, 3mm and 5mm thickness. The results are given in **Table (2)** the following can be concluded:

1. For different steel plate thickness the average increase in μ_ϕ under strain rate of 0.1/sec is about 14% as compared to the static loading.

2. For a strain rate of 0.1/sec the strengthening of the beam by steel plates of 1mm, 3mm and 5mm respectively decreases the curvature ductility by 8%, 9% and 10% respectively as compared to the unplated sections.
3. For the static strain rate the strengthening of the beam by steel plates of 1mm, 3mm and 5mm respectively decreases the curvature ductility by 6%, 12% and 18% respectively as compared to the unplated sections.
4. For higher strain rates the increase in thickness of steel plates is become insignificant on the curvature ductility of the beam section, **Fig.(13-e)**.
5. For different steel plate thickness the average increase in moment capacity at strain rate of 0.1/sec over the static rate is (19%), **Fig.(12)**.

Table (1) Curvature ductility $\mu_{\emptyset}$ for beams under different strain rates

Strain-Rate ($\acute{\varepsilon}$) 1/sec	*0. 1*	*0. 01*	*0.001*	*0.0001*	*Static 0.00001*
f_y (MPa)	*f_c'=28 MPa, f_{yt} =414 MPa, S=100mm*				
276	45.28	43.50	40.08	37.16	34.20
345	30.23	30.39	29.05	25.62	22.58
414	18.08	17.53	17.02	16.95	16.28
f_{yt} (MPa)	*f_c'=28 MPa, f_y =414 MPa, S=100mm*				
276	15.58	15.05	14.17	13.86	13.26
345	17.01	16.67	16.17	15.98	14.89
414	18.08	17.53	17.02	16.95	16.28
f_c' (MPa)	*f_y =414 MPa, f_{yt} =414 MPa, S=100mm*				
21	14.39	13.92	13.57	13.32	13.10
28	18.08	17.53	17.02	16.951	16.28
35	19.39	18.90	18.48	18.22	17.47
S(mm)	*f_c'=28 MPa, f_y =414 MPa, f_{yt} =414 MPa*				
100	18.08	17.53	17.02	16.95	16.28
150	13.77	13.14	12.49	12.32	12.01
200	11.82	11.76	11.18	10.88	10.54
250	10.76	10.99	10.37	10.17	9.80

Table (2) Effect of Plate Thickness and Strain Rate on the Curvature Ductility $\mu_{\emptyset}$ for Beam Sections

Strain-Rate ($\acute{\varepsilon}$) 1/sec	*0. 1*	*0. 01*	*0.001*	*0.0001*	*Static 0.00001*
Plate Thickness (mm)	*f_c'=28 MPa, f_y =414 MPa, f_{yt} =414 MPa, S=100mm*				
0	18.08	17.53	17.02	16.951	16.28
1	16.75	16.48	15.99	15.94	15.30
3	16.55	16.06	15.89	15.43	14.57
5	16.35	15.86	14.78	14.25	13.81

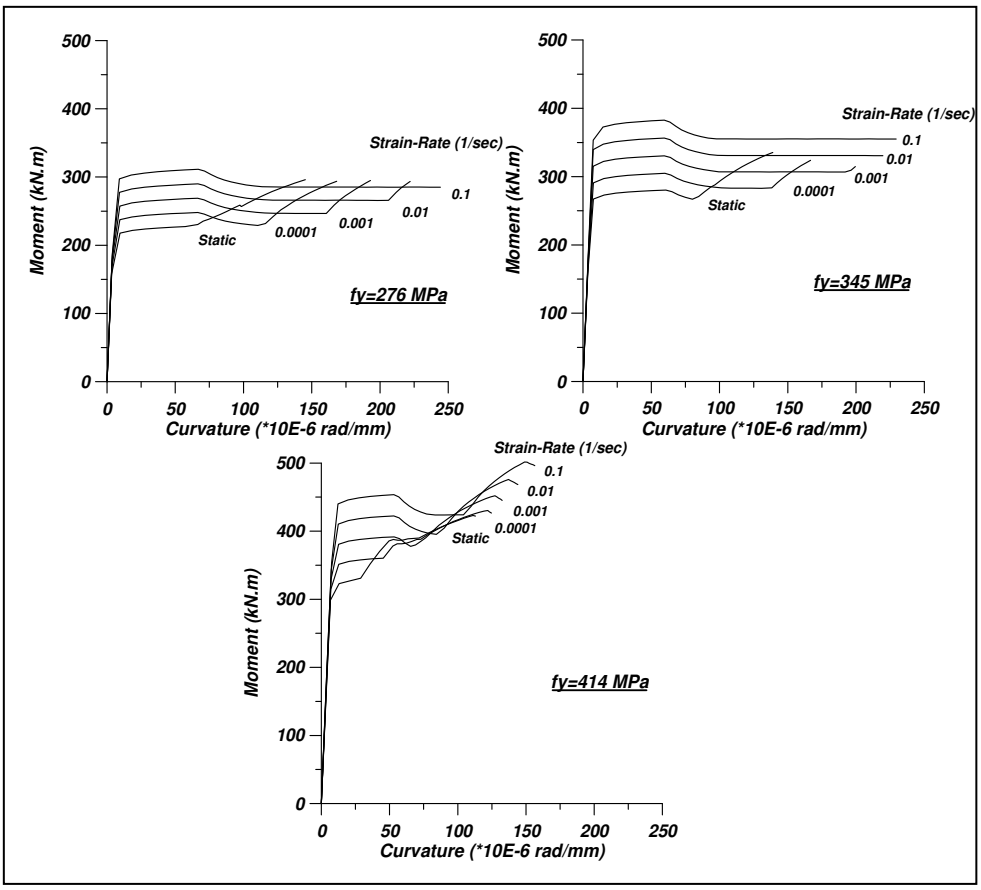

Fig (8) Effect of strain-rate on the moment curvature relationship for different yield strength of main reinforcement f_c'=28 MPa, f_{yt} =414 MPa, S=100mm

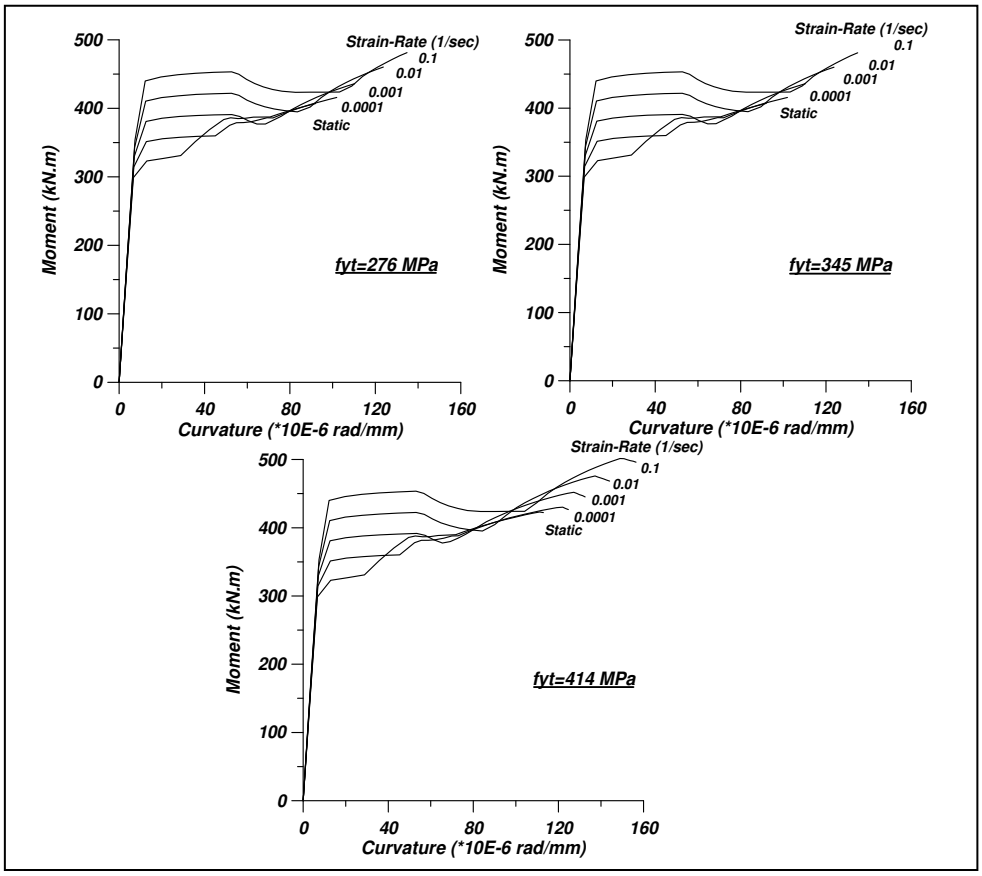

Fig (9) Effect of strain-rate on the moment curvature relationship for different yield strength of transverse reinforcement f_c'=28 MPa, f_y =414 MPa, S=100mm

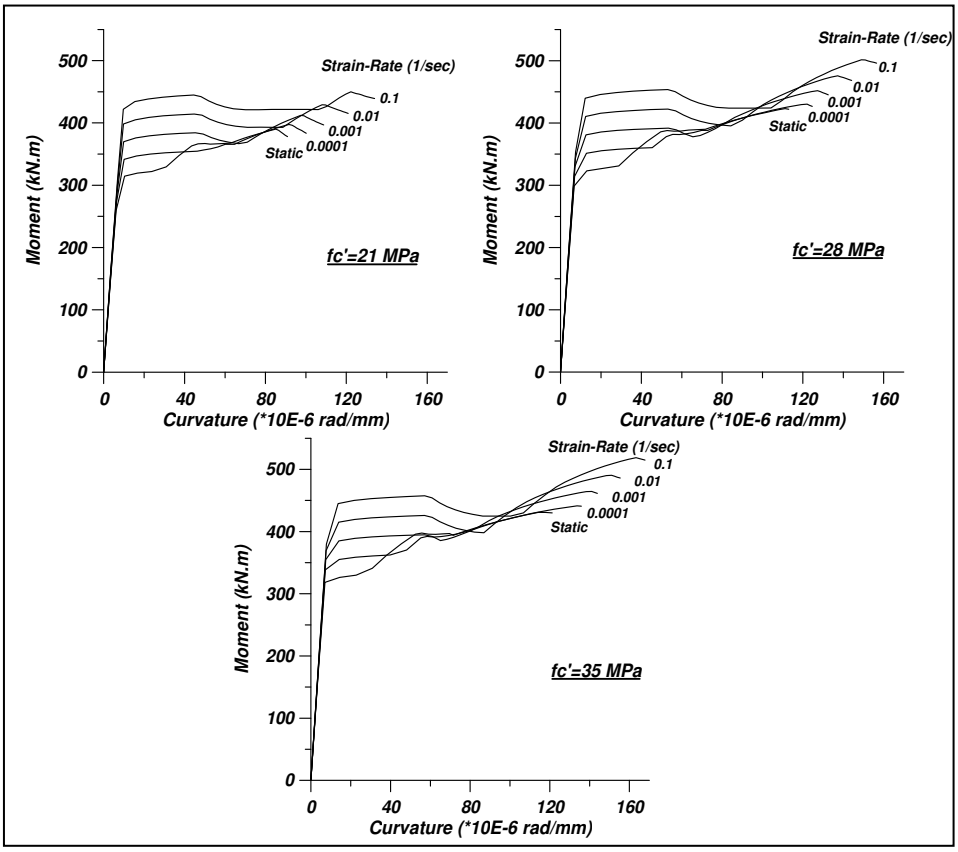

Fig (10) Effect of strain-rate on the moment curvature relationship for different compressive strength of concrete f_y =414 MPa, f_{yt} =414 MPa, S=100mm

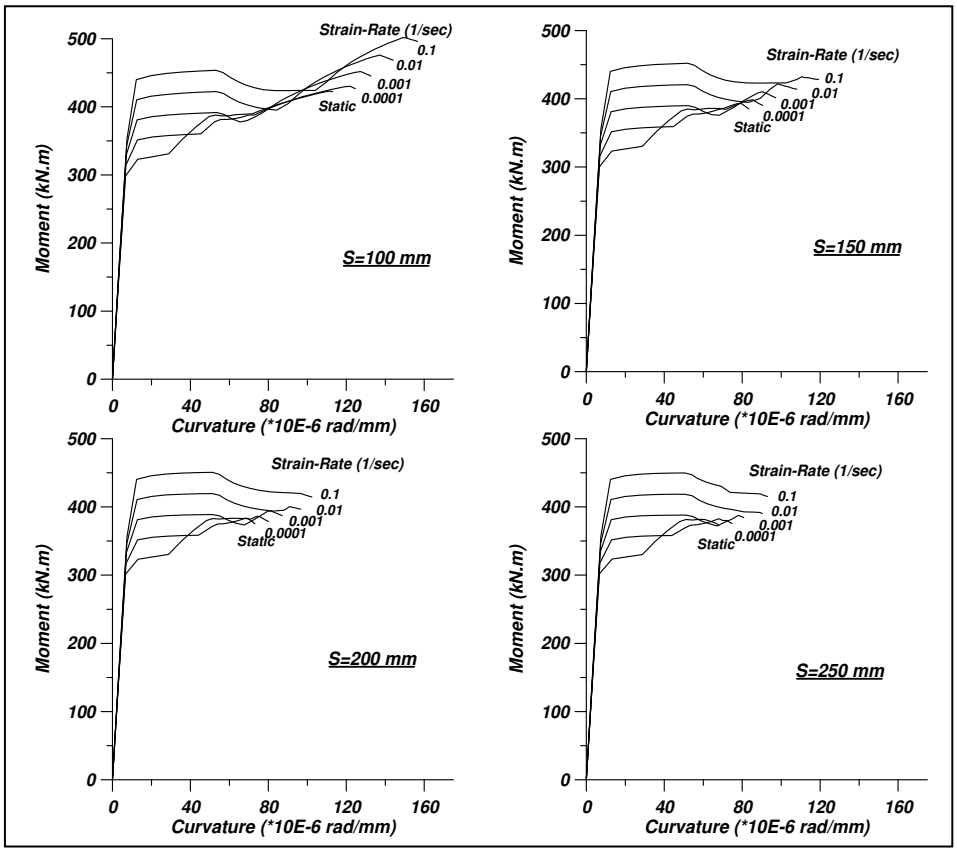

Fig (11) Effect of strain-rate on the moment curvature relationship for different spacing of transverse reinforcement f_c'=28 MPa, f_y =414 MPa, f_{yt} =414 MPa

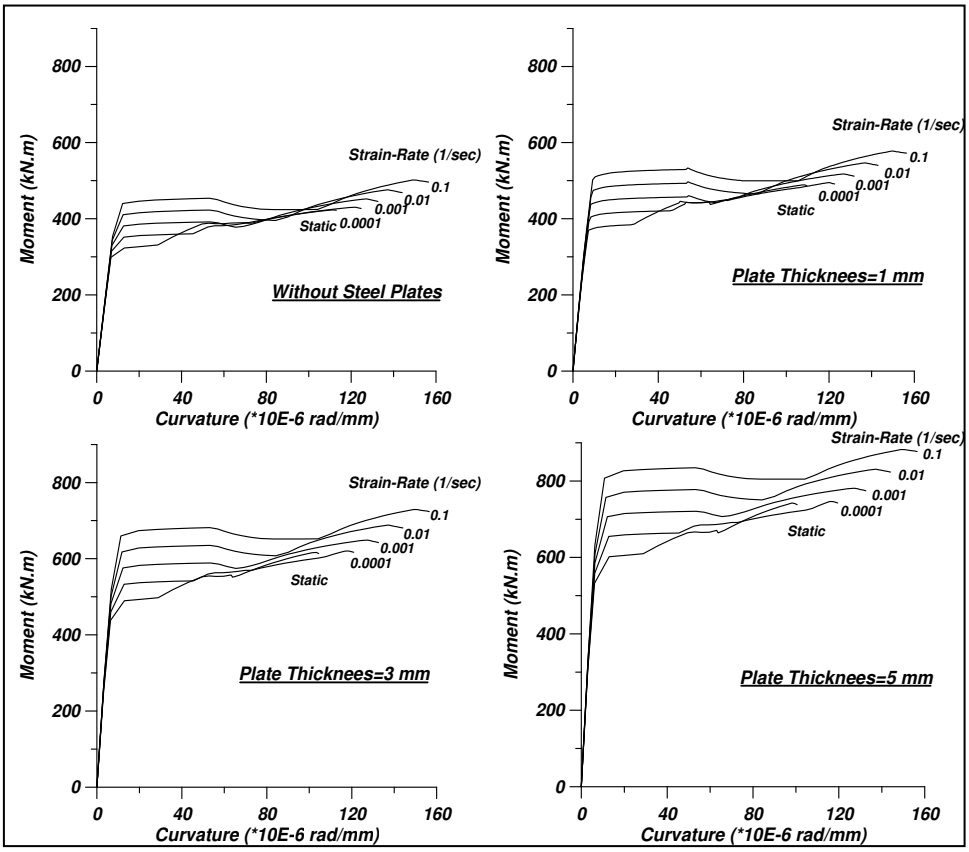

Fig (12) Effect of strain-rate on the moment curvature relationship for beams with and without steel plates f_c'=28 MPa, f_y =414 MPa, f_{yt} =414 MPa, S=100mm

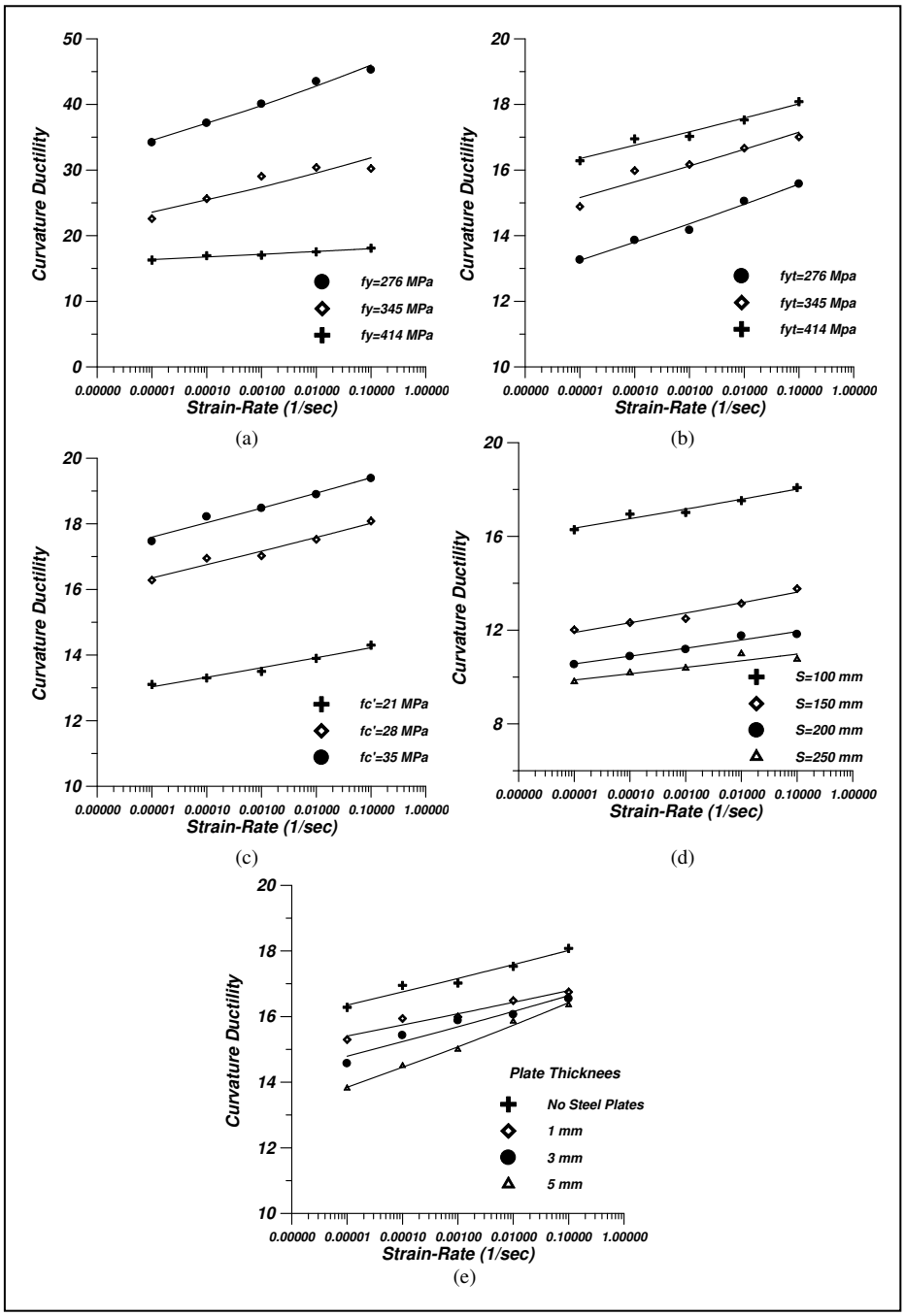

Fig(13). Effect of strain rate on curvature ductility for different:

(a) Effect of steel yield strength for main reinforcement (f_c'=28 MPa, f_{yt} =414 MPa, S=100mm)

(b) Effect of steel yield strength for transverse reinforcement (f_c'=28 MPa, f_y =414 MPa, S=100mm)

(c) Effect of concrete compressive strength (f_y =414 MPa, f_{yt} =414 MPa, S=100mm)

(d) Effect of spacing of stirrups (f_c'=28 MPa, f_y =414 MPa, f_{yt} =414 MPa)

(e) Effect of steel plate thickness (f_c'=28 MPa, f_y =414 MPa, f_{yt} =414 MPa, S=100mm)

CONCLUSIONS:

Based on the results obtained in the present study, the following conclusions can be drawn:

1. The curvature ductility factor increased by about (14%) for a strain rate of (0.1/sec) as compared to the static loading for different yield strengths of the transverse reinforcement and different steel plate thickness
2. The curvature ductility factor increased on average by (20%) under the strain rate of (0.1/sec) over the static strain rate for different yield strengths of the main reinforcement.
3. The moment capacity increased on average by (20%) for the strain rate of (0.1/sec) as compared to the static load condition for different yield strengths of the main reinforcement, strengths of the transverse reinforcement, compressive strength of concrete, spacing of stirrups and steel plate thickness.
4. The curvature ductility under different strain rates for the sections strengthened by steel plates as compared to the unplated sections decreased for the beam sections by about (10%).

NOTATIONS:

A_{sx}, A_{sy}=area of one leg of transverse reinforcement in x and y directions.
b_{cx}, b_{cy}=core dimensions measured c/c of perimeter hoop in x and y directions.
E_c =modulus of elasticity for concrete.
E_s =modulus of elasticity for steel.
E_{sec} =secant modulus of elasticity for concrete.
f_c' = concrete cylinder strength (in MPa).
f_{cc}',f_{co}'= confined & unconfined concrete compressive strength in members (in MPa).
f_L = average confinement pressure (in MPa).
f_{Le}' = equivalent uniform lateral pressure (in MPa).
f_u =static ultimate yield strength of steel (in MPa).
f_u' =dynamic ultimate yield strength of steel (in MPa).
f_y =steel yield strength (in MPa).
f_y' =dynamic yield strength of steel (in MPa).
f_{yt} =yield strength of transverse reinforcement (in MPa).
m, n =number of tie legs in x and y directions.
S =spacing of transverse reinforcement.
S_L =spacing of longitudinal reinforcement laterally supported by corner of hoop or hook of cross tie.
$\acute{\varepsilon}$ =strain rate $\geq 10^{-5}$
ρ_c =total transverse steel area in two orthogonal directions divided by corresponding concrete area.
ε_{01} =strain corresponding to peak stress of unconfined concrete.
ε_{085} =strain corresponding to 85% of peak stress of unconfined concrete on the descending branch.
ε_1 =strain corresponding to peak stress of confined concrete.
ε_{85} =strain corresponding to 85% of peak stress of confined concrete.
ε_c =concrete strain.
ε_h =static strain hardening initiation strains of steel.
ε_h' =dynamic strain hardening initiation strains of steel.
ε_u =static ultimate strains of steel.
ε_u' =dynamic ultimate strains of steel.

REFERENCES:

1. Al Haddad, M. S. "Curvature Ductility of R.C. Beams Under Low & High Strain Rates" ACI Structural Jor. , Vol. 92, No. 5, Sep. – Oct. 1995, pp 526 – 534.
2. Bing, L., Park, R. and Tanka, H. "Stress-Strain Behavior of High Strength Concrete Confined by Ultra High and Normal Strength transverse Reinforcements" ACI Str. Journal Vol.98, No.3, May-June 2001, pp. 395–406.
3. Corley, W. G. "Rotational Capacity of Reinforced Concrete Beams" Journal Str. Divi. ASCE Vol. 92, No. st5, October, 1966, pp. 121-146.
4. Hussain, M., Sharif, A., Basunbul, I. A., Baluch, M. H. and Al-Sulaimani, G. J. "Flexural Behavior of Precracked R/C Beams Strengthened Externally by Steel Plates" ACI Str. Journal Vol. 92, No. 1, Jan.–Feb., 1995 pp. 14-22.
5. Park and Paulay "Reinforced Concrete Structures" 1975.
6. Razvi,S. & Saatciaglu ,M. "Confinement Model for High Strength Concrete" Jor. Str. Eng. ASCE, March, 1999.
7. Scott, B. D., Park, R. and Priestley, M. J. N. "Stress-Strain Behavior of Concrete Confined by Overlapping Hoops at Low and High Strain Rates" ACI Jor. January – February, 1982, pp 13 – 27.
8. Soroushian, P. "Steel Mechanical Properties at Different Strain Rates" ASCE Jor. Str. Eng., Vol. 113, No. 4, April, 1987, pp. 663 – 672.
9. Soroushian, P. and Sim, J. "Axial Behavior of R.C. Columns Under Dynamic loads" ACI Jor. November – December 1986, pp 1018 - 1025.

DEFLECTION OF STRAIGHT AND CAMBERED BEAMS MEASURED DURING FOURTEEN HOURS PER DAY

Dr. Kanaan Sliwo Youkhanna Athuraia

ABSTRACT

Straight and camber beams in portal frames [Footings + Columns + Beams] were studied. Deflection for period of fourteen hours in a day was measured for ten days.

Peak value of deflection within a day is predicted for each one of the beams under a sustained load uniformly distributed.

It is suggested that the load test is to be performed during critical period, within a day, that gives peak deflection.

الخلاصة

تمت دراسة عتبات مستقيمة ومقوسة (**Camber**) ضمن هياكل حاملة حقيقية [أسس + أعمدة + عتبات]. تم قياس الإنحراف (الأود) لفترة أربع عشرة ساعة باليوم ولمدة عشرة أيام.

تم الحصول على القيمة العظمى (**Peak**) للإنحراف (الأود) ضمن اليوم ولكل عتبة تحت حمل مستمر موزع بالتساوي (**Uniformly Distributed Load**).

يمكن أن نقترح بأن يتم عمل فحص التحميل (**Load Test**) خلال الفترة الحرجة ضمن اليوم والتي تعطي أعظم إنحراف (أود).

KEY WORDS

: **camber, deflection, load test, peak, straight.**

INTRODUCTION

Reinforced concrete has taken its place as one of the most important structural material due to its relatively high compressive strength, durability, adaptability to various forms and its relatively low cost. It, however, has the unfavorable characteristic of relatively low tensile strength.

Reinforced concrete buildings respond quite significantly to changes in loading and environment in addition to the natural laws which govern the behavior of the materials, leading to the inevitable deflection. To the engineer, these movements (deformations) should take an important considerations in ensuring that the structure is safe and will satisfactorily fulfil its purpose.

Arching is the oldest structural method for bridging too long spans. Arches are made of masonry, steel, timber and reinforced concrete.

Introducing some camber (shallow curvature) to flexural members (beams or slabs) may mobilize end restraint forces. Curved flexural members tend to straighten when a load is applied on them under the action of “angular deformation”. This tends to increase the span of a curved member. To maintain the original span, a horizontal thrust reaction will be initiated by the action of the restraining supports. This axial restraint force acts in a similar manner as the axial pre-stressing force.

LITERATURE REVIEW

Generally, all codes recommend the practice of providing an initial camber, to overcome excessive deflections due to vertical loads.

CEB-FIB Model Code [2] states that in order to balance the deflections, fully or in part, and to prevent the unwanted effects, adequate cambers are introduced in the form-work during construction.

ACI [1] and Iraqi Building Code [3] specify that the maximum permissible deflection may be exceeded if camber is provided so that the total deflection minus camber does not exceed the permissible limit.

An upward deflection is sometimes introduced to the member. This deflection is equal to the downward deflection caused by dead loads only, especially when the dead load represents the largest share of loads [4].

SCOPE OF RESEARCH

An attempt is made, in this research, to study the deflection of straight and camber beams in actual portal frames [Footings + Columns + Beams]. The deflection was measured during months July and September of the year **2003** every two hours in a day [readings start at **8:00 a.m.** and finished at **10:00 p.m.**] for ten days.

An attempt is made to search for the peak period, i.e. the period which the deflection takes its peak value (maximum value)within a day. It is believed that it is possible to make use of this peak period in actual buildings [as an example, reducing the load (live load) during this period depending on the type and performance of each building (commercial, industrial, residential, . . .)]. Also, it may be possible to make use of this peak period for load test, i.e. to perform load test on buildings during this peak period in order to give the decision of the load test taking into account the worst situation of environment daily changes.

An attempt is also made, to study the effect of camber beams (whether it is interior or not). To ensure the accuracy, all dial gages have been calibrated at the central Institution for Measuring and Quality Control.

EXPERIMENTAL WORK

Three model portal frames were prepared [for general information of the portal frames, see **Appendix (A)**] as follows:

1- Single span frame (with straight beam) [Frame (**A**)], shown in **Fig. (1)**.
2- Single span frame (with cambered beam) [Frame (**B**)], shown **Fig. (2)**.
3- Triple span frame (with cambered beam) [Frame (**C**)], shown **Fig. (3)**.

The upward camber is chosen to be 4.6 % upward curvature (gives best results [5]). Dead load was applied on beams after frames were about more than **100 days** age. The date of the dead load application is **12/5/2003**, and that of live load application is **20/6/2003**. Deflection readings for frames (**A** & **C**) were from **15/7/2003** to **24/7/2003**, and that for frames (**A** & **B**) were from **11/9/2003** to **20/9/2003**. These periods were chosen to study the effect of Baghdad climate of hot weather (frames **A** & **C**) and moderate weather (frames **A** & **B**).

Structural analysis indicates that the total ultimate load is (**5.383 kN/m**). According to load test requirements, **85%** of the total load should be considered as total test load, hence:

Total Test Load = 0.85 (5.383) = 4.576 kN/m

Beam self weight = 0.072 kN/m

Super imposed dead load = 2.461 kN/m (assumed, to use equal concrete block rows, each row contain equal number of concrete blocks**)**

Total dead load = 2.533 kN/m

Hence test live load = 4.576 – 2.533 = 2.043 kN/m

Dead and live loads were applied (experimentally) using concrete blocks and sags filled with gravel and hanged on steel pipes. The loads were applied at the same time for all frames.

Tables (1), **(2)**, **(3)** and **(4)** give the measured deflection of the portal frames during fourteen hours of ten days of the research.

Fig. (1) shows the relationship between the average measured deflection and daily hours for frames (**A** & **C**), whereas **Fig. (2)** shows the same relationship for frames (**A** & **B**). **Fig. (3)** shows the same relationship for frame (**A**) at both months (**July and September**).

To ensure that there is no settlement in the foundation, the soil is compacted, then a brick layer is placed under a thin concrete blinding layer on which experimental models were cast.

For theoretical verification of the deflection results obtained experimentally, the following formulas were applied [1,6]:

$$\Delta_{2i} = \frac{5L^2}{48E_cI_e}[M_2 - \tfrac{1}{10}(M_1 + M_3)] \quad \text{.....(1)}$$

and

$$\Delta_{(cp+sh)} = \lambda.(\Delta_i)_{sust} \quad \text{.....(2)}$$

$$\lambda = \frac{\xi}{1+50\rho`} \quad \text{.....(3)}$$

where

E_c is the modulus of elasticity.

I_e is the effective moment of inertia.

M_1 & M_3 are the moments at the left and right ends respectively.

M_2 is the moment at mid-span of the beam.

λ & ξ are the long term deflection multiplier and coefficient respectively.

$(\Delta_i)_{sust}$ is the immediate deflection due to sustained load.

$\Delta_{(cp+sh)}$ is the long term deflection due to creep and shrinkage.

Δ_{2i} is the immediate deflection.

Total (immediate plus long term) theoretical deflections are given at the bottom of Tables (1, 2, 3 & 4), which indicate that the experimental results are acceptable.

It can be seen from **Tables (1)**, **(2)**, **(3)** and **(4)** and **Figs. (4)**, **(5)** and **(6)**, the following remarks:

1- Straight beam (Frame **A**) reaches peak value (maximum deflection) within a day faster than camber beams (Frames **B** & **C**).

2- Straight beam (Frame **A**) is able to rebound the deflection starting from the time of the peak value up to **8:00 a. m.** of the following day, while the cambered beam is able to rebound the deflection starting from the time of the peak value up to about **11:00 a. m.** (as an average). This situation makes the cambered beam capable to withstand the action of sustained load and environment more than the straight beam.

3- The ability of a cambered beam to rebound the deflection is better than that of straight beam. Hence, it is possible to suggest increasing the service life time in the design codes for buildings with camber members (beams and slabs) more than service life time of buildings with straight members only.

4- Straight beam suffers from temperature difference (Morning, Noon, Evening) more than camber beam.

5- Frame (**A**) reaches peak value of deflection at **6:00 p.m.** in **July**, and at **4:00 p. m.** in **September**. This means that due to the environment changes and due to sustained load, the straight beam will suffer from the reduction of its ability to withstand the external action (effect) done on it.

6- From **Tables (1)**, **(2)**, **(3)** and **(4)**, it can be seen that the range of daily hours for peak values of deflection is as follows:

4:00 to **8:00 p.m.**] for frame (**A**) in **July** and **September**.
[**6:00** to **8:00 p.m.**] for frame (**B**) in **September**.
[**8:00** to **10:00 p.m.**] for frame (**C**) in **July**.

7- It is possible to conclude that the cambered beam (Frames **B** & **C**) is better than straight beam (Frame **A**).

8- It is possible to conclude that the camber beam will be better if it is interior beam (Frame **C**) compared to single span beam (Frame **B**).

CONCLUSIONS

1- It is preferable to perform load test on straight members during the period [**4:00 p.m. – 8:00 p.m.**], and for cambered members during the period [**6:00 p.m. – 10:00 p.m.**] in order to give load test decision taking into account the worst case of daily deflection changes (peak value).

2- It is preferable for a straight beam to be cambered one to improve the beam behavior.

REFERENCES

[1] "Building Code Requirements For Structural Concrete", ACI 318M-2002, and Commentary – ACI 318MR-2002, American Institute, Detroit, Michigan.

[2] CEB-FIB Model Code for Concrete Structures, 3rd Edition, 1978.

[3] "Iraqi Building Code Requirements for Reinforced Concrete", Code 1/ 1987, Building Research Center, Scientific Research Council.

[4] Salvadori and Heller, "Structure in Architecture ", Prentice - Hall, Inc., Englewood Cliffs, New Jersey.

[5] Shasha, Kais A. O., " Control of Camber of Concrete Beams to Minimize Steel Reinforcement ", M. Sc. Thesis, University of Baghdad, 1990.

[6] الدكتور هاني محمد فهمي ، "تصاميم الخرسانة المسلحة"، مركز التعريب والنشر، الجامعة التكنولوجية، بغداد، 1986.

Table (1) Deflection around day for frame (A) (mm) [during July 2003].

Day	Hour							
	8:00	10:00	12:00	2:00	4:00	6:00	8:00	10:00
15/7	3.291	3.311	3.313	3.331	3.375	3.376	3.380	3.378
16/7	3.286	3.295	3.313	3.331	3.376	3.376	3.376	3.358
17/7	3.287	3.304	3.322	3.347	3.394	3.392	3.395	3.395
18/7	3.295	3.331	3.349	3.362	3.404	3.401	3.385	3.369
19/7	3.318	3.349	3.368	3.388	3.412	3.422	3.412	3.398
20/7	3.322	3.349	3.369	3.393	3.421	3.430	3.428	3.412
21/7	3.349	3.371	3.383	3.396	3.438	3.443	3.434	3.421
22/7	3.351	3.369	3.371	3.386	3.434	3.440	3.434	3.434
23/7	3.358	3.377	3.380	3.403	3.447	3.439	3.443	3.443
24/7	3.347	3.359	3.368	3.394	3.430	3.434	3.435	3.435
Aver-age	**3.320**	**3.342**	**3.354**	**3.373**	**3.413**	**3.415**	**3.412**	**3.404**
Final average deflection = 3.379 mm								
Theoretical average deflection = 5.479 mm								

Table (2) Deflection around day for frame (C) (mm) [during July 2003].

Day	Hour							
	8:00	10:00	12:00	2:00	4:00	6:00	8:00	10:00
15/7	2.111	2.099	2.091	2.095	2.101	2.132	2.137	2.137
16/7	2.108	2.100	2.095	2.090	2.110	2.130	2.146	2.145
17/7	2.110	2.095	2.090	2.100	2.115	2.150	2.158	2.157
18/7	2.103	2.100	2.098	2.105	2.115	2.140	2.152	2.150
19/7	2.117	2.112	2.108	2.110	2.120	2.126	2.150	2.150
20/7	2.118	2.110	2.105	2.121	2.133	2.152	2.155	2.158
21/7	2.140	2.130	2.125	2.118	2.139	2.152	2.160	2.160
22/7	2.143	2.140	2.130	2.133	2.135	2.160	2.165	2.163
23/7	2.148	2.144	2.141	2.143	2.150	2.164	2.170	2.170
24/7	2.151	2.130	2.115	2.120	2.140	2.160	2.163	2.162
Aver-age	**2.125**	**2.116**	**2.110**	**2.114**	**2.126**	**2.147**	**2.156**	**2.155**
Final average deflection = 2.131 mm								
Theoretical average deflection = 3.468 mm								

Table (3) Deflection around day for frame (A) (mm) [during September 2003].

Day	Hour							
	8:00	10:00	12:00	2:00	4:00	6:00	8:00	10:00
11/9	4.135	4.155	4.152	4.252	4.358	4.365	4.358	4.358
12/9	4.138	4.154	4.155	4.251	4.357	4.402	4.357	4.357
13/9	4.140	4.163	4.161	4.258	4.365	4.365	4.365	4.365
14/9	4.143	4.177	4.180	4.280	4.396	4.384	4.390	4.385
15/9	4.146	4.179	4.182	4.279	4.391	4.382	4.389	4.379
16/9	4.148	4.190	4.189	4.286	4.398	4.387	4.393	4.392
17/9	4.151	4.199	4.204	4.299	4.413	4.397	4.410	4.407
18/9	4.155	4.210	4.206	4.306	4.410	4.396	4.410	4.407
19/9	4.158	4.217	4.221	4.318	4.427	4.406	4.423	4.421
20/9	4.161	4.227	4.232	4.328	4.437	4.414	437	4.433
Aver-age	**4.148**	**4.187**	**4.188**	**4.286**	**4.395**	**4.390**	**4.393**	**4.390**
Final average deflection = 4.297 mm								
Theoretical average deflection = 6.324 mm								

Table (4) Deflection around day for frame (B) (mm) [during September 2003].

Day	Hour							
	8:00	10:00	12:00	2:00	4:00	6:00	8:00	10:00
11/9	3.606	3.585	3.604	3.638	3.726	3.766	3.760	3.663
12/9	3.595	3.579	3.598	3.634	3.721	3.762	3.705	3.636
13/9	3.600	3.573	3.585	3.602	3.623	3.764	3.634	3.609
14/9	3.600	3.529	3.560	3.595	3.616	3.767	3.641	3.624
15/9	3.605	3.560	3.594	3.622	3.673	3.770	3.723	3.662
16/9	3.610	3.564	3.583	3.609	3.684	3.768	3.673	3.624
17/9	3.611	3.534	3.561	3.584	3.637	3.762	3.672	3.623
18/9	3.611	3.535	3.553	3.573	3.586	3.760	3.602	3.573
19/9	3.598	3.515	3.547	3.558	3.579	3.765	3.596	3.579
20/9	3.599	3.496	3.536	3.562	3.578	3.780	3.597	3.585
Aver-age	**3.604**	**3.547**	**3.572**	**3.598**	**3.642**	**3.766**	**3.660**	**3.618**
Final average deflection = 3.626 mm								
Theoretical average deflection = 5.602 mm								

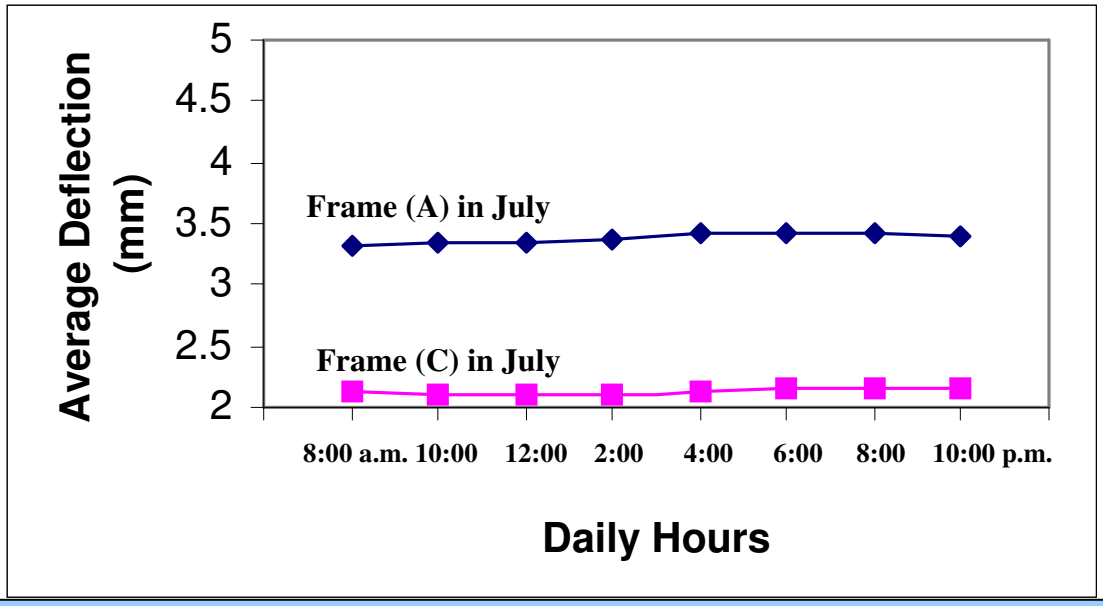

Fig. (4) Deflection – Hour relationship for frames (A & C).

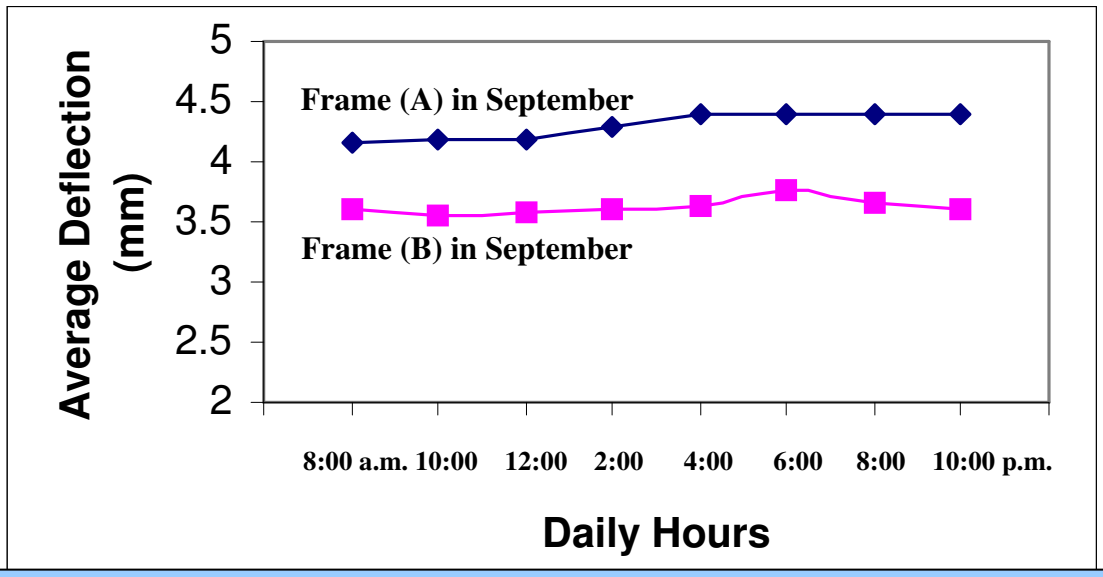

Fig. (5) Deflection – Hour relationship for frames (A & B).

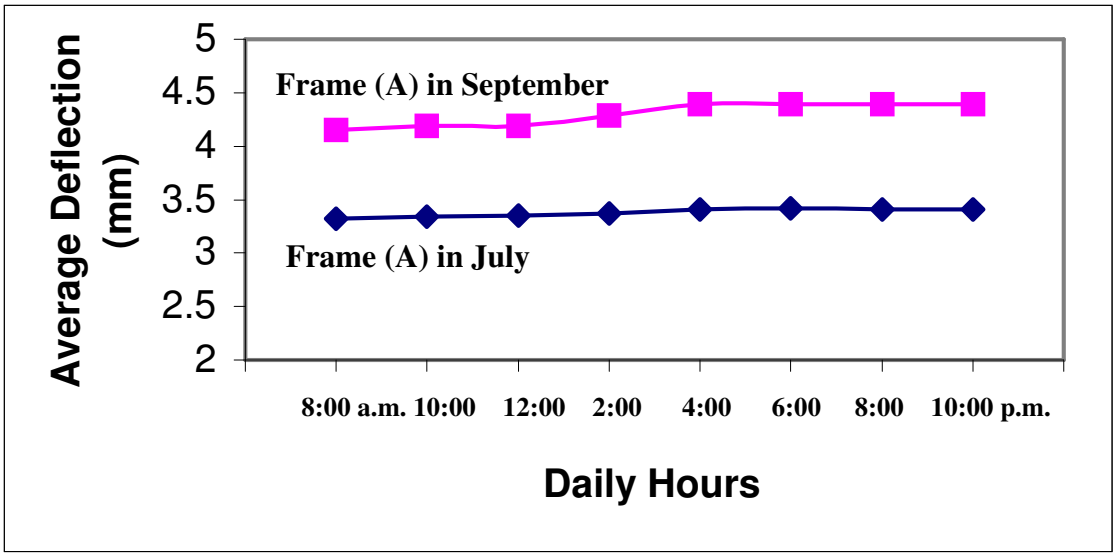

Fig. (5) Deflection – Hour relationship for frames (A & B).

APPENDIX (A)

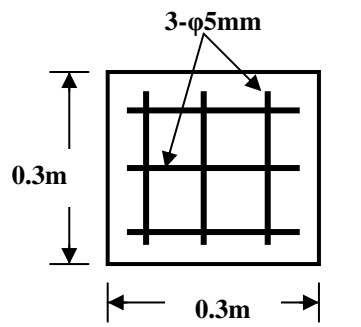

[A] Footing of all portal frames (thickness=0.1m)

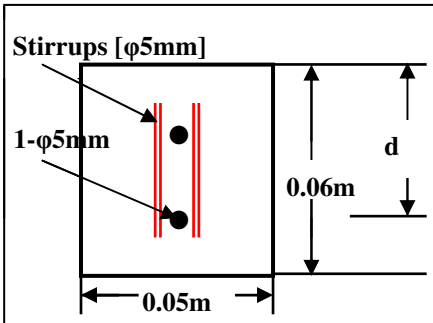

(B) Beam section for portal frames [d is variable].

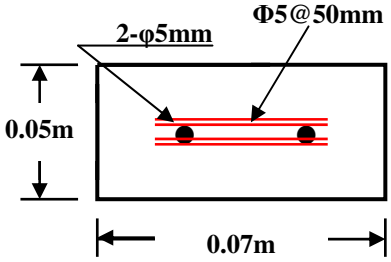

(C) Column section for all portal frames

STIRRUP DISTRIBUTION

1st stirrup @ 0.11m 2nd stirrup @ 0.26m 3rd stirrup @ 0.41m	From face of support

General Information:
For all portal beams :
f'_c = 26.59 MPa (Concrete).
f_y = 774 MPa (Steel Reinforcement).
Degree Of curvature (C_r) = 4.6 %
Portland Cement (Type I).

THEORETICAL SIMULATION OF STRESS-STRAIN RELATIONS FOR SOME IRAQICLAYS USING THE ENDOCHRONIC MODEL

Dr. Mohammed Yousif Fattah
Prof., University of Technology

Maysam Th. Al-Hadidi
Lecturer, University of Baghdad,

Akeel A.S. Al-Gharbawi
Lecturer, University of Baghdad,

ABSTRACT

A constitutive law can be defined as a mathematical functional relation between physical quantities such as stress and strain and may take other factors like time, temperature and additional material properties into account.

In this paper, the endochronic model is used to predict the stress-strain relations of two Iraqi clays. This model is a viscoplastic one but without introducing a yield surface. It encompasses material behaviour such that the current stress state is a function of strain history through a time scale called "intrinsic time" which is not the absolute time but a material property.

The simulation showed that the model overestimates the strains for all cases studied. This may be attributed to the material parameters which require a parametric study to determine their actual values for Iraqi clays.

KEYWORDS

Clay, End chronic Model, Stress, Strain, Model Parameters

الخلاصة

يمكن تعريف قوانين العلاقات التكوينية بأنها دوال رياضية تربط بين كميات فيزياوية مثل الإجهاد و الانفعال و قد تأخذ عوامل عديدة أخرى مثل الزمن و الحرارة و خصائص أخرى للمادة بنظر الاعتبار.

أستعمل في هذا البحث نموذج الزمن الضمني للتنبؤ بعلاقات الإجهاد–الانفعال لتربتين طينيتين عـــراقيتين. إن هذا النموذج هو من النوع اللدن – اللزج و لكنه لا يود خل سطح خضوع. و يعبر عـــن ســـلوك المـــادة بحيث أن حالة الإجهاد الحالية تكون دالة لتاريخ الانفعال من خلال مقياس زمني يدعى "الزمن الضمني" الذي يختلف عن الزمن المطلق من حيث أنه خاصية من خواص المادة. لقد بين التمثيل أن هذا النموذج يعطي قيما عالية للانفعال لكل الحالات التي تمت دراستها. و يعزى هذا إلى معاملات المادة التي يتضمنها النمـــوذج و التي تحتاج إلى دراسة معاملات لتحديد قيمها الحقيقية بالنسبة للترب الطينية العراقية.

INTRODUCTION

Endochronic theory was first introduced by Valanis in 1971. He coined this Greek name "Endochronic" that consists of two roots, endos (meaning inner) and chronos (meaning time). This theory encompasses material behaviour such that the current stress state is a function of the strain

history through a time scale called " intrinsic time" which is not the absolute time measured by a clock as in viscoplasticity but a material property. Hence, the endochronic theory is a "viscoplastic" one but without introducing a yield surface. Therefore, all the complexities and difficulties that develop in introducing a suitable yield criteria are avoided, (Valanis,1971).

Bazant in 1974 and later with his coworkers extended Valanis theory to predict the behaviour of different engineering materials such as concrete , and soils.

GENERALIZED CONSTITUTIVE RELATIONS:

To generalize the uniaxial concept of the endochronic theory into three dimensions, first, the definition of the intrinsic time increment, dz, which is used in stead of real time increment, dt, is introduced. The intrinsic time for time-dependent behaviour is function of strain increments, $d\in_{ij}$ and time, dt. The dependence of dz upon $d\in_{ij}$ is assumed to be gradual to exclude ideal plastic reponse. The function of dz will be continuous, smooth, and monotonically increasing. Thus, function $(dz)^S$ with an appropriate exponent "s" , can be expanded in a tensorial power series in $d\in_{ij}$ and dt , i.e., (Bazant and Bhat,1976):

$$(dz)^s = p + p_{ij}\, d\in + p_4\, dt + p_{ijkl}\, d\in_{ij}\; d\in_{kl} + p_{ij4}\; d\in_{ij}\; dt + p_4\; dt^2 + p_{ijklmn}\, d\in_{ij}\; d\in_{kl}\, d\in_{mn} + \ldots\ldots \quad (1)$$

where:

P= coefficient matrices, the subscripts refer to the components in the Cartesian coordinates x_i, i = 1, 2, 3, and number (4) refers to the time axis.

Since, dz must vanish as $d\in_{ij} \to 0$ and $dt \to 0$, thus P=0. Setting s=1, and neglecting all quadratic terms, then dz = P_4. dt which is of no interest, thus $P_4 = 0$. Setting s=2, and satisfying the conditions of isotropy, the quadratic form of Equation (1) can be written in terms of the first two invariants of $d\in_{ij}$, as follows, (Bazant and Bhat,1976):

$$(dz)^2 = P_o J_2 + (P_1 I_1 + P_2 dt)^2 + P_3 (dt)^2 \quad (2)$$

where:

P_o, P_1 , P_2, P_3 = non-negative coefficients.

J_2 = second deviatoric strain increment invariant, and

I_1 = first strain increment invariant.

Then, dz must vainish for both instantaneous time, dt =0, and pure volumetric deformation, J_2=0, hence P_1= 0. Thus, the remaining terms in Equation (2) can be rewritten in the following form:

$$(dz)^2 = \left(\frac{d\xi}{Z_1}\right)^2 + \left(\frac{dt}{\tau_1}\right)^2 \quad (3)$$

where:

$$d\xi = f_1(\sigma, \in) \cdot d\zeta \quad (4.a)$$

$$d\zeta = \sqrt{J_2} = \sqrt{\frac{1}{2} de_{ij} \cdot de_{ij}} \quad (4.b)$$

de_{ij} = deviatoric strain increment tensor

$$= d\in_{ij} - \frac{1}{3}\delta_{ij} \cdot d\in$$

δ_{ij} = Kronecker delta.

$d\in$ = Volumetric strain increment = $d\in_{kk}$

z_1, τ_1 = Constants.

$d\xi$ is scalar called "damage measure" that depends on strain increments and stresses to predict hardening and softening. $d\zeta$ is called "deformation measure" that depends on strain increments only. From Equations (3) and (4), $d\zeta$ and dz represent geometrically the length of path traced by material states in a six-dimensional strain space for $d\zeta$, or in a strain-time space for dz., (Ansal et al., 1979).

Secondly, generalizing of equations to three dimensions using dz instead of dt, and splitting the strain components into deviatoric and volumetric components to satisfy isotropy conditions, the following differential constitutive equations are deduced:

$$de_{ij} = \frac{dS_{ij}}{2G} + \frac{S_{ij}}{2G} \cdot dz \qquad \textbf{(5.a)}$$

$$d\in = \frac{d\sigma_m}{3k} + \frac{\sigma_m \cdot dt}{3k\tau_1} + d\lambda + d\in^o \qquad \textbf{(5.b)}$$

where:

$de_{ij} = d\in_{ij} - \frac{1}{3}\delta_{ij} \cdot d\in$

$d\in = d\in_{11} + d\in_{22} + d\in_{33}$

$d\lambda$ = inelastic dilatancy,

S_{ij} = deviatoric stress tensor,

$= \sigma_{ij} - \delta_{ij} \cdot \sigma_m$

σ_m = mean stress = $\frac{1}{3}\sigma_{kk}$

G, K = shear and bulk elastic moduli, and

$d\in^o$ = stress-independent inelastic strains (e.g. thermal strains).

Both of the first terms of Equations (5.a) and (5.b) represent the elastic strain increments, while the remaining terms represent the inelastic strain increments. For instance, the term $(\sigma_m \cdot dt / 3K\tau_1)$ represents the time-dependent inelastic volumetric strain, i. e. creep, while $d\lambda$ represents the time-independent volumetric strain.

To develop a quasi-linear elastic incremental constitutive law for simplicity, the plastic stress increment tensor $d\sigma_{ij}^p$ can be obtained from Equations (5) by multiplying Equation (5.a) by 2G, and Equation (5.b) by 3K, hence:

$$d\sigma_{ij}^p = 2G \cdot de_{ij}^p + \delta_{ij}(3K \cdot d\in^p)$$
$$= S_{ij}\, dZ + \delta_{ij}\, (\sigma_m\, dt/\tau_1 + 3K\, d\lambda + 3K\, d\in^o) \qquad \textbf{(6)}$$

The stress increments $d\sigma_{ij}$ are related to the elastic strain increments $d\in_{ij}^e$ by the following equations:

$$d\sigma_{ij} = 2G \cdot de_{ij}^e + \delta_{ij}(3K \cdot d\in^e) \qquad \textbf{(7)}$$

Hence, the summation of Equations (7) and (8) yields:

$$d\sigma_{ij} + d\sigma_{ij}^p = D_{ijkl} \cdot d\in_{kl} \qquad \textbf{(8)}$$

where:

D_{ijkl} = elastic coefficient matrix

THE NUMERICAL PROCEDURE:

The basic constitutive law, Equation (5), is of a differential form, and the variables that govern inelastic deformations are (dz) and ($d\lambda$). Bazant and Bhat (1976) used the step-by-step integration or step-iterative algorithm in which for each loading step, a number of iterations are performed till satisfaction of equilibrium of stresses and strains occurs. This is assured when the change in values of (dz) and ($d\lambda$) for the same loading step becomes very small.

In this algorithm, the values of (dz) and ($d\lambda$) computed from the previous loading step provide an initial estimate for the next loading step.

Endochronic Hardening Functions and Parameters:

The function f_1 in Equation (4) that accounts for hardening or softening, should decrease as the inelastic strains accumulate, because $d\xi$ is adopted as a measure of the accumulated inelastic strain, hence:

$$d\xi = \frac{d\eta}{f(\eta)} \quad ; \quad d\eta = F(\sigma,\in)\cdot d\zeta \tag{9}$$

where:

$f(\eta)$ = Strain-hardening function.

$F(\sigma,\in)$ = Strain-softening function.

Thus, the function $f(\eta)$ has a significant effect on the non-linearity of the stress-strain relations, while the function $F(\sigma,\in)$ allows for a gradual decrease of these relations on approach to peak stress. Both functions depend mainly on material type.

Hardening Functions and Dilatancy for Normally Consolidated Clays:

The function F in Equation (9) is determined semi-empirically from experimental data. The function F is governed by the effective confining stress I_1^{σ}, the volume change, I_1^{ε}, and the second deviatoric strain invariant, J_2^{ε}. Bazant et al. (1979) introduced the following formulation for function F:

$$F(\sigma,\in) = a + \frac{\left|1 - a_1 I_1^{\in}\right| / (1 + a_3 J_2^{\in})}{0.01 + a_2 (I_1^{\sigma} / Pa)} \tag{10}$$

where: a's = material constants.

Pa = atmospheric pressure = 101.3 kN/m^2

The division of I_1^{σ} in Equation (10) by Pa is to make the relation dimensionless. Constant "a" must be positive to ensure irreversible strain increment for the critical case of no hardening or softening, (Bazant et al., 1979).

The function f (η) represents the limiting critical case of no hardening or softening. Thus, for large values of η, this function, f (η), must converge to one. The function f (η) takes the following form:

$$f(\eta) = 1 + \frac{\beta_1}{1 + \beta_2 \eta} \tag{11}$$

where: β_1 and β_2 = constants.

The dilatancy or densification function dλ of clays depends on shear and volumetric stresses and strains. Hence, the function dλ depends on J_2^{ε}, I_1^{σ} and I_1^{ε}. Moreover, dλ depends on λ itself because the volumetric strain increment should decrease monotonically till zero as a limit in the case of failure. Hence dλ is equal to (Bazant et al., 1979):

$$d\lambda = \frac{C_o \left|1 + C_1 I_1\right| \, d\zeta}{(1 + C_2 I_1^{\sigma} / Pa)(1 + C_3 J_2^{\epsilon})(1 + C_4 \lambda)} \tag{12}$$

where: c_o, c_1, c_2, c_3, c_4 = material constants.

$d\lambda$ is determined empirically from tests and it depends on the clay type, stress path and stress history.

The tensile strengths of soils are very small and hence neglected.

The elastic moduli G and K of the soil element change during loading, and thus the accumulated densification-dilatancy measure λ and the effective normal stress also change. Thus, the effect of void ratio is:

$$\frac{de}{e_o} = \frac{\varepsilon_v \, (1 + e_o)}{e_o} = \frac{3(1 + e_o) \, \lambda}{e_o} = \frac{3\lambda}{n} \tag{13}$$

where: e_o = initial void ratio

ε_v = volumetric strain = ε_{kk}

n = porosity.

while the effect of normal stress is the ratio $(I_1^{\sigma} - I_1^{\sigma_o}) / I_1^{\sigma_o}$, where $I_1^{\sigma_o}$ is the initial first stress invariant. Hence, the elastic moduli will be equal to:

$$G = G_o (1 + b_1 \frac{I_1^{\sigma} - I_1^{\sigma_o}}{I_1^{\sigma_o}} + b_2 \frac{3\lambda}{n}) \tag{14}$$

where: b_1 and b_2 = constants,

and $$K = \frac{2}{3} G(1 + \nu)/(1 - 2\nu) \tag{15}$$

MODEL PARAMETERS OF CLAYS

All material parameters in the previous equations are based on best fit of experimental results.

Constant "a" in Equation (10) affects the value of the peak stress. Constant a_3 which is called "distortion coefficient" is determined by the following correlation proposed by Ansal et al. (1979). Based on general pattern of results:

$$a_3 = 153.8(e_o Pa / Po) + 34.62 \tag{16}$$

where:

Po = consolidation pressure.

Similarly, the plasticity coefficient Z_1 in Equation (3) that accounts for rigidity and deformibility of clays, is determined from the following correlation:

$$Z_1 = 0.00294(e_o P_o / P_a)^2 - 0.0177(e_o P_o / P_a) + 0.0396 \tag{17}$$

Ansal et al. (1979) determined an approximate correlation for densification coefficient C_o in Equation (12), softening coefficient β_2 in Equation (11), and the elastic modulus E, as shown in Figure (1). This correlation depends on the consolidation pressure P_o, and the liquidity index of the clay I_L, where (Mitchel, 1993):

$$I_L = \frac{w_{nat} - w_p}{I_P} \tag{18}$$

where:

w_{ant} = natural water content.
w_p = plastic limit
I_p = plasticity index = w_L -w_P
w_L = liquid limit.

Choice of appropriate ratio of the liquidity index to the consolidation stress is tempered by judgement in the absence of test results.

All other constants are determined experimentally. The values of the parameters as proposed by Bazant et al. (1979) are shown in Table (1):

Table (1) – Material parameters of endonchronic model for normally consolidated clays.

	Value
a_o	4
a_1	500
a_2	0.75
β_1	5n (n = porosity)
C_1	2500
C_2	0.25
C_3	1000
C_4	9000
b_1	0.1
b_2	0.1

Computer Program

The computer program **Endoch**, coded in Fortran laguage, was written by the authors. The algorithm used in the endochronoc model incorporates an iterative procedure. The program computes stresses, strains, all functions like F, f (η), and variables like λ, η, at mid-step loading. Iterations are then performed till the tolerance of the values of dz and dλ becomes less than 0.05 %. The values of strain increments, dε, intrinsic time, dz, and inelastic dilatancy, dλ, or the previous step are taken as an estimate for the current step.

APPLICATIONS:

This model have been applied for simulating stress-strain relationships of two Iraqi soils:

i) **First application** Al- Mufty (1990) carried out a series of tests on al-Fao soft clay.

Block samples were obtained from an area close to the river Shatt-Al-Arab.

The top layer of Fao soil was found to be stiff to very stiff brownish gray silty clay with a desiccated crust. This layer is followed by a soft to very soft gray silty clay.

According to the unified classification system, the soil from both layers may be classified as CL-CH, inorganic clays of medium to high plasticity. According to, AASHTO M145-73, the soil is classified as A-7-6 (16).

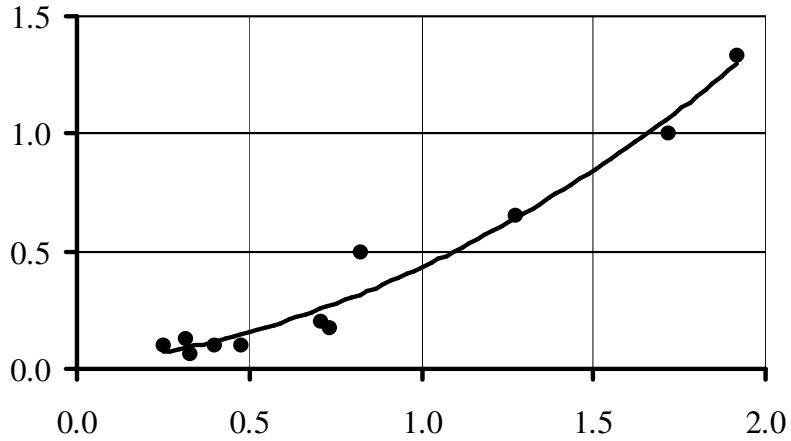

(a)

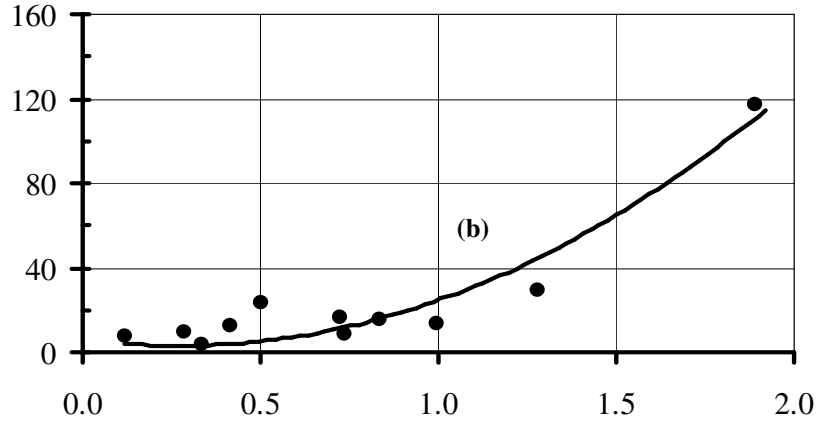

b) Softening coefficient, β_2.

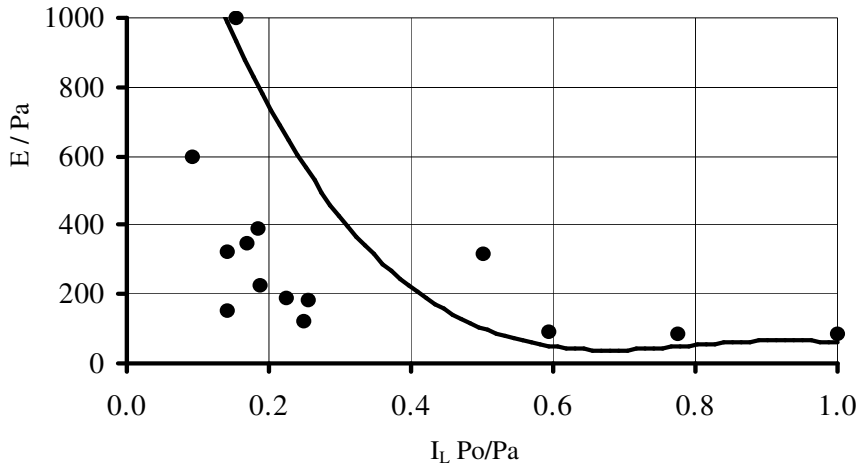

(c)

c) Elastic modulus, E.

The average properties of the soil at sampling depths 1.25 m and 3 m respectively are listed in Table (2).

Table (2). - Average properties of the soft clay from Al-Fao, (from Al-Mufty, 1990).

Property	1.25 m depth	3 m depth
Total unit weight γ_t , kN/m^3	17.9	17.7
Water content w %	30	45
Liquid limit w_L %	54	50
plasticity index Ip %	27	24
Liquidity index I_L	0.11	0.79
Specific gravity G	2.7	2.72
Sand size fraction %	9	12
Silt size fraction %	58	60
Clay size fraction %	33	28
Activity A	0.82	0.86

Among the tests carried out by Al-Mufty (1990) unconsolidated undrained triaxial compression tests on samples compacted by the standard compaction test to the maximum dry density and optimum moisture content. These results are compared with those predicted by the endochronic model in Figures (2) to Figure (6).

Fig (2) and (3) represent the samples that are taken from the top layer, and the figures from (4) to (6) represent the samples that are taken from the layer below the top layer.

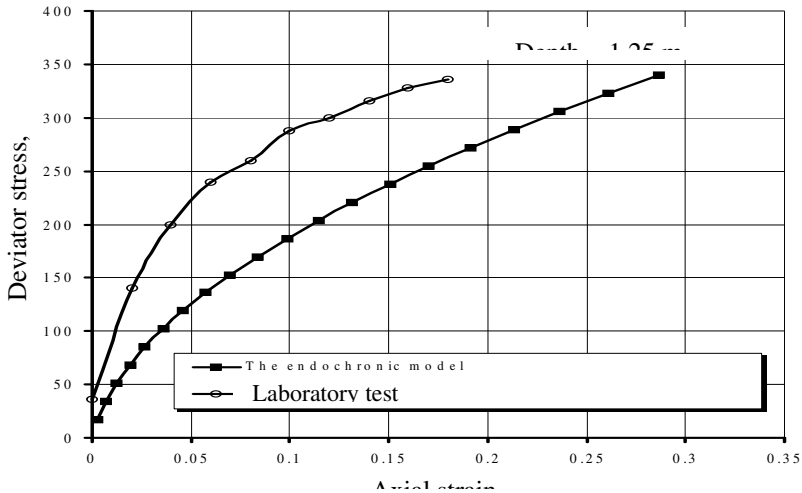

Fig.(2). - A comparison between the stress-strain relationships predicted by the endochronic model with laboratory tests of Al – Mufty (1990), σ_3 =300 kPa.

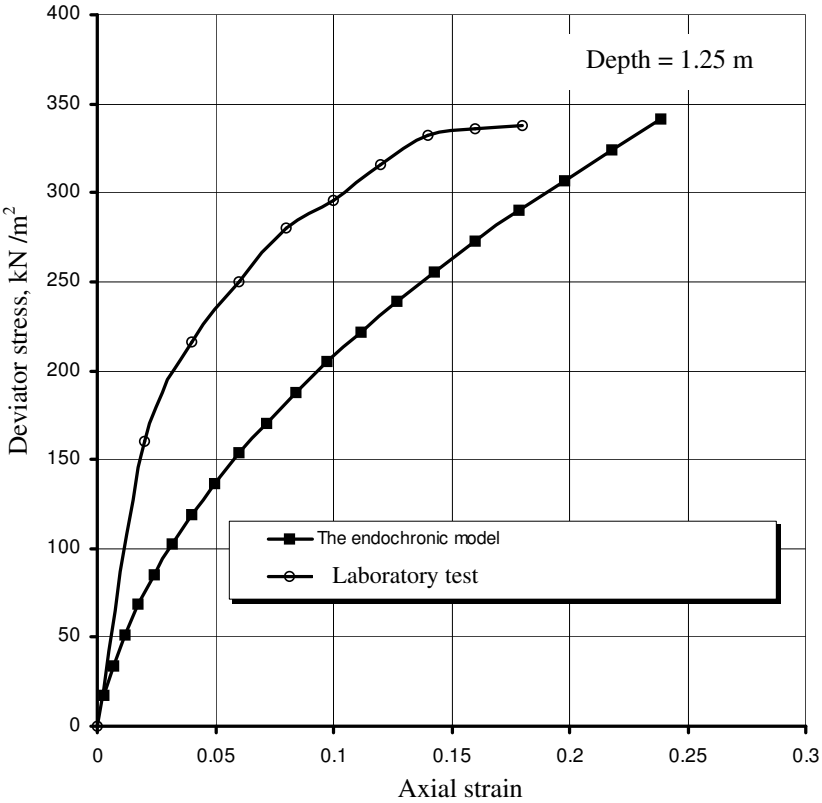

Fig.(3). - A comparison between the stress-strain relationships predicted by the endochronic model with laboratory tests of Al – Mufty (1990), σ_3 =300 kPa.

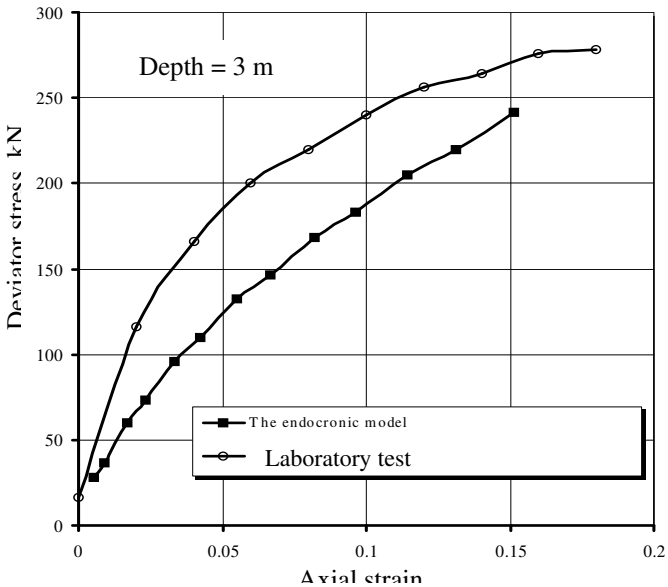

Fig.(4). - A comparison between the stress-strain relationships predicted by the endochronic model with laboratory tests of Al – Mufty (1990), σ_3 =100 kPa.

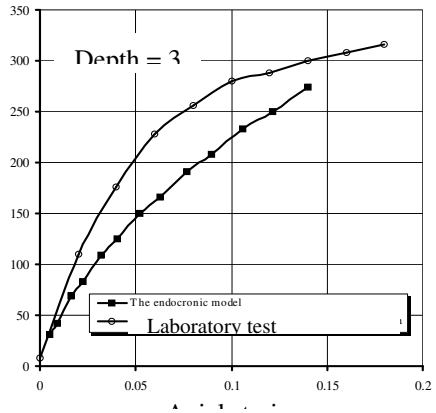

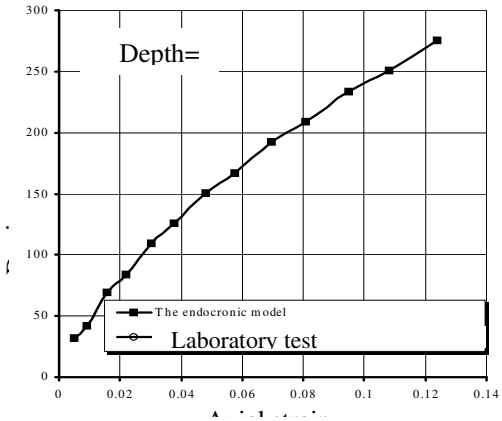

Fig. (5). - A comparison between the stress-strain relationships predicted by the endochronic model with laboratory tests of Al – Mufty (1990), σ_3 =200 kPa.

Fig (6). with laboratory tests of Al – Mufty (1990), σ_3 =300 kPa.

It can be observed in these figures that the model overestimates the strains for all the cases studied under high stress increments.

In addition, there is no definite yield point can be obtained. Thus it is approximately suitable for normally consolidated clays where ductile behaviour of the stress-strain is expected.

ii) Second application

Al- Saady (1989) carried out laboratory tests on an A-6 soil during construction of a road embankment. A representative area located at Al – Zafarania (south of Baghdad), was chosen for the research. The site covers an area of soil composed of silty clay with varying thickness. This stratum behaves as normally or slightly overconsolidated soil, have an upper desiccated crust 0.5-0.75 m thick.

The distribution of the particle sizes indicated:

Clay fraction = 45 %, silt fraction = 37 %, sand fraction = 18 %.

It is classed as “CL” in a Casagramde classification chart.

Among the tests carried out by Al- Saady (1989) consolidated undrained triaxial test which was designated as series D as shown in Table (3).

In addition, unconsolidated undrained triaxial test which was designatd as series G as shown in Table (4).

Consolidated undrained triaxial test results are compared with those predicted by the endochronic model in Figures (7) to (12) which show a comparison between the stress-strain relationships predicted by the endochronic model with laboratory tests of Al – Saady, (series, D).

Consolidated drained triaxial test results are compared with those predicted by the endochronic model in Figures (13) to (18). Figures (19) to (24) show a comparison between the volumetric strain–axial strain relationships predicted by the endochronic model with laboratory tests of Al-Saady, (series, G).

Table(3). - The results of series (D), (from Al-Saady, 1989).

Test No.	σ'_c kN/m^2	e_o	w_c %	$(\sigma_1-\sigma_3)_f$ kN/m^2	$\left(\sigma_1/\sigma_3\right)_f$ kN/m^2	Δu_f kN/m^2
1	79	0.76	26.0	123.24	3.50	30.81
2	100	0.70	24.3	123.00	3.55	52.22
3	150	0.74	25.6	189.21	3.30	72.45
4	200	0.69	24.6	219.60	3.25	104.45
5	300	0.75	25.4	279.00	3.25	176.68
6	376	0.73	26.0	348.01	3.30	224.07

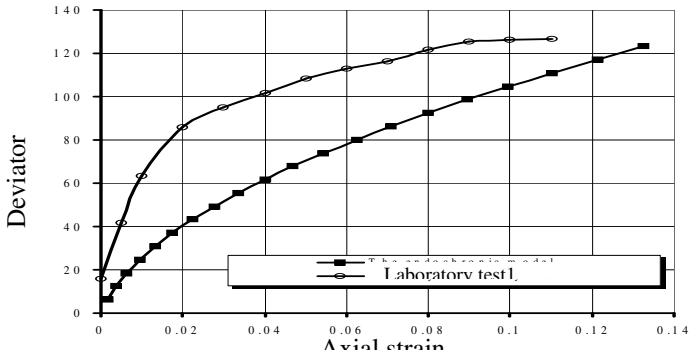

Fig.(7). - A comparison between the stress-strain relationship predicted by the endochronic model with laboratory tests of Al – Saady, Test 1, Series D.

Fig. (8) - A comparison between the stress-strain relationship predicted by the endochronic model with laboratory tests of Al – Saady, Test 2, Series D.

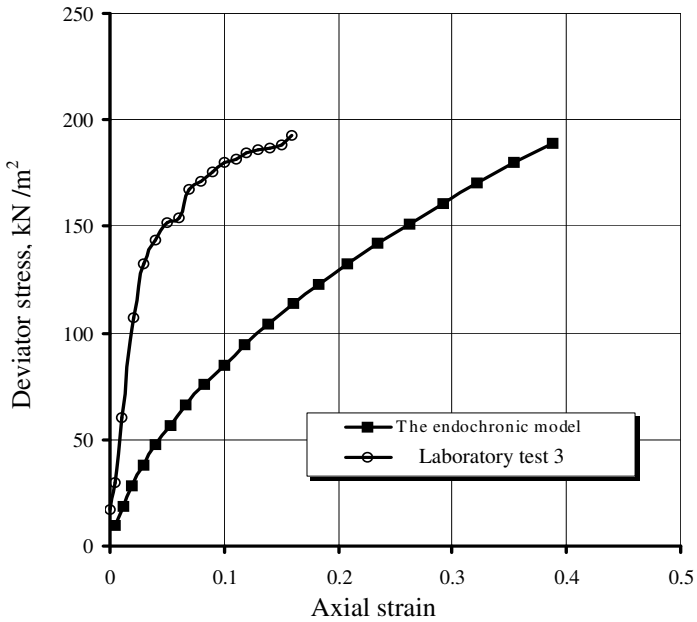

Fig. (9) - A comparison between the stress-strain relationship predicted by the endochronic model with laboratory tests of Al – Saady, Test 3, Series D.

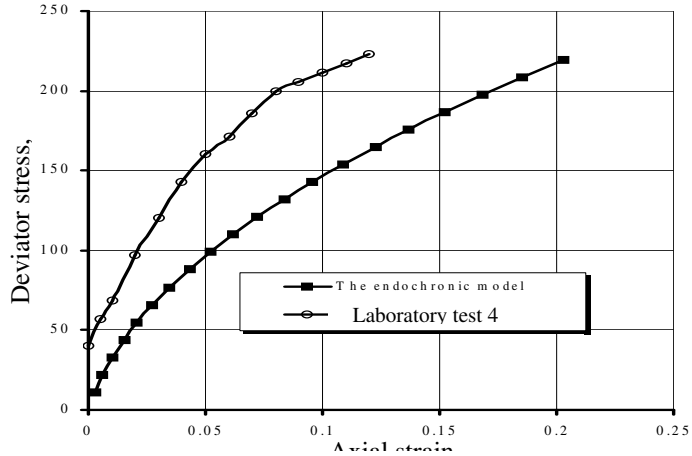

Fig. (10) - A comparison between the stress-strain relationship predicted by the endochronic model with laboratory tests of Al – Saady, Test 4, Series D.

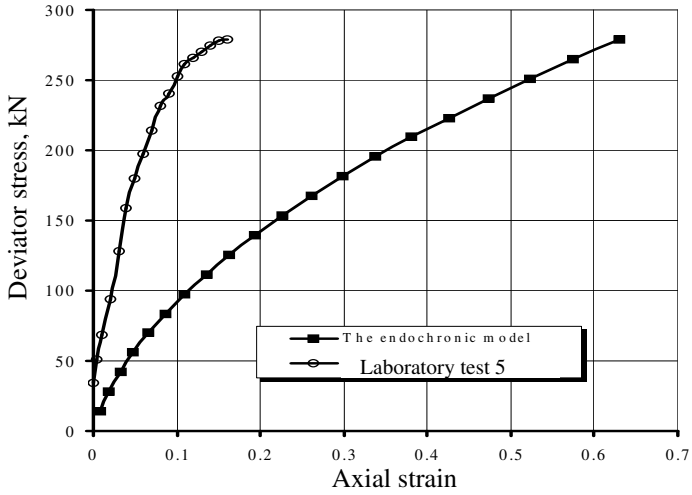

Fig. (11) A comparison between the stress-strain relationship predicted by the endochronic model with laboratory tests of Al – Saady, Test 5, Series D.

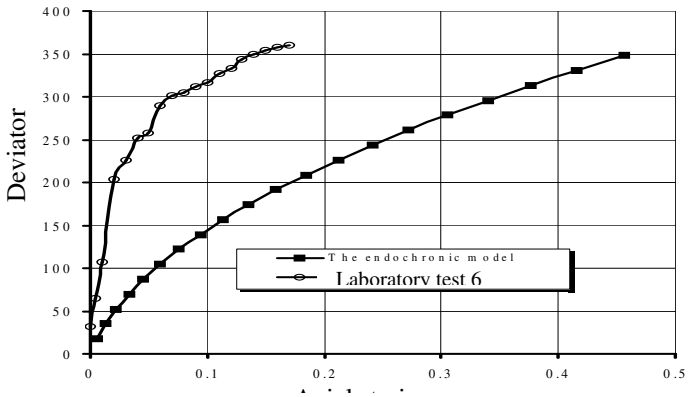

Fig. (12). A comparison between the stress-strain relationship predicted by the endochronic model With laboratory tests of Al – Saady, Test 6, Series D.

Table (4). - The results of series (G), (from Al-Saady, 1989).

Test No.	$\sigma_c^{'}$ kN/m^2	e_o	w_c %	$(\sigma_1-\sigma_3)_f$ kN/m^2	$\left(\Delta V/V_o\right)_f$ kN/m^2
1	79	0.66	23.5	198.87	2.300
2	100	0.69	24.7	281.18	2.283
3	150	0.75	26.0	348.03	3.026
4	200	0.75	27.0	405.03	3.016
5	300	0.69	25.2	752.55	3.590
6	376	0.72	25.0	913.52	3.710

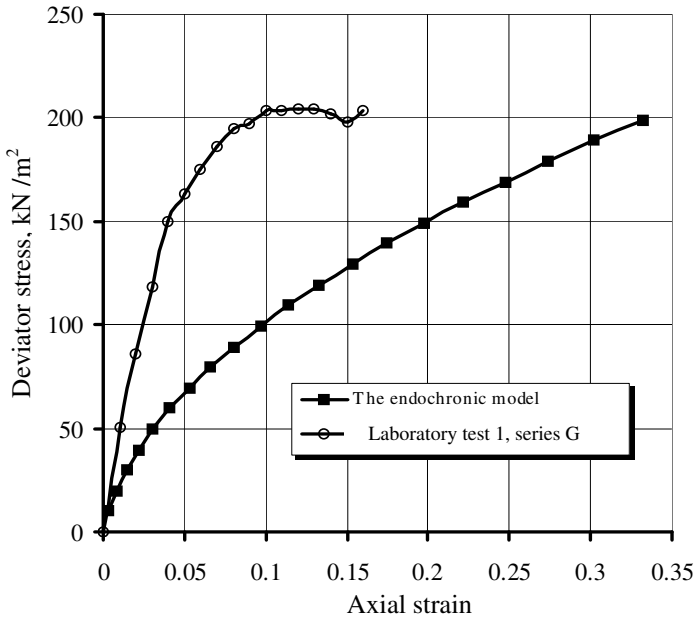

Fig. (13). - A comparison between the stress-strain relationship predicted by the endochronic model with laboratory tests of Al – Saady, Test1, series G.

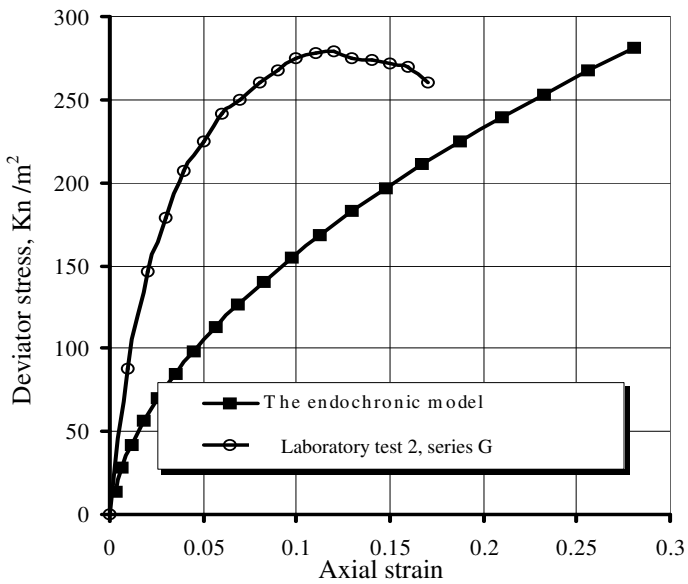

Fig. (14). - A comparison between the stress-strain relationship predicted by the endochronic model with laboratory tests of Al – Saady, Test2, series G.

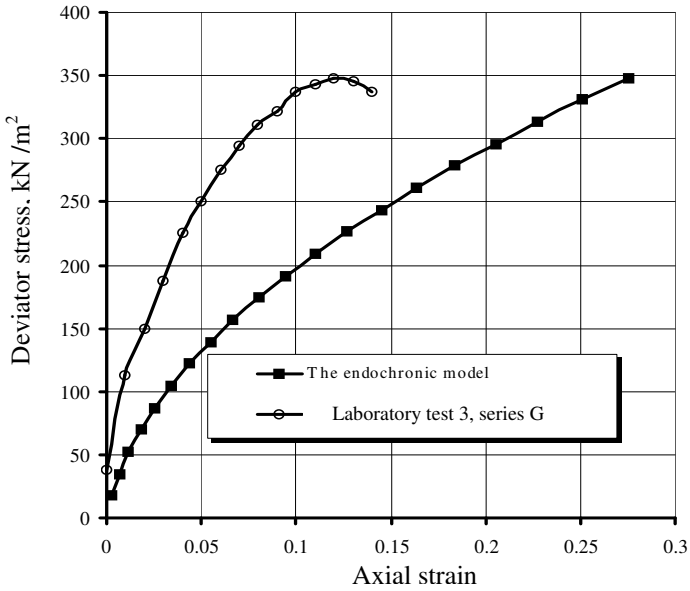

Fig.(15) - A comparison between the stress-strain relationship predicted by the endochronic model with laboratory tests of Al – Saady, Test3, series G.

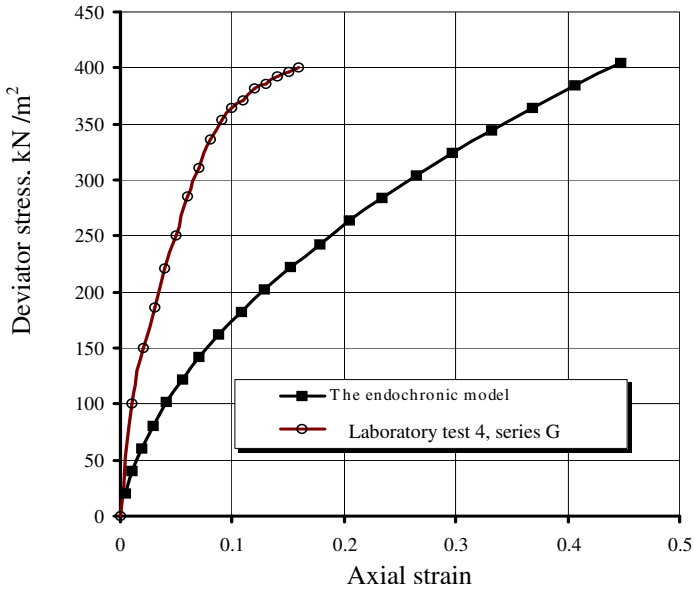

Fig.(16) - A comparison between the stress-strain relationship predicted by the endochronic model with laboratory tests of Al – Saady, Test4, series G.

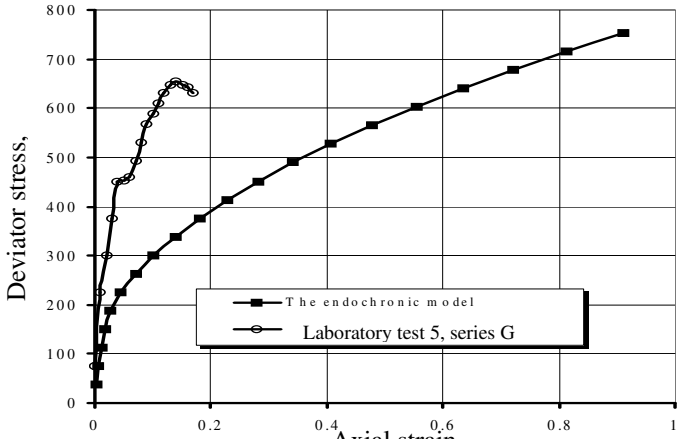

Fig.(17) - A comparison between the stress-strain relationship predicted by the endochronic model with laboratory tests of Al – Saady, Test5, series G.

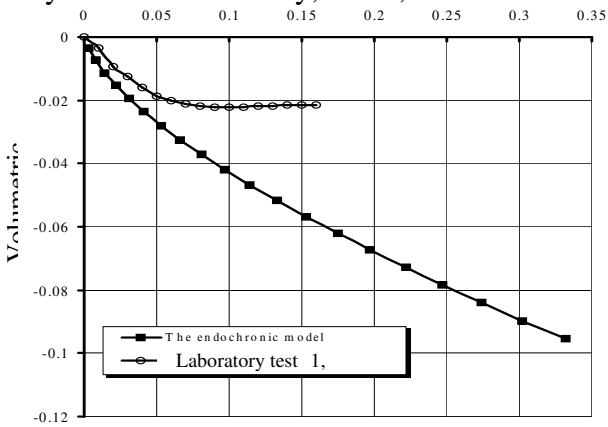

Fig.(18) - A comparison between the volumetric strain – axial strain relationship predicted by the endochronic model with laboratory tests of Al – Saady, Test1, series G.

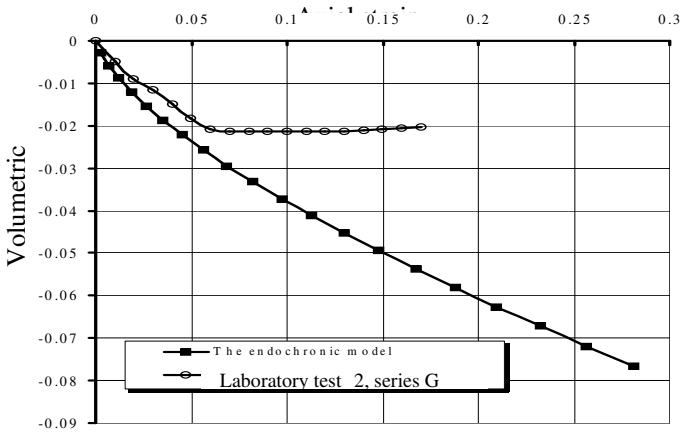

Fig.(19) - A comparison between the volumetric strain – axial strain relationship predicted by the endochronic model with laboratory tests of Al – Saady, Test2, series G.

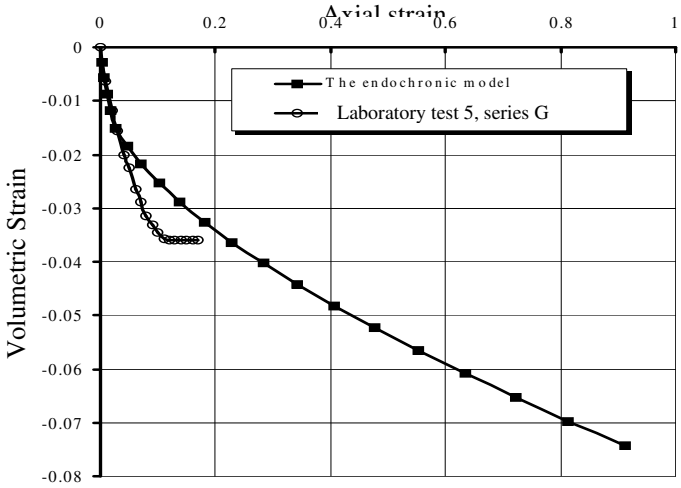

Fig.(20) - A comparison between the volumetric strain – axial strain relationship predicted by the endochronic model with laboratory tests of Al – Saady, Test3, series G.

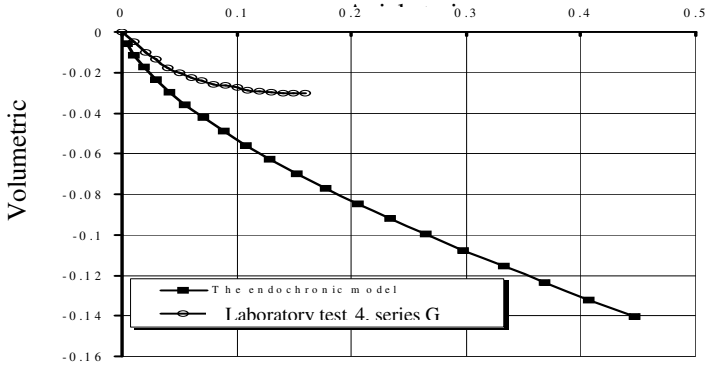

Fig.(21). - comparisons between the volumetric strain – axial strain relationship predicted by the endochronic model with laboratory tests of Al – Saady, Test 4, series G.

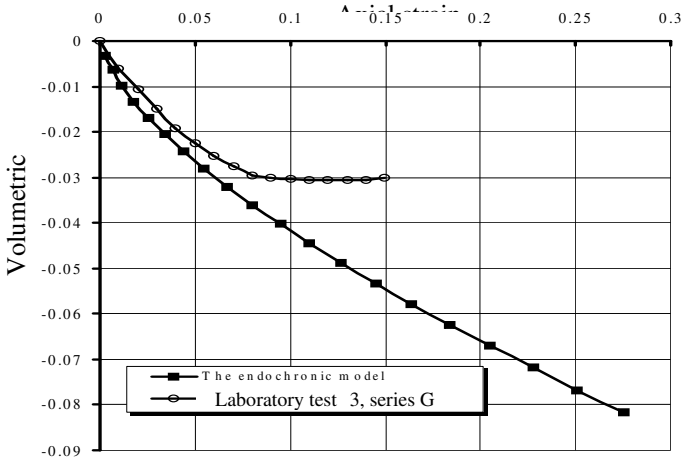

Fig.(22) - A comparison between the volumetric strain – axial strain relationship predicted by the endochronic model with laboratory tests of Al – Saady, Test 5, series G.

The same behaviour is noticed in this clay. The predicted volumetric strains are closer to measured strains under small stress increments. At large stresses, the predicted strains became larger.

CONCLUSIONS:

1- The endochronic model overestimates the strains for all the cases simulated under high stress increments.

2- There is no definite yield point can be obtained when simulating the laboratory tests. This means that this model can be adopted for normally consolidated clays where ductile behaviour of the stress-strain is expected.

3- The error in simulation may be attributed to the model parameters, which need to be evaluated by carrying out parametric study for Iraqi clays.

REFERENCES:

- Al-Mufty, A. A. E., (1990). (Analysis of Stress Deformation Behaviour of Fao Soil), M.Sc. thesis, Civil Engineering Department, University of Baghdad.
- Al- Saady, N. H., (1989). (Analysis of an A-6 Soil During Construction of Road Embankment), M.Sc. thesis, Civil Engineering Department, University of Baghdad.
- Ansal, A. M., Bazant, Z. P. and Krizek, R. J., (1979). (Viscoplasticity of Normally Consolidated Clays), Journal of Geotechnical Engineering, ASCE, Vol. 105, No. GT4, p.p. 519 – 537.
- Bazant, Z. P. and Bhat, P. D. (1976). (Endochronic Theory of Inelasticity and Failure of Concrete), Journal of Engineering Mechanics, ASCE, Vol. 102, No. EM4, p.p. 701 – 722.
- Bazant, Z. P., Ansal, M. and Krizek, R. J., (1979). (Visco-Plasticity of Transversely-Isotropic Clays), Journal of Engineering Mechanics, ASCE, Vol. 105, No. EM5, p.p. 549 – 565.
- Mitchel, J. K. (1993). (Fundamentals of Soil Behaviour), Second Edition, John Wiley and Sons.
- Valanis, K. C., (1971). (A Theory of Viscoplasticity without a Yield Surface – Part I: General Theory, Part II: Application to Mechanical Behaviour of Metals), Archieves of Mechanics, Vol. 23, No. 4, p.p. 517 – 551, Warszawa.

NOTATION:

$d\in_{ij}$	Strain increments
dt	Time increments
P	Coefficient matrices
J_2	second deviatoric strain increment invariant
I_1	first strain increment invariant
de_{ij}	deviatoric strain increment tensor
δ_{ij}	Kronecker delta
$d\in$	Volumetric strain increment
z_1, τ_1	Constants
$d\xi$	damage measure
$d\zeta$	deformation measure
$d\lambda$	inelastic dilatancy
S_{ij}	deviatoric stress tensor
σ_m	mean stress
G	shear elastic moduli
K	bulk elastic moduli
$d\in^o$	stress-independent inelastic strains
$d\sigma_{ij}$	The stress increments
D_{ijkl}	elastic coefficient matrix
$d\in^e_{ij}$	elastic strain increments
$f(\eta)$	Strain-hardening function.
$F(\sigma,\in)$	Strain-softening function.
$\boldsymbol{I}_1^{\sigma}$	effective confining stress
$\boldsymbol{I}_1^{\varepsilon}$	the volume change
$\boldsymbol{J}_2^{\varepsilon}$	the second deviatoric strain invariant
a's	material constants
Pa	atmospheric pressure
β_1	constants
c's	material constants
β_2	softening coefficient
e_o	initial void ratio
ε_v	volumetric strain
n	porosity
b's	constants
Po	consolidation pressure
C_o	densification coefficient
E	elastic modulus
I_L	the liquidity index of the clay
w_{ant}	natural water content.
w_p	plastic limit
I_p	plasticity index
w_L	liquid limit.

EFFECT OF COMPACTION ON THE BEHAVIOUR OF KIRKUK GYPSEOUS SOIL

Dr. Yousif Jawad **M. Abdul Jabbar**

ABSTRACT

The purpose of the present work is to investigate the effect of compaction on the behaviour of gypseous soil. A testing program carried out to study the geotechnical properties and the behaviour of gypseous soil (gypsum content χ = 37% & 56%) taken from Kirkuk city.

The tests include classification tests, chemical tests, X-ray diffraction analysis, compaction characteristics, compressibility & collapsibility, California Bearing Ratio (CBR) & shear strength tests.The effect of dry unit weight, water content, compactive efforts, relative compaction & soaking on the engineering properties of the soil tested are included in the program. All tests were carried out using Standard and Modified Proctor.

Based on the results, several conclusions have been obtained. The soil compacted at the dry side of optimum tends to collapse upon soaking while the soil compacted at the wet side of optimum tends to swell . The percent of swelling for soil with χ =37% is more than that with χ =56%.

Through the observation of shear strength test results, for the two compactive efforts and the two types of gypseous soil,the cohesion(c) increases with decreasing gypsum contents.The angle of internal friction (φ) decreases with increasing moulding water content and increases with increasing gypsum contents.The soaked CBR values increase with increasing compactive efforts and gypsum content.

الخلاصة

الغرض من هذا البحث هو التحري عن تأثير الرص على تصرف التربة الجبسية. وقد تضمنت الفحوص المختبرية برنامج لدراسة الخصائص الجيوتكنيكية والسلوك الهندسي للتربة تحت الدراسة بمحتوى جبسي% 37 و56% مأخوذة من مدينة كركوك. هذا وقد اشتملت الفحوص تصنيف التربة والفحوص الكيميائية وتحليل انحراف الاشعة السينية وخصائص الرص وفحوص الانضغاطية والانهيارية و نسبة التحمل الكاليفورني CBR وفحوص مقاومة القص .وتضمن البرنامج ايضاً دراسة وحدة الوزن الجاف والمحتوى المائي و جهد الرص والرص النسبي والغمر على الخصائص الهندسية للترب المفحوصة,و قد جرت كل الفحوص باستخدام بروكتور القياسي والمحسن.

وعلى ضوء النتائج فقد تم الحصول على استنتاجات عديدة .لوحظ أن الترب المرصوصة بمحتوى مائي الى الجانب الجاف تكون معرضة للانهيار عند غمرها بالماء بينما الترب المرصوصة بمحتوى مائي الى الجانب الرطب تكون معرضة للانتفاخ .كما و ان النسبة المئوية للانتفاخ للترب بمحتوى جبسي % 37 كانت اكثر من تلك ذات المحتوى الجبسي% 56 .

من خلال ملاحظة نتائج فحوص مقاومة القص ,نستنتج أنه لكل من جهديّ الرص وكلا النوعين من التربة الجبسية , التماسك يزدادمع نقصان نسبة الجبس.أما زاوية الاحتكاك الداخلي فتقل مع ازدياد المحتوى المائي وتزداد مـــع ازديـــاد نـــسبة الجبس. لوحظ ان قيم نسبة التحمل الكاليفورني المغمورة تزداد مع ازدياد جهد الرص ونسبة الجبس.

KEY WORDS

standard compaction, modified compaction, optimum, water content, maximum dry unit weight, gypsum content, cohesion, angle of friction,collapse potential, and CBR.

INTRODUCTION

Soil compaction is the process where by soil particles are constrained to pack more closely together through a reduction in the air voids ,generally by mechanical means, **Ingles and Metcalf(1972)**.

Gypseous soil is that soil which contains enough gypsum($CaSO_4.2H_2O$) to interfere with engineering construction .It is the worst among the problematic soils as it contains soluble salt and its chemical reactions.Gypseous soil in Iraq constitutes (11 to 15)% of the area of Iraq. Many major projects suffered from several problems related to construction on or by gypseous soils such as cracks, tilting, collapse and leaching the soil, **Mahdi(2004).**

Proper construction of gypseous soil embankment essentially requires a careful and slow process of compaction control since it involves a prior selection of proper fill borrow areas which have the potential contractual degree of compaction.The compaction control of gypseous soils also requires the slow heating in temperature ranging between (60-80)°C for 48 hrs ,instead of 24 hrs for non gypseous soils, **Al-Khafaji(1997).**

MATERIALS USED:

To achieve the purpose of this study, natural gypseous soil of two different percentages of gypsum (37%,56%) was taken from Kirkuk city.The chemical properties of these samples are shown in **Table (1).**

Table (1). Chemical Properties of Soils

Chemical composition, %	K1 (χ=37%)	K1 (χ=56%)
Al_2O_3	5.9	4.96
CaO	21.98	25.2
SO_3	13.8	22.6
Gypsum content	37	56
Cl^-	0.088	0.096
pH	7.8	7.8

The components of the minerals for each type of saline soil are given in **Table (2).** It can be noted that gypsum, quartz, calcite, and Palygroskite are the predominated minerals in the soils.

Table (2). Mineralogical composition of soils

Soil Type	Non Clayey Mineral	Clayey Mineral
χ=37%	Gypsum, Calcite, Quartz.	Palygroskite
χ=56%	Gypsum, Calcite, Quartz, Dolomite, Feldspar.	Palygroskite

Classification tests were performed first. Physical tests include specific gravity Gs, grain size distribution and Atterberg limits. Standard and modified compaction tests were carried out to determine the moisture-density relationships.Series of engineering tests were conducted on compacted samples. The tests performed include standard oedometer test, double oedometer test, triaxial and CBR tests.
The physical and compaction characteristics are given in **Table (3)**.

Table (3). Summary of physical and classification tests results.

Soil Property	Soil Designation	
	K1	K2
Gypsum Content,%	37	56
Specific gravity	2.51	2.46
Liquid limit,%	29	29
Plasticity Index,%	8	7
%Sand	82.31	77.18
%Fines	17.66	22.82
Moisture-density relations (D698) Optimum water content (%) Maximum dry unit weight(kN/m3)	13.5 17.73	13.85 17.6
Moisture-density relations (D1557) Optimum water content (%) Maximum dry unit weight(kN/m3)	10.75 18.75	9 18.8
Soil Classification According to ASTM D 2487	SM	SM

PREPARATION OF COMPACTED SAMPLES:

The following procedure was adopted in preparing the compacted soil samples for the oedometer and collapse tests. The soil was compacted using standard and modified Proctor procedure, and then the compacted samples were extruded from compaction mould by pushing the test ring to the required thickness. The faces were leveled after trimming

A manufactured hammer was adopted to carry out the preparing of compacted soil samples for triaxial shear tests. A hammer of 1.9 cm diameter, 500 gm mass and 30 cm drop as shown in **Plate (1). Table (4)** shows the required number of blows that gives the same compactive effort of the standard and modified compactive effort. The drop height, weight of hammer and number of blows were determined on the basis of the standard and modified compactive efforts.

.

Plate (1). Manufactured hammer.

Table (4). Corresponding compactive efforts in the manufactured hammer.

Type of compaction	No. of blows / layer in the compaction mould	Compactive effort, CE in compaction mould ($kN.m/m^3$)	No. of blows / layer in manufactured mould	Compactive effort, CE in manufactured mould ($kN.m/m^3$)
Standard compaction	25 blows (*3 layers*)	593.7	3 layers (*2 of them compacted @12 blows and the other @ 11 blows*)	597.525
Modified compaction	25 blows (*5 layers*)	2710	5 layers (*4 of them compacted @ 32 blows and the other @ 31 blows*)	2714.48

* Compaction Mould of 4 " diameter.

COMPRESSIBILITY TESTS:

A series of Oedometer tests were carried out using standard back loading Oedometer. The sample size used 50 mm in diameter by 19 mm in height.

The series of Oedometer tests include two tests as follows:

Standard consolidation tests:

These tests were carried out on compacted samples to determine the compressibility characteristics. These tests were performed on samples prepared at different water content and dry unit weights of the standard and modified compaction tests.

Double Oedometer Tests:

This test was conducted according to **Jennings & Knight (1957)**. In this test, two samples were tested. The first one was loaded at its initial water content throughout the test without addition any water (dry test). Precautions were taken to minimize the evaporation of water from specimen by covering the cell with a nylon bag. The other sample was primarily saturated them loaded progressively as in the standard consolidation test. The difference between the two curves quantifies the amount of deformation that would occur at any stress level if the soil to be saturated during it is loading history.

SHEAR TESTS

The purpose of those tests was to investigate the shear strength characteristics of the compacted gypseous soil. Further more the effects of soaking on the strength characteristics were studied.

Triaxial Compression Tests:

To study the effect of water content and dry unit weight on shear strength of the soil tested, Unconsolidated Undrained tests, U-U were conducted on specimens (38 mm in diameter and 76 mm in height) compacted at different water contents and dry unit weights of the standard & modified compaction tests by mean of manufactured hammer .

California Bearing Ratio (CBR) test

Two series of tests were conducted on each soil sample (K1, K2). For the first series, the preparation of specimens and testing procedure were generally in accordance with **AASHTO** T143-81. Three specimens were prepared at optimum water content of the standard compaction test. And compacted in three layers using 2.5 kg hammer dropped from a height of 30.5 cm. Ten, thirty and sixty-five blows per layer were used for compacting the three specimens.

Identified specimens were prepared and testing after soaking in water until the swelling is ended to simulate the effect of saturation on the bearing characteristics.

In the second series, the whole program was repeated on specimens prepared at optimum water content of the modified compaction test and compacted in five layers using 4.5 kg hammer dropped from height of 45 cm.

In these entire tests, surcharge weights of 4.5 kg, in form of annular steel rings, were placed on the top surface of the prepared specimens before testing. The surcharge simulates the effect of the thickness of road construction overlaying the layer being tested.

RESULTS AND DISCUSSION:

Grain size distribution:

Table (5) shows the grain size distribution data. This table revealed that both soils with gypsum content χ=37%, χ=56% consist of coarse, medium and fine sand. The data for both soils reflects a significant difference between the dry and wet sieving by water, with respect to soil with

gypsum content equal 37% the dry sieving showed only 13.84% fines while the wet sieving or natural specimen results in 70.02% fines.

The variation in the grain size distribution by both techniques (dry andwet by water) is attributed to the cementing agent (gypsum), which softens or dissolves in water, **Ismael and Mollah (1998).**

However, depending on either dry or wet sieving by kerosene, the soils can be classified according to **ASTM** D 2487 as (SM), i.e., silty sand.

Table (5). Results of Sieve Analysis.

Sample Type		Sieving method	Gravel (>4.75) mm	Coarse (2-4.75) mm	Medium sand (0.427-2) mm	Fine sand (0.075-0.425) mm	Silty clay (<0.075) mm	Specific gravity Gs
χ =37%	Natural	Dry	0.04	11.15	42.61	32.36	13.84	-
	Natural	Wet (water)	0	0.64	8.7	20.63	70.02	2.49
	Natural	Wet (kerosene)	0.03	10.93	38.59	32.79	17.66	2.51
χ =56%	Natural	Dry	0	2.52	42.28	30.52	24.69	-
	Natural	Wet (water)	0	0.25	12.38	20.46	66.91	2.47
	Natural	Wet (kerosene)	0	2.48	42.53	32.17	22.82	2.46

COMPACTION TESTS:

Relationships between dry unit weight and water content for the tested soil are shown in **Fig. (1)** for compactive efforts associated with the modified and standard Proctor.It is noticed that the standard maximum dry unit weight of the soil with gypsum content χ =37% is somewhat higher than the standard maximum dry unit weight of the soil with gypsum content χ=56%, while the opposite is true for modified compaction test as shown in **Fig. (1)**.

This behaviour may be explained by the role of gypsum in the soil as stated by **Al-Mufty (1997).** In other words, the standard compaction curve where specific gravity and cementing of gypsum (both of them decreases as the gypsum content increase which tends to decrease the unit weight) are the predominate factors, while in the modified compaction tests, filling the voids which tends to increase the unit weight with increasing gypsum content is the controlled factor rather than the other two factors (specific gravity and cementing of gypsum).

It can be concluded from the water-unit weight relationships, that the test results are depending on the soluble salt content (gypsum content) water content, soil components, the solubility degree of gypsum in water and compactive effort.

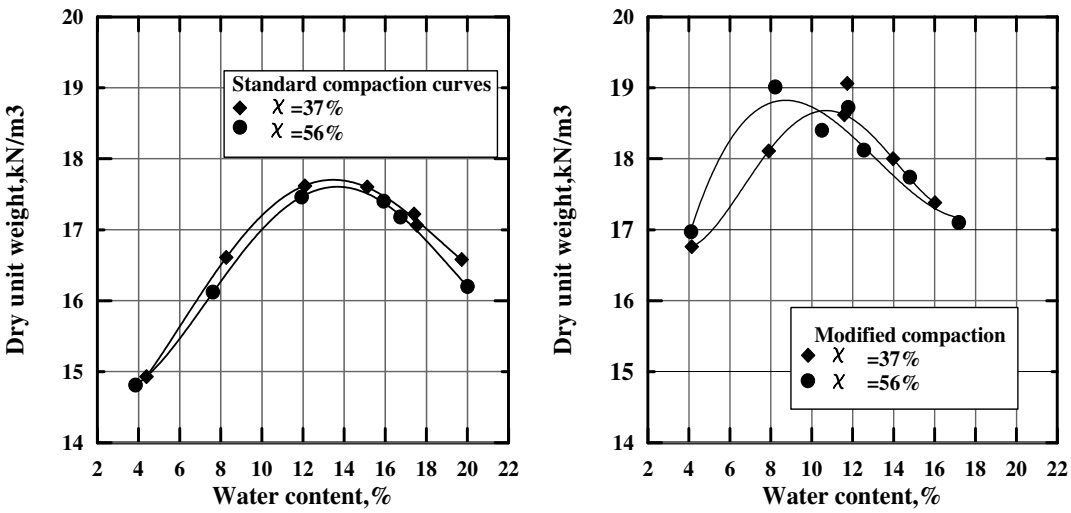

Fig. (1). Compaction curves for χ=37% and χ=56%.

OEDOMETER TESTS:

Compression Tests:

The results are presented as void ratio versus logarithm of vertical pressure and are shown in **Figs (2) and (3)** for all tested specimens.

It can be seen that the shape of e-log pressure curves for compacted samples with gypsum content χ=56% is steeper than the curves of samples with gypsum content χ=37%. This is due to the effect of gypsum content.

Table (6) and **Figs (2)** and **(3)** show the tests results for the two groups. It is noticed from **Table (6)** that compression index increased for soaked specimens. This is due to soften and dissolve of gypsum.

Double Oedometer:

The effect of compaction on the collapse behaviour of the tested soil was investigated by conducting the double oedometer test. To give a clear picture of tests results, collapse potential, CP, % for both gypsum contents and both compactive efforts as a function of moulding water content for all vertical pressures are plotted as shown in **Figs (4) to (5).**

Table (6). Results of compression tests.

Soil type	Compaction	As compacted specimens					Soaked specimens				
		γd kN/m^3	w.c %	e_o	Cc	Cr	γd kN/m^3	w.c %	e_o	Cc	Cr
χ=37%	Standard	17.73	13.5	0.416	0.128	0.024	17.73	13.5	0.416	0.1	0.020
		17.46	11	0.437	0.161	0.021	17.46	11	0.437	0.173	0.023
		17.46	16.1	0.437	0.131	0.026	17.46	16.1	0.437	0.134	0.023
		16.5	8	0.52	0.171	0.0193	16.5	8	0.52	0.146	0.022
	Modified	18.75	0.75	0.339	0.156	0.024	18.75	10.75	0.339	0.071	0.029
		17.46	6.25	0.437	0.134	0.023	17.46	6.25	0.437	0.128	0.028
		17.46	15.75	0.437	0.203	0.01	17.46	15.75	0.437	0.125	0.011
		18.125	8	0.385	0.116	0.019	18.125	8	0.385	0.111	0.027
χ=56%	Standard	17.6	13.85	0.396	0.11	0.017	17.6	13.85	0.396	0.095	0.022
		17.46	11.6	0.4078	0.1	0.019	17.46	11.6	0.408	0.164	0.023
		17.46	16	0.7078	0.133	0.017	17.46	16	0.408	0.166	0.019
		16.25	8	0.513	0.181	0.016	16.25	8	0.513	0.17	0.025
	Modified	18.8	9	0.307	0.097	0.027	18.8	9	0.307	0.091	0.023
		17.46	4.75	0.4078	0.117	0.025	17.46	4.75	0.408	0.11	0.028
		17.46	15.5	0.4078	0.137	0.022	17.46	15.5	0.408	0.199	0.037
		18.75	8	0.311	N.D	N.D	18.75	8	0.311	N.D	N.D

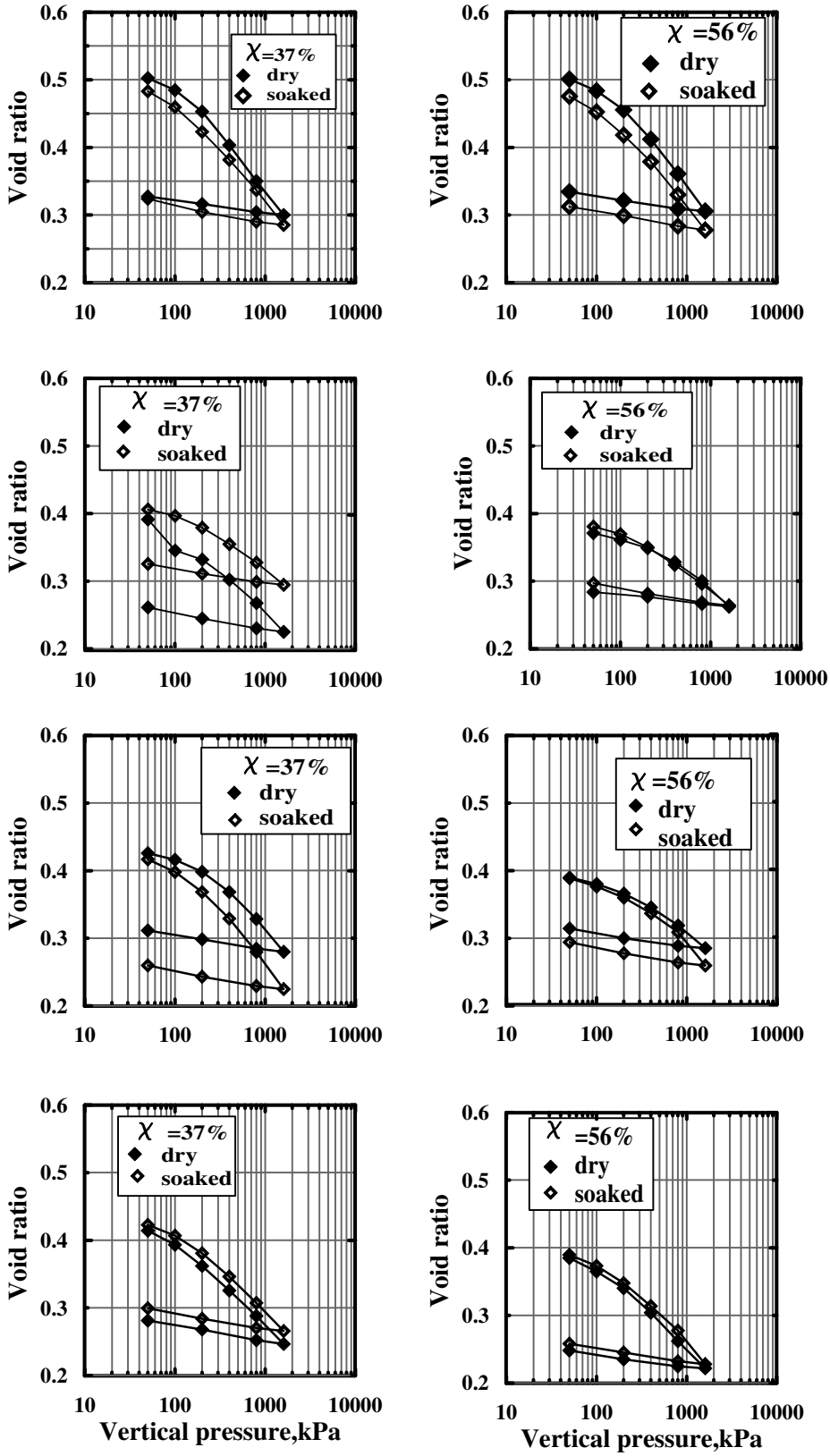

Fig.(2). Compression curves for soil samples of standard compaction at: (a) w.c=8%, (b) dry side, (c) optimum water content, (d) wet side.

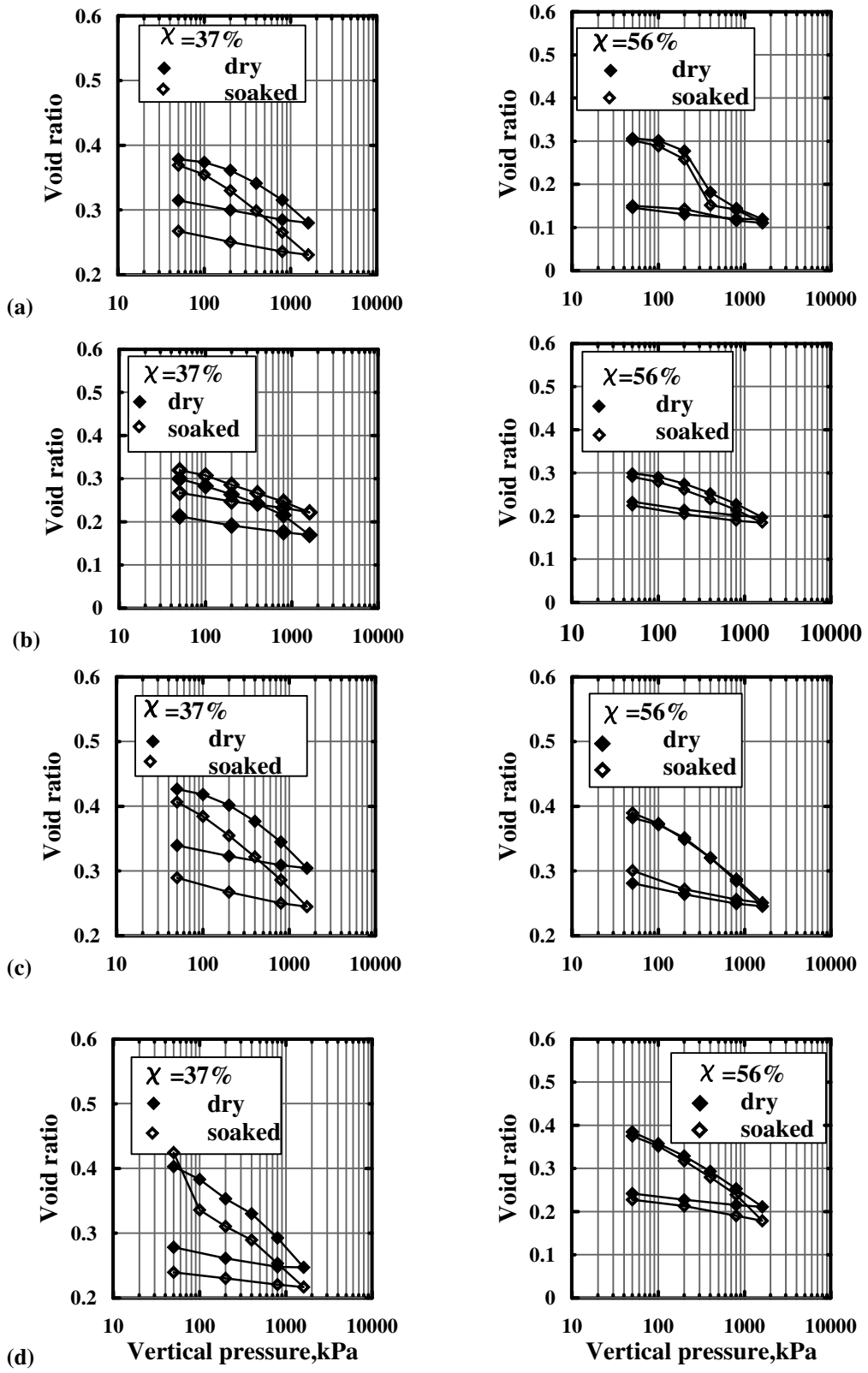

Fig. (3). Compression curves for soil samples of modified compaction at: w.c=8%, (b) dry side, (c) optimum water content, (d) wet side

From these figures, in general, the trend of the tested samples were found to collapse from dry side of optimum for both gypsum contents and both compactive efforts until it reached the optimum water content the trend was changed to swell where the swelling is higher for samples of gypsum content 37%. This behaviour can be explained as follows: as the water enters the soil void leads to soften the cementing bonds that took place in term of collapse potential. Collapse potential increased with a decrease in gypsum content. This may be attributed to the effect of sand-silt mixture, as the amount of silt size particles become angular in shape due to crushing of sand by compaction. As a result of that, the collapse decreased. This behaviour was noticed by **Assallay, Rogers and Smalley (2004).** They found that higher collapse values were obtained when the angular silt fraction was replaced with smooth, spherical glass balls thus confirming that the geometrical properties of the silt particles have a significant effect on the hydro collapse behaviour of loess deposits.

As the water content increased, the role of Palygroskite will begin in term of swelling which increased then decreased. The swelling can occur when anhydrous calcium sulphate imbibes water ,**Abduljawad (1994).**This process of gypsification refers to the addition of water crystallization to the mineraland is associated with a volume increase of up to 62%,**Blatt et al.(1980).** The swelling was noticed to increase as the gypsum content decreased. This phenomenon could be attributed to the effect of gypsum in limiting the amount of swelling at higher water content as reported by **Bridge and Tunny (1973).** They explained this effect to the replacement of ions in the clay mineral by the calcium on the clay exchange sites.

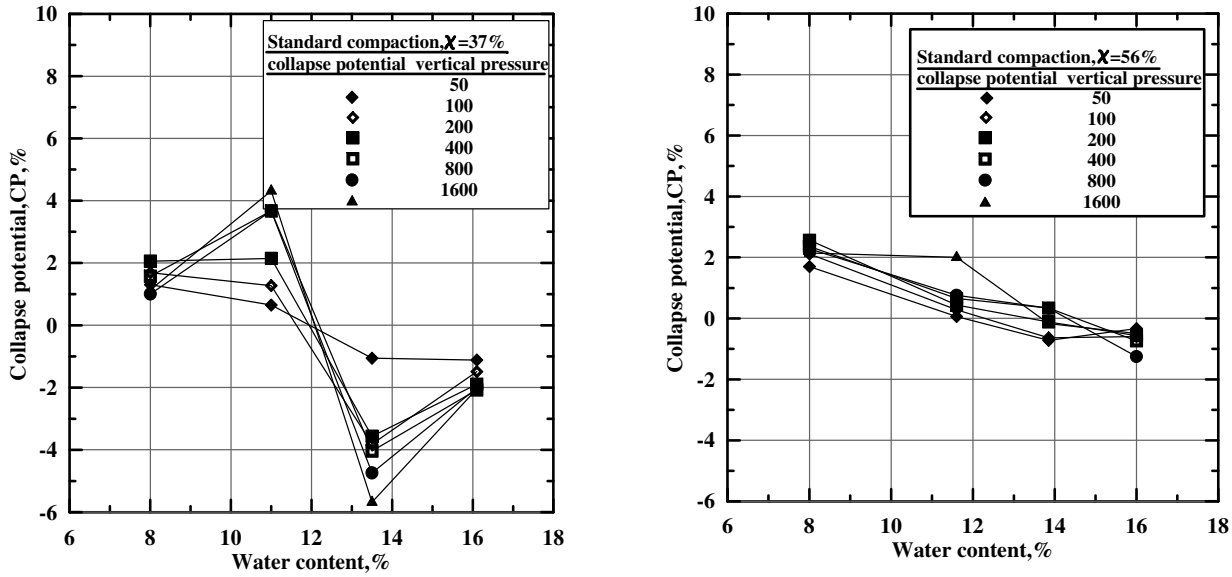

(a) (b)

Fig. (4). Influence of moulding water content on collapse potential from double oedometer of compacted soil specimens: (a) χ =37% (b) χ =56% of standard compaction.

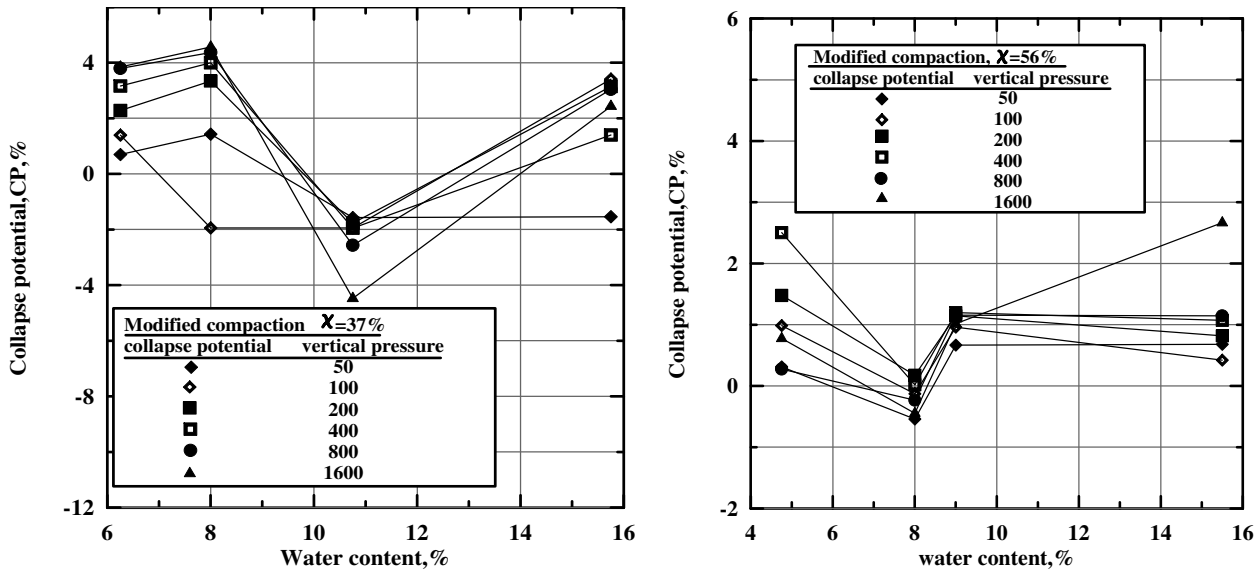

(a) (b)

Fig. (5). Influence of moulding water content on collapse potential from double oedometer of compacted soil specimens: (a) χ =37%, (b) χ =56% of modified compaction.

SHEAR STRENGTH CHARACTERISTICS:

Triaxial Compression Tests:

Different dry unit weights and moulding water contents of the standard and modified compaction tests were adopted to obtain a complete picture of effect compactive effort on shear behaviour of the tested gypseous soils.

Fig.(6) shows the shear strength parameters cohesion c and angle of internal friction φ as a function of compactive effort for both gypsum contents. From the results, the following can be observed:

a- The cohesion c increased as the compactive effort increased for both gypsum content.

b- The angle of internal friction **φ** also increased with an increase in compactive effort for both gypsum content with a decrease in moulding water content.

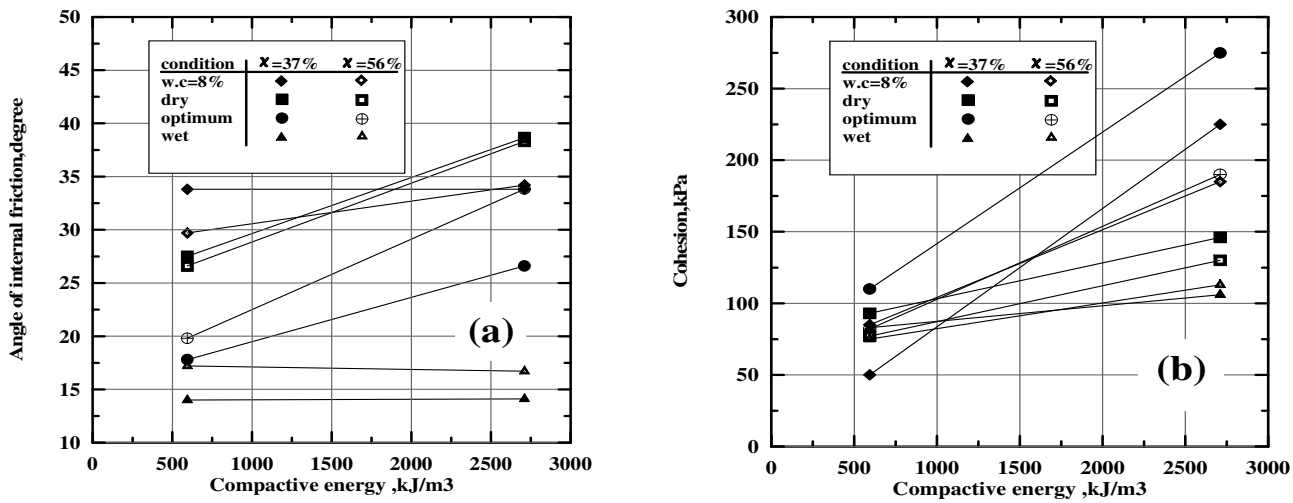

Fig. (6). (a) Angle of internal friction, (b) cohesion versus compactive energy.

To show a clear picture of effect moulding water content on shear strength parameters c and φ, **figs (7)** and **(8)** are plotted.

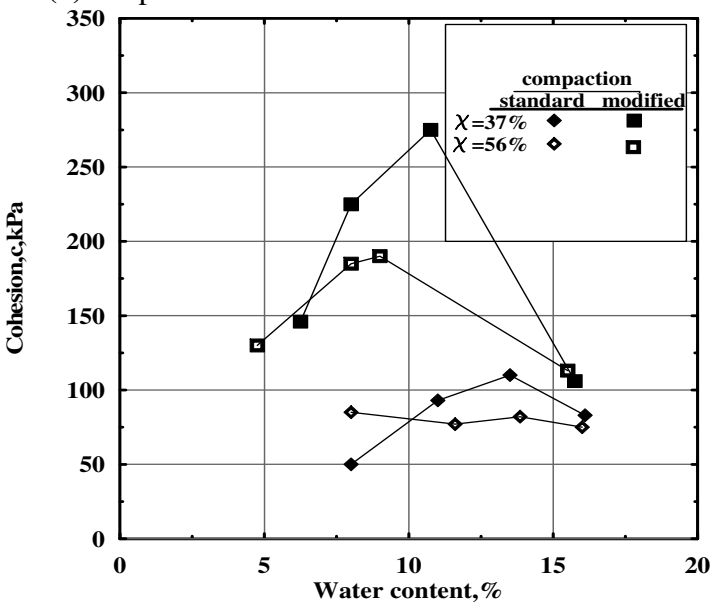

Fig. (7). Relationship between cohesion and moulding water content of soil tested.

Fig. (7) shows that the cohesion c increased with increasing compactive effort and decreased with increasing gypsum content. The increase in cohesion for all compactive efforts and gypsum content with increasing moulding water content till it reaches a maximum value at optimum water content then tends to decrease in similar manner of compaction curve.

As the cohesion which is due to internal forces holding soil particles together in a solid mass so, as the gypsum content increased, the generated crystal formation pressure in the pore spaces increased leading to rupture of primary and newly bond, as a result of which cohesion is reduced.

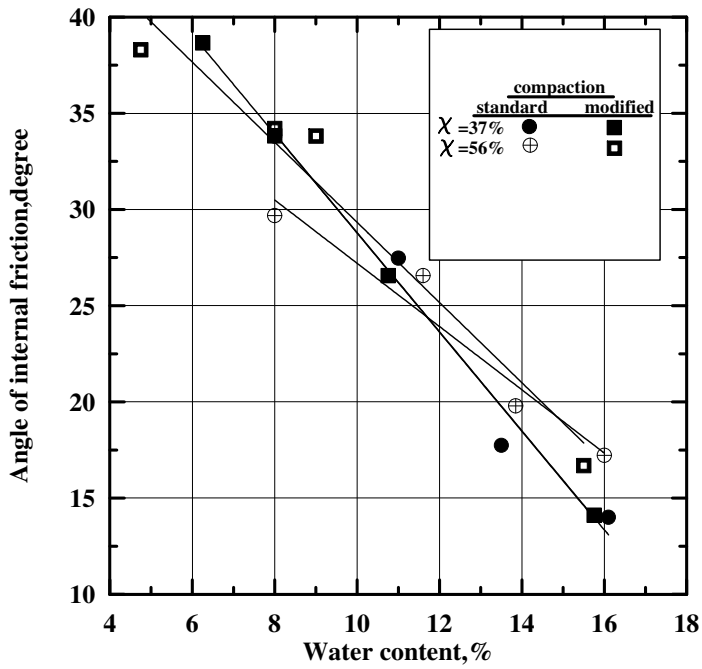

Fig. (8). Relationship between angle of internal friction and moulding water content of soil tested.

Examining **Fig.(8)** revealed that the angle of internal friction decreased with increase moulding water content because water acts as a lubricant reducing friction and minimizing the sliding effect, which leads to reduce the angle of friction. It is also clear that angle of internal

friction increased with increasing gypsum content for both compactive efforts. This may be attributed to the fact that φ increased with increasing coefficient of uniformity *Cu* of the soil, where *Cu*=17 for soil with gypsum content=37% while *Cu*=25 for soil gypsum content=56%. Furthermore, the friction between gypsum particles is greater than mineral components of the soil.

Figs (9.a) and **(9.b)** show the shear strength as a function of moulding water content. From the results, the following can be observed:

a- The shear strength tends to increase with increasing confining pressure for both compactive efforts and both gypsum contents. This increased is somewhat little at wet side of optimum. As seen in compaction curves for both soils (χ=37%and χ=56%), the selected points at wet side of optimum could be considered nearly saturated soils (S=92.35% and S=90.3%for standard and modified compaction tests of χ=37% and S=96.44% and S=93.42% for standard and modified compaction tests of χ=56%). This behaviour can be explained in terms of pore pressure in the saturated soil, the pore water takes up which is a portion of applied load.

b- In standard compactive effort for both gypsum content, shear strength decreases as the moulding water content increased, while in modified compactive effort the shear strength increased as the moulding water content increased until it reached the optimum water content then decreased as the water content increased.

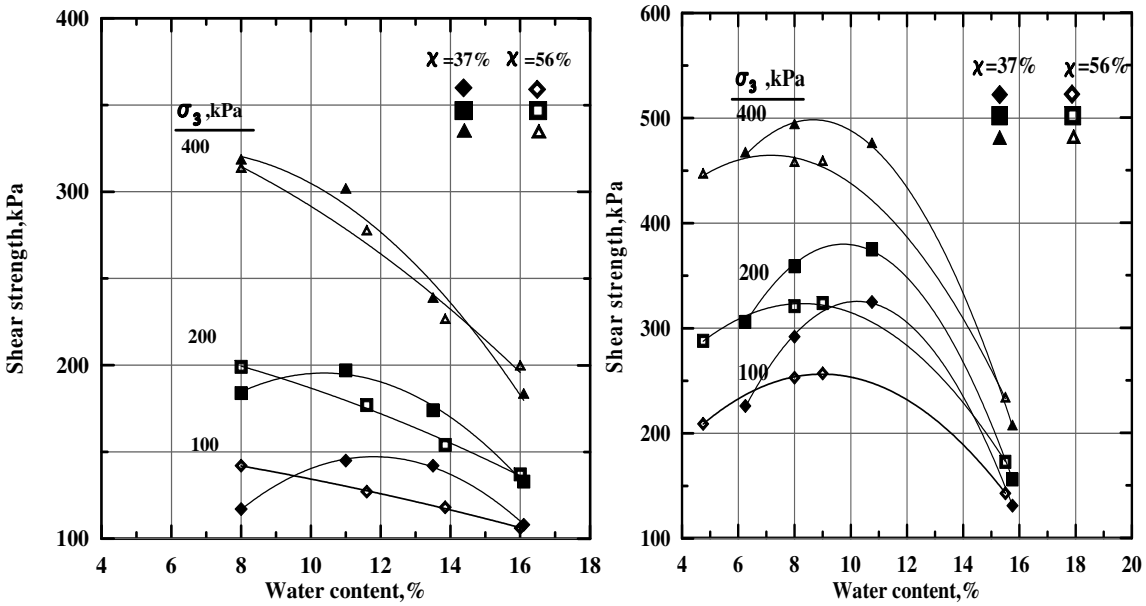

Fig. (9). Influence of moulding water content on shear strength compacted soil samples of χ =37%and χ =56%: (a) standard, (b) modified.

<u>California Bearing Ratio (CBR) Tests:</u>

The tests were performed on samples prepared at optimum water content and compacted to various unit weights. A second series of tests were performed on specimen soaked in water for 4 days to give an indication of strength loss due to saturation and to give information concerning

Soaked CBR values at 2.5 and 5 mm penetration are summarized in **Table (7).**

Table (8). Results of CBR Tests.

Soil type	No. of blows	2.5 kg hammer		4.5 kg hammer	
		CBR @2.5mm penetration	CBR @5.0mm penetration	CBR @2.5mm penetration	CBR @5.0mm penetration
K1 χ =37 %	10	1.133	2.987	4.0	4.13
	30	3.437	2.8557	7.93	8.767
	65	5.589	4.959	10.196	12.024
K2 χ =56 %	10	2.077	1.754	2.832	3
	30	9.479	9.143	7.55	10.52
	65	13.784	14.024	35.876	42.08

It can be seen that CBR values are greater at 2.5 and 5 mm penetration for gypsum content χ =56% than the corresponding values for gypsum content χ =37%. This may be attributed to the gypsum content as this result coincides with the effect of gypsum in reducing the plasticity of the tested soil, since the plasticity index can be considered as a shear index as well **Rodrigues, Castillo and Sowers (1988).** A summary of all CBR soaking test results for both gypsum contents at 2.5 and 5 mm penetration are presented in **Fig. (10).**

The soaked values of CBR are plotted against the number of blows per layer in **Fig (11).** In all cases shown in this figure, CBR values found to increase with increase in number of blows, weight of hammer used and gypsum content. Fifty six blows per layer are generally required to mould CBR specimen to hundred percent of the maximum dry unit weight determined by **ASTM D 678-70 and D 1557-70**, at this number of blows, a soaked CBR values of 5% and 11% are obtained for soil with gypsum content χ =37% whereas, for soil with gypsum content χ =56%, soaked CBR gives high values in the range (12.5 - 34%).

It is worth to mention that at this stage: by relating the soaked CBR values obtained at 100% of the maximum dry unit weight and optimum water content of the standard and modified compactive efforts with the shear parameters cohesion c and angle of internal friction φ that gained from triaxial tests of samples compacted at maximum dry unit weight and optimum water content of the standard and modified compactive efforts for both gypsum content as shown in **Fig. (12).**

From this figure, the cohesion is observed to decrease with increasing soaked CBR values while the angle of internal friction is seemed to increase with increasing soaked CBR values with increasing compactive efforts.

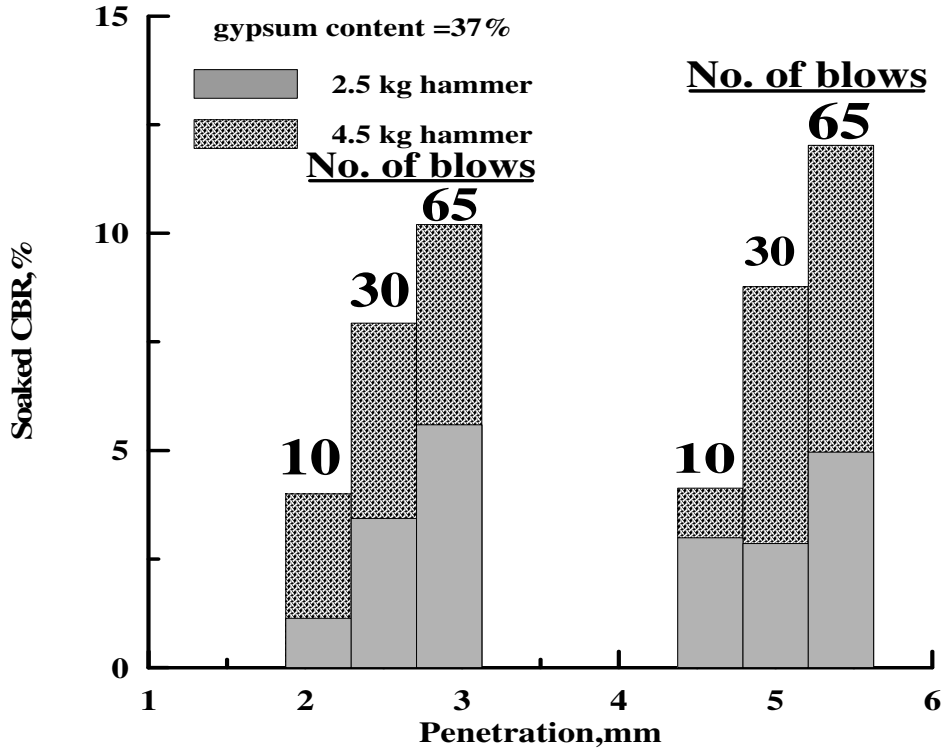

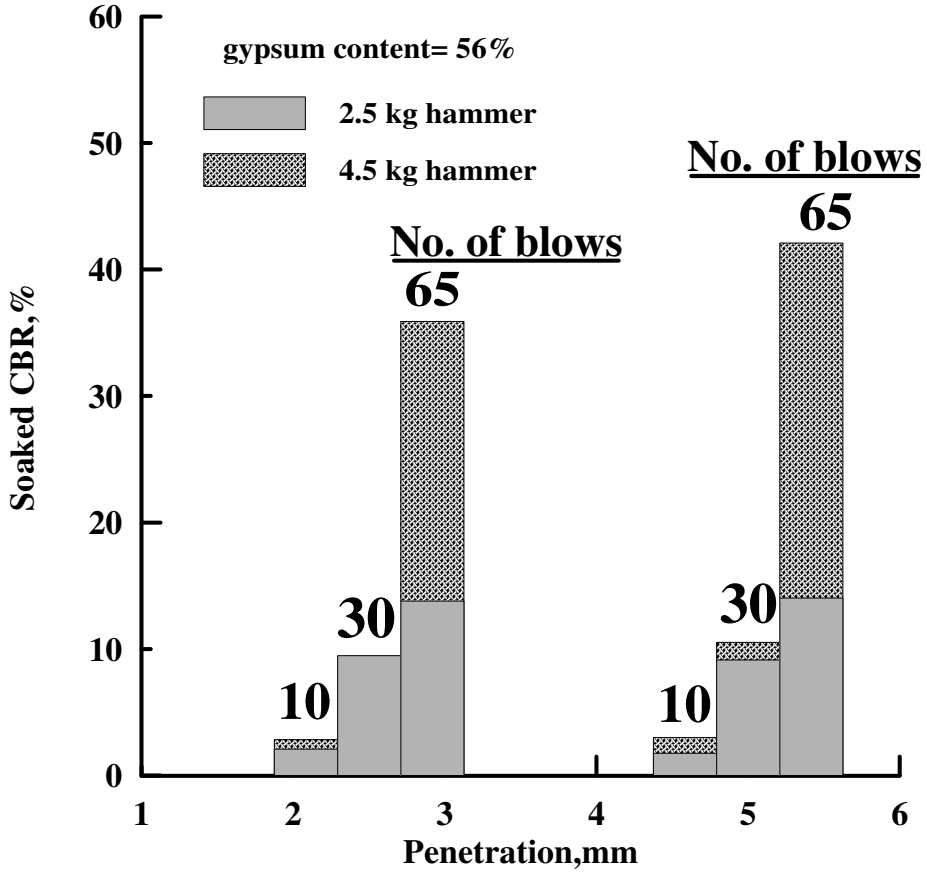

Fig. (10). CBR values at 2.5 and 5 mm penetration for gypsum content: (a) χ =37%, (b) χ =56%.

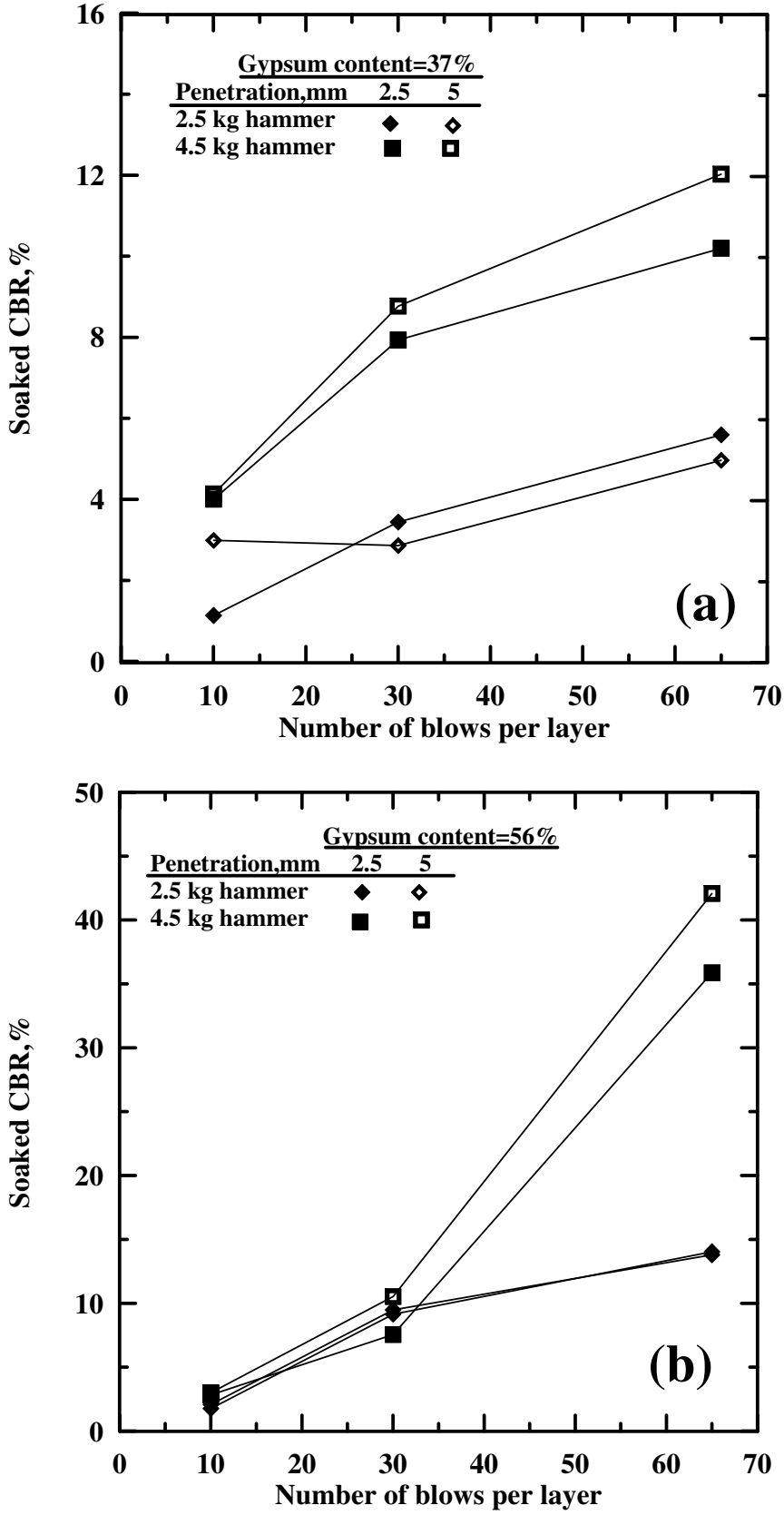

Fig. (11). Number of blows per layer versus CBR: (a) χ =37%, (b) χ =56%.

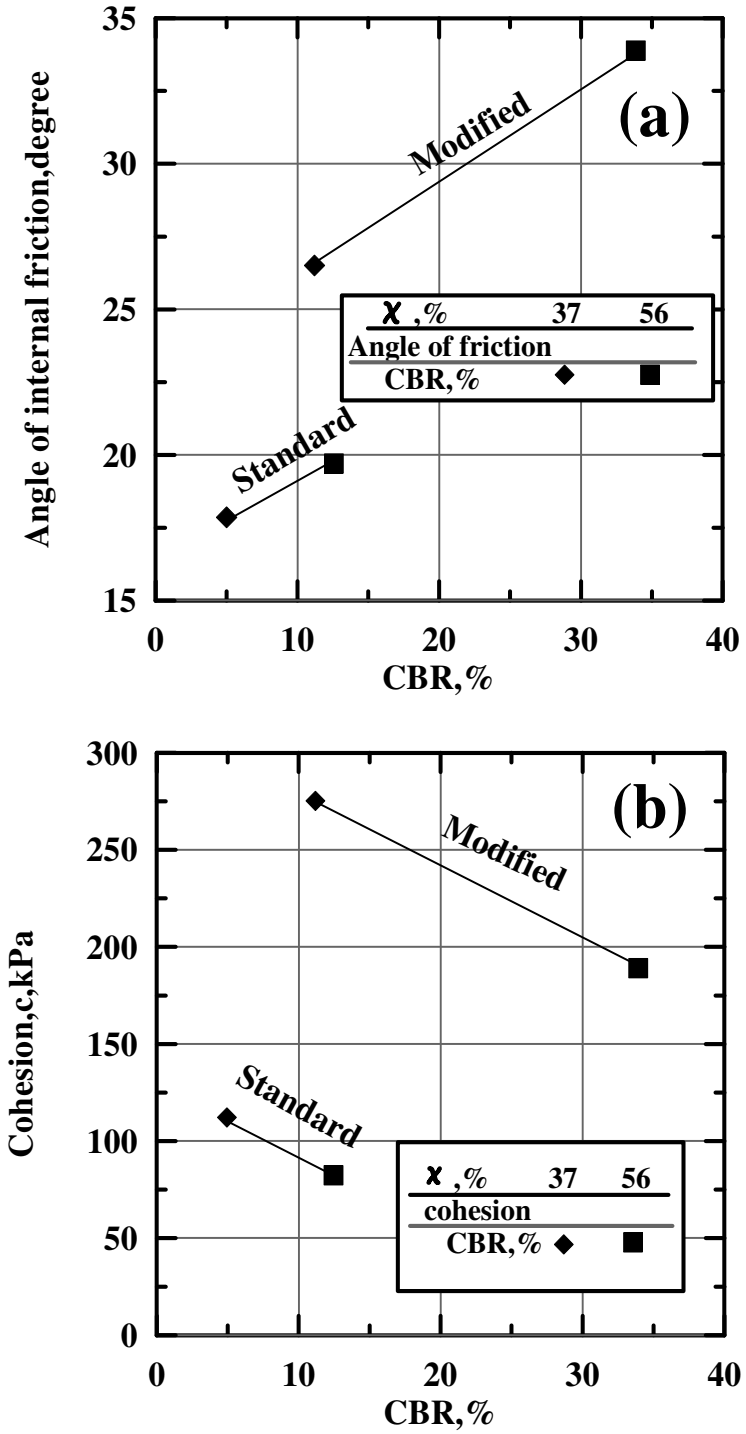

Fig. (12). Variation of shear strength parameters with soaked CBR values: (a) Angle of internal friction, (b) Cohesion.

CONCLUSIONS

A program of laboratory tests was carried out on two types of gypseous soil taken from Kirkuk city. Tests were performed on compacted soil samples using Standard and Modified Proctor. Based on the results, the following conclusions are made:

-With the increase in compactive effort, the maximum dry unit weight increases and the optimum water content decreases for both types of gypseous soil. The percent increase in dry unit weight is 5.75% and 6.82% and the percent decrease in optimum water content is 20.4% and 35.02%for soils with gypsum content χ=37% and χ=56% respectively.

-Compacted soil specimens at dry side of optimum tend to collapse after soaking with water while soil specimens compacted at wet side of optimum tend to swell for both compactive efforts. The percent of swell of soil with χ =37% is more than that with χ =56%.

-Shear strength parameters (***cohesion and friction***) increase with increase in gypsum content. The cohesion (c) increases with the increase in moulding water content till it reaches a maximum value at optimum water content then tends to decrease in a manner similar in shape of compaction curve. This behaviour is independent of compactive effort and gypsum content.

The angle of internal friction (φ) decreases with the increase in moulding water content and with the decrease in gypsum content for both compactive efforts.

- Values of California Bearing Ratio (CBR) at 2.5 mm and 5 mm penetration are higher for soil with gypsum content χ=56% as compared with the corresponding values for gypsum content χ =37%.
- The soaked CBR values increase with the increase in compactive efforts (number of blows, weight of hammer used) and gypsum content.

-The increase in soaked CBR values obtained at maximum dry unit weight and optimum water content were found to be compatible with the increase in angle of friction and decrease in cohesion for both types of compactive efforts.

REFERENCES

- Al-Khafaji, A. (1997): "Densification of Gypseous Soils by Compaction", Ground Improvement Geo Systems London, pp. 96-102.
- Al-Mufty, A. A. (1997): "Effect of Gypsum Dissolution on The Mechanical Behaviour Of Gypseous Soils", Ph. D. Thesis, Civil Engineering Department, College of Engineering, University of Baghdad.
- Ingles, O. G. and Metcalf, J. B. (1972): "Soil Stabilization Principles and Practice" Butter Worths Pty Limited, Australia.
- Ismael, N. F. and Mollah, M. A. (1998): "Leaching Effects on Properties of Cemented Sands in Kuwait", ASCE, Journal of Geotechnical and Goeenvironmental Engineering, Vol. 124, No. 10, pp. 997-1004.
- Jennings, J.E. and Knight, K. (1957): “The addition settlement of Foundation Sandy Subsoil on Wetting”, Proceeding of 4th International Conference on Soil Mechanics and Foundation Engineering, Vol.1, pp. 316-319.
- Mahdi, B. O. (2004): "Some Aspects of Gypseous Soil of the Middle Part of Iraq", Ph. D. Thesis, Civil Engineering Department, College of Engineering, University of Baghdad.
- Rodriguez, A. R., Castillo, H. D. and Sowers, G. F. (1988): "Soil Mechanics in Highway Engineering", Transportation Technical Publication.
- Abduljawad, S.N. (1994): Swell Behaviour of Calcareous Clays from the Eastern Province of Saudi Arabia, Quarterly Journal of Engineering Geology, Vol.27, pp333-351.

- Assallay, A. M., Rogers, C. D. F. and Smalley, I. J. (2004): "Influence of Particle Shape and Clay Content on the Hydro-Collapse Behaviour of Loess", International Conference, Future Vision & Challenges for Urban Development, Cairo, Egypt.
- Blatt, H., Middleton, G., and Murray,R.(1980):Origin of Sedimentary Rocks,2nd Eddition ,Printice –Hall,New York,538-567.
- Bridge, B. J. and Tunny, J. (1973): "The Effect Of Gypsum Treatment On The Swelling Of Natural Loads Of A Clay Soil", soil science, Vol. 115, No. 6.

ABBREVIATIONS AND NOTATIONS

AASHTO:	American Association of State Highway and Transportation Officials
ASTM:	American Sociaty of Testing Material
CBR:	California Bearing Ratio,%
Cu:	Coefficient of uniformity
CP:	Collapse potential, %
c:	Cohesion(kPa)
Gs:	Specific gravity
K1:	Soil with gypsum content 37%
K2:	Soil with gypsum content 56%
S:	Degree of saturation
SM:	Silty Sand
U-U:	Unconsolidated Undrained
χ:	Gypsum content
f:	Angle of internal friction

PREDICTION OF THE EFFICIENCY OF SIEVE TRAY USING AIR-WATER SYSTEM

Prof. Dr. Adil A. Al-Hemiri
University of Baghdad

Muhannad Abdul Razaq Hassan
Chemical Engineering Department

ABSTRACT

This investigation deals with the effect of weir height, liquid and gas flow rate on tray efficiency. The tests were carried out on a single pass cross flow tray of air-water system of 0.3 m diameter for clear liquid height over sieve tray with weir height 3, 4 and 5 cm.

Point efficiency values were found to be in the same range for different weir height, but it improves slightly with weir height. And the average values of point efficiency were 83 % for 3 cm weir height, 85 % for 4 cm weir height and 89 % for 5 cm weir height. While, point efficiency of 90 % was obtained for 5 cm weir height and liquid flow rate ranging between 5.8 to 7.32 m^3/s.

In the range of clear liquid height over hole diameter (h_L/d_H) between 2 to 10, increasing the Reynolds number ranging between $2.0*10^5$ to $1.6*10^6$ for gas phase increases point efficiency.

Prediction of Murphree (Tray) efficiency using Lopez and Castells (1999) equation shows that the ratio of E_{MV}/Ep is equal to 1, due to low value of calculated Peclet number (degree of liquid mixing), which ranged between 0.07 to 1.5.

الخلاصة

درس هذا البحث تاثير تغير كل من إرتفاع السد و جريان السائل و الغاز على إرتفاع السائل فوق الصينية المنخلية و كفائتها لنظام هواء-ماء.

يزداد ارتفاع السائل فوق صينية اختبار واحدة ذات قطر 0.3 متر وعدد فتحات 213 فتحة و ارتفاع سد3 و4 و5 سم بزيادة جريان السائل بين 0.12 الى 0.58 متر مكعب \ساعة ويقل مع زيادة جريان الغاز من 35 الى 100 متر مكعب \ ساعة.

كانت قيم الكفاء ة النقطية متقاربة لكنها تتحسن قليلا مع زيادة ارتفاع السد . وكانت معدلاتها مع ارتفاع السد هي 83% لارتفاع سد3 سم و85% لارتفاع سد 4 سم و 89% لارتفاع سد 5 سم . في حين اعلى قيمة للكفاءة النقطية كانت 90% لارتفاع سد 5 سم و جريان ماء بين 8.5 و 7.32 م^3/ ثا .

كذلك زيادة عدد رينولدز للطور الغازي يزيد من الكفاءة النقطية للصواني المنخلية في حالة كون نسبة إرتفاع السائل إلى قطر ثقب الصينية تتراوح بين 2 إلى 10.
تم تخمين كفاءة ميرفري للصينية باستخدام معادلة لوبيز و كاستلز (1999) والتي اشارت إلى إن نسبة كفاءة ميرفري إلى الكفاءة النقطية كانت تساوي واحد بسبب إنخفاض قيم عدد بكلت للسائل والتي تراوحت بين 0.07 و 1.5.

KEYWORDS
Sieve tray, Tray efficiency, Point efficiency, Murphree plate efficiency

INTRODUCTION

The tray efficiency governs the number of actual trays needed to achieve the desired product purity specifications. With highly efficient trays one can install a lower number of these highly efficient trays to achieve the separation desired.

Several tray efficiency definitions in use. Three different efficiencies are useful, in particular (Wijn, 2003).

- The overall efficiency (*Eo*), the socalled: Fenske efficiency.
- The average tray efficiency, first defined by Murphree (E_{MV}).
- The local (or point) efficiency (*Ep*).

For nonreactive systems, several methods are available for estimating the Murphree tray efficiency from point efficiency estimates made either from laboratory-scale measurements, such as using an Oldershaw column, or from published correlations (Dribika and Biddulph, 1986; Bennett and Grimm, 1991; AIChE, 1958). Klemola 1998 lists references for more than a dozen tray efficiency correlations. For each of these methods, the conversion of point efficiency to tray efficiency relies on the choice of the mixing model to be used.

The liquid mixing on the tray has been modeled using several approaches. Lewis (1936) analyzed the ideal case of plug flow across the tray, which may be approached for large diameter columns. Gautreaux and O'Connell (1955) treated the flow as a series of perfectly mixed pools across the tray. The primary difficulty in the utility of their method is incorrectly estimating the number of mixed pools on the tray. The AIChE (1958) study used a more rigorous mixing model based on eddy diffusivity for diffusive backmixing based on the dimensionless Peclet number AIChE, (1958). Foss et al. (1958) developed a method for relating the Peclet number to the number of perfectly mixed pools across the tray. More recent work has included mixing models of increasing complexity Prado and Fair, (1990); Garcia and Fair, (2000).

For nonreactive systems with cross-flow trays, the concentration varies across the tray as a result of nonideal mixing. In the limit of perfect liquid mixing on the tray, the concentration is constant across the tray and the point efficiency and tray efficiency are the same. For nonideal mixing, concentration gradients develop across the tray that lead to differences in the tray and point efficiencies. In the extreme limit of plug flow across the tray, the concentration gradient is maximized and the difference is also at a maximum.

Bennett et al. (2000) used the recent correlation reported by Bennett et al. (1997), they address point efficiency, entrainment, mixing within the froth, weeping, and cross-flow and parallel-flow tray types. Their correlation for point efficiency is:

$$E = 1 - \exp\left[\frac{-0.0029}{1 + m\dfrac{\rho_{MV}}{\rho_{ML}}\sqrt{\dfrac{D_V(1-\varphi_e)}{D_L\left(\dfrac{A_H}{A_B}\right)}}} (\mathrm{Re})^{0.4236}\left(\frac{h_L}{d_H}\right)^{0.6074}\left(\frac{A_H}{A_B}\right)^{0.3195} \right] \qquad (1)$$

There are no generalized correlations that apply to all types of tray deck designs. So, this approach will use the broadly based correlations developed for sieve trays to develop some optimization rules and then to discuss the implications of using other types of trays on these rules. The optimization goals are:

1. Maximizing theoretical stages per section or column height,
2. Minimizing pressure drop per theoretical stage, and
3. Maximizing the operational range, turn-down, or turn-up.

MURPHREE AND POINT EFFICIENCIES

The Murphree vapor efficiency for a tray is defined as the ratio of the actual change in vapor mole fraction for a component divided by the change in mole fraction that would be experienced if the vapor leaving the tray were in equilibrium with liquid leaving the tray.

$$E_{MV} = \left(\frac{\bar{y}_{n+1} - \bar{y}_n}{y_{n+1} - y_n^*} \right)_{Tray} \qquad (2)$$

When E_{MV} is Murphree vapor efficiency, $\overline{y}_{n+1}$ is average mole fraction in the vapor entering the tray, $\overline{y}_n$ is average mole fraction in the vapor leaving the tray, and y^*_n is the mole fraction that would be in equilibrium with liquid leaving the tray.

The point efficiency *Ep* is defined similarly, but applies to a particular point on the tray, with a particular liquid-phase composition.

$$Ep = \left(\frac{y_{n+1} - y_n}{y_{n+1} - y_n^*} \right)_{point} \qquad (3)$$

The point efficiency follows from application of the two-film-mass-transfer model for point of vapor as it travels up-ward through the liquid phase and engages in mass-transfer exchange with the liquid. The liquid composition is assumed to be constant in the vertical direction.

The key point in introducing the above equations is to realize that difference between point efficiency and Murphree vapor efficiency arises as a result of the variation in y^* that occurs across the tray as liquid phase composition changes. These changes result from mass balance consideration (as components are absorbed or desorbed) for no reactive system, and from both mass balance and chemical reactive consideration for reactive system. Thus, it is necessary to perform some type of integration across the tray, that is to invoke a mixing model, to account for these changes. In addition, for fast reactions where local mass-transfer coefficients are enhanced depending on the local concentration of reactants, the resulting gradient in mass-transfer enhancement factor must also be accounted for (Fisher and Rochelle, 2002).

EFFECT OF MIXING AND SIGNIFICANCE OF LIQUID PECLET NUMBER (*PE*) ON E_{MV}/ *EP* RELATIONSHIP

The assumption of Lewis (1936) concerning lack of liquid mixing (backmixing) on the gas-liquid contacting tray (although mathematically expedient at the time) is in reality not true; just as total liquid mixing equally not true in traditional industrial-size columns (diameter equal to or grater than one meter). In fact, a degree of liquid backmixing always exists in the liquid as it traverses the tray of such columns. The degree of liquid mixing is characterized by the Peclet number (*Pe*).

$$Pe = \frac{Q_L Z_o^2}{A_a h_L De} \qquad (4)$$

A small Peclet number indicates a high degree of mixing and vice versa. According to (Lo'pez and Castells, 1999), if *Pe* is less than 0.2 the liquid is considered well-mixed such that E_{MV} can be considered equal to *Ep*. On the other hand a *Pe* value of about 39 indicates condition approaching liquid plug flow on the tray (Dribika and Biddulph, 1986). Hence a *Pe* value of 50 and higher indicates definite liquid plug flow condition. In such a case the tray efficiency will be larger than point efficiency; the difference between them increasing as *Pe* increases.

Of the above models, the AlChE study (1958) seems to be still the most popular (Lo'pez and Castells, 1999) and is as follows:

$$\frac{E_{MV}}{E_P} = \frac{1-e^{-(\eta+Pe)}}{(\eta+Pe)\left(1+\frac{\eta+Pe}{\eta}\right)} + \frac{e^{\eta}-1}{\eta\left(1+\frac{\eta}{\eta+Pe}\right)} \tag{5}$$

Where

$$\eta = \frac{Pe}{2}\left[\sqrt{\left(1+\frac{4\lambda_o E}{Pe}\right)}-1\right] \tag{6}$$

Eddy diffusivity (*De*)

As pointed out in the previous section, one of the parameters affecting the liquid Peclet number value (and consequently the degree of liquid mixing as it traverses the tray) is the eddy diffusivity (*De*). Usually specific eddy diffusivity is measured experimentally (Chan and Fair, 1984),

To develop a simple relationship and to approximately account for eddy diffusion and the liquid continuous region , droplet mass exchange was assumed to occur over the entire two-phase layer height $h_{2\Phi}$,. Hence, Bennett and Grimm (1991) correlation was:

$$De = 0.02366\left(gh_{2\Phi}^3\right)^{1/2} \tag{7}$$

Where for the correlation (equation (7)):

$$h_{2\Phi} = h_{Fe} + \left[\frac{0.794K_s^2}{(A_h/A_a)\Phi_e}\right] \tag{8}$$

$$h_{Fe} = C'\left[\frac{Q_L}{\Phi_e}\right]^{2/3} + h_w \tag{9}$$

$$\Phi_e = \exp\left(-12.55K_s^{0.91}\right) \tag{10}$$

$$C' = 0.501 + 0.439\exp(-137.8h_w) \quad (11)$$

The correlation (equation (7)) was modified later by Bennett et al. (1997) taking also into consideration diffusion resulting from turbulence in the liquid continuous region. This modified correlation was given by Lo'pez and Castells (1999) as follows:

$$De = (4)(0.024)\left(gh_{2\Phi}^{3}\right)^{1/2} \quad (12)$$

Where for this correlation

$$h_{2\Phi} = h_{Fe}\left[1 + \left(1 + 6.9\left(\frac{h_L}{d_H}\right)^{-1.85}\right)\frac{Fr_G}{2}\right] \quad (13) \qquad Fr_G = \frac{V_{ej}^2}{gh_{Fe}}$$

(14)

$$Ve_j = 3K_s\sqrt{\frac{\sqrt{3}}{(A_h/A_a)\Phi_e}} \quad (15)$$

EXPERIMENTAL WORK

Equipment

The experimental laboratory apparatus used is shown in Fig. 1 and consisted of the following:

i. Glass column. (QVF)
ii. Liquid storage tank.
iii. Blower.
iv. Centrifugal pump.
v. Connecting piping.
vi. Measuring instruments

Geometrical parameters

The following specifications were used which were concluded from Coulson (1985), Treybal (1981) and Ludwig (1979).The plate used is shown in **Fig. (2)**

Material of construction of sieve plate	aluminum alloy A-1050 (99.5 % by wt. Al)
Column diameter	30 cm
Hole diameter	5 mm
Plate thickness	5 mm
Weir height	3 cm, 4 cm, 5 cm
Weir length	22 cm

Length of liquid path	22 cm
Total no. of holes	213
% Free area	7.7
Active or bubbling area	0.05372 m^2
Vapor density (air) standard	1.1982 kg/m^3
Liquid density (water) standard	997.94 kg/m^3
Hole pitch	13.5 mm triangular
Hole area /Active area	13.16 %
Active area /Column area	76.1 %
Outlet calming zone width	18 mm

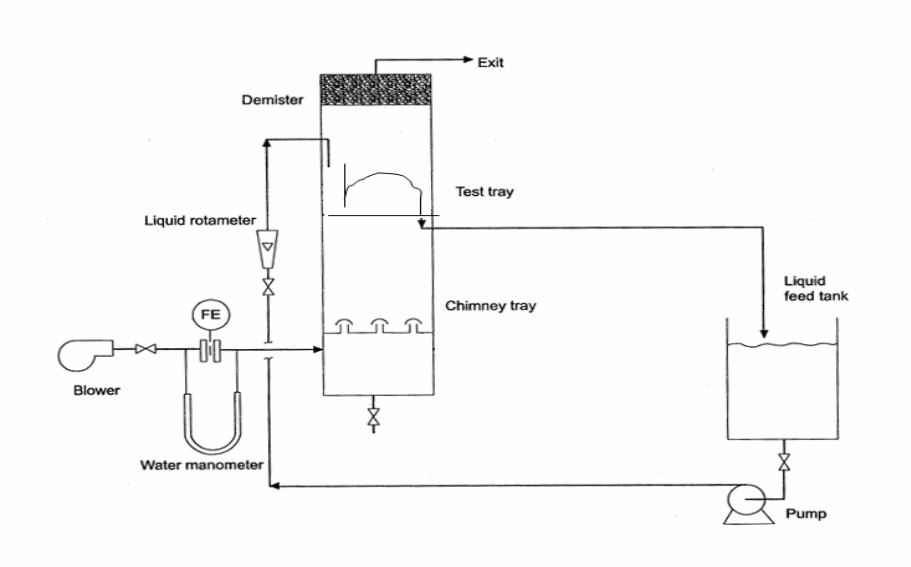

Fig. (1), Schematic diagram of the experimental rig

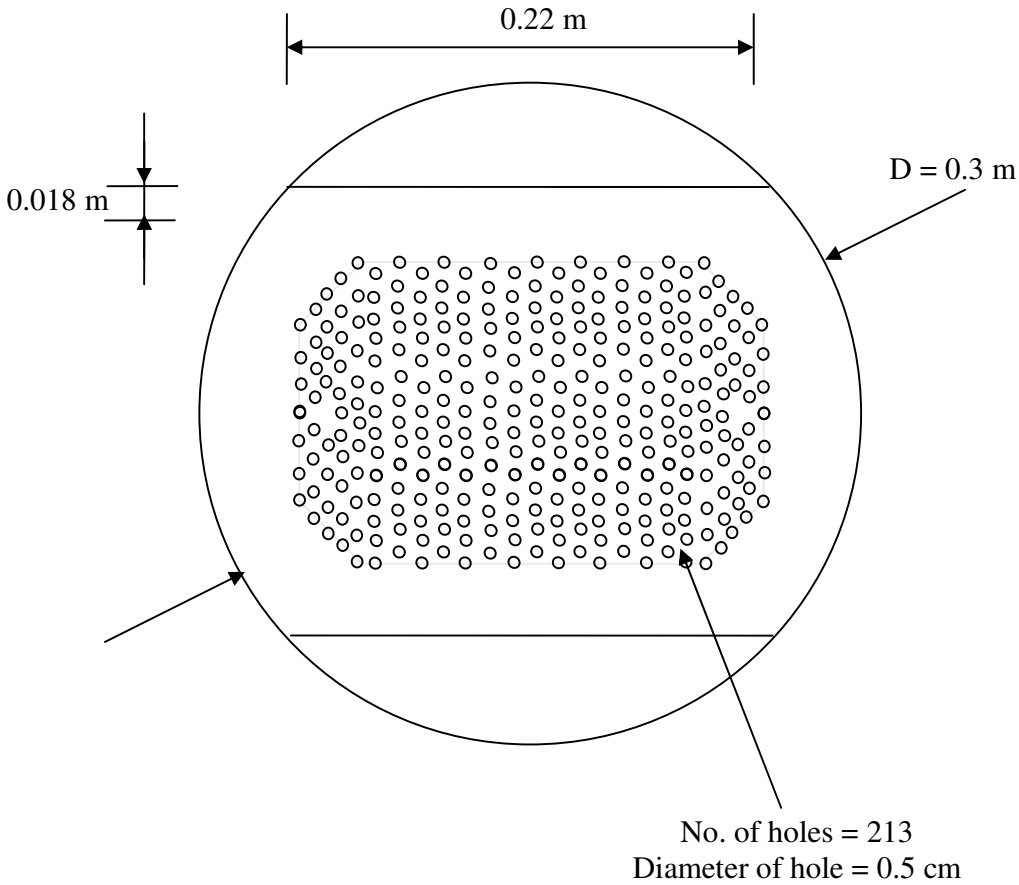

Fig. (2)., Schematic diagram of the sieve tray

Experimental procedures

The experimental program related to the laboratory rig consisted of the following particular steps employed for the operational system:

1. Initially, a sufficient quantity of the liquid to be used was prepared and introduced to the larger of the one liquid tank. This liquid quantity amounted to about $50*10^{-3}$ m^3.
2. The air blower was operated and the air flow was adjusted by a manual gate valve (placed on the 3" ND pipe) utilizing the installed calibrated orifice meter for this purpose. This value of air flow corresponded to the minimum required to avoid dumping of the liquid from the perforated test tray at its minimum adopted inlet flow rate of 0.25 m^3/h.
3. The main supply/recirculating liquid pump was then operated and the liquid flow was adjusted at 0.1 m^3/h by the globe valve upstream of the area flow meter which was utilized for this purpose. This value of liquid flow rate was practically the minimum stable rate of

flow achievable in the rig due to the variation in the reservoir tank liquid level over the duration of an experimental run.

4. The glass column was then observed to ensure that some liquid overflowed the outlet weir. If that was not the case, the air flow rate was gradually increased to achieve this overflow and subsequently fixed and recorded at this overflow occurrence. This procedure was necessary to keep away from the weep point.
5. The next step was to increase the air flow was used to values corresponding approximately to 35, 50, 60, 70, 86 and 100 m^3/h while maintaining the liquid flow are at 0.1 m^3/h. Hence, it was possible to decrease the value of the weeping fraction and/or increase the value of liquid flow over the outlet weir.
6. The procedure pointed out in points 2 and 5 above was repeated over for increasing in the liquid flow rate to the test tray; namely 0.1, 0.14, 0.18, 0.22, 0.26, 0.3, 0.34, 0.38, 0.46and 0.58 m^3/h and measuring the clear liquid height and froth height for each change.

DISCUSSIONS

Effect of weir load (Q_L/L_w), clear liquid height (h_L) and weir height (h_w) on point efficiency (Ep)

Figure (3) shows the effect of changing liquid flow rate (weir load) on the point efficiency. The point efficiency appears increase with clear liquid height as shown in Figure (4), when the liquid flow rate increasing the liquid height increases over the tray deck which will increase the interfacial area and contact time and hence point efficiency.

Maximum values of point efficiency for 5 cm weir height 90 % for liquid flow rate ranging between 5.8 to 7.32 m^3/s m and clear liquid height between 3.5 to 4 cm.

Point efficiency values appear in the same range for different weir height. The average values of point efficiencies versus weir height are summarized in Table (1) and appear improve slightly with weir height. This improvement of point efficiency is due to increasing of liquid height above the tray deck.

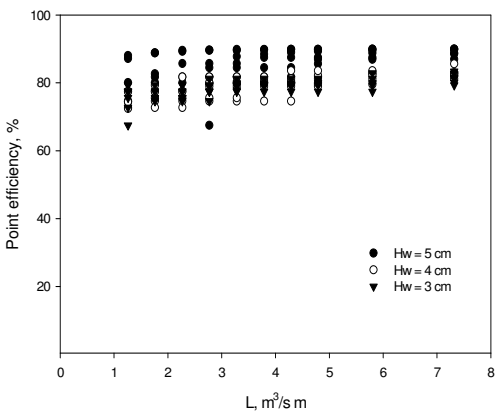

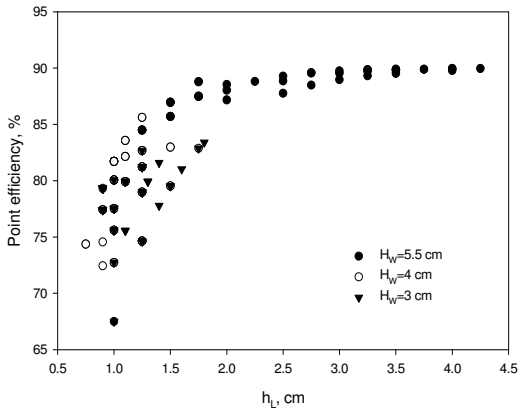

Fig. (3)., The point efficiency versus weir Fig.(4)The point efficiency versus clear liquid height liquid load

The results of point efficiency versus liquid height are compared with Porter (1992) results, who worked on air-water system with 6.35 mm hole diameter, weir height 10, 20, 50 mm and liquid weir load from 0.00125 to 0.025 m^3/m.s and Prado (1987), who worked on the same system but with weir height 25.4, 50.8, 76.2 mm and liquid weir load from 0.0015 to 0.0028 m^3/m.s as shown in Figure (5) Comparison between the results obtained from Porter (1992), Prado (1987) and the present work shows good agreement.

Table (1)., Average values of point efficiency versus weir height

Weir height, cm	Average point efficiency, %
3	83
4	85
5	89

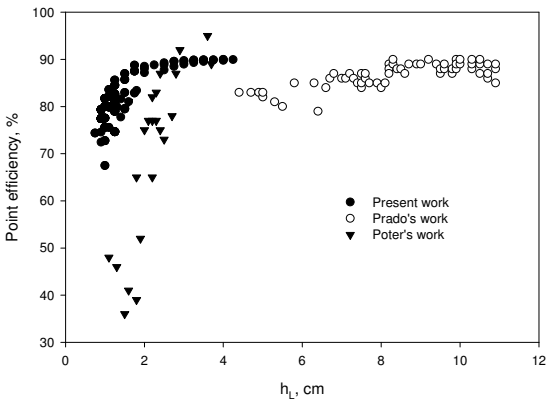

Fig. (5). Comparison of various air-water systems and present work

Effect of F-factor on tray point efficiency (*Ep*)

Bennett et al. (1997) correlation (equation (1)) was used to calculate the point efficiency which is shown that point efficiency increases with gas velocity (Reynolds number Re) as shown in Figure (6).

Large values of gas velocity through the perforation (large *Re*) yield higher interfacial area. As expected the ratio of h_L/d_H plays a significant role and the efficiency increases with h_L/d_H which is ranging between 2 to about 10, as shown in Figure (7).

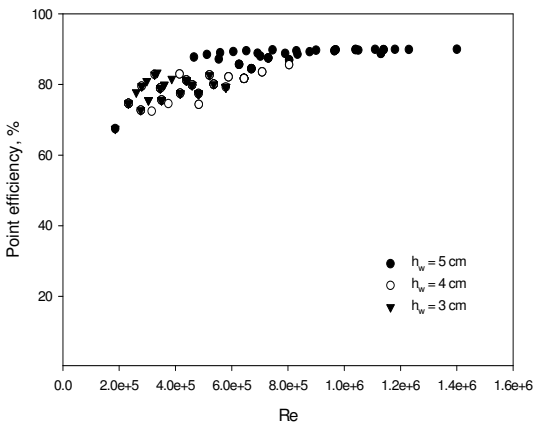

Fig. (6)., The point efficiency versus Reynolds number

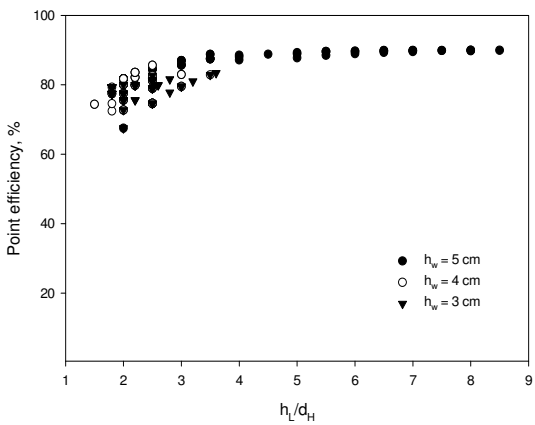

Fig. (7), the point efficiency versus h_L/d_H

The above results (effect of weir load and gas velocity on point efficiency) are in good agreement with Bennett et al. (2000).

Bennett et a 2000) reported that the denominator of the term within the major bracket is the correction required hen liquid phase resistance is important. No significant effect of changing the diffusivities of CO_2 and NH_3. This gives good evidence that the liquid phase resistance is not important.

Predicted Murphree tray efficiency (E_{MV})

The prediction of Murphree tray efficiency is done by using recently equation of Lopez and Castells (1999). This equation predicts the ratio of Murphree tray efficiency over point efficiency as function of Peclet's number (*Pe*). *Pe* for experimental data are calculated and ranged between 0.07 to 1.5.

Referring to equation (4); namely:

$$Pe = \frac{Q_L Z_o^2}{A_a h_L De} \qquad (4)$$

It is apparent that h_L and *De* must be evaluated in order to establish the value of *Pe*. Clear liquid height was used in equation 2.13 was determined experimentally for three weirs height (3, 4, and 5 cm),

while the *De* correlation given by Bennett et al. (1997), being most recent in the literature was used in this study. Accordingly *De* values shown in appendix were obtained.

According to Lopez and Castells (1999) equation E_{MV} is equal to *Ep* obtained from the experimental data as shown in Figure (8).

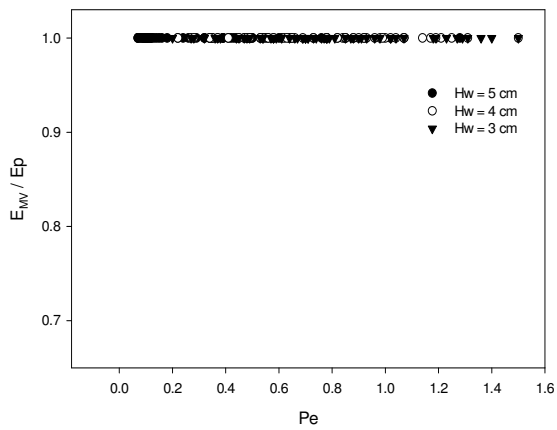

Fig. (8)., Murphree tray efficiency per point Efficiency versus Peclet number

CONCLUSIONS

The following conclusions can be drawn from the results obtained:

1. Maximum calculated value of point efficiency for 5 cm weir height is 90 % for liquid flow rate ranging between 5.8 to 7.32 m^3/s and clear liquid height between 3.5 to 4 cm.
2. Point efficiency values are in the same range for different weir height, but it improves slightly with weir height and the average values of point efficiency are 83 % for 3 cm weir height, 85 % for 4 cm weir height and 89 % for 5 cm weir height.
3. At large values of Reynolds number for gas phase, the point efficiency increases with h_L/d_H in the range 2 to 10 to about 90 %.
4. Evaluation of liquid Peclet number by equation of Lopez and Castells (1999), shows that *Pe* ranged between 0.07 to 1.5.

5. Prediction of Murphree efficiency by using Lopez and Castells (1999) equation shows that the ratio of E_{MV}/Ep is equal to 1 for all experimental data due to low value of liquid Peclet number.

REFERENCES

. American Institute of Chemical Engineers (1958), *"Bubble-tray design manual"*, AIChE, New York.

. Bennett, D. L. and Grimm, H. J., "Eddy dffusivity for distillation sieve trays", AIChE J 37, 4 (1991) 589-596.

. Bennett, D. L. and Kovak, K. W. (2000), *"Optimize distillation columns"*, AIChE.

. Bennett, D. L., Kovak, K. W. and Zak, D. (1997), *"Optimization of sieve type distillation trays"*, AIChE Annual Meeting, Los Angeles.

. Bennett, D. L., Watson, and Wiescinski, M. A.(1997), *"New correlation for sieve-tray point efficiency, entrainment and section efficiency"*, AIChE J., 43(6), p 1,611.

. Chan, H. and Fair, J. R. (1984), *"Prediction of point efficiencies on sieve trays"*, Ind. Eng. Chem. Process Des. Dev., 23, 4, 814-819.

. Coulson, J. M. and Richardson, J. F. (1985), *"Chemical Engineering"* Vol.6, 1st ed., Pergamon.

. Dribika, M. M., Bidduiph, M. W. (1986), *"Scaling-up distillation efficiency",* AIChE J., 32, 11, 1864-1875.

. Fisher, K. S. and Rochelle, G. T. (2002), *"Effect of mixing on efficiencies for reactive tray contactors"*, AIChE J., 11 (48), 2537.

. Foss, A. S., Graster, J. A. and Pigford, R. L. (1958), *"Effect of liquid mixing on the performance of bubble trays"*, AIChE J., 4(2), 231.

. Gautreaux, M. F. and O'Connell, M. E.(1955), *"Effect of length of liquid path on plate efficiency"*, Chem. Eng. Prog., 51, 232.

. Gracia, J. and Fair, J. R. (2000), *"A fundamental model for prediction of distillation sieve tray efficiency. 2. Model development and validation"*, Ind. Eng. Chem. Res., 39, 1818.

. Klemola, K. T. (1998), *"Efficiencies in distillation and reactive distillation"*, Acta Poly. Scand., Chem. Tech. Ser., No. 257.

. Lewis, W. K. (1936), *"Rectification of binary mixtures: Plate efficiency of bubble cap columns"*, Ind. Eng. Chem. 28, 399-402.

. Lo'pez and Castelles (1999), *"Influence of tray geometry on scaling up distillation efficiency from laboratory data"*, Ind. Eng. Chem. Res. 38, 2747- 2753.

. Ludwig, E. E. (1979), *"Applied process design for chemical and petrochemical plants"*, Vol.2, 2nd ed., p.109 Gulf Publishing Company.

. Porter, K. E., Chambers, S. Yu, K. T. and Zhang, M. O. (1992), *"Flow patterns and temperature profiles on a 2.4 m diameter sieve tray"*, I. Chem. Eng. Symposium Series, 128, A257-A272.

. Prado, M. and Fair, J. R. (1990), *"Fundamental model for prediction of sieve tray efficiency"*, Ind. Eng. Chem. Res., 29, 1031.

. Treybal (1981), *"Mass transfer operations"*, McGraw-Hill international edition.

. Wijn, E. F., (2003), *"Development of distillation tray efficiency model"*, Chem. Eng. J75, 171-184.

NOMENCLATURE

Symbol	Description	Units
A_a	Active area	m^2
A_h	Hole area	m^2
C'	Constant defined by equation 11	
d_H	Hole diameter	m
De	Eddy diffusivity for liquid mixing	m^2/s
D_L	Liquid molecular diffusivity	m^2/s
D_V	Vapor molecular diffusivity	m^2/s
E_{MV}	Murphree gas-phase tray efficiency	-
E or E_p	Point efficiency	-
E_o	Overall column efficiency	-
F	F factor $=V_{gh}\sqrt{\rho_g}$	m/s
Fr_G	Gas Froude number defined in equation 14	-
g	Gravity acceleration	m/s^2
$h_{2\Phi}$	Two-phase layer height on the tray (sum of liquid continuous region + gas continuous region)	m
h_{Fe}	Effective froth height	m
h_L	Clear liquid height in the two phase layer on the tray	m
h_w	Outlet weir height	m
K_S	Density corrected superficial gas velocity over active area ($=V_{ga}[\rho_g/($	m/s

	$\rho_L - \rho_g)^{1/2}]$)	
L_w	Weir length	m
m	Slope of equilibrium line	
Pe	Liquid Peclet number	-
Q_g	Volumetric gas flow rate	m^3/s
Q_L	Volumetric liquid flow rate	m^3/s
Re	Reynolds number	-
V_{ej}	Gas velocity defined by equation 15	m/s
y	Gas concentration (mole fraction)	
y^*_n	Mole fraction that would be in the equilibrium with liquid leaving the tray	
$\bar{y}_n$	Average mole fraction in the vapor leaving the tray	
$\bar{y}_{n+1}$	Average mole fraction in the vapor entering the tray	
Z_o	Liquid flow path length	m

Greek Letters

η	Defined by equation 6
Φ_e	Effective relative froth density as defined in equation 10

Subscripts

0	Evaluate at z = 0
1	Evaluate at z = 1
g	Gas
h	Hole
hor	Horizontal
L	Liquid
w	Weir

Superscripts

__	Mean value
*	Equilibrium value if used with x or y

EVOLUTIONARY ALGORITHMS FOR TRANSFERRING PROPERTIES BETWEEN IMAGES PART I: GRAYSCALE IMAGE COLORIZATION

Dr. Bara'a Ali Attea
Computer Science Department, niversity of Baghdad

Aminna Dahim Aboud
Computer Science Department, niversity of Baghdad

ABSTRACT

In this paper, an evolutionary algorithm (EA) for "colorizing" grayscale images is introduced by evolving color patch transfer process between a source colored image and a target grayscale image. As the general problem of inverting a gray palette to a color palette is a severely under-constrained, ambiguous problem and has no exact, objective solution, human labor and costly semantic knowledge are required. The presented EA attempts to minimize the amount of human work by automatically choosing colored patches from the source image and applying their colors to the grayscale patches of the target image. Furthermore, the best patch matching over all EA parent individuals are recombined in a single multi-sexual recombination scheme to form a single offspring individual. Mutation, on the other hand, forms all other EA individuals. The simple technique of the proposed EA can be successfully and efficiently applied to a variety of images.

الخوارزميات التطورية لنقل الصفات بين الصور الجزء الأول: تلوين الصور الرمادية

الخلاصه

يهتم هذا البحث بأيجاد خوارزميات تطورية لحل مشكلة نقل الصفات بين الصور. في هذا الجزء نقدم خوارزمية تطورية تلائم مشكلة نقل الألوان من صورة مصدر ملونة الى صورة هدف رمادية. تعتمد الخوارزمية التطورية المقترحة على نقل رقع من الألوان من الصورة المصدر الى الصورة الهدف في آن واحد. يرجع سبب أختيارنا الخوارزمية التطورية الى طبيعة مشكلة التلوين نفسها, حيث تعد هذه المشكلة من المشاكل الغامضة والتي لاتمتلك الى حل صحيح ودقيق. الخوارزمية التطورية المقترحة تحاول التقليل من التدخل البشري في عملية التلوين بوساطة الأختيار الأتوماتيكي للرقع الملونة من الصورة المصدر ونقل الوان هذه الرقع الى الرقع الرمادية للصورة الرمادية. أقترحت طريقة التزاوج متعدد الأجناس لخلط أفضل الرقع المتطابقة لتوليد فرد واحد. من جهة أخرى، تتولى عملية الطفرة الوراثية توليد بقية الأفراد للجيل الجديد. طبقت الخوارزمية المقترحة بنجاح وبكفاءة على أنواع مختلفة من الصور.

KEYWORDS

Image colorization, genetic algorithm, multi-sexual crossover, color patch

INTRODUCTION

Colorization is a useful technique in increasing the visual appeal of black-and-white photos, classic movies or scientific visualizations. Further, colorization has applications in color editing and compression. The problem of coloring a grayscale image involves assigning three-dimensional (RGB) pixel values from a source, color image to a target, grayscale image whose pixels are varied along only one dimension (luminance). As several hues and/or saturation levels may carry the same luminance value, colorization problem has no inherently correct solution. Moreover, it has several other challenges including ambiguity, fuzzy boundary identification, and user expert. [1] [2]. In other words, colorization is in general a severely under-constrained and ambiguous problem for which it makes no sense to try to find an ”optimum” solution, and for which even the obtainment of “reasonable” solution requires some combination of strong prior knowledge about the scene depicted and decisive human intervention. Even in the case of pseudo coloring, where the mapping of luminance values to color values is automatic, the choice of the color map is commonly determined by human decision.

Several techniques are published for digital colorization. Readers please refer to recent papers. Some (but mostly used) colorization work are color transfer of Reinhard et al [3], image analogies of Hertzmann et al [4], the classical full search of Welsh et al [5], and the Antypole strategy of Di Blasi and Reforgiato [1]. The main concept of these colorization techniques is to exploits textural information. For example, the work of Welsh et al, which is inspired by the color transfer [3] and by image analogies [4], examines the luminance values in the neighborhood of *each pixel* in the target image and add to its luminance the chromatic information of a pixel from a source image with best neighborhoods matching. This technique works well on images were differently colored regions give rise to distinct textures. Otherwise, the user must specify rectangular swatches indicating corresponding regions in the two images. Di Blasi and Reforgiato [1] propose an improvement to Welsh et al work, where Antipole clustering strategy is adopted as an efficient data structure for fast color retrieving. Their approach provides a way to speed up the searching process but at the expense of increasing implementation complexity.

In this paper, the technique of evolutionary algorithms (EAs), probabilistic search algorithms based on the model of natural evolution will be applied, for colorization problem. The procedure of evolution works by minimizing the matching error (in term of luminance and texture information) between pairs of source and target square patches. Then transfer color mood from the best evolved source patches to the target patches. In what follow, the characteristic components of this EA will be presented.

THE PROPOSED EVOLUTIONARY ALGORITHM

An Evolutionary Algorithm (EA) is inspired by biological evolution, and is widely believed to be an effective global optimization algorithm. There are a variety of evolutionary algorithms emerged:”evolutionary programming-EP” [6], “evolution strategies-ESs” [7] and “genetic algorithms-GAs” [8]. Moreover, since EAs are motivated by natural principles, when faced with problem, natural remedies are often emulated.

An EA consists of a population of individuals, which are evaluated using fitness function. The individuals (mostly fittest individuals) are reproduced and perturbed via three main EA's operators: selection, recombination, and mutation. The processes used to select which parents will produce

offspring varies significantly from one EA to another, and includes strategies such as uniform random selection, rank-proportional selection, and fitness-proportional selection. In addition to these selection processes, the mechanisms used for offspring reproduction also varies. They range from asexual reproduction with no mutation (in which offspring are exact replicas of parents), asexual reproduction with mutation, to sexual reproduction with recombination. Moreover, sexual reproduction can be in either local form with 2-parent recombination or global form with multi-parent recombination. Historically, the EP and ES communities have emphasizes asexual reproduction while the GA community has emphasized sexual reproduction.

In the proposed EA, square patches of pre-selected size- $w_p \times w_p$ - of the target, grayscale image are colorized from suitable $w_p \times w_p$ source patches. The evolution of the patch colorization scheme is manipulated by formulating individual representation, penalty function, and individual evolution via perturbation operators.

Search space representation

In order to apply an EA to a particular problem, it is appropriate to select an internal representation of the space to be searched and define an external evaluation function, which assign utility to candidate solutions. Both components are critical to the successful application of the EA to the problem of interest. Here, to represent a solution (an individual's genotype), a two-dimensional array of $m \times n$ genes is used such that:

$m = h_t / w_p$, and

$$n = w_t / w_p \qquad (1)$$

Where

h_t : Height of the target grayscale image,

w_t : Width of the target grayscale image, and

w_p : Patch width (e.g., we use $w_p = 3,\ 5,\ 7,\ 9,$ or 11).

Gene (i, j) of an individual identifies an un-overlapped $w_p \times w_p$ target patch (i, j) and can contain x and y coordinates of the center of a $w_p \times w_p$ source patch. To start the EA, a population of p_{size} individuals is randomly created, and each individual can represent the genotype of a potential solution to the colorization problem.

The total number of possible solutions represents the search space size (which here, grows exponentially as increasing the number of un-overlapped source patches).

Penalty function

Next, it is important to define a suitable penalty function which rewards the right kinds of individuals. For the colorization problem reported here, it would be desirable to minimize luminance matching error between pairs of target patches and source patches. In other words, each gene (i, j) in an EA individual has associated with it a luminance matching error (i, j) computed as:

$$error(i, j) = match(p_t(i, j), p_s(i, j)) \qquad (2)$$

Where:

$p_t(i, j)$: Target patch being identified by the gene (i, j) ;

$p_s(i, j)$: Source patch referred to by the gene (i, j) ;

and the $match$ between two patches p_t and p_s of a given gene (i, j) is defined to be:

$$0.5\left|\mu_s(i,j)-\mu_t(i,j)\right|+0.5\left|\sigma_s(i,j)-\sigma_t(i,j)\right| \qquad (4)$$

Where μ and σ are the luminance average and standard deviation both taken with respect to a $w_p \times w_p$ source or target patch as referred to by subscript *s* or *t* respectively. Then, an EA individual has a penalty function E computed as the sum of all its gene luminance matching errors:

$$E=\sum_{i=1}^{m}\sum_{j=1}^{n} error(i,j) \qquad (5)$$

In order to match luminance information, both source and target images must be converted from RGB color space to a de-correlated space (de-correlated YIQ color space is used here).

Evolutionary operators

In our EA, we breakdown the traditional views found in the EA communities and make a hybrid collection of evolutionary processes that would be useful for the colorization problem. The main issues made in the proposed EA are: extinctive selection, single multi-sexual discrete recombination, and preservative mutation operator.

The first character of the proposed EA is the strict denial of selection process; letting all offspring to be created from all parents using recombination and mutation. First a multi-sexual discrete recombination process is applied among all parents to produce only one mated offspring. Genes among all parents are competed and the best ones (with smallest matching errors) are inherited to that offspring.

Next, mutation is used to fulfill the new population with $p_{size}-1$ new offspring. 90% offspring are created by mutating the genes of the mated offspring while others 10% offspring are created randomly from the total search space.

Genotype decoding: phenotype re-coloring

After stopping the EA to a pre-selected maximum number of generations, a population of individuals that may have some promising solutions is obtained. The best individual (with smallest *E*) has to be decoded to its colored result. In EA literatures, the output of the genotype decoding is normally known as phenotype. Here, phenotype coloring includes the following sequence of steps:

1. Go through the best EA individual genes and the target image in scan-line order in steps of one gene (for the individual) and one $w_p \times w_p$ patch (for the target image).
2. Select from the source image a $w_p \times w_p$ patch in which its center has coordinates *x* and *y* referred to by the current gene.
3. For each pixel in the target patch, search the selected source patch in scan-line order for the closest pixel (in term of luminance value). Add the chromatic components (I and Q) of that pixel to the luminance value of the current target pixel.
4. Repeat the sequence 1, 2, and 3 for all target patches.
5. Transform the target image from YIQ to RGB color space to display the result on the screen.

EXPERIMENTAL RESULTS

This section reports some results obtained by running the proposed EA with $p_{size}=40$ to a maximum number of generations equals to 30 for coloring a range of image domains with different sizes. Generally, the experimented images are classified as homogeneous ones. These images include

a single object in the foreground and this object is clearly discernible from a mostly homogeneous background. First, (if needed) luminance histogram matching of Hertzmann et al [4] is applied to match the first- and second- order statistics of the luminance distribution of the source image according these of the target image. More concretely, if $l(p)$ is the luminance of a pixel in the source image, then we remap it as

$$l(p)' = \frac{\sigma_t}{\sigma_s}(l(p) - \mu_s) + \mu_t \qquad (6)$$

EA results are compared with the Welsh et al classical full search method [5] (both are implemented using un-optimized visual Basic code.) The neighborhood statistics required in both algorithms are pre-computed over the source and target images. In the full search method, we need to pre-compute neighborhood average and standard deviation of each pixel, while in the EA; the statistics are needed for each un-overlapped patch. Different patch size was used. Obviously, decreasing patch size results in more acceptable results but at the expense of increasing maximum required number of generations. Each EA result is formulated by depicting the phenotype of the best individual obtained after only 30 generations together with the result of the full search algorithm (see figures 1 and 2). Quantitative EA results are also pointed out by including average of penalty function ($E/m*n$) of the best individual in the initial and the last generations. Processing time required for a single Pentium IV PC computer is also included for both colorization algorithms (see table 1). Actually, EA algorithm requires less computation time than presented in the table. By comparing EA results with those of Welsh et al, we can easily demonstrate that the proposed easy to implement EA can produce visually accepted results in a number of image domains although there are some failure (yet tolerable) patch colorization cases. Running time will vary depending on the patch size, size of source and target images (total search space size), p_{size} and the maximum number of generations. In most of experimented results, the computation time of EA colorization algorithm to obtain visually accepted results was better than the classical full search algorithm of Welsh et al.

CONCLUSIONS

This paper introduces a simple colorization technique based on combing the concept of evolutionary algorithms with a patch-based luminance matching strategy. A new multi-sexual recombination strategy is given to recombine, in a single EA step, the best patches found between source color and target gray images. Without user expert, the algorithm can give pleasing visual results for homogenous images. Both EA and patch-based luminance matching could be the subject of future research. For example, try to test this colorization algorithm on more complicated images, i.e. heterogeneous images where the scene has multiple objects on the foreground, or has a cluttered background, or is illuminated in an uneven way.

REFERENCES

[1] G. Di Blasi, and R. D. Reforgiato, "Fast colorization of gray images", *In proceedings of Eurographics Italian Chapte,* 2003.

[2] L. F. M. Vieira, R. D. Vilela, and E. R. Nascimento, "Automatically choosing source color images for coloring grayscale images", *16th Brazilian Symposium on Computer Graphics and Image Processing (SIBGRAPI 2003), Sao Carlos, Brazil. IEEE Computer Society*, ISBN 0-7695-2032-4, pp. 151-158, 2003.

[3] E. Reinhard, M. Ashikhmin, B. Gooch, and P. Shirley, "Color transfer between images", *IEEE Transactions on Computer Graphics and Applications 21*, 5, pp. 34-41, 2001.
[4] A. Hertzmann, C. E. Jacobs, N. Oliver, B. Curless, and D.H. Salesin, "Image analogies", In *Proceedings of ACM SIGGRAPH 2002*, pp. 341-346.
[5] T. Welsh, M. Ashikhmin, and K. Mueller, "Transferring color to grayscale images", *ACM Transactions on Graphics 21*, 3 (July) 2002, pp. 277-280.
[6] J.R. Koza, *Genetic Programming: on the programming of computers by means of natural selection.* Cambridge, MA: MIT Press, 1992.
[7] H.-P. Schwefel, *Numerical Optimization of Computer Models.* New York: John Wiley & Sons, 1981.
[8] D.E. Goldberg, *Genetic Algorithms in Search, Optimization, and Machine Learning.* New York: Addison Wesley, 1989.

Table (1). Mean of penalty and processing time comparison between EA and full search.

Target image	$E/m*n$		Time (sec.)	
	gen. no.0	gen. no.30	EA	Full search
	77.565	0.644	1225	2918
	55.686	0.670	964	2086
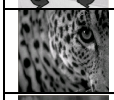	393.646	8.673	1121	3061
	217.278	3.129	398	417
	62.396	3.161	444	552
	489.798	13.854	482	534
	363.182	12.938	653	733
	469.055	11.7	235	333
	359.201	18.7	575	688
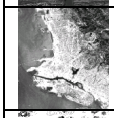	493.716	13.410	565	697
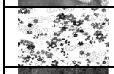	656.273	13.788	279	324
	43.373	1.059	529	812

EFFECTS OF NON-LINEAR MAGNETIC CHARGE ON INDUCTION FURNACE OPERATION DURING THE HEATING CYCLE

Adil H. Ahmad, PhD **Fadhil A. Abood, PhD** **Akram F. Bati, PhD** **Essam M. Abdul-Baki, MSc.**
University of Technology Baghdad / Iraq

خلاصة

أن هذا البحث هو عبارة عن دراسة لسلوك المجال الكهرومغناطيسي للفرن الحثي عندما يكون قلبه مادة مغناطيسية اخذين بنظر الاعتبار العلاقة اللاخطية لكثافة الفيض المغناطيسي B المتولد في القلب الحديدي للفرن كداله للشدة المغناطيسية H المسلطة على ملفاته.

بما أن كلا من الخواص ألمغناطيسيه للقلب الحديدي ومقاومته النوعية تتأثران بشدة بارتفاع الحرارة فأن الدراسة تضمنت تأثير الحرارة على كلا العاملين آنيا لتوضيح السلوك الكهرومغناطيسي للفرن خلال عملية التسخين. أن توزيع كل من كثافة التيار و كثافة الفيض و شدة المجال المغناطيسي داخل القلب الحديدي وعلى سطحه الخارجي قد تم تحديدها. وكذلك فأن توزيع الفيض المغناطيسي قد تم رسمه لدرجات حرارة مختلفة.

أن هذه الدراسة قد أظهرت أهمية تضمين اللاخطية المغناطيسية وتأثرها بالحرارة في دراسة الأفران الحثية لذا، فأنها ستكون كأساس للعمل المستقبلي الذي سيتضمن التعشيق بين التحليلات الحرارية و الكهرومغناطيسية لهذه الأفران.

ABSTRACT

This research studying the electromagnetic behavior of the induction furnace when its core is a magnetic material taking into consideration the effect of the non-linear dependence of the magnetic flux induced in it due to the applied magnetizing force.

Since the magnetic characteristics are severely affected by temperature rise in a non-linear way, so as the specific electric resistance of the charge material, this work deals with studying the effect of temperature on the non-linear characteristics of a magnetic core simultaneously with that on the specific electric resistance to show the electromagnetic behavior of the furnace during heating operation. The distribution of the current density, flux density and the magnetizing force at different temperatures inside the furnace and on the charge surfaces are determined for different temperatures. Also the flux distribution is plotted at these cases. This study will be the base for future work on the electromagnetic-thermal coupled analysis for the induction furnace.

INTRODUCTION

This work represents the second step of analyzing the electromagnetic behavior of the induction furnace when its core is a ferromagnetic material. The results of the first step analysis have already been published and presented on a linear induction furnace [1] using a FEM package (ANSYS 5.4). In this work the analysis is extended to take into consideration the effect of three types of non-linear relations on the furnace parameters these are:

a) The effect of the non-linearity of the permeability μ with the magnetic field intensity H, or $B = \mu(H) \cdot H$.
b) The non-linear effect of the temperature T on the permeability $\mu(T, H)$.
c) The non-linear variation of the specific electric resistance of the charge material with temperature $\rho(T)$.

The new analysis was done using numerical technique based on a general-purpose finite element package "ANSYS 7". Two previous applications [2] are considered in order to verify the results of this work. The first example is an induction furnace with magnetic core and operating at low frequency of 60 Hz, while the second furnace using the same material as a core operating at medium frequency of 4KHz. The results obtained by ANSYS 7 show a good agreement with the published work. The magnetic material used is a carbon steel SAE 1045 (C45). The data of steel C45 are extracted from references [2],[3] & [4].

It is very interesting in this work to show clearly what is going on inside the magnetic charge of the induction furnace during its operation by studying the effect of temperature increase on the distribution of flux lines, B, H & J (from room temperature up to Curie temperature). Such knowledge will lead to expect the effect of non-linearity and temperature increase on Skin depth $\delta = 1/\sqrt{\varpi\mu\sigma}$. Also, it is an important step to prepare for the electromagnetic-thermal coupled analysis, which will complete the simulation of the induction heating process to be as real as possible.

The Magnetic Non-linearity Problem:

When the magnetic non-linearity is considered, the conventional transient analysis method will elapse a long time to solve such problem. In FEM, harmonic analysis assumes that all quantities are sinusoidally varying, but if a sinusoidal exciting field H is used, non-linearity distorts the waveforms of the flux density B, while considering sinusoidal B will lead to a non-sinusoidal H. Therefore, non-linearity cannot be included in the analysis directly and iron saturation requires special treatment. Hence, Several methods [5–9] for determining appropriate permeability have been used to make account of time variation. These methods include the use of time-averaged value of the permeability over a complete cycle. The problem can then be simplified by considering only the fundamental frequency component of B and H. The problem, in this case, is cast in time harmonic form with (d/dt) being replaced by $(j\varpi)$. The package " ANSYS 7 " deals with this problem to investigate the accurate results [10].

Accurate data for carbon steel SAE 1045 (C45) about the dependence of its relative magnetic permeability on temperature are not readily available but it could be approximated as [4]

$$\mu_r(T,H) = 1 + (\mu_r(H)_{T=0} - 1)\cdot\left[1 - (T\cdot 750^{-1})^2\right] \qquad \text{when} \qquad T < 750^o C$$

$$\mu_r(T,H) = 1 \qquad \text{when} \qquad T \geq 750^o C$$

The family of curves of $B(T,H)$ is shown in Fig. (1) for steel C45, This figure

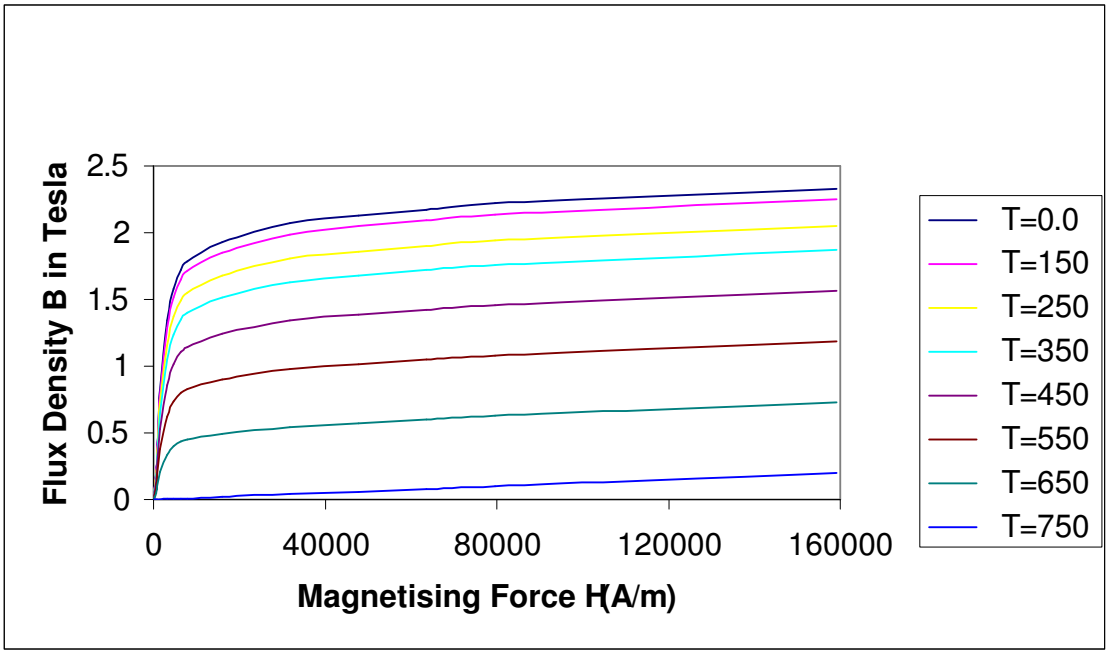

Fig. (1) The Magnetic Characteristics (B-H curves) for Steel C45 at different temperatures

Shows that Curie-temperature for this kind of steel is 750°C, so the characteristics at that degree is linear and $\mu_r = 1$.

It is already known that the specific electric resistance of conducting materials is a function of temperature; hence, this factor should be included in this analysis in order to make the simulation as real as possible. Fig. (2) represents $\rho(T)$, the specific electric resistance or the resistively of the carbon steel C45 as a function of temperature [3].

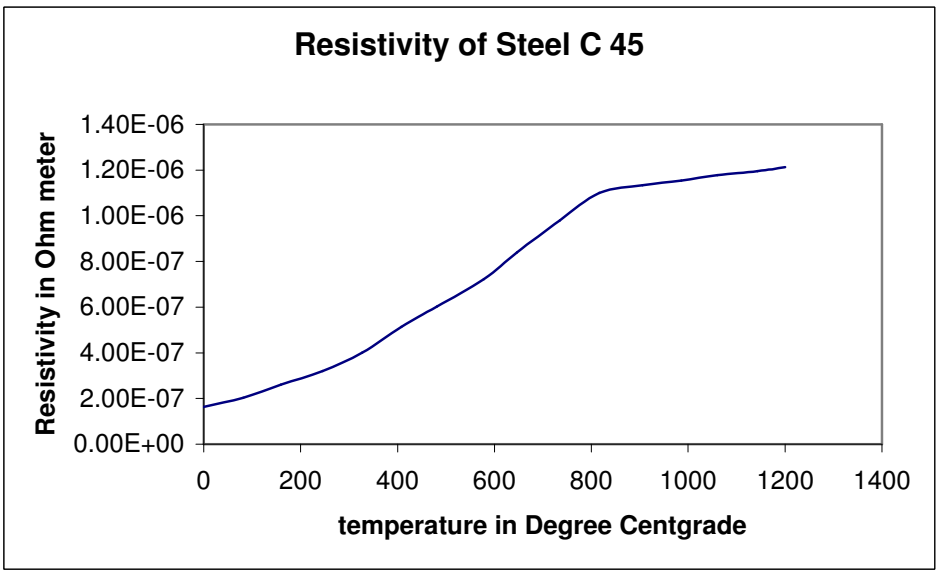

Fig. (2). the electrical resistively of steel C45 as a function of temperature

SIMULATION RESULTS

a - Effect of non-linear magnetic charge

As mentioned before two examples have been applied to verify the present results. The first example for a low frequency furnace of 60Hz Its data shown in table (1) .

Table (1)

Coil inner diameter (m)	0.08256
Coil length (m)	0.254
Number of turns	29.5
Frequency (Hz)	60
Charge material	Steel SAE1045 (C45)
Charge diameter (m)	0.06032
Charge length (m)	0.254
Charge conductivity (mho/m)	5E6
Relative Permeability	18

In this example two solutions are obtained, (applying constant current density source), the first solution is done assuming linear magnetic material with μ_r=18, and in the second solution the (B-H) non-linear relation at ($T = 0^o C$) as shown in Fig. (1) is considered. The finite element model of the furnace under consideration is shown in Fig. (3). The distribution of the normalized value of the current density magnitude $J_n = |J| / |J_{surf}|$ on charge mid-plane is drawn as a function of normalized charge radius for the linear and non-linear case is shown in Fig. (4). The results show that the current density distribution

for the ANSYS and that of reference [2] are exactly the same, while, there is a difference in a nonlinear case, because they consider the non-linearity in different ways. The power loss in each case is calculated and the "Non-Linear Factor" NLF is about 1.524. Where, NLF is the ratio of the power loss inside the core in the non-linear case to that of the linear one. This computed value of NLF is about 5.4% more than Boden's experimental value of this factor that has been found to be 1.47 [11].

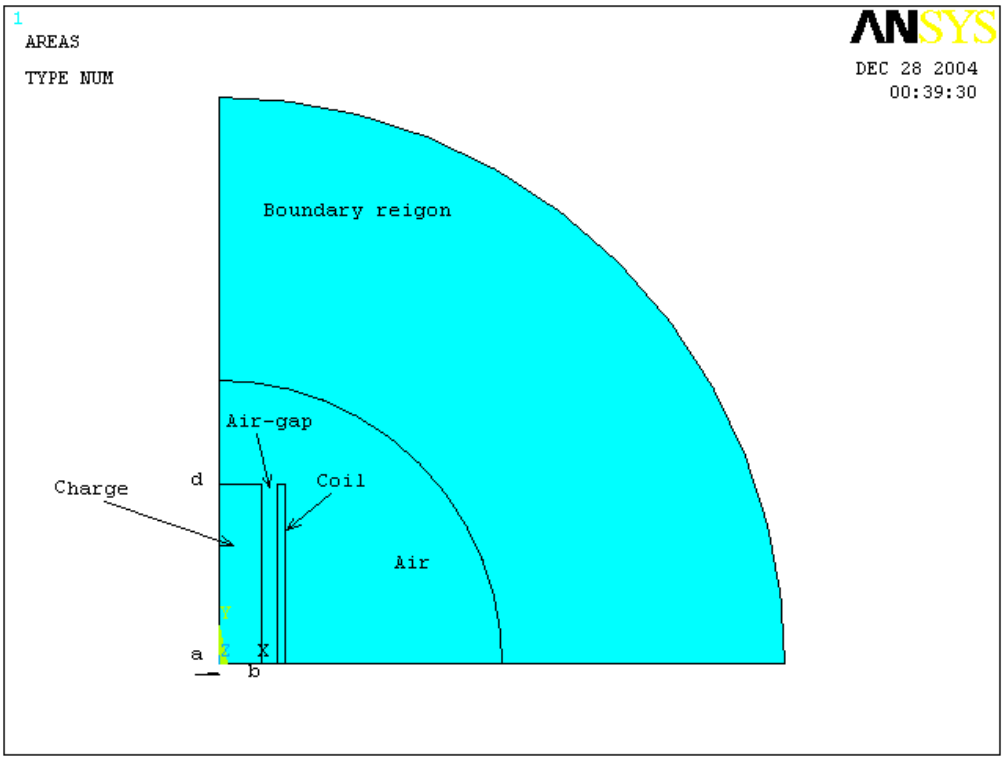

Fig. (3). Quarter of the longitudinal section in the finite element model of the furnace.

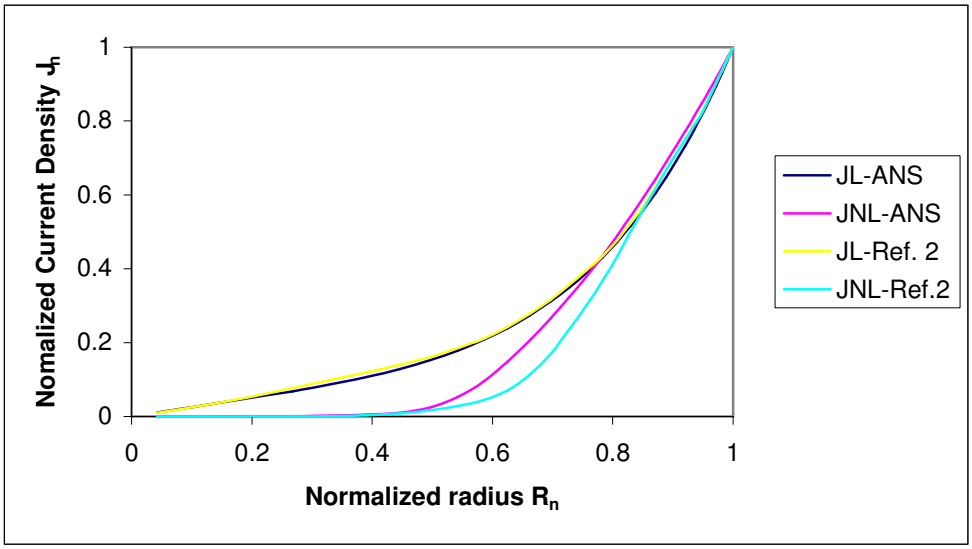

Fig. (4) Distribution of normalized current density magnitude for linear and non-linear cases for a 60 Hz furnace

The second example is for the medium frequency range furnace with the data shown in table (2). The same graph is drawn as that for example (1), given in Fig. (5). The results show reasonable agreement with that of reference [2]. The NLF in this case is calculated to be 1.266, which is 20.4% less than Boden's value. The obtained results verifies the method used by ANSYS 7 to treat the non-linearity of the magnetic circuit.

Table (2)

Coil inner diameter (m)	0.0412
Coil length (m)	0.5842
Number of turns	61
Frequency (Hz)	4000
Charge material	Steel SAE1045 (C45)
Charge diameter (m)	0.0254
Charge length (m)	0.5842
Charge conductivity (mho/m)	4.878E6
Relative permeability	88

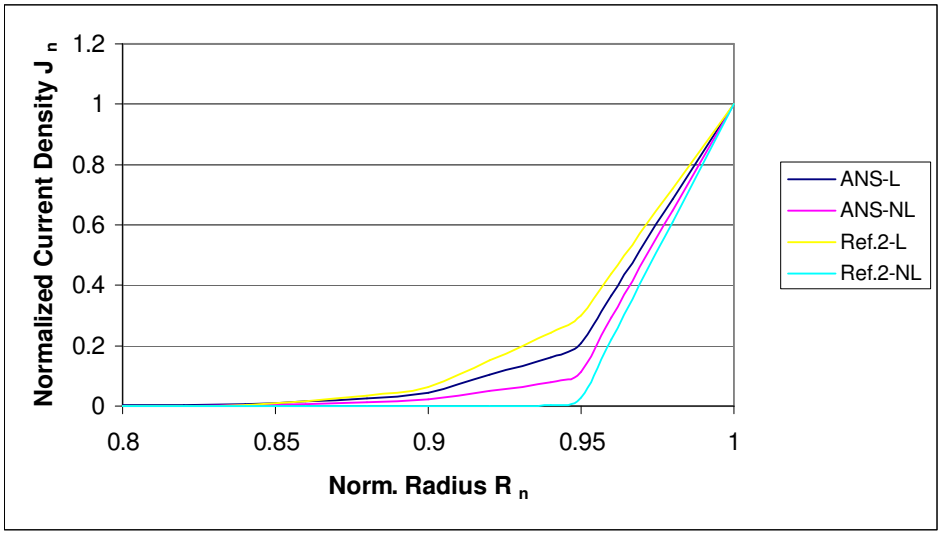

Fig. (5) Distribution of normalized current density magnitude for linear and non-linear case for a 4000 Hz furnace

b- Effect of temperature increase

In order to study the electromagnetic parameters during the temperature increase inside the furnace, five different temperatures are assumed for the furnace under test, these are (0.0°C, 250°C, 450°C, 650°C, &750°C). The (60Hz) furnace of example (1), is analyzed at these temperatures. This analysis done on the low frequency furnace only, because, in such a kind of furnaces the heat distribution inside the core seems to be approximately uniform, so, the results will give the most logical descriptions can be obtained for the given temperature. While, this assumption is quiet wrong in the medium frequency furnaces due to the sever skin effect in such frequencies, which leads to non-uniform distribution of the temperature inside the core. The magnitudes of H, B, and J for three different positions in the charge, (the mid-plane, the external side surface and the top surface) for each temperature are calculated and plotted as shown in Fig. (6.a.b.c), (7.a.b.c), &(8.a.b.c.) respectively.

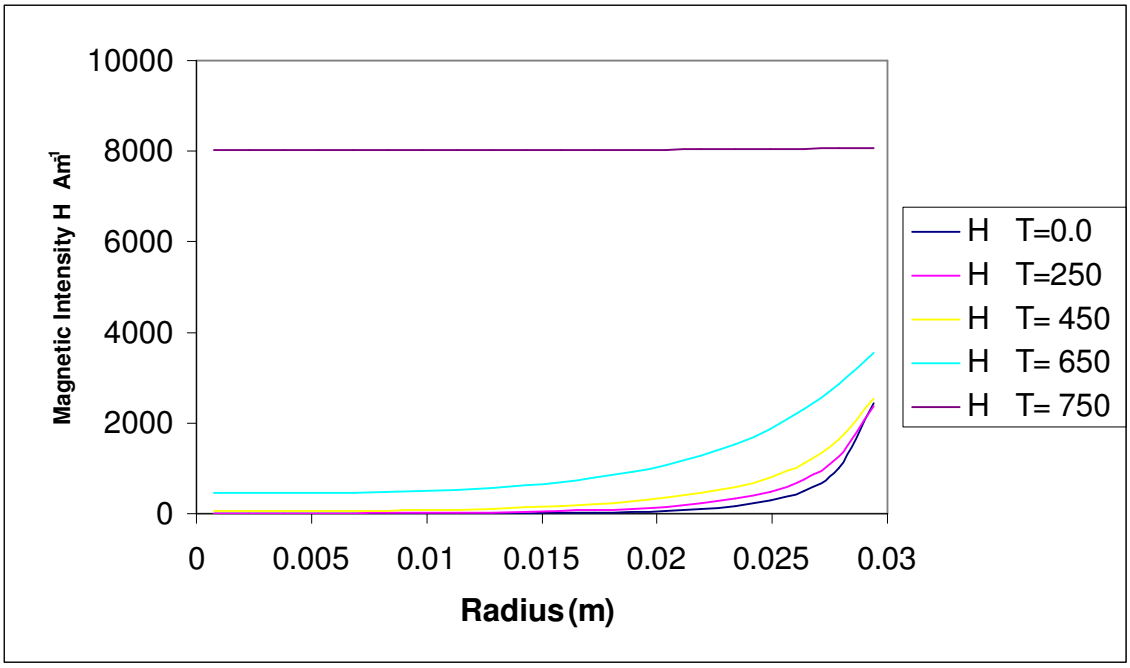
10000
8000
6000
4000
2000
0
Magnetic Intensity H Am-1
0
0.005
0.01
0.015
0.02
0.025
0.03
Radius (m)
H T=0.0
H T=250
H T= 450
H T= 650
H T= 750

(6-a)

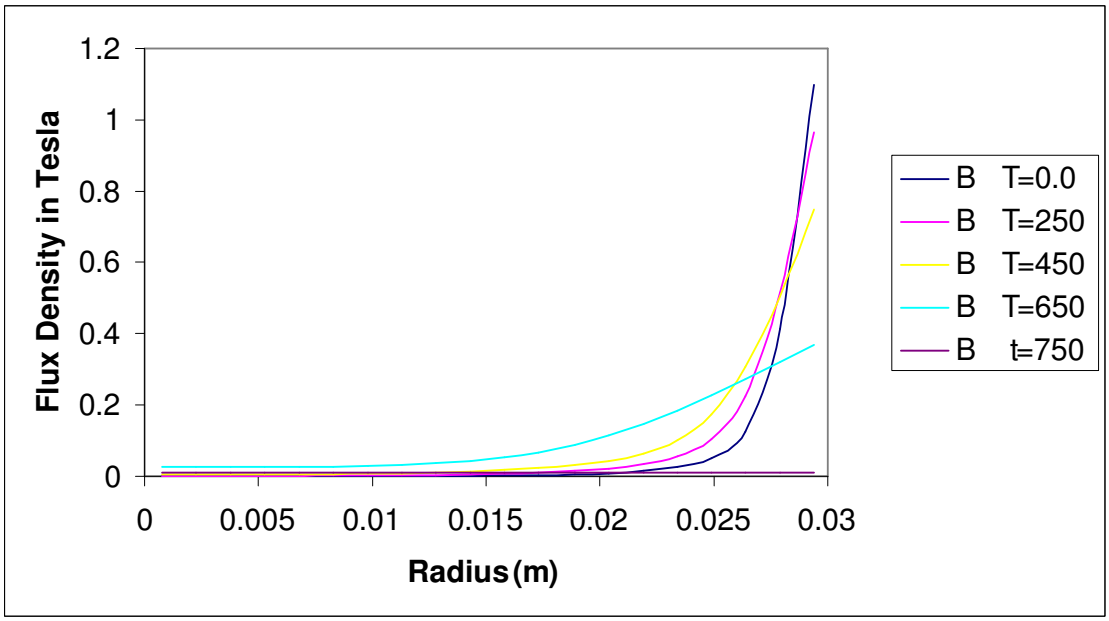
1.2
1
0.8
0.6
0.4
0.2
0
Flux Density in Tesla
0
0.005
0.01
0.015
0.02
0.025
0.03
Radius (m)
B T=0.0
B T=250
B T=450
B T=650
B t=750

(6-b)

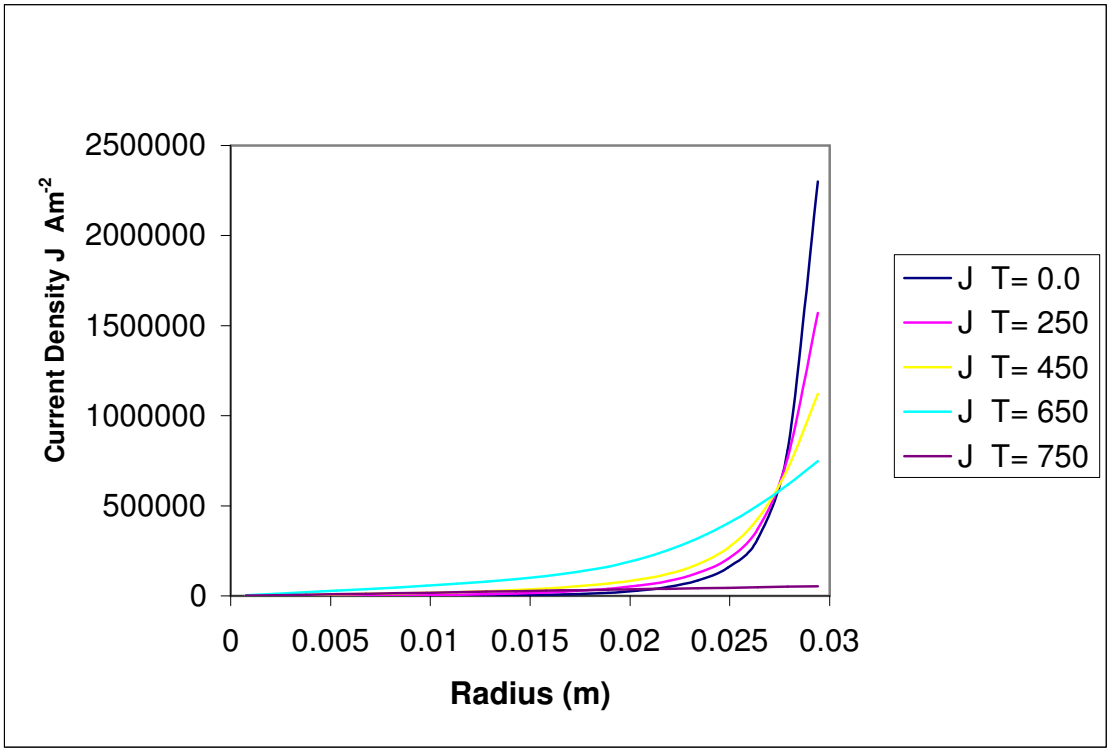

(6-c)

Fig. (6-a, b, c) Distribution of $|H|$, $|B|$, and $|J|$ as a function of the core radius in the mid-plane of the core for different temperatures

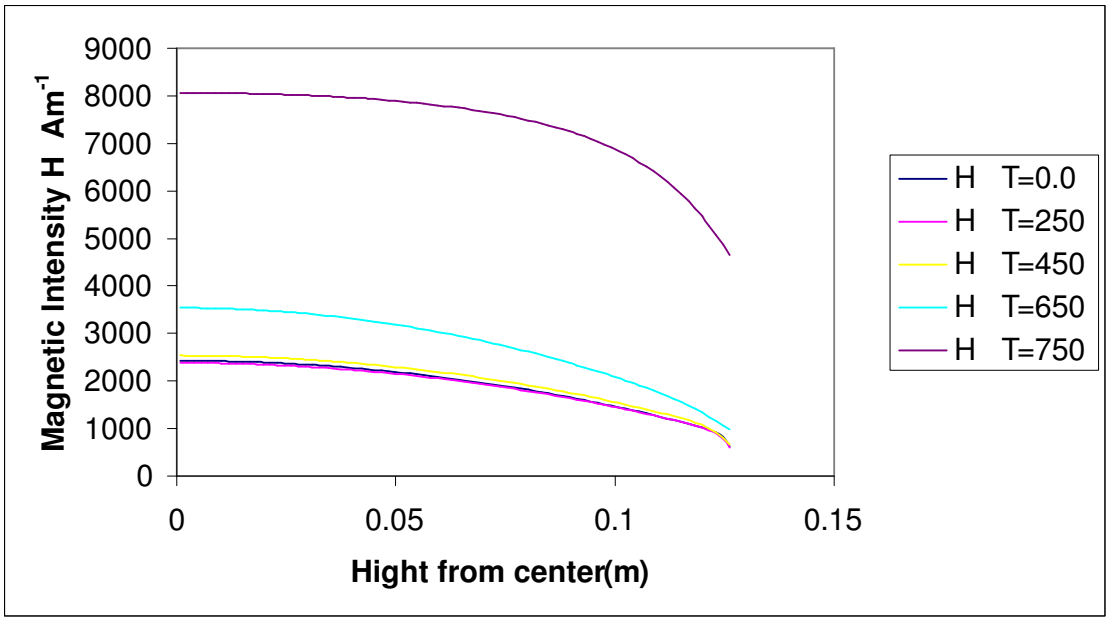
Magnetic Intensity H Am-1
9000
8000
7000
6000
5000
4000
3000
2000
1000
0
0
0.05
0.1
0.15
Hight from center(m)
H T=0.0
H T=250
H T=450
H T=650
H T=750

(7-a)

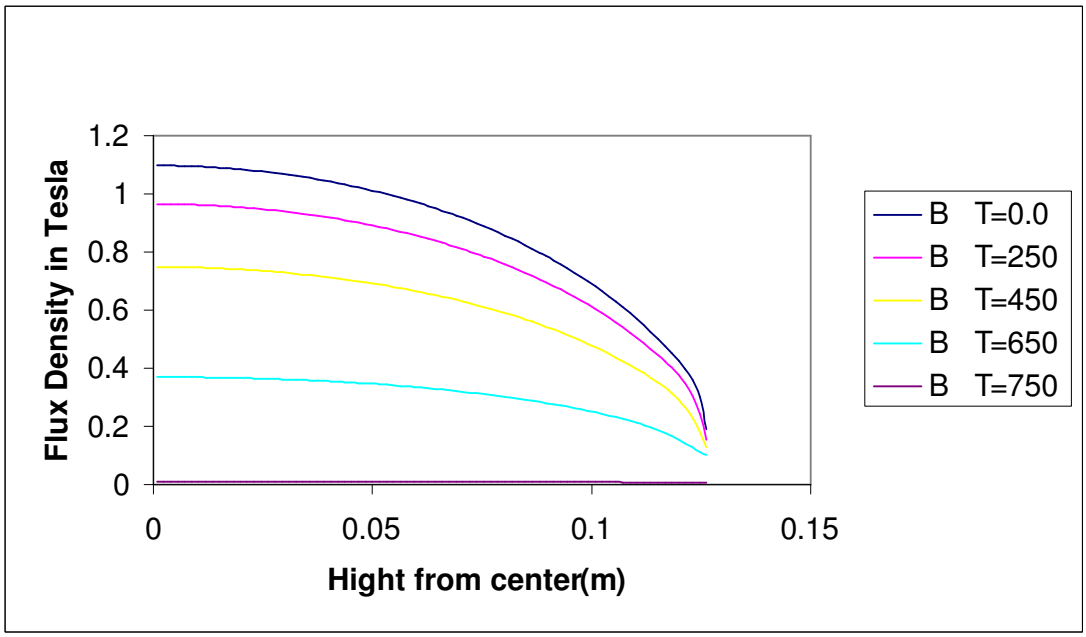
Flux Density in Tesla
1.2
1
0.8
0.6
0.4
0.2
0
0
0.05
0.1
0.15
Hight from center(m)
B T=0.0
B T=250
B T=450
B T=650
B T=750

(7-b)

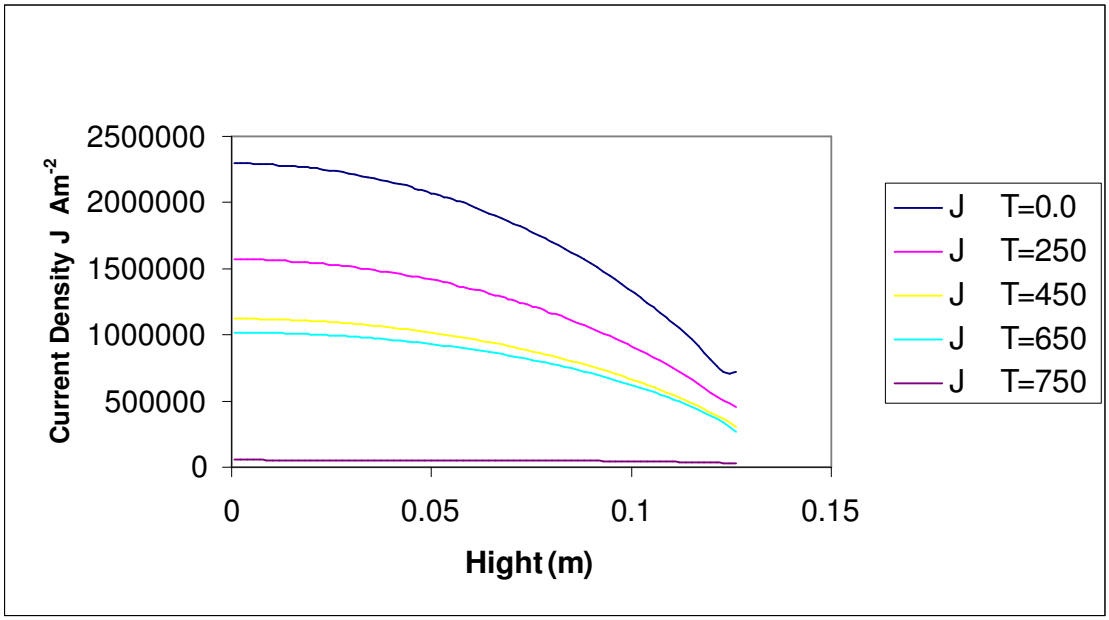

(7-c)

Fig. (7-a,b,c) Distribution of $|H|$, $|B|$, and $|J|$ at the external side surface for different temperatures

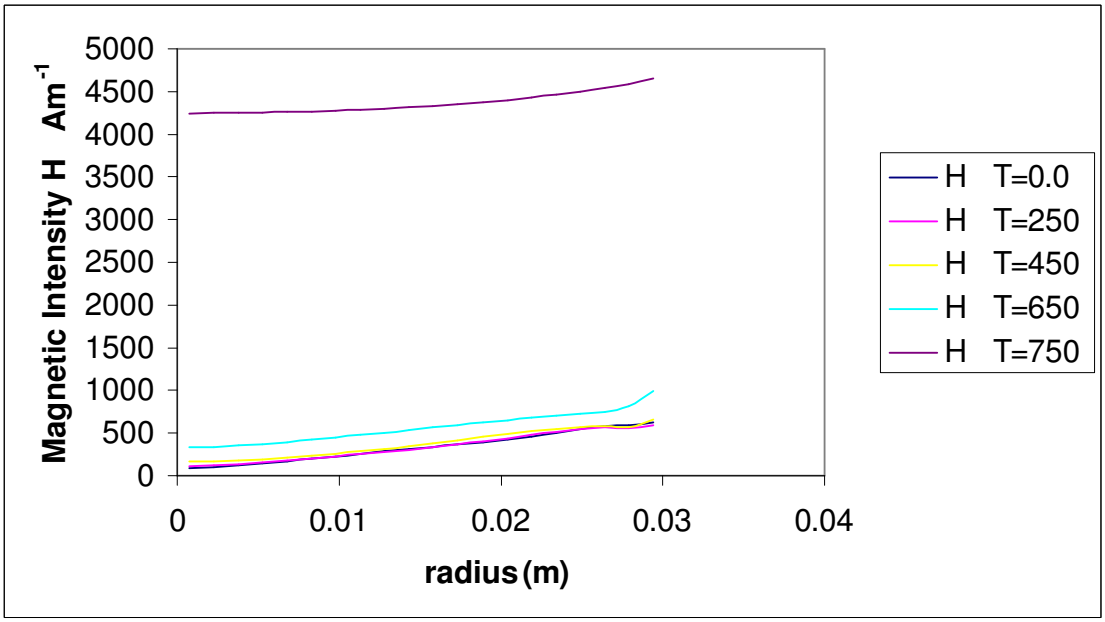

(8-a)

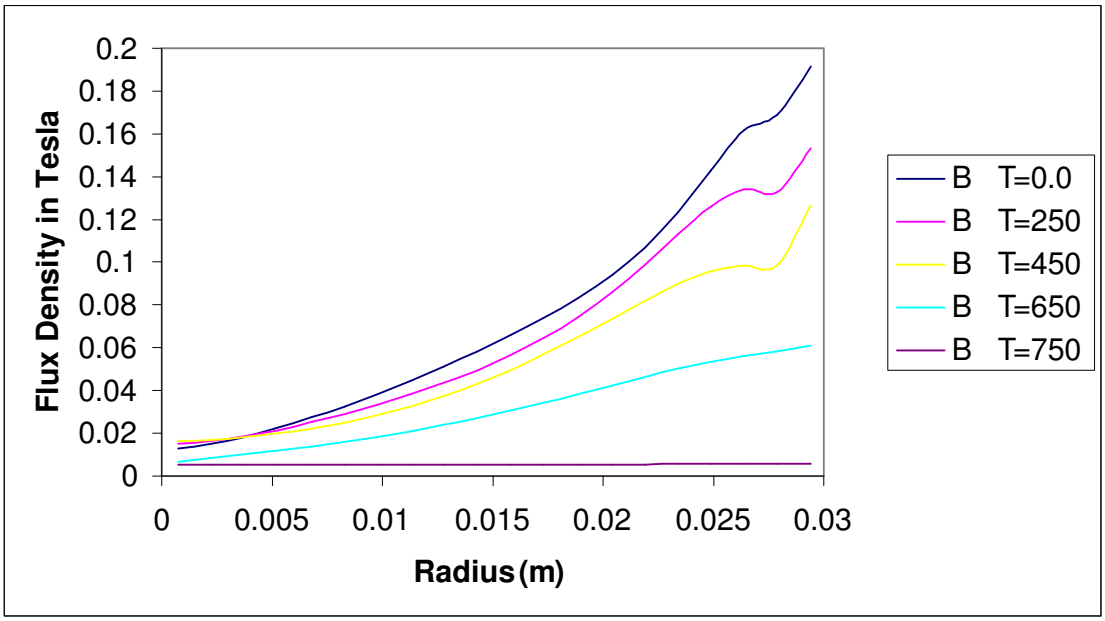

(8-b)

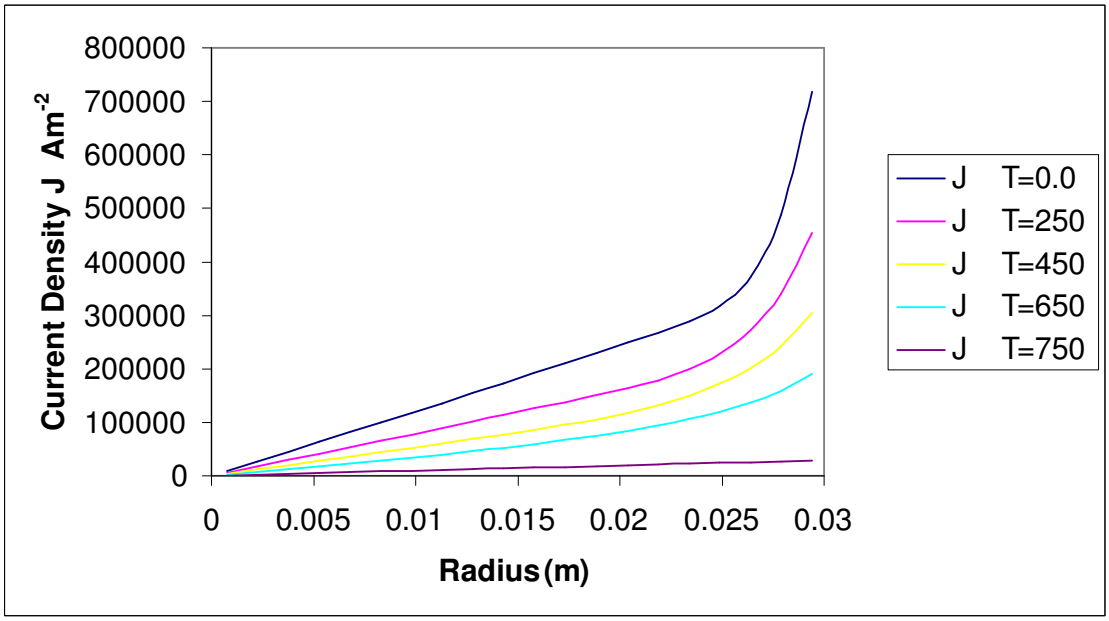

(8-c)

Fig. (8-a, b, c) Distribution of $|H|$, $|B|$, and $|J|$ as a function of the core radius in the mid-plane of the core for different temperatures

DISCUSSION

This paper declares the effect of the non-linearity in the (B-H) curve of the magnetic charge of the furnace on the flux distribution and on other parameters like $J, B, \& H$. The results obtained seems to be quite reasonable, and agrees with that

published to deal with non-linearity at room temperature only. Two kinds of furnaces are used for verification of the work, low frequency, and medium frequency one. The analysis extended to deal with other temperatures taking into consideration the effect of temperature increase on the permeability and the electrical resistivity of the steel charge

The results obtained in the first part of this research show that the power delivered to the charge is more than that calculated by the linear analysis, because NLF is always more than one. Also, it is clear that the skin depth is less than that in the linear case, while the eddy current magnitude increases especially behind the side external surface of the charge.

When the effect of temperature increase studied, the results show that the flux density reduced as the temperature increased due to the associative reduction in the permeability and the magnetizing force increased. This is quite reasonable because the magnetizing force is severely opposed by the flux generated due to the induced eddy currents, but, when the permeability reduced, the induced eddy currents reduced too leading to reduce the reduction of the magnetizing force. But the magnetizing force is constant since the input current to the coil from the power supply is constant, so the resultant H will increase with the reduction of the permeability, which is the case here. Also, as a result of eddy current reduction, the distribution of the magnetic intensity H will be approximately uniform everywhere inside the core when Curie temperature reached. This will lead to the conclusion that, the power losses due to eddy currents will be reduced with the increase of charge temperature

The flux distribution for each temperature is shown in Fig. (9) inside and outside the furnace. It is clear that the density of flux lines increased near the side surface of the charge at (T=0.0^{o}C), and it tends to be approximately uniform at Curie temperature.

Conclusion and Future Work

The results show that the permeability of the charge material is the dominant parameter due to its sever effect on the distribution of $J, B, \& H$, and the depth of penetration of the power inside the charge, is a function of temperature also during the heating cycle (for constant frequency).

It is very obvious that the distribution of $B, H, \& J$ is approximately uniform inside the core at Curie temperature. This study prepares to complete the simulation of the induction furnace using the FEM in that it helps to expect the furnace behavior during the heating process. In order to reach the most real study of the furnace, an electromagnetic-thermal coupled analysis should be done considering $\mu(T,H) \& \rho(T)$ simultaneously and continuously for each element inside the FE model during the increases in temperature of the furnace. Such a study will be the aim of the authors in future.

From the power supply point of view, it is clear that the furnace is a non-linear load. Hence an electromagnetic-thermal coupled analysis will lead to calculate the variation in load impedance during operation and this will help very much to expect the design parameters of the power supply needed for certain load.

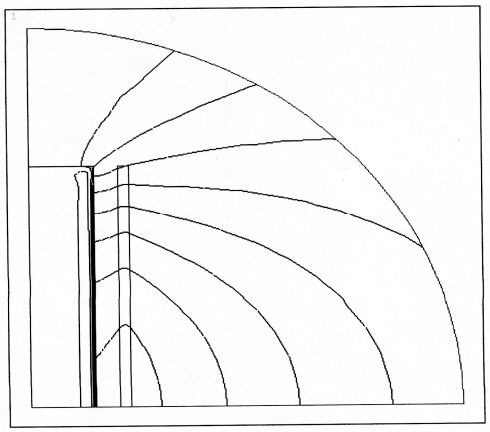

T=0.0°C

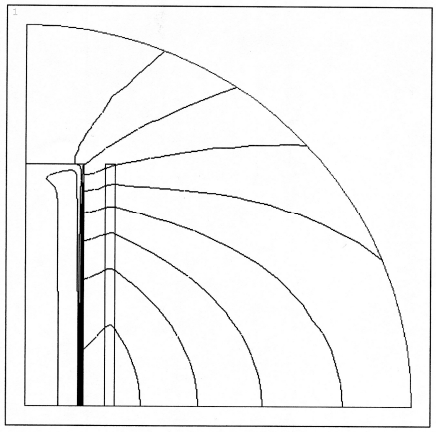

T=250°C

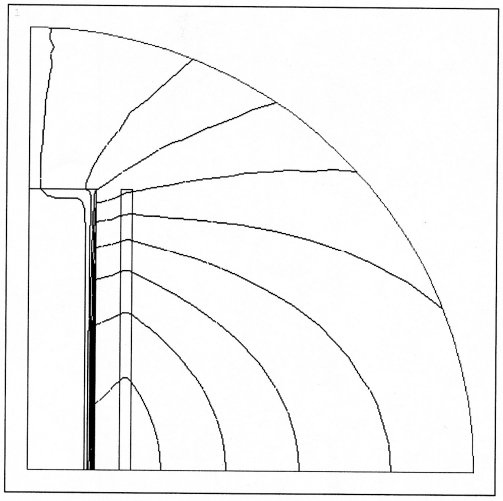

T=450°C

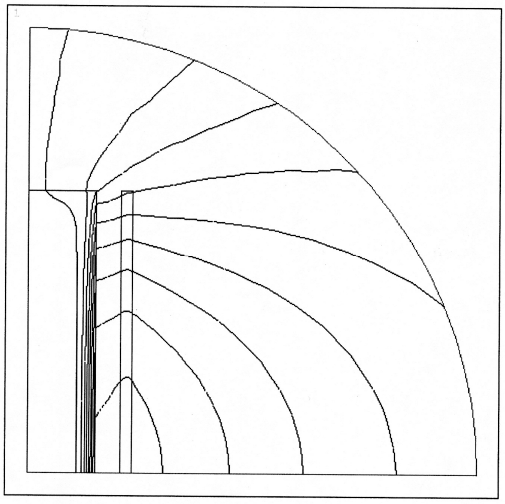

T=650°C

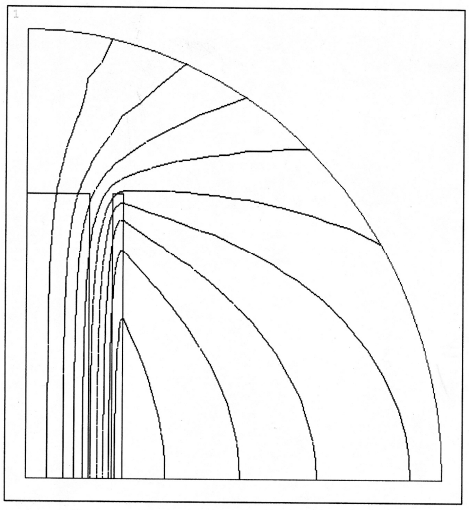

T=750°C

Fig. (9)
The distribution of flux during operation at different temperatures

B	: Magnetic flux density	Tesla.
H	: Magnetic field intensity	$Amp.m^{-1}$.
I	: Current	Amp.
J	: Current density	$Amp.m^{-2}$.
T	: Temperature.	^{o}C
μ	: The permeability	$Henry.m^{-1}$.
μ_r	: The relative permeability.	
δ	: The Skin depth	m
ρ	: The resistivity	Ω.m.
σ	: The conductivity	$(\Omega.m)^{-1}$.
ϖ	: The angular Frequency	$Rad.\ Sec^{-1}$

REFERENCES

1. Dr. Adil H. Ahmed, Dr. Akram F. Batti, Mr. Essam. M. Abdul-Baki, "A Study of Eddy Currents in a Linear Induction Furnace Using Finite Element Method",2004

2. Razzaq A. Marsuq, , "Analysis and Study of Design Criteria of Induction Furnaces", M.Sc. Thesis, University of Baghdad, (1994).

3. Jorg Cstrowski, "Boundary Element Methods for Inductive Hardening", Ph.D. Thesis, University of Tubingen, 2003.

4. A. Vasiliev, I. Poniak, V. Greshnov, "Modeling and Investigation of Hardening Process", International Scientific Colloquium "Modeling For Electromagnetic Processing", Hannover, March 24-26,2003.

5. Gillott, D.H. and Calvert, J.F., "Eddy Current Loss in Saturated Solid Magnetic Plates, Rod and conductors", IEEE Trans. On Magn., Vol. MAG-1, 1965, pp. 126-137.

6. El-Markaby, M.S., Fawzi, T.H. and Ahmed, M.T., "Approximate Treatment of Non-linear Eddy Current Problems", *ibid,* Vol. MAG-18, No.6. Nov. 1982. pp. 1737-1739.

7. Lavers, J.D., "Finite Element Solution of Non-linear Two Dimensional TE-Mode Eddy Current Problems", *ibid,* Vol. MAG-19, No.5, Sept. 1983, pp. 2201-2203.

8. Marchand, ch. and Foggia, A., "2-D Finite Element Program for Magnetic Induction Heating", *ibid,* Vol. MAG-19, No.6, Nov. 1983, pp2647-2649.

9. Lavers, J.D., Ahmed, M.R., Cao, M. and Kalaichelvan, S., "An Evaluation of loss Models for Non-linear Eddy Current Problems", *ibid,* Vol. MAG-21, No.5, Sept. 1985, pp. 1850-1852.

10. Demerdash, N.A. and Gillott, D.H., "A New Approach for Determination of Eddy

Currents and Flux Penetration in Non-linear Ferromagnetic Materials", *ibid*, Vol. 10, 1974 pp. 682-685.

11. Davies, J. and Simpson, P., "Induction Heating Handbook", McGraw-Hill Book Company (UK), 1979.

DESIGN AND IMPLEMENTATION OF A TRANSPARENT SECURE LAN

Dr. Sufyan T. Faraj and Firas R. Barjas

ABSTRACT

Many attacks may be carried out against communications in Local Area Networks (LANs). However, these attacks can be prevented, or detected, by providing confidentiality, authentication, and data integrity security services to the exchanged data.

This paper introduces a security system that protects a LAN from security attacks. On each host in the protected LAN, the security system transparently intercepts each outbound IP (Internet Protocol) packet, and inserts a crypto header between the packet IP header and payload. This header is used to detect any modification to the content of the packet in transit, and to detect replayed packets. Then, the system encrypts the IP packet payload and some fields of the inserted crypto header. On the other hand, the system transparently intercepts each inbound IP packet, decrypts its encrypted portions, and then uses its crypto header to authenticate the packet. If the packet is properly authenticated, the system indicates it to upper protocols.

To be transparent to applications, the security system part that processes inbound and outbound IP packets was implemented as a NDIS (Network Driver Interface Specification) intermediate driver that resides between the LLC (Logical Link Control) and MAC (Medium Access Control) data link sublayers.

الخلاصة

هنالك العديد من الهجمات التي يمكن تنفيذها ضد اتصالات الشبكات المحلية (LANs). ألا أنه بالأمكان منع أو اكتشاف هذه الهجمات عن طريق توفير السرية للمعلومات المتبادلة، و التأكد من سلامتها و صدق مصدرها.

يقترح هذا البحث نظاماً أمنياً يمكن استعماله لحماية شبكة محلية من الهجمات التي قد تستهدف أمنها. في كل حاسبة مرتبطة بالشبكة المحمية، يقوم النظام الأمني المقترح بمقاطعة مسار كل رزمة خارجة من نوع IP packet بصورة شفافة، ثم يقوم بادخال معلومات أمنية (crypto header) بين الـــ IP header و الـــ IP payload. تستعمل هذه المعلومات لكشف أي تغيير لمحتويات الرزمة أثناء تنقلها، و لكشف الرزم التي أعيد بثها. بعد ذلك، يقوم النظام بتشفير الـــ IP Payload، و بعض الأجزاء من المعلومات الأمنية المضافة. من جهة أخرى، يقوم النظام بمقاطعة مسار كل رزمة داخلة الى الحاسبة بصورة شفافة، ثم يقوم بفتح تشفير الأجزاء المشفرة منها. بعد ذلك، يفحص النظام المعلومات الأمنية الموجودة في الرزمة المُستلمة للتأكد من صدق و سلامة معلوماتها. فأذا كانت الرزمة سليمة، يقوم النظام بتسليمها الى البروتوكولات العليا.

لكي يكون النظام المقترح شفافاً للتطبيقات العليا، فأن ذلك الجزء من النظام الذي يعامل الرزم الخارجة و الداخلة تم تنفيذه كسواقة (NDIS intermediate driver)، و التي تقع بين طبقتي الـــ data link layer : LLC و MAC.

KEYWORDS
LAN, **security**, **encryption**, **authentication**, **transparent**, **NDIS intermediate driver**

ABBREVIATIONS

API:	Application Programming Interface
CIMD:	Cryptographic Intermediate Miniport Driver
DDK:	Driver Development Kit
DIX:	Digital equipment Intel Xerox
DoS:	Denial of Service
ESP:	Encapsulating Security Payload
GUI:	Graphical User Interface
ICMP:	Internet Control Message Protocol
IETF:	Internet Engineering Task Force
IM:	Intermediate Miniport
IP:	Internet Protocol
IPX/SPX:	Internet Packet Exchange/ Sequenced Packet Exchange
IV:	Initialization Vector
LAN:	Local Area Network
LLC:	Logical Link Control
LSP:	Layered Service Provider
MAC:	Medium Access Control
MAC:	Message Authentication Code
MD:	Message Digest
MTU:	Maximum Transmission Unit
NDIS:	Network Driver Interface Specification
NIC:	Network Interface Card
OSI:	Open Systems Interconnection
PMTU:	Path Maximum Transmission Unit
SDL:	Security Descriptors List
SHA:	Secure Hash Algorithm
SSM:	Security System Manager
TCP/IP:	Transport Control Protocol/ Internet Protocol
TDI:	Transport Driver Interface
WLAN:	Wireless LAN

INTRODUCTION

Networks have become indispensable for conducting business in government, commercial, and academic organizations. Networked systems allow people to access needed information rapidly, improve communications while reducing their cost, collaborate with partners, provide better customer services, and conduct electronic commerce. While computer networks revolutionize the way people do business, the risks they introduce can be fatal to a business. Attacks on networks can lead to lost money, time, products, reputation, sensitive information, and even lives [ALL01].

The problem of network security is a very complex issue. By definition, network security means a protection of the network assets from different kinds of threats in the network by implementation of different security services using various security mechanisms [TRC99].

The above definition introduces the following three aspects of network security [STA99]:

- *Security Attack:* Any action that compromises the security of information, such as eavesdropping, masquerading, replay attacks, Denial of Service (DoS) attacks, and active change to the exchanged information.
- *Security Service:* A service that enhances the security of data processing systems and information transfers. It is intended to counter security attacks. A security service makes use of one or more security mechanisms. The most important security services are confidentiality, integrity, and authentication.
- *Security Mechanism:* A mechanism that is designed to detect, prevent, or recover from a security attack. Encryption is the security mechanism that can be used to provide confidentiality, whereas hash functions or Message Authentication Codes (MACs) can be used in different ways to provide authentication and data integrity.

Some important insights in the literature concerning the subject of network security are summarized as follows:

- IPSec (IP Security) is a subset of IPv6 and a set of extension to IPv4. It has been developed by the Internet Engineering Task Force (IETF) to provide secure packet transmission over networks.
- A. Ganz, S. H. Park, and Z. Ganz [GAN00] had developed a security broker for Wireless LANs (WLANs). This system implements a number of security services such as authentication and real-time encryption/decryption for the communications in WLANs. The real time encryption/decryption service is implemented as a Layered Service Provider (LSP), and uses Microsoft's CryptoAPI. The use of a LSP allows a Trojan horse, or a worm to directly call the kernel-mode TCP/IP (Transport Control Protocol/ Internet Protocol) driver via the Transport Driver Interface (TDI), and completely bypass the provided security processing.
- The CIPRESS [RAD01] (Cryptographic Intellectual Property Rights Enforcement SyStem) from Mitsubishi Corporation and Fraunhofer-IGD was an attempt for providing transparent network access control, auditing, and encryption on the Microsoft Windows NT platform. CIPRESS provides these services by enforcing an automatic security policy that was implemented using LSP technique. However, CIPRESS supports only complete files, and does not support streaming data.
- B. S. Shaker [SHA02], Al-Nahrain University developed in 2002 an on-line end-to-end cryptography software system for LANs. An NDIS intermediate driver was used to process sent IP packets, and encrypt each IP packet payload using MARS algorithm if its upper protocol is TCP, whereas decryption of received packets was performed at the IP filter hook driver. While encrypting exchanged TCP data provides confidentiality, and some degree of data integrity (depending on encrypted TCP checksum), this system does not protect networks against masquerading because it does not authenticate the source of received packets. Moreover, replay attacks can be launched freely and successfully against the hosts that use this system. On the other hand, the use of IP filter hook driver for decryption instead of the used NDIS intermediate driver unnecessarily introduces additional processing overhead.

The purpose of this paper is to introduce the design of a security system that can be used to provide confidentiality, authentication, and integrity to the data exchanged within a LAN, so that attacks against the exchanged data are prevented (or detected). The security system provides the security services transparently, i.e. there is no need to change software on a user computer that benefits from the provided security services. Users can continue to use their usual network applications (without any change) while the security system provides security services to the exchanged data.

SYSTEM SPECIFICATIONS AND DESIGN APPROACH

The following points shed the light on the specifications of the proposed security system:

- The security system provides confidentiality to the exchanged data.
- The security system provides authentication and integrity to the exchanged data.
- The security system provides access control.
- If received data is not properly authenticated or if it is replayed data, the security system collects audit information from it, and produces an alert to the network security administrator indicating the reception of such invalid data along with the collected audit information. In turn, the network security administrator could monitor the audit information, and take an appropriate action to prevent a possible attack that might cause the reception of the unauthenticated or replayed data.
- The security system is able to prevent DoS attacks launched by hosts unknown to the system.
- The security system is transparent to applications.
- The security system does not affect the work of routers that may exist in the protected network.
- The security system is able to protect itself from attacks.
- Due to the rapid increase of networks, many people who are not so experienced in network security have become network administrators. For this reason, the security system provides a friendly and easy to use interface for them.

To achieve the features and specifications stated above, the following choices were adopted:

- Microsoft Windows 2000 was chosen as the platform under which the proposed security system works, for of its reliability, high performance, and security.
- TCP/IP protocol was chosen as the transport protocol for the protected LAN.
- The LAN protected by the proposed security system was chosen to be Fast Ethernet. The security system assumes that Ethernet frames encapsulate IP packets according to the Ethernet II (DIX Ethernet) encoding, because by default, Microsoft Windows 2000 TCP/IP stack transmits Ethernet frames using this encoding [MAC00].
- The NDIS Intermediate Miniport (IM) driver was chosen to apply the required transparent security processing to inbound and outbound network traffic. NDIS IM driver was chosen for the following reasons:
  1- It is well documented.
  2- It is a kernel mode driver, and all incoming or outgoing packets should pass through this driver. This feature prevents network packets from bypassing the security policy enforced by the security system.
  3- The NDIS IM driver lies below the network layer (between the LLC and MAC data link sublayers [DDK00]). This feature gives NDIS IM drivers a lot of control over network packets, without affecting other network protocol stack components. As an example, the position of NDIS IM drivers make them appropriate to be used to authenticate the source IP address of received IP packets.

The transparent security processing performed by the security system NDIS IM driver mostly follows the way in which the IPSec protocol processes network packets, but it avoids some problems that exist in the IPSec design. These problems are:

1- IPSec is too complex to be secure. The design obviously tries to support many different situations with different options. The number of major modes of operation can be drastically reduced without significant loss of functionality. IPSec is well beyond the level of complexity that can be

analyzed or properly implemented with current methodologies. Thus, no IPSec system will achieve the goal of providing a high level of security [SCH99].

2- The ESP (Encapsulating Security Payload) protocol allows the payload to be encrypted without being authenticated. In virtually all cases, encryption without authentication is not useful. ESP should be modified to always provide authentication; only encryption should be optional [SCH99].
3- When both encryption and authentication are provided, IPsec performs the encryption first, and then authenticates the ciphertext. This is the wrong because going by the "Horton principle", the protocol should authenticate what was meant, not what was said. The meaning of the ciphertext still depends on the decryption key used. Authentication should thus be applied to the plaintext, and not to the ciphertext [SCH99].
4- The specifications of IPSec allow predictable -but random- Initialization Vectors (IVs) to be used in IPsec ESP encryption, and explicitly allow the common practice of using the last ciphertext block of encrypted data from an encryption process as the IV for the next encryption process. Predictable initialization vectors compromise IPsec confidentiality. By using an adaptive chosen plaintext attack, an attacker can break low entropy plaintext blocks using brute force, and confirm guesses of the contents of arbitrary plaintext blocks. However, the preconditions of this attack are restrictive, and the vulnerability is thus difficult, but probably not impossible, to exploit in practice [NUO02].
5- Since IPSec is used to secure IP packets only, packets of transport protocols other than TCP/IP (IPX/SPX -Internet Packet Exchange/ Sequenced Packet Exchange- for instance) are not affected by the processing of IPSec. Hence, the packets of these protocols can still be used to launch attacks against a network, if they are installed on the hosts of that network, even if IPSec is deployed.

The developed security system avoids the complexity and many modes of operation inherent in the IPSec protocol, it always provides authentication and encryption for IP packets, it authenticates the plaintext instead of the ciphertext, it uses a random IV for each IP packet, and it prevents communications using transport protocols other than the TCP/IP protocol (the security system can be improved to secure the packets of these transport protocols instead of blocking them). However, the security system implemented now does not provide automatic key exchange, and this can be considered as a future work.

SECURITY SYSTEM ARCHITECTURE AND COMPONENTS

The security system consists mainly of the following three components:

1- The Security Descriptors List (SDL), which stores security descriptors corresponding to hosts in the protected network.
2- The Security System Manager (SSM), which is a Win32 application that allows the network security administrator to control the operation of the CIMD, and alerts him (or her) if a suspicious packet is received.
3- The Cryptographic IM Driver (CIMD) that applies the transparent security processing to inbound and outbound IP packets.

Fig.(1 illustrates the security system architecture and the interaction among its components. The following subsections introduce these components in more details.

The Security Descriptors List (SDL)

The SDL stores security descriptors corresponding to hosts in the protected network. In other words, the SDL is essentially a list of the IP addresses of other hosts in the protected network, and their security parameters. If the network security administrator wants to enable communication with a certain host, he (or she) must specify a security descriptor corresponding to that host. This security descriptor is used by the security system to process packets exchanged with that host. The security policy enforced by the security system blocks all inbound and outbound packets exchanged with a host, if the SDL does not contain a security descriptor corresponding to that host.

The security system stores the SDL in the Windows 2000 Registry encrypted with a master key, so that it is inaccessible to unauthorized users. Moreover, choosing the Registry to store the SDL prevents non-administrator users from modifying the contents of the SDL.

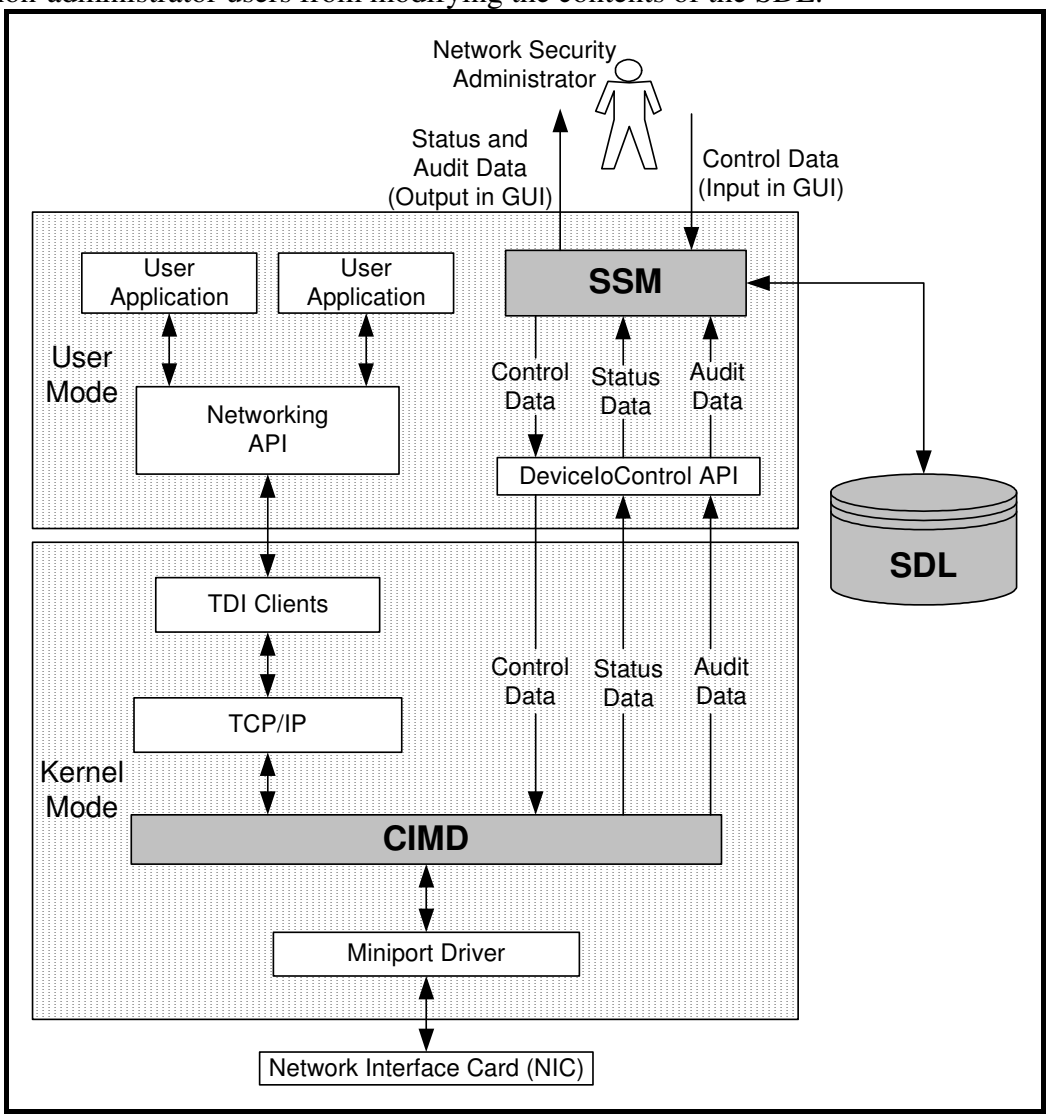

Fig.(1). Security System Architecture

Each security descriptor consists of the following security parameters:

- *IP Address:* This is the IP address of the host represented by the security descriptor.
- *Secure Packets:* This parameter states whether packets exchanged with the host represented by the security descriptor must be secured or not. This parameter is a Boolean flag. If its value is False, all other parameters except the IP Address parameter are ignored.

- *Hash Algorithm:* This parameter specifies the hash algorithm used in the authentication of packets exchanged with the host represented by the security descriptor. The security system implements two hash algorithms: SHA-1 (Secure Hash Algorithm-1) and MD5 (Message Digest 5).
- *Encryption Algorithm:* This parameter specifies the encryption algorithm used to encrypt or decrypt packets exchanged with the host represented by the security descriptor. The security system implements two encryption algorithms: Rijndael and Twofish.
- *Key Length:* This parameter specifies the length of the encryption key used to encrypt or decrypt packets exchanged with the host represented by the security descriptor. The length could be either 128 bits or 256 bits.
- *Encryption Key:* This parameter stores the encryption key used to encrypt or decrypt packets exchanged with the host.
- *Sequence Number Counter:* A monotonically increasing 32-bit value, written in the crypto headers of packets that will be sent to the host represented by the security descriptor. This number is used to detect replayed packets. It is also used as the number of packets, which have been secured with the security descriptor currently used key and algorithms, and which have been sent to the host represented by the security descriptor. This parameter is reset to zero if the security descriptor key or algorithms are changed.
- *Packets Received:* This parameter holds the number of packets that have been received from the host represented by the security descriptor, and processed with the security descriptor currently used key and algorithms. This parameter is reset to zero if the security descriptor key or algorithms are changed.
- *Anti-Replay Window:* A window that is used to detect replayed packets previously received from the host represented by the security descriptor. This parameter is reinitialized if the security descriptor key or algorithms are changed.
- *Bytes Sent:* This parameter holds the number of bytes that have been encrypted with the currently used key and encryption algorithm, and sent to the host represented by the security descriptor.
- *Bytes Received:* This parameter stores the number of bytes received from the host represented by the security descriptor and that have been decrypted with the currently used key and algorithm.

THE SECURITY SYSTEM MANAGER (SSM)

The SSM presents a Graphical User Interface (GUI) to the network security administrator, so that he (or she) can interact with the security system, and control its operation. The SSM provides the following functions:

- At initialization time, the SSM loads the encrypted SDL from the Registry, decrypts it, and passes its security descriptors to the CIMD. The CIMD stores the passed security descriptors in a linked list in its own memory context for fast access. The CIMD uses the security parameters of each security descriptor to process inbound and outbound packets exchanged with the host represented by that security descriptor, and it updates some of these parameters during processing.
- The network security administrator can use the SSM to add, remove, or change the parameters of a security descriptor corresponding to a host in the protected network. The SSM updates the SDL accordingly, and uses the DeviceIoControl API (Application Programming Interface) (The DeviceIoControl API sends a control code directly to a specified device driver, causing the corresponding device to perform the corresponding operation [SDK01]) to communicate with the CIMD, and inform it of the changes.
- The SSM periodically communicates with the CIMD using the DeviceIoControl API to get status data reported by the CIMD, and display it to the security administrator. The status data encompasses the mutable security parameters (that are updated by the CIMD) of all the security

descriptors. These parameters are: Sequence Number Counter, Packets Received, Anti-Replay Window, Bytes Sent, and Bytes Received.

- The SSM periodically communicates with the CIMD using the DeviceIoControl API to get the audit data associated with unauthenticated or replayed packets that were received by the CIMD, if any. The audit data associated with each suspicious received packet is stored in an entry in a linked list maintained by the CIMD. The audit data of each suspicious packet includes: the packet source IP address, the packet source MAC address, whether the suspicious packet is unauthenticated or replayed, the upper protocol data encapsulated by the IP packet, the packet total length, and the time when the suspicious packet was received. If there is audit data, the SSM alerts the network security administrator, and indicates the audit data to him (or her).

The Cryptographic NDIS IM Driver (CIMD)

The CIMD consists of two parts (like any other NDIS IM driver): the miniport part and the protocol part. The miniport part exposes miniport entry points (MiniportXxx functions), which NDIS calls to communicate the requests of one or more overlying protocol drivers. The miniport part in turn forwards these requests to the underlying miniport NIC (Network Interface Card) driver after performing the required security processing, if any.

The protocol part exposes protocol entry points (ProtocolXxx functions), which NDIS calls to communicate requests from underlying miniports. The protocol part in turn forwards these requests to overlying protocols after performing the required security processing, if any.

The CIMD inserts into each outbound IP packet that should be secured a 40-byte crypto header between its IP header and payload. This header consists of three fields:

1- The IV field (16 bytes) that holds the random initialization vector used in the encryption.
2- The Hash field (20 bytes) that holds a hash code calculated over the immutable fields of the IP header, the IP payload, and the Sequence Number field of the inserted crypto header. This hash code provides support for data integrity and authentication of the IP packet. The data integrity service detects any modification to the content of the packet in transit. The authentication service enables the receiving host to authenticate the sending host, and thus prevents address spoofing attacks.
3- The Sequence Number field (4 bytes), which is used to detect replayed packets. Each time that a packet is sent to a host, the sender increments the Sequence Number Counter of the security descriptor corresponding to that host, and places the resulting value in the Sequence Number field of the packet crypto header.

Then, the CIMD encrypts the payload of the IP packet along with the Hash and Sequence Number fields of the inserted crypto header using the encryption key of security descriptor representing the packet destination host. The encryption provides the required confidentiality to the exchanged data, and it protects the hash code held in the crypto header. Fig.(2 shows a typical outbound IP packet that becomes as shown in Fig.(3 after being processed by the CIMD.

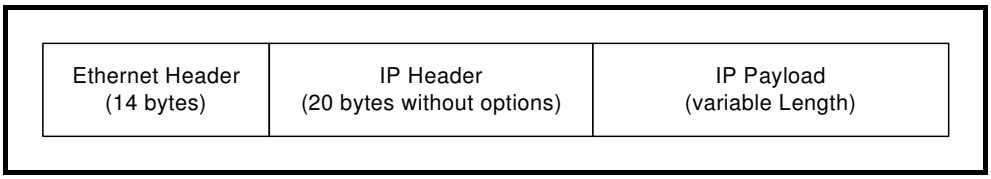

Fig.(2). A Typical Outbound IP Packet

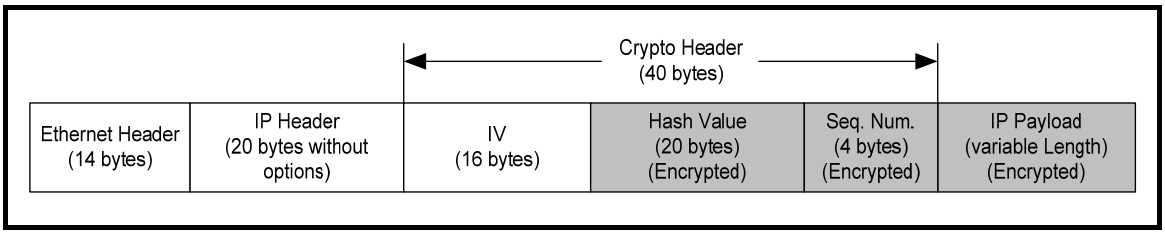

Fig.(3). The Outbound IP Packet after Being Processed by the CIMD

On reception, the CIMD decrypts the encrypted portions of each received IP packet, and then it inspects its crypto header. If the packet is properly authenticated and it is not a replayed packet, the CIMD strips off the crypto header, and then it delivers the packet to upper drivers. Otherwise, if the received packet is not properly authenticated or if it is a replayed packet, the CIMD collects audit information from this packet to be indicated to the network security administrator.

When the CIMD processes an outbound packet, it inserts the crypto header between the packet IP header and IP payload, so that routers in the protected LAN (if any) need not be changed, and they can route the packet properly. Leaving routers unaffected requires also that the CIMD does not encrypt the IP headers of outbound IP packets. However, the CIMD changes the value of the Total Length field of the IP header of each outbound secured packet to reflect the new packet length resulting after the insertion of the crypto header. The Checksum field of the IP header is also changed to a new value calculated over the new IP header.

The security system processes packets in layer 2 (data link layer) of the OSI (Open Systems Interconnection) protocol stack (between the LLC and MAC sublayers). Nevertheless, it does not provide link encryption, and it is considered to be an end-to-end cryptographic system.

LARGE PACKETS RESTRICTIONS

Since the CIMD increases the length of outbound IP packets by the size of the inserted crypto header (40 bytes), the processing of large IP packets may impose the following two problems:

The First Problem

If the CIMD inserts the crypto header into a large IP packet, whose size is larger than 1460 bytes, the size of the packet will become more than 1500 bytes after the insertion of the crypto header. This will cause the sending NIC to drop the packet, because maximum size of IP packets over Ethernet II is 1500 bytes [HOR84].

Hence, to resolve this problem, the security system explicitly sets the MTU (Maximum Transmission Unit) of each network interface to 1460 bytes instead of the default value (i.e. 1500 bytes). This must be done so that the TCP/IP protocol will not send to the CIMD IP packets larger than 1460 bytes. In Windows 2000, the MTU of an *interface* can be changed by modifying the following Registry value [MAC00]:
HKEY_LOCAL_MACHINE\SYSTEM\CurrentControlSet\Services\Tcpip\Parameters\Interfaces*interface*\MTU.

The Second Problem

This problem results from the solution of the first problem. It occurs when a router that uses the security system routes a secured packet of size larger than 1460 bytes, and which was received from another host. Since the MTUs of the router network interfaces are set to 1460 bytes by the security system installed on it, the router will fragment the received secured packet. Apparently,

fragmentation of a secured packet conflicts with the work of the security system. This is because the packet fragments other than the first one will not have crypto headers, and so will be considered unauthentic by the security system on the target host. The first fragment will not be authentic also, because its crypto header originally authenticates the total packet, not only the first fragment. The security system resolves this problem by disabling the Path MTU (PMTU) Discovery [MOG90] that is used by default by Windows 2000 for packets destined to a non-local host [MAC00].

Since the IP layer on the sending host is unaware of the existence of the CIMD that increases the length of outbound packets, PMTU discovery cannot resolve the problem of large packets sent to a non-local host stated above. This is because even if the IP layer adheres to the Next-Hop MTU value in the ICMP (Internet Control Message Protocol) Destination Unreachable messages reported by some router in the packet path, the CIMD still increases the length of outbound packets by the size of the inserted crypto header after it receives them from the IP layer. Thus, resulting packets will have a length 40 bytes more than the Next-Hop MTU reported by the router, and thereby causing the router to drop these packets.

In Windows 2000, when PMTU Discovery is disabled (which is the solution to the problem), an MTU of 576 bytes is used for all non-local destination addresses [MAC00]. Hence, after the CIMD inserts the crypto header into an outbound packet destined to a non-local host, the packet length will not exceed 616 bytes (576 bytes, the MTU + 40 bytes, the size of the crypto header). This packet length is well below the MTU of intermediate routers that use the security system. Thus, packets having this length will not be fragmented by the intermediate routers. The PMTU Discovery can be disabled by setting the following Windows 2000 Registry value to 0 [MAC00]:
HKEY_LOCAL_MACHINE\SYSTEM\CurrentControlSet\Services\Tcpip\Parameters\EnablePMTU Discovery

SECURITY SYSTEM IMPLEMENTATION AND PERFORMANCE RESULTS

The CIMD was written in C language and using NDIS library support routines, then it was compiled and built using the Windows 2000 DDK (Driver Development Kit). The SSM was developed using Microsoft Visual C++ language.

To measure the performance results, the security system was installed on 5 machines, which were connected as 100BaseTX Fast Ethernet by using Linksys 10/100 dual speed 16-port stackable Hub. The specifications of each machine were as follows:

- Processor: Intel Pentium III, 866 MHz
- Physical Memory: 128 Mbytes
- Hard Disk: Western Digital Caviar, 20 Gbytes
- LAN Card: Realtek RTL8139(A)
- Operating System: Windows 2000 Advanced Server

Three tests were performed on two machines (from now on, they will be called A and B) during the transfer of a 710-Mbyte file between them: network performance test, memory usage test, and processor usage test. The file was located in A, while B was used to get the file from A. All the results were measured using the Performance tool of Windows 2000. The tests were repeated on the two machines when they used the security system in each of the following cases:

1- The encryption algorithm is Rijndael, and the hash algorithm is SHA-1.
2- The encryption algorithm is Rijndael, and the hash algorithm is MD5.
3- The encryption algorithm is Twofish, and the hash algorithm is SHA-1.
4- The encryption algorithm is Twofish, and the hash algorithm is MD5.

For comparison purposes, the tests were also repeated in the following cases:

1- When the two machines deployed Windows 2000 IPSec with a pre-shared key as the authentication method, ESP as the used IPSec protocol, 3DES as the encryption algorithm, and SHA-1 as the hash algorithm used by the IPSec HMAC.
2- When nothing was used to secure network traffic. This situation will be referred to as: "Normal Case".

The following subsections present and discuss the results of all the performed tests.

Network Performance Test

The average packets/sec Performance tool counter was used to measure the network performance. Table shows the results of the average packets/sec counter in all the cases.

When the security system is deployed, the degradation in the average packets/sec rate with respect to the Normal Case was about: 31.7% for (Rijndael,MD5), 35.6% for (Rijndael,SHA-1), 44.4% for (Twofish,MD5), and 45.5% for (Twofish,SHA-1). On the other hand, the use of the IPSec service with a pre-shared key as the authentication method, ESP as the used IPSec protocol, 3DES as the encryption algorithm, and SHA-1 as the hash algorithm caused a degradation of about 30.9%. The degradation in the average packets/sec rate is a normal result because of the delay introduced by the security related processing on the two machines.

Table (1). The Results of the Network Performance Test

Case	Packets/sec at A	Packets/sec at B
Normal Case	10574.911	10572.754
IPSec	7307.058	7306.679
Security System (Rijndael,SHA-1)	6807.960	6809.903
Security System (Rijndael,MD5)	7218.649	7217.341
Security System (Twofish,SHA-1)	5761.566	5759.622
Security System (Twofish,MD5)	5879.617	5879.498

Processor Usage Test

Processor usage was measured using the %Processor Time Performance tool counter, which is the percentage of time the processor is executing a non-Idle thread. This counter was designed as a primary indicator of processor activity. It is calculated by measuring the time that the processor spends executing the thread of the Idle process in each sample interval, and subtracting that value from 100% (Each processor has an Idle thread, which consumes cycles when no other threads are ready to run) [MSP01].

Notice that the results of this performance measure may not be too accurate because they may be affected by other services and applications that were running on A and B during the file transfer operation. The results of the test are shown in

Table (1. Before the transfer operation started, the %Processor Time was measured at A and B, and its average was nearly 0.2% at each one of them.

When either the security system or IPSec is used to secure network traffic, %Processor Time increases apparently due to the required security related processing. However, the increase in processor usage does not differ much for all the cases that have security processing.

Table (1 shows that the processor usage at B is larger than its usage at A in all the cases. This may be due to the fact that B was the machine that initiated and drove the file transfer operation.

Table (1). The Results of the Processor Usage Test

Case	%Processor Time at A	%Processor Time at B
Normal Case	41.757 %	47.903 %
IPSec	84.787 %	85.212 %
Security System (Rijndael,SHA-1)	84.522 %	89.804 %
Security System (Rijndael,MD5)	83.674 %	88.590 %
Security System (Twofish,SHA-1)	85.060 %	90.825 %
Security System (Twofish,MD5)	86.638 %	88.600 %

Memory Usage Test

Memory usage was investigated using the Available Mbytes counter of the Performance tool. As for the processor usage test, the results of this performance test may not be too accurate because they may be affected by other services and applications that were running on A and B when the file was transferred between them.

Before the file transfer operation started, the memory available at A was: 25.5 Mbytes, while that available at B was: 42 Mbytes. This difference is due to the fact that different services and applications were running on the two machines. Table (3 shows the results of the Available Mbytes counter at A and B when the file was transferred between them in all the cases. The memory used for file transfer at each machine was calculated by subtracting the available memory during the file transfer from the available memory before the file transfer started.

As shown in the table, the memory used at each machine does not differ much for all the cases. It may also be noticed that the memory used at B is more than that used at A in all the cases. This may be because B is the machine that initiated and drove the file transfer operation.

Table (3). The Results of the Memory Usage Test

Case	Available Mbytes at A	Used Mbytes at A	Available Mbytes at B	Used Mbytes at B
Normal Case	22.500	3	36.383	5.617
IPSec	22.680	2.8	37.030	4.97
Security System (Rijndael,SHA-1)	21.000	4.5	35.230	6.77
Security System (Rijndael,MD5)	21.000	4.5	36.770	5.23
Security System (Twofish,SHA-1)	20.090	5.41	34.000	8
Security System (Twofish,MD5)	21.170	4.33	33.570	8.43

CONCLUSIONS

The most important points concluded throughout the design and implementation of the security system are listed below:

- To provide security to the data exchanged within a network, encryption and message authentication mechanisms must be used. However, these mechanisms impact the average packets/sec rate in the network, which degrades by a percentage depending on the complexity of the used algorithms. Moreover, these security mechanisms increase processor usage on the hosts that perform them approximately to the double.
- The development of an end-to-end cryptographic system that works in layer 2 (data link layer) of the OSI reference model can be made much easier, if the protected protocol that works in layer 3 (network layer) is aware of the existence of the cryptographic system. This may require that the

protected protocol and the cryptographic system be developed by the same party, or by cooperative parties.

- Windows network drivers represent a powerful and efficient method to transparently intercept and process inbound and outbound network data. Among the well-documented network drivers, the NDIS intermediate driver is the more powerful, and more efficient one.
- If a network driver below the IP layer (such as a NDIS intermediate driver) inserts a number of bytes into outbound packets that will be sent on a certain network interface, the MTU of that interface must be decreased by the number of bytes that will be inserted, so that large packets are not dropped by the network interface.
- If a NIC has its NDIS task offload capabilities enabled, these capabilities may improperly affect the work of installed packet-modifying NDIS intermediate drivers. Hence, these capabilities should be turned off for the modifying intermediate drivers to work properly.

REFERENCES

[ALL01] J. H. Allen, *"The CERT Guide to System and Network Security Practices"*, Addison Wesley Professional, June 2001.

[DDK00] Microsoft Corporation, Microsoft Windows 2000 Driver Development Kit, *"Network Drivers"*, 2000.

[GAN00] A. Ganz, S. H. Park, and Z. Ganz, *"Security Broker for Multimedia Wireless LANs"*, Elsevier Science B.V., 2000.

[HOR84] C. Hornig, *"A Standard for the Transmission of IP Datagrams over Ethernet Networks"*, RFC 894, April 1984.

[MAC00] D. MacDonald and W. Barkley, *"Microsoft Windows 2000 TCP/IP Implementation Details"*, Microsoft Corporation, 2000.

[MOG90] J. Mogul and S. Deering, *"Path MTU Discovery"*, RFC 1191, November 1990.

[MSP01] Microsoft Corporation, Microsoft Development Network, Windows 2000 Resource Kit Reference, "Windows 2000 Performance Counters Reference", April 2001.

[NUO02] A. Nuopponen and S. Vaarala, *"Attacking Predictable IPsec ESP Initialization Vectors"*, Helsinki University of Technology, 2002.

[RAD01] E. Rademer and S. D. Wolthusen, *"Transparent Access to Encrypted Data Using Operating System Network Stack Extensions"*, Mitsubishi Corporation and Fraunhofer-IGD, 2001.

[SCH99] B. Schneier and N. Ferguson, *"A Cryptographic Evaluation of IPSec"*, Counterpane Internet Security, Inc., 1999.

[SDK01] Microsoft Corporation, Microsoft Development Network, Platform SDK Documentation, April 2001.

[SHA02] B. S. Shaker, *"Design and Implementation of an Online Cryptography System for LANs"*, M.Sc. thesis, College of Engineering, Al-Nahrain University, 2002.

[STA99] W. Stallings, *"Cryptography and Network Security: Principles and Practice"*, Second Edition, Prentice Hall, 1999.

[TRC99] D. Trcek, T. Klobucar, B. Jerman-Blazic, and F. Bracun, *"CA-Browsing System - a Supporting Application for Global Security Services"*, a white paper, Jozef Stefan Institute, 1999.

EXPERIMENTS ON BIOMASS TRANSPORT INSIDE UPFLOW SLUDGE BLANKET REACTORS INTERMITTENTLY FED

Mohanad Jasim Mohammed
Assistant Teacher
Environmental Engineering Department
College of Engineering, University of Baghdad

ABSTRACT

This work describes the experimental activities developed to study the biomass transport phenomena occurring in upflow anaerobic reactor influencing the biomass washout. The experimental investigations have been carried out on pilot UASB fed with the aim to determine the height to which washout is affected by: daily flow distribution; upflow velocity; concentration and sedimentation properties of the biomass. The experiments had shown a considerable influence on the biomass behavior of the time interval between two successive feeds of the reactor. It was found that, if this period is more than 1 hr larger losses of the biomass into the effluent were obtained, independent of the upflow velocity. Shorter time periods give rise to a regular sludge expansion of the interface even with very high upflow velocities (up to 4 m/hr), and accordingly exhibit limited sludge washout.

KEYWORDS
UASB, sludge washout, solids transport, upflow velocity, intermittently fed.

الخلاصة

يصف البحث الفعاليات المختبرية لدراسة ظاهرة انتقال الكتلة الحية التي تحدث في مفاعل الجريان الصاعد الاهوائي للحمأة وتأثير سرعة الجريان الصاعد على عملية انجراف الكتلة الحية خارج المفاعل، الشيء الذي يودي بدوره الى انخفاض كفاءة المفاعل بسبب هذه الظاهرة. تمت هذه التجارب باستخدام منظومة الجريان الصاعد الاهوائي للحمأة بعد تقليمها بحمأة حبيبية من نفس موقع الدراسة لغرض إيجاد الارتفاع الحرج الذي يؤثر على عملية جرف الكتلة الحية من خلال تغير كل من: كمية الجريان الداخل الى المفاعل، سرعة الجريان الصاعد، إضافة الى تركيز وكثافة الكتلة الحية الداخلة الى المفاعل. وخلال البحث تبين بصورة واضحة تأثر سلوك الكتلة الحية بالمدة الزمنية الفاصلة بين كل دورة تغذية بمياه الفضلات، وفي الحقيقة إذا كانت هذه الفترة أكثر من ساعة واحدة فان عملية جرف الكتلة الحية خارج المفاعل سيكون كبيرا وبشكل مستقل عن تأثير سرعة الجريان الصاعد. بينما خلال الفترات الزمنية الأقل من ساعة واحدة سببت تمدد منتظم للحمأة حتى في حالة زيادة سرعة الجريان الصاعد الى (4 متر/ ساعة) مما سبب في تقليل ظاهرة انجراف الكتلة الحية خارج المفاعل.

INTRODUCTION

The anaerobic biological sludge blanket systems proposed over recent years have been considerable interest because of their good removal efficiencies of organic substrates, their relatively of simple layout and the low capital and operating costs. The most successful systems include the upflow anaerobic sludge blanket (UASB - Lettinga et al., 1980). UASB is consisting of a tank fed from below in which the wastewater to be treated flows vertically upwards: the biomass forms a thick layer of sludge on the bottom under a suspension composed of biologically formed granules (blanket). The granule washout into the final effluent of UASB is obviously a critical feature in the operation of these systems (Barber and Stuckey, 1999). If this were to happen, system performance would drop because of the presence of organic solids in the effluent (Lettinga and Hulshoff Pol, 1991) and the reduction of the biomass in the system (Nachaiyasit and Stuckey, 1997). However, continuously fed systems have shown small washout even with high average upflow velocities, in the order of 1 to 1.5 m/hr (Barber and Stuckey, 1999), a result that is essentially attributable to the good sedimentation properties of anaerobic sludge. There is essentially no information available on the washout in systems intermittently fed, which is convivially exist in the wastewater treatment plants of small communities (Garuti et al., 1992).

This work describes the problem of washout in intermittently fed anaerobic systems by referring to experimental tests carried out in a variety of working conditions. These were made possible by using the pilot UASB located at the Al-Mansour company wastewater treatment plant (WWTP) (Baghdad, Iraq). The tests are purposed to determine the extent to which treatment performance is affected by factors such as: daily flow distribution; upflow velocity; concentration and sedimentation properties of biomass.

The work was organised in two phases. **Phase 1** analyses of the wastewater characteristic in the anaerobic sections of the Al-Mansour WWTP by monitoring the sludge concentration under different flow conditions.

Phase 2 of the work was carried out in the laboratory using a glass pilot plant UASB inoculated with the sludge from the Al-Mansour WWTP. UASB was fed with a flow having the same organic matter concentration to reproduce operating conditions close to those of the actual system and physically observe sludge dynamics in the system. Repeated measurements of the total suspended solids (TSS) and soluble chemical oxygen demined (COD) content of the effluent made it possible to determine washout and removal efficiencies according to the way the blanket expanding.

MATERIALS AND METHODS

The experimental activities were carried out at the Al-Mansour WWTP, which consist of an activated sludge biological system with an aeration tank, a settling tank, a thickening tank, a digester for the excess sludge at the end of the treatment processes for an overall volume of 70 m^3. The organic substrate content of influent wastewater is partially degraded by the biomass in anaerobic conditions.

The UASB pilot plant was made from a glass tube with a diameter of 0.1 m and a height of 2.5 m, the wastewater enters the reactor from the bottom across distribution system to allow equal contact between granular bacteria and wastewater. The total volume of the reactor is 0.0196 m^3. The active volume is 0.0094 m^3 (Fig.1). Wastewater is pumped up by a pipeline system, flow meters and valves controlled by a timer system. The system was designed to control discharge and upflow velocity.

The TSS concentration was measured for all sludge samples in compliance with the Standard Methods (1989). The pilot plant was filled up to a height of 1.20 m with 0.0094 m^3 of sludge and $7.30 \cdot 10^{-3} \cdot m^3$ of wastewater from the Al-Mansour WWTP. During the tests, the system was fed generally with a mixture of tap water and glucose having a total COD of 230 g/m^3 (equal to the mean value measured in the influent flow at the Al-Mansour WWTP). In order to check the experimental results, some tests were repeated using wastewater from the Al-Mansour WWTP and these gave acceptable results. In all cases, the temperature and pH of the flow fed to the pilot plant were maintained at almost constant values of 25° C and 6.9, respectively. Experimentation consisted of 10 different tests (Table 1, Figure 1 Schematic representation of the UASB reactor).

TESTS CARRIED OUT ON THE UASB PILOT PLANT

The results of tests were conducted using the glass pilot UASB set up in the laboratory and varying the duration of the feed interruption phases (D_i), the upflow velocity of the flow being treated (*u*), the duration of the feed phases (D_f), the duration of the cycle (D_c), which is given by the sum of the above two times . The main advantage of this series of experiments consists in observing the expansion of the sludge blanket. Ten tests were carried out with different values of D_i: for the first five tests it was less than or equal to 1 hr; for the others it was > 1 hr. The results of the first five tests (Table 1, Columns 7 and 8) show that the sludge blanket almost expanded regularly, regardless of the upflow velocity (some contractor were observed only for *u* close to 4 m/hr or higher). Under these conditions, a clear interface in the sludge blanket was seen to form, a maximum expansion, small TSS concentrations were always measured (Fig.2, for Test 1). Increases in D_i (Tests 6 to 10) showed a significantly thickened sludge blanket on the bottom during the feed interruption phases; the formation of many channels in the sludge blanket when the feed started; most of the wastewater flow passing at high speed (much higher than *u*) through these channels during the feed phases, with a for impotence 'short circuiting' of the sludge blanket, the formation of an irregular interface which disappeared for D_i greater than 3 hr and high TSS concentrations in the effluent. Moreover, increases in D_i led to a greater volume of biogas trapped in the sludge blanket, which was obviously released in the form of large bubbles at the start of feeding and further contributed to the irregular expansion of the sludge blanket in the form of explosion. The influence of upflow velocity on sludge blanket expansion was assessed on the considerations made above, by referring to regular expansion conditions. In particular, the results of Test 1 were used. These results were obtained with D_i equal to 10 min and relative to nine different values of u, the determination over time of the height of the sludge blanket interface during four cycles is reported in Figure 3 as can be seen periodic steady–state conditions were reached in all cases after just two cycles. Obviously, the interface reached gradually higher levels as u increased. The height increase was particularly significant when the upflow velocity passed from 2.30 m/hr to 3.00 m/hr. All the curves show a rapid rise in the sludge at constant speed immediately following the start of feeding and as it continues, the curves show indicating the fall in the interface rising speed after the gradual dispersion of the granular, which were less subject to wastewater flow transport effects. The influence of upflow velocity on washout was proved by means of the measurements of suspended solids in the plant effluent (Fig. 2).

As these measurements are held to be coincident with the mean value of TSS concentration in the effluent during five minutes intervals around the moment of maximum sludge blanket expansion. It was possible to calculate sludge mass escaping into the effluent during this interval. This value was held to be significant index of the measurement of overall system washout (M_w column 2, Table 2) as it constituted the high percentage of the washout and was generally increasing as *u* increased.

Column 3 of Table 2 reports the values indicated with m_w and obtained by the ratio of M_w with the

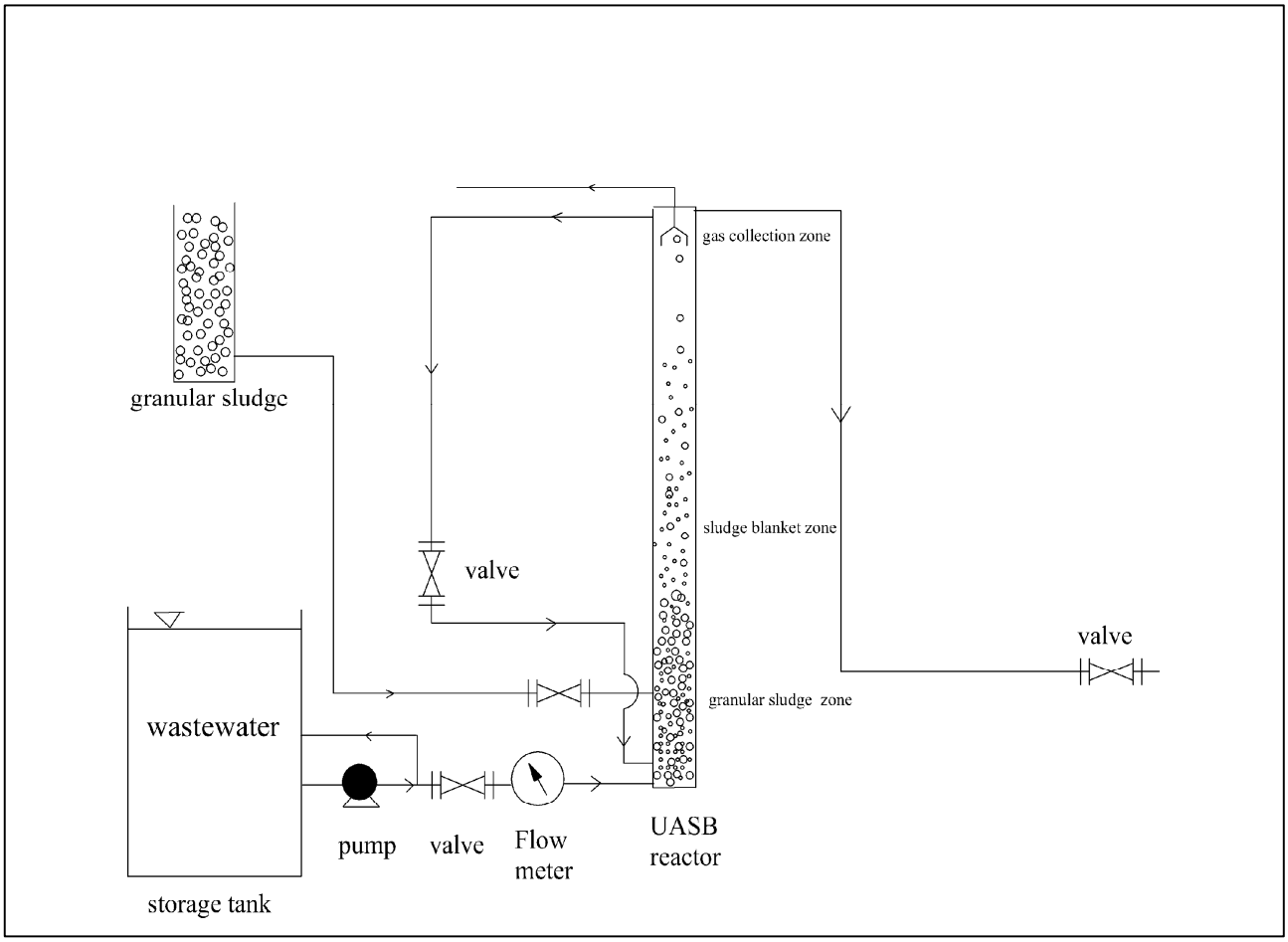

Fig(1).: Schematic Diagram of the UASB Pilot Plant

Table (1) Operating conditions and results of tests on the UASB pilot plant.

Test No.	Df (min)	Di (min)	Dc (min)	u (m/hr)	Number of Investigations	Investigations with blanket regular expansion	Investigations With blanket Regular expansion (%)
1	3	4	2	5	6	7	8
1	10	10	20	2.00	20	20	100
	10	10	20	2.30	20	20	100
	10	10	20	2.50	20	20	100
	10	10	20	3.00	20	20	100
	10	10	20	3.30	20	20	100
	10	10	20	3.45	20	19	95
	10	10	20	4.00	20	19	95
	10	10	20	4.30	20	18	90
	10	10	20	5.15	20	18	90
2	10	20	30	2.00	10	10	100
	10	20	30	2.30	10	10	100
	10	20	30	4.00	10	10	100
	10	20	30	5.15	10	9	90
3	10	30	40	2.30	10	10	100
	10	30	40	4.00	10	10	100
	10	30	40	5.15	10	10	100
4	10	40	50	2.30	10	10	100
	10	40	50	4.00	10	9	90
	10	40	50	4.30	10	9	90
	10	40	50	5.15	10	9	90
5	10	06	70	2.00	10	9	90
	10	60	70	2.30	10	10	100
	10	60	70	3.30	10	9	90
	10	60	70	3.45	10	9	90
	10	60	70	5.15	10	8	80
6	10	90	100	2.30	10	7	70
	10	90	100	4.00	10	4	40
	10	90	100	4.30	10	2	20
	10	90	100	5.15	10	0	0
7	10	180	190	2.30	6	3	50
	10	180	190	4.00	6	2	33
	5	180	185	4.30	6	1	17
	5	180	185	5.15	6	0	0
8	10	480	490	2.30	3	0	0
	5	480	485	4.00	3	0	0
	5	480	485	4.30	3	0	0
	5	480	485	5.15	3	0	0
9	5	1440	1445	2.00	3	0	0
	5	1440	1445	2.30	3	0	0
	5	1440	1445	4.00	3	0	0
10	5	4320	4325	2.15	3	0	0
	5	4320	4325	2.34	3	0	0
	5	4320	4325	3.70	3	0	0

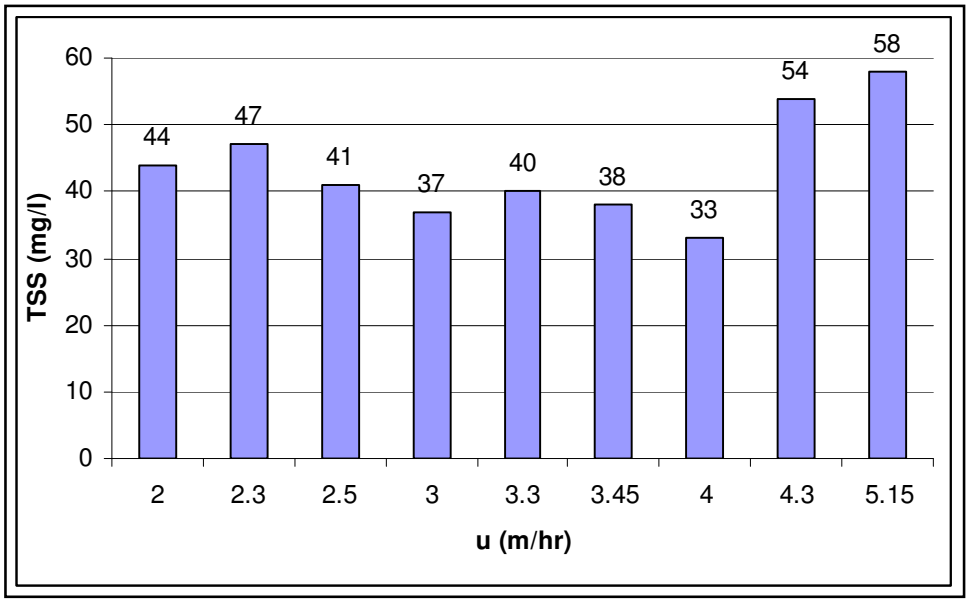

Fig(2). Mean TSS concentrations detected in the effluent of the pilot UASB during Test 1 at the moment of maximum sludge blanket height

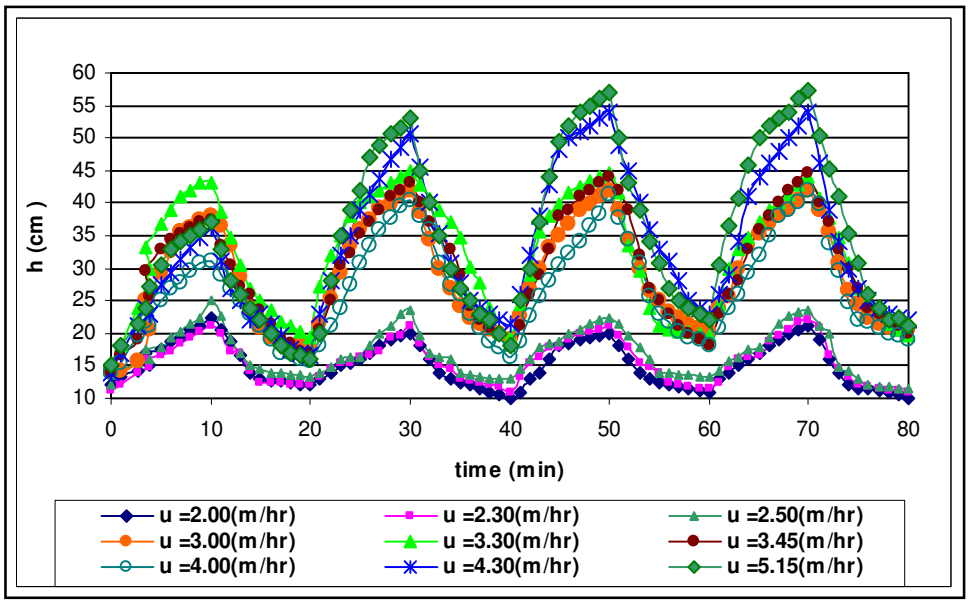

Fig(3). The sludge blanket interface height detected in the pilot UASB during Test No. 1

sludge mass present in the plant at the beginning of the test. The value of m_w was seen to range between 0.17 and 0.25 % when *u* was less than 4.00 m/hr. Moreover, in these conditions the correlation between upflow velocity and washout was second order law (Fig. 4). With values of *u* higher than 4.00 m/hr, m_w exceeded 0.3 % even with regular sludge blanket expansion. This determination was caused by turbulence, which increases separation of the sludge blanket interface. During each investigation in Test 1 the COD of effluent from the pilot plant was determination. The mean values corresponding to each upflow velocity and relative removal efficiencies are reported in Table 2 (column 4 and 5 respectively). Efficiencies are shown in the diagram in (Fig. 5) with a second degree polynomial fitting of the experimental data. It is seen that the best results quadrate to values of *u* between 3.00 and 4.00 m/hr with removal efficiencies values above 60 % with lower values of *u*, the removal efficiencies decrease because of the formation of small channels for the wastewater being treated in the sludge blanket, and although this dose not give rise to the washout that results in the incomplete degradation of organic substrate.

The following observations were obtained:

_If velocity between 3 and 4 m/hr then will be not effect on the washout and assures very high removal efficiencies.
_For velocity values below, 3 m/hr a negligible blanket expansion will aims, but at the same time results in a channeling phenomenon, which lowers treatment efficiency.
_If velocity is higher than 4 m/hr, an increase in the washout and reducing in performance in organic substrate removal will be obtained.

Table (2). Washout flows and filtered COD values in the effluent during Test No. 1

u **(m/hr)**	**M_w (mg)**	**m_w (%)**	**Filtered COD (mg/l)**	**COD Removal efficiency**
1	**2**	**3**	**4**	**5**
2.00	52.20	0.172	129.4	41.90
2.30	61.67	0.177	148.3	38.10
2.50	64.00	0.184	120.8	50.00
3.00	71.08	0.204	76.60	66.67
3.30	94.50	0.272	83.00	63.89
3.45	87.17	0.205	83.00	63.60
4.00	79.40	0.205	76.60	61.10
4.30	126.30	0.364	127.5	44.58
5.15	122.50	0.358	161.0	30.00

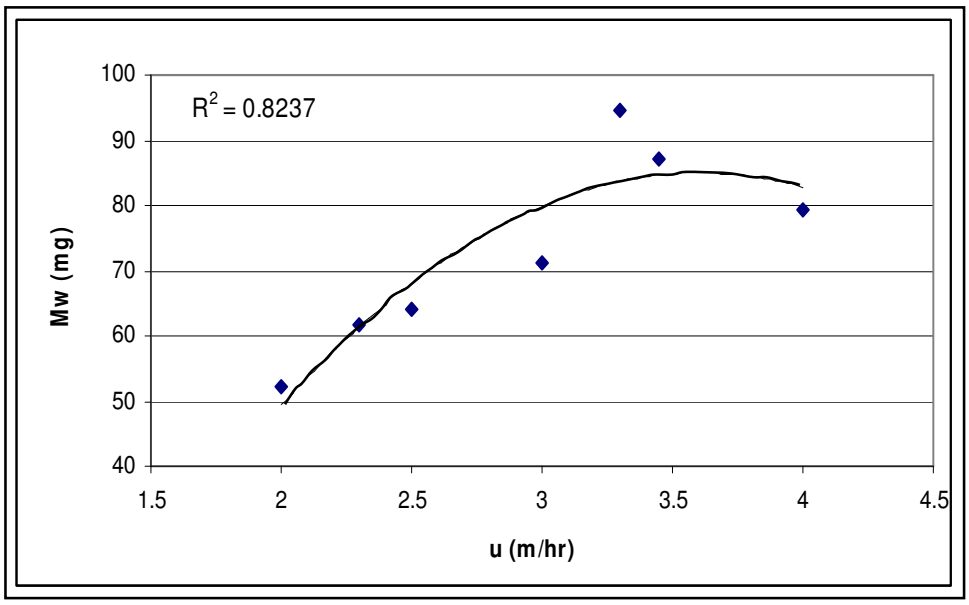

Fig(4). Variation of washout with upflow velocity ($R^2 = 0.8237$)

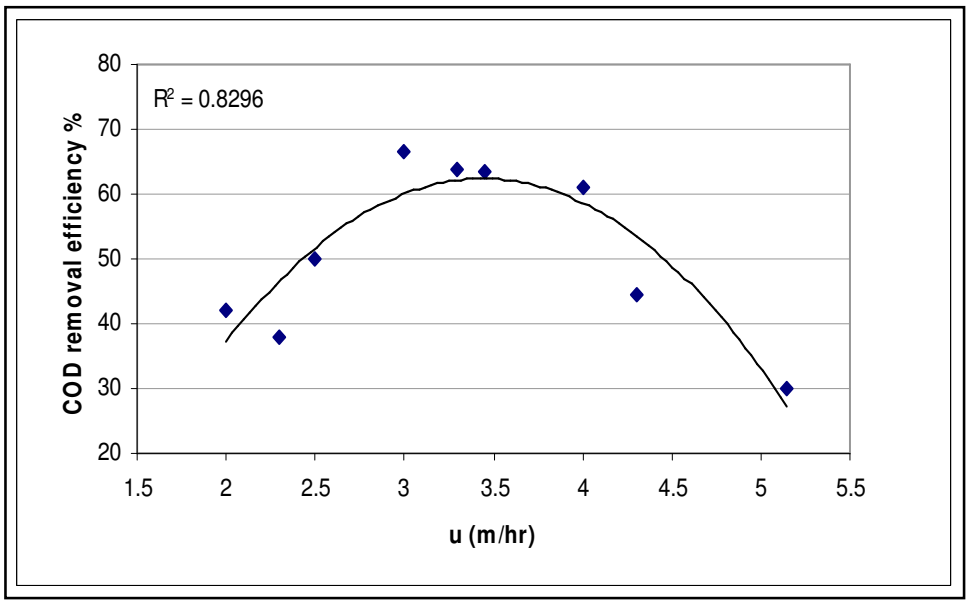

Fig(5). Removal efficiency for filtered COD for different upflow velocity ($R^2 = 0.8296$)

CONCLUTIONS

The study shows that, when velocity between 3 and 4 m/hr the effect on the washout decreased and assures very high removal efficiencies.

The results illustrate that, for velocity values below, 3 m/hr a negligible blanket expansion will aims, but at the same time results in a channeling phenomenon, which lowers treatment efficiency.

It seen that, if velocity is higher than 4 m/hr, an increase in the washout and reducing in performance in organic substrate removal will be obtained.

The results illustrate that the when the feed flow is interrupted for long periods (above 1 h) considerable losses of biomass into the effluent will be obtained.

From the results it seen that, with shorter periods blanket expansion takes place on a regular basis even with very high upflow velocities (up to 4 m/hr), giving rise to limited washout and high removal efficiencies, especially with velocities ranging between 3 and 4 m/hr.

REFERENCES

BARBER WP and STUCKEY DC (1999) "The use of anaerobic baffled reactor (ABR) for wastewater treatment" Water Res. 33 (7) 1559-1578.

GARUTI G, DOHANYOS M and TILCHE A (1992) "Anaerobic-aerobic wastewater treatment system suitable for variable population in coastal areas" Water Sci. & Technol. 25 (12) 185-195.

GROBICKY A and STUCKEY DC (1991) "Performance of the AnaerobicBaffled Reactor under steady-state and shock loading conditions"Biotech. Bioeng. 37 344-355.

LETTINGA G, VAN HELSEN AFM, HOBMA SW, DE ZEEUW W and KLAPWIJK A (1980) "Use of the upflow sludge blanket (USB) reactor concept for biological wastewater treatment " Biotech. Bioeng. 22 699-734.

LETTINGA G and HULSHOFF POL LW (1991) "UASB-Process design for various types of wastewaters". Water Sci. Technol. 24 (8) 87-107.

MAZZOLANI G, PIROZZI F and D'ANTONIO G (1998) "A generalized settling approach in the numerical modeling of sedimentation tanks". Water Sci Tech. 31 (3) 95-102.

NACHAIYASIT S and STUCKEY DC (1997) " The effect of shock loads on the performance of an Anaerobic Baffled Reactor (ABR). 1 – Step changes in feed concentration at constant retention time". Water Res. 31 (11) 2737-2746.

OROZCO A (1997) "Pilot full-scale anaerobic treatment of low-strength wastewater at sub-optimal temperature (15°C) with a hybrid plug flow reactor". Water Res. 28 (15) 267-276

STANDARD METHODS (1989) " Standard Methods for the Examination of Water and Wastewater" (17th edn.). Edited by Clesceri LS, Greenberg AE and Trussel RR. APHA, AWWA, WPCF.

Stability Issues of Welded Pipe Containing Pulsatile Flows

Dr. Nabeel K. Abid Al-Sahib
Ass. Prof.
University of Baghdad
AL-Khwarizmi College of Eng.

ABSTRACT:

This paper deals with the dynamics and stability behavior of a welded pipe containing flowing fluid having a small harmonic component superposed. The equation of motion was derived to represent the motion of a welded pipe conveying a pulsatile flow using a tensioned Euler- Bernoulli beam theory. The finite element analysis was used to simulate the harmonic motion of a welded pipe conveying fluid. It was shown that welded pipes with clamped-clamped and clamped-pinned supports are subject to a multitude of parametric instabilities in all their modes. Stability maps are presented for parametric instabilities of welded pipe with clamped-clamped and clamped-pinned ends. It is found that the extent of the instability regions increases with flow velocity for clamped-clamped and clamped-pinned welded pipes. The most important consideration from a practical point of view is to avoid the onset of parametric resonance.

الخلاصة

يتناول البحث السلوك الديناميكي و أستقرارية الأنابيب الملحومة الناقلة للموائع ذات السرع المتغيرة. تم أشتقاق معادلة الحركة للأنابيب الملحومة الناقلة للموائع ذات السرع المتغيرة بأستخدام نظرية أويلر-برنولي للعتبات كما تم أستخدام طريقة العناصر المحددة لمماثلة الأنابيب الملحومة الناقلة للموائع التوافقية. لوحظ بأن الأنابيب الملحومة ذات حدود التثبيت مثبت-مثبت و مثبت-مدبس خاضعة لعدد من المتغيرات اللامستقرة في جميع أنماطها. تم رسم خارطة اللاأستقرارية للأنابيب الملحومة ذات حدود التثبيت الأنفة الذكر. لقد وجد بأن وجود المناطق الغير مستقرة يزداد مع زيادة سرعة جريان المائع داخل الأنابيب الملحومة ذات حدود التثبيت المذكورة أنفا.

KEYWORDS
Pustule Flow, Stability Regions, Dynamics of Pipes, Parametric Instabilities.

INTRODUCTION:

Welded pipe conveying fluid are widely used in engineering applications. One of the design challenges is to avoid pipe buckling and flutter under various operation conditions. It's clear that if the velocity of a fluid conveying in pipe is not constant, but has a harmonic fluctuation over and above a constant mean value, then the pipe experiences instability, this phenomenon is similar to a beam

subjected to a periodic axial load **[Bolotin, 1964]**. The dynamic behavior of the system strongly depends on the different kinds of boundary conditions and on the fact whether the pipe is considered to be inextensible, i.e the cross-sectional area of the pipe is constant.

Many recent researches have been carried out on the vibration of a pipe conveying fluid. Zsolt Szabo et al **[Zsolt Szabó, 1997]** studied the dynamics of a pipe containing pulsative flow, the stability analyses of the linearized systems were performed in autonomous and nonautonomous (time-periodic) case. Zsolt Szabó **[Zsolt Szabó, 2000]** investigated the dynamic behavior of a continuum inextensible pipe containing fluid flow having a velocity relative to the pipe has the same but time-periodic magnitude along the pipe at a certain time instant. Wang and Bloom **[Wang, 2001]** studied the static and dynamic instabilities of submerged and inclined concentric pipes conveying fluid, Zsolt Szabó **[Zsolt Szabó, 2003]** investigated the nonlinear dynamics of a cantilever elastic pipe that contains pulsatile flow. The equation of motion was derived by using Hamiltonian action function. He used Galerkin's technique to include only finite number of spatial modes in the solution. The stability chart of the time-varying system was computed in the space of the relative perturbation amplitude of the flow velocity and dimensionless forcing frequency using an efficient numerical method based on Chebyshev polynomials. In the near of some critical regions bifurcation diagrams were also computed which show secondary bifurcations and phase locking followed by chaotic motion.

In the industry welded pipe conveying fluid encountered, for example, in the form of exhaust pipes in engines, stacks of fuel gases, air-conditioning ducts, pipes carrying fluid (chemicals) in chemical and power plants, risers in offshore platforms, and tubes in heat exchangers and power plants. The fluid inside the pipe dynamically interacts with the pipe motion, possibly causing the pipe to vibrate.

Also, pipelines play a significant role in the economic and environmental considerations of countries. Some carry water to help irrigate desert areas; others deliver gas over vast distances, and those that carry liquid fuels often unseen as they are buried underground **[Lee and Mote, 1997]**.

In this paper an attempt to study, analytically and numerically, the effect of harmonic fluctuation of the fluid velocity on the dynamic behavior of a welded pipe conveying unsteady flow.

EQUATION OF MOTION:

The system under consideration consists of a uniform welded pipe conveying unsteady fluid sketched in Fig. (1). the pipe is initially straight, stressed, and finite length.

The equation of motion for pre-stressed single-span pipe conveying unsteady fluid as a function of the axial distance z and time t, based on beam theory is given by **[Kuiper, 2006]**:

$$EI\frac{\partial^4 y}{\partial z^4} + \left(m_f U^2 - T_{eff.}\right)\frac{\partial^2 y}{\partial z^2} + 2m_f U\frac{\partial^2 y}{\partial z \partial t} + m_f\frac{\partial U}{\partial t}\frac{\partial y}{\partial z} + m\frac{\partial^2 y}{\partial t^2} = 0 \tag{1}$$

Where: EI is the bending stiffness of the pipe, m=mf+mp, mf is the mass of fluid per unit length, mp is the mass of the pipe per unit length, $T_{eff.} = T \pm A_i P_i$ so-called effective force, Ai is the internal cross sectional area of the pipe, Pi is the hydrostatic pressure inside the pipe, T is a prescribe axial force due to welding, and U is a fluid velocity.

The left end of the pipe is rigidly support, whereas the right end is assumed to allow no lateral displacement but to provide a restoring moment proportional to the rotation angle of the pipe. The clamped-clamped or clamped-pinned pipe is obtained from this formulation in the limit of the restoring rotational moment going to infinity or zero respectively. Thus, the boundary conditions at ends of the pipe are given as **[Paidoussis, 1998]**:

$$y(0,t)=0 \tag{2}$$

$$\frac{\partial y(0,t)}{\partial z}=0 \tag{3}$$

$$EI\frac{\partial^2 y(L,t)}{\partial z^2}= K_{rs}\frac{\partial y(L,t)}{\partial z} \tag{4}$$

$$y(L,t)=0 \tag{5}$$

Where Krs is the stiffness of the rotational spring at the right end.

The statement of the problem eqs. (1) ~ (5) can be written in a non-dimensional form as follows:

$$\frac{\partial^4\eta}{\partial\xi^4}+(\gamma+V^2)\frac{\partial^2\eta}{\partial\xi^2}+2\beta V\frac{\partial^2\eta}{\partial\xi\partial\tau}+\beta\frac{\partial V}{\partial\tau}\frac{\partial\eta}{\partial\xi}+\frac{\partial^2\eta}{\partial\tau^2}=0 \tag{6}$$

$$\eta(0,\tau)=0 \tag{7}$$

$$\frac{\partial\eta(0,\tau)}{\partial\xi}=0 \tag{8}$$

$$\frac{\partial^2\eta(1,\tau)}{\partial^2\xi}=-K\frac{\partial\eta(1,\tau)}{\partial\xi} \tag{9}$$

$$\eta(1,\tau)=0 \tag{10}$$

With the following dimensionless variables and parameters:

$$\eta = y/L$$
$$\xi = z/L$$
$$\tau = t\sqrt{EI/m}/L^2$$
$$V = LU\sqrt{m_f/EI}$$
$$\gamma = L^2T_{eff.}/EI$$
$$\beta = \sqrt{\frac{m_f}{m}}$$

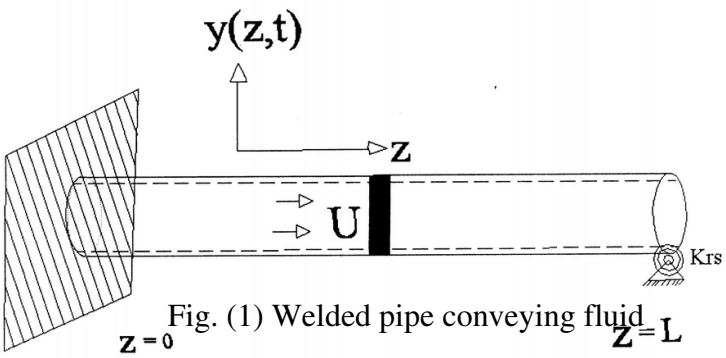

Fig. (1) Welded pipe conveying fluid

ANALYTICAL ANALYSIS:

It is clear that if a velocity of a fluid conveying in a welded pipe is not constant, but has a harmonic fluctuation under and above a constant mean value, then the pipe experiences instability.

To describe the function of this unsteady flow harmonically, Fourier series with one harmonic for the periodic velocity may be used to obtain **[Bolotin, 1964]**,

$$V = V_o[1 + \Delta \mathrm{Cos}(w\tau)] \tag{11}$$

Where Δ is an excitation parameter, w is a non-dimensional circular frequency, and τ is a non-dimensional time.

Substituting eq. (11) into eq. (6) yields:

$$\frac{\partial^4 \eta}{\partial \xi^4} + (\gamma + V_0^2 \Phi^2)\frac{\partial^2 \eta}{\partial \xi^2} + 2\beta V_0 \Phi \frac{\partial^2 \eta}{\partial \xi \partial \tau} - \beta V_0 w \Delta \mathrm{Sin}(w\tau)\frac{\partial \eta}{\partial \xi} + \frac{\partial^2 \eta}{\partial \tau^2} = 0$$

Where (12)

$$\Phi = (1 + \Delta \mathrm{Cos}(w\tau))$$

Regions of Instabilities:

The regions of instability of eq. (12) are separated from the stable region by periodic solution with periods (T) and (2T), where ($T=2\pi/w$) hence there are two solutions of identical periods bound the region of instability, the regions enclosed by the solution having period (2T) correspond to the "primary instabilities", while the region of "secondary instabilities" are enclosed by the solution having period (T), for example, if a system with natural frequency (w_n), the primary instabilities occurs at ($w=2w_n/q$) where (q=1,3,5 …) while the secondary instability region occurs at ($w=2w_n/q$) where (q=0,2,4 …) furthermore, instabilities corresponding to (q=1 and 2) are known as the principal primary and the principal secondary instabilities respectively.

Primary Instability Regions:

To determine the region of primary instability the displacement η may be expressed as follows **[Singh, 1979]**:

$$\eta(\xi,\tau) = \sum_{q=1,3,5,...} H_q(\xi)\mathrm{Sin}(\frac{1}{2}qw\tau) + R_q(\xi)\mathrm{Cos}(\frac{1}{2}qw\tau) \tag{13}$$

Where Hq and Rq are unknowns function of ξ, substituting eq. (13) into eq. (12) gives,

$$\sum_{q=1,3,5,...} [\{\frac{d^4H_q}{d\xi^4} + (\gamma + V_0^2 + \frac{V_0^2\Delta^2}{2})\frac{d^2H_q}{d\xi^2} - \beta V_0 qw\frac{dR_q}{d\xi} - (\frac{q}{2})^2 w^2 H_q\}\mathrm{Sin}(\frac{qw\tau}{2}) \tag{14}$$

$$+\{\frac{d^4R_q}{d\xi^4} + (\gamma + V_0^2 + \frac{V_0^2\Delta^2}{2})\frac{d^2R_q}{d\xi^2} + \beta V_0 qw\frac{dH_q}{d\xi} - (\frac{q}{2})^2 w^2 R_q\}\mathrm{Cos}(\frac{qw\tau}{2})$$

$$+\{V_0^2\Delta\frac{d^2H_q}{d\xi^2} - \frac{\beta V_0\Delta qw}{2}\frac{dR_q}{d\xi} - \frac{\beta V_0\Delta w}{2}\frac{dR_q}{d\xi}\}\mathrm{Sin}(\frac{(q+2)w\tau}{2})$$

$$+\{V_0^2\Delta\frac{d^2R_q}{d\xi^2} + \frac{\beta V_0\Delta qw}{2}\frac{dH_q}{d\xi} + \frac{\beta V_0\Delta w}{2}\frac{dH_q}{d\xi}\}\mathrm{Cos}(\frac{(q+2)w\tau}{2})$$

$$+\{V_0^2\Delta\frac{d^2H_q}{d\xi^2} - \frac{\beta V_0\Delta qw}{2}\frac{dR_q}{d\xi} + \frac{\beta V_0\Delta w}{2}\frac{dR_q}{d\xi}\}\mathrm{Sin}(\frac{(q\quad 2)w\tau}{2})$$

$$+\{V_0^2\Delta\frac{d^2R_q}{d\xi^2} + \frac{\beta V_0\Delta qw}{2}\frac{dH_q}{d\xi}\quad\frac{\beta V_0\Delta w}{2}\frac{dH_q}{d\xi}\}\mathrm{Cos}(\frac{(q\quad 2)w\tau}{2})$$

$$+\frac{V_0^2\Delta^2}{4}\frac{d^2H_q}{d\xi^2}\{\mathrm{Sin}(\frac{(q+4)w\tau}{2}) + \mathrm{Sin}(\frac{(q\quad 4)w\tau}{2})\}$$

$$+\frac{V_0^2\Delta^2}{4}\frac{d^2R_q}{d\xi^2}\{\mathrm{Cos}(\frac{(q+4)w\tau}{2}) + \mathrm{Cos}(\frac{(q\quad 4)w\tau}{2})\}] = 0$$

The region of principal primary instability can be obtained by truncating the series in eq. (14) at (q=1), now equating the coefficients of [Sin (wτ/2)] and [Cos (wτ/2)] from both sides of eq. (14) yield,

$$\frac{d^4H_1}{d\xi^4} + (\gamma + V_0^2 + \frac{V_0^2\Delta^2}{2} - V_0^2\Delta)\frac{d^2H_1}{d\xi^2} - \frac{w^2}{4}H_1 - \beta V_0 w\frac{dR_1}{d\xi} = 0 \tag{15}$$

$$\frac{d^4R_1}{d\xi^4} + (\gamma + V_0^2 + \frac{V_0^2\Delta^2}{2} + V_0^2\Delta)\frac{d^2R_1}{d\xi^2} - \frac{w^2}{4}R_1 + \beta V_0 w\frac{dH_1}{d\xi} = 0 \tag{16}$$

Neglecting (β) results in an accuracy of the order (98%) furthermore, the effect of neglecting (β) should not be mean that the effect of fluid mass (mf) is also negligible, this is attributed to the fact that the non-dimensional flow velocity (V) and the natural frequency (w) are also function to (mf), neglecting (β) in eqs. (15) and (16) results **[Chen, 1971]**,

$$\frac{d^4H_1}{d\xi^4} + (\gamma + V_0^2 + \frac{V_0^2\Delta^2}{2} - V_0^2\Delta)\frac{d^2H_1}{d\xi^2} - \frac{w^2}{4}H_1 = 0 \tag{17}$$

$$\frac{d^4R_1}{d\xi^4} + (\gamma + V_0^2 + \frac{V_0^2\Delta^2}{2} + V_0^2\Delta)\frac{d^2R_1}{d\xi^2} - \frac{w^2}{4}R_1 = 0 \tag{18}$$

Note that eq. (17) gives the upper limit of the primary instability region, while eq. (18) represents the lower instability region; the solution of eq. (17) may be written as,

$$H_1 = E_1 Sin(f_1\xi) + E_2 Cos(f_1\xi) + E_3 Sinh(f_2\xi) + E_4 Cosh(f_2\xi) \tag{19}$$

While the solution of eq. (18),

$$R_1 = T_1 Sin(k_1\xi) + T_2 Cos(k_1\xi) + T_3 Sinh(k_2\xi) + T_4 Cosh(k_2\xi) \tag{20}$$

Where: $f_1 = \sqrt{\frac{a_1 + \sqrt{a_1^2 + w^2}}{2}}$, $f_2 = \sqrt{\frac{-a_1 + \sqrt{a_1^2 + w^2}}{2}}$

$k_1 = \sqrt{\frac{a_2 + \sqrt{a_2^2 + w^2}}{2}}$, $k_2 = \sqrt{\frac{-a_2 + \sqrt{a_2^2 + w^2}}{2}}$

$a_1 = V_0^2 + \gamma + \frac{V_0^2\Delta^2}{2} - V_0^2\Delta$, $a_2 = V_0^2 + \gamma + \frac{V_0^2\Delta^2}{2} + V_0^2\Delta$

And E1…E4, T1……T4 are arbitrary constants.

The upper limit can be evaluated by substituting eq. (19) into the boundary conditions eqs. (7)~(10) to give the following equation in matrix form:

$$[A_{i,j}]\{E_j\} = 0 \tag{21}$$

While the lower limit can be evaluated by substituting eq. (20) into the boundary conditions eqs. (7)~(10) yields.

$$[B_{i,j}]\{T_j\} = 0 \tag{22}$$

Both eqs. (21) and (22) are functions of many physical parameter such as (w, Δ, V_0) searching for values of any of these parameters which vanish the above determinants gives the appropriate limit of the primary region.

Secondary Instability Regions:

To determine the regions of secondary instability, the displacement ξ, is expressed as **[Singh, 1979]**,

$$\eta(\xi,\tau) = \sum_{q=0,2,4,\ldots} H_q(\xi)\mathrm{Sin}(\frac{1}{2}qw\tau) + R_q(\xi)\mathrm{Cos}(\frac{1}{2}qw\tau) \tag{23}$$

Substituting eq. (23) into eq. (12) result in eq. (14) with summation over q=0, 2, 4, … the region of the principal secondary instability can be prediction by truncated the series in the resulting equation (with q=0,2,4,…) at q=0,2 and neglecting (β) result the following equations:

$$\frac{d^4H_2}{d\xi^4} + (\gamma + V_0^2 + \frac{V_0^2\Delta^2}{2})\frac{d^2H_2}{d\xi^2} - w^2H_2 = 0 \tag{24}$$

$$\frac{d^4R_0}{d\xi^4} + (\gamma + V_0^2 + \frac{V_0^2\Delta^2}{2})\frac{d^2R_0}{d\xi^2} + V_0^2\Delta\frac{d^2R_2}{d\xi^2} = 0 \tag{25}$$

$$\frac{d^4R_2}{d\xi^4} + (\gamma + V_0^2 + \frac{V_0^2\Delta^2}{2})\frac{d^2R_2}{d\xi^2} - w^2R_2 + V_0^2\Delta\frac{d^2R_0}{d\xi^2} = 0 \tag{26}$$

Note that eq. (24) is an uncoupled differential equation related to the upper limit and may have a solution of the form:

$$H_2 = D_1\mathrm{Sin}(g_1\xi) + D_2\mathrm{Cos}(g_1\xi) + D_3\mathrm{Sinh}(g_2\xi) + D_4\mathrm{Cosh}(g_2\xi) \tag{27}$$

Where: $g_1 = \sqrt{\frac{b_1 + \sqrt{b_1^2 + 4w^2}}{2}}$, $g_2 = \sqrt{\frac{-b_1 + \sqrt{b_1^2 + 4w^2}}{2}}$

$$b_1 = V_0^2 + \gamma + \frac{V_0^2\Delta^2}{4}$$

While eqs. (25) and (26) are coupled differential equations related to the lower limit and can be solved by using the series solution as,

$$R_0 = \sum_{j=1}^{8} d_{0j}e^{\Lambda_j\xi} \tag{28}$$

And

$$R_2 = \sum_{j=1}^{8} d_{2j}e^{\Lambda_j\xi} \tag{29}$$

Where Λj's are the roots of the polynomial

$$\Lambda^4 + (\gamma + v_0^2 + \frac{v_0^2\Delta^2}{2})\Lambda^2 \qquad v_0^2\Delta\Lambda^2$$

$$2v_0^2\Delta\Lambda^2 \qquad \Lambda^4 + (\gamma + v_0^2 + \frac{3v_0^2\Delta^2}{4})\Lambda^2 - w^2 \tag{30}$$

Note that d0j's and d2j's are related to each other by,

$$d_{0j} = \frac{v_0^2\Delta\Lambda_j^2}{[\Lambda_j^4 + (\gamma + v_0^2 + \frac{v_0^2\Delta^2}{2})\Lambda_j^2]} d_{2j}$$

There are two limits which bound the principal secondary instability regions, the upper and lower limits; the upper limit can be evaluated by substituting eq. (27) into the boundary conditions equations eqs. (7)~ (10) Which gives,

$$[A_{i,j}]\{D_j\} = 0 \tag{31}$$

While the lower limit can be evaluated by substituting eqs. (28)& (29) into the boundary conditions eqs. (7)~ (10) yields,

$$[B_{i,j}]\{d_j\} = 0 \tag{32}$$

Both equations (31) and (32) are functions of many physical parameters such as (μ, w, Δ, and V) searching for values of any of these parameters which vanishing the above determinants gives the appropriate limit of the secondary region.

FINITE ELEMENT MODELING PROCEDURE:

The FE analysis was carried out using a general purpose FE package ANSYS V9.0. The approach is divided into five parts: thermal analysis, coupled field thermal-structure analysis, computational fluid dynamics (CFD), coupled field fluid-structure analysis, and modal analysis.

A non- linear transient thermal analysis was conducted first to obtain the global temperature history generated during and after welding process. A stress analysis was then developed with the temperatures obtained from the thermal analysis used as loading to the stress model.

The solutions of the governing Navier-Stokes equations for the axisymmetric geometries modeled are obtained using ANSYS FLOTRAN analysis. The governing flow equations are discretized in space according to the spectral element method. Spectral elements combine high order accuracy with the geometric flexibility of low-order finite element methods. The computational domain is divided into a number of non-degenerate spectral elements within which all information on geometry, flow

initial and boundary conditions and solutions is approximated by high order polynomial expansions. A local mesh is constructed within each element, and points on this mesh are used as interpolate points for the expansion of all dependent variables. All the simulations were performed with no-slip (zero velocity) conditions at all walls and zero pressure at the flow outlet.

The coupled field fluid-structure analysis solved the equations for the fluid and solid domains independently of each other. It transfers fluid forces and solid displacements, velocities across the fluid-solid interface. The algorithm continues to loop through the solid and fluid analyses until convergence is reached for the time step (or until the maximum number of stagger iterations is reached). Convergence in the stagger loop is based on the quantities being transferred at the fluid-solid interface.

Finally used modal analysis to determine the vibration characteristics (natural frequencies and mode shapes) of a welded pipe conveying fluid. The natural frequencies and mode shapes are important parameters in the design of a structure for dynamic loading conditions.

RESULTS AND DISCUSSIONS:

Study the stability issues for particular single span ASTM214-71 mild steel welded pipe system with (1 m) length, (50.8 mm) outer diameter, (1.5 mm) thickness. The welded pipe was formed by joining two (0.5 m) pipes by fusion arc welding with a current of 30 A and voltage equal 460 volt using an electrode type E7010-G to make a straight pipe 1m length with welding on its mid span.; the welding procedure was modeled as a single pass in this analysis.

The analytical analysis is performed using Matlab V6.5 software to determine the limits of primary and secondary instability regions. The program was developed to be used for any specified pipe dimensions, length, pipe material stiffness, different flow velocities, and welding specifications. The FE analysis is performed using ANSYS V9.0 software. The parameters used in the calculations are listed in table (1).

Table (1) Parameters used in the calculation

EI	**$1.4122*10^4$**	**Nm^2**
m_f	**1.795**	**Kg/m**
m	**3.608**	**Kg/m**
R	**25.4**	**mm**
$T_{eff.}$	**$3.0243*10^5$**	**N**
L	**1**	**m**
ρ_f	**1000**	**Kg/m^3**
β	**3.264**	

Clamped-Clamped Welded Pipe:

Fig. (2) Shows the regions of parametric instability in the range 0.5 <w/ w_{01}< 6.0 for a clamped-clamped welded pipe (V_0 =2), where w_{01} is the first mode natural frequency at zero flow. If instead of w/ w01, the ordinate w/ w_n had been utilized, where w_n is the actual natural frequency for the mode concerned at V_0=2, then the principal primary regions of all the modes would begin at w/ w_n=2, the second primary region at w/w_n=2/3, the principal secondary region at w/ w_n=1, and so on.

With the ordinate used here, associated with the first mode are:

1- The principal primary region beginning at w/ w_{01}= 1.8.
2- The principal secondary at w/ w_{01}=0.9.
3- The secondary primary region beginning at w/ w_{01}=0.6.

Similarly, associated with the second mode, the corresponding regions begin at w/ w_{01}= 5.1, 2.6, and 1.7, respectively. Associated with the third mode are the (1) principal secondary region beginning at w/ w_{01}= 5.1, and second primary region at w/ w_{01}=3.4.

Fig. (3) Shows the effect of flow velocity on the principal regions of instability associated with the first mode of a clamped-clamped welded pipe. It is noted that as the flow velocity increases the regions of instability are displaced downwards, which reflects the decrease of the first mode frequency with flow. It is also noted that the regions of instability become broader with increasing flow.

Fig. (4) Shows the effect of β on parametric instabilities. It is seen that with increasing β the regions of instability become broader and displaced downwards, which reflects the lowering of the natural frequencies as β increases for this particular flow velocity.

Clamped-Pinned Welded Pipe:

Fig. (5) Shows the parametric instability regions for a clamped-pinned welded pipe for V_0=4.5, 5.5, 6 in the range w/w02 < 2.4. the large regions of instability in the middle of the figure are the principal primary regions associated with the second mode, while at the bottom is a principal secondary region which occurs for V_0=6 only. The small regions at the top are principal secondary regions associated with the third mode.

Figures (6a, b) show, respectively, the primary and secondary instability regions, for the range of frequencies shown, of a welded pipe. The three uppermost regions of instability in figure (6a), for V_0=6, 7.5, 8 and 9, are principal primary regions associated with the third mode, while the two large regions in the middle, for V_0=8 and 9, are a mixture of principal primary regions associated with the second and third modes.

Finally, the smaller regions at the bottom of figure (6b) may similarly be divided into the following two groups: (i) the regions for V_0=6, 7.5, and 8 are mixtures of principal primary regions associated with the second mode and of second primary regions associated with the third mode, (ii) the regions for V_0=8 and 9 are mixtures of second primary regions associated with the second and third modes. This fusion of the regions of instability is shown particularly well in the cases of v0=8 and 9, where each of the regions is formed of two interlinked distinct zones, the upper of which is related to the second mode and the lower to the third mode.

In figure (6b) the upper region (V_0=6) is the principal secondary one associated with third mode, while the remaining regions are all mixtures of principal secondary regions associated with the second and third modes. The upper areas of the latter are associated with the third mode and the lower areas with the second, except for V_0=8 where no such distinction may be made.

It would be of interest to compare the results of dynamic stability obtained for a pipe conveying unsteady flow without welding by Chen **[Chen, 1971]**. We can see that the effect of welding is to reduce the range of beginning the principal primary, principal secondary, and second primary regions of instability for clamped-clamped and clamped-pinned boundary conditions.

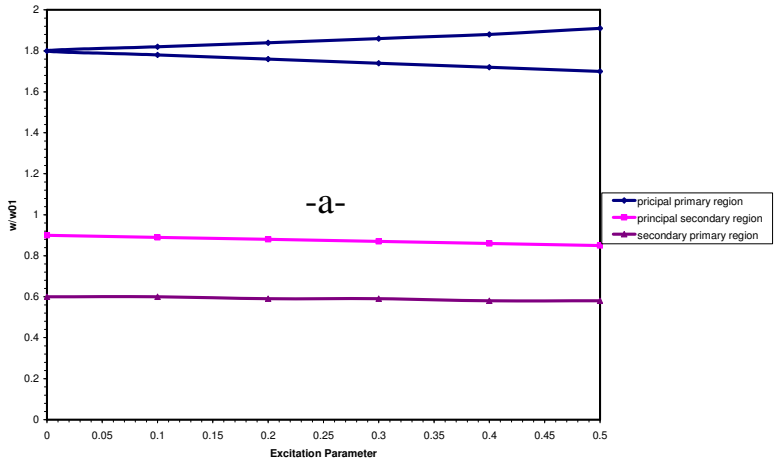
-a-
w/w01
Excitation Parameter
pricipal primary region
principal secondary region
secondary primary region

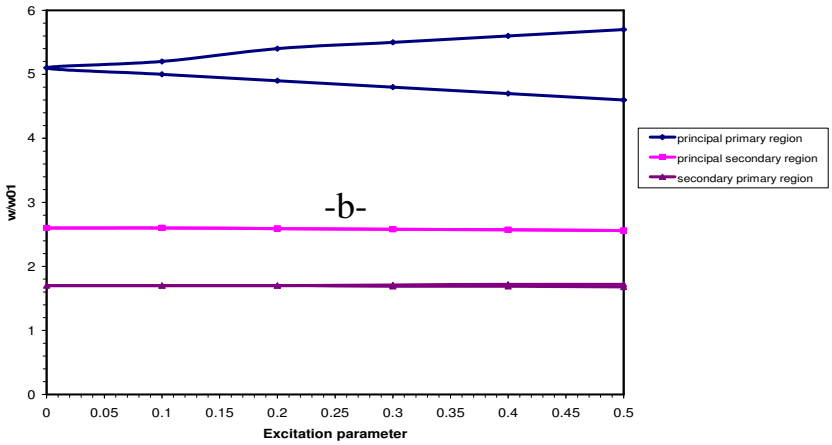
-b-
w/w01
Excitation parameter
principal primary region
principal secondary region
secondary primary region

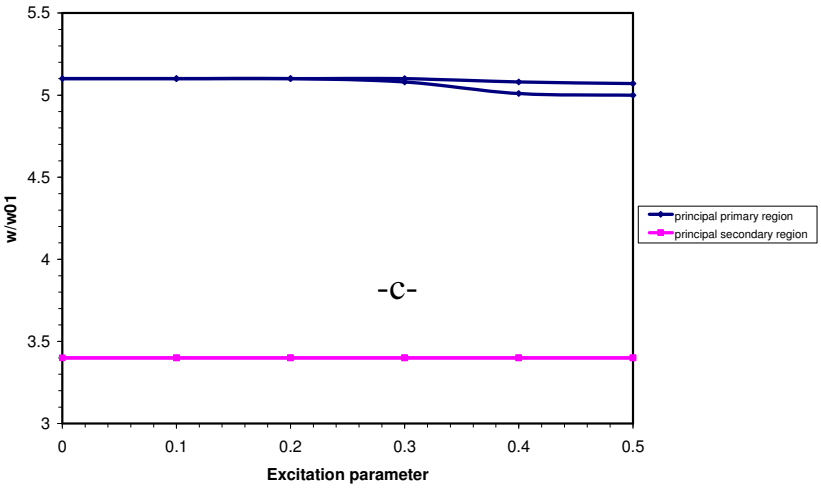
-c-
w/w01
Excitation parameter
principal primary region
principal secondary region

Fig. (2) Parametric instability boundaries for a clamped-clamped welded pipe (V_0=2). The system is unstable within the triangular regions
a- First mode b- Second mode c- Third mode

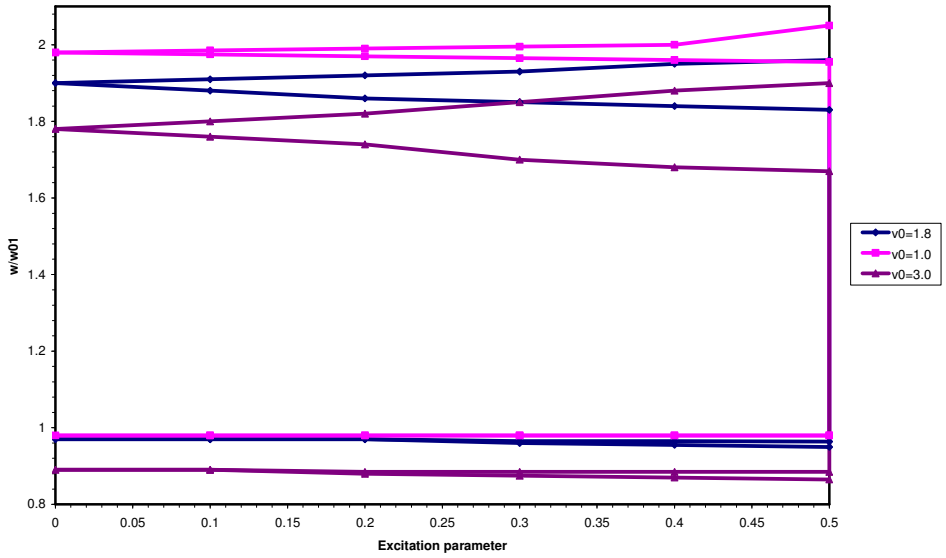

Fig. (3) The effect of flow velocity, V_0, on the principal instabilities associated with the first mode of a clamped-clamped welded pipe, for three values of V_0

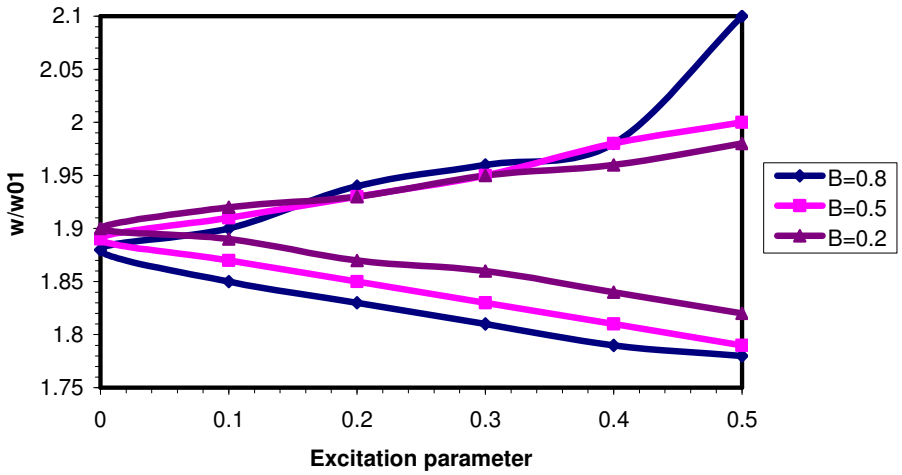

Fig. (4) The effect of β on parametric instabilities

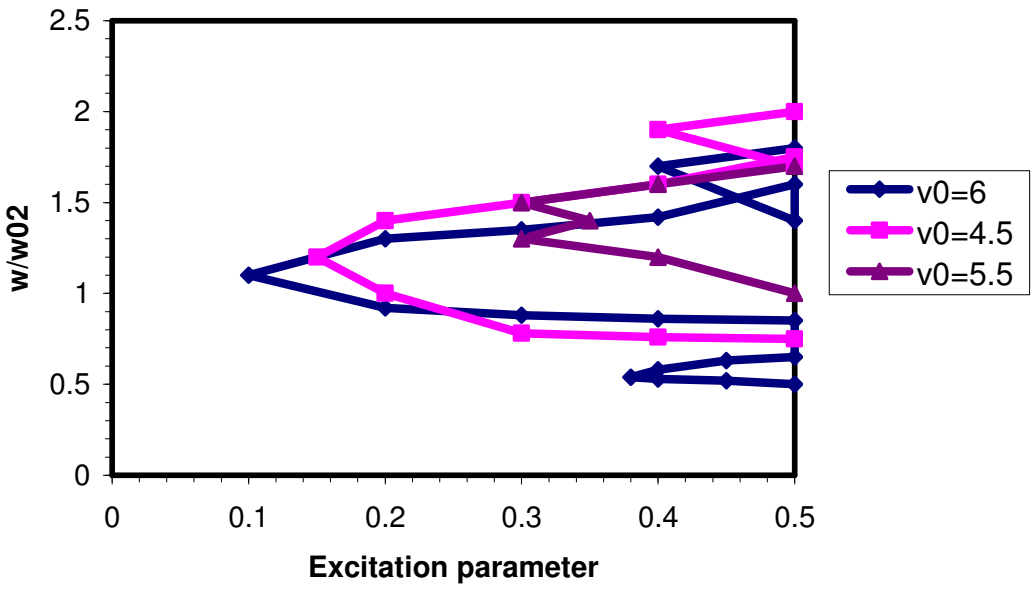

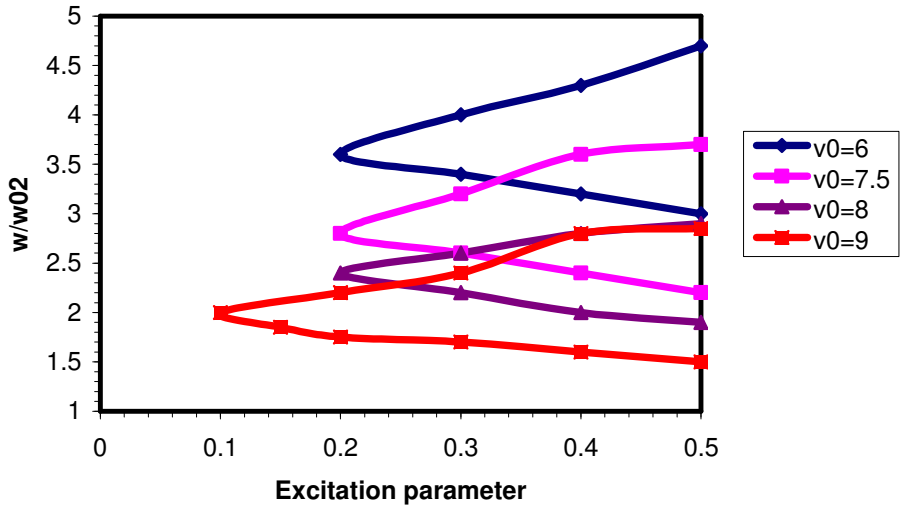

Fig. (5) Parametric instability boundaries for a clamped-pinned welded pipe

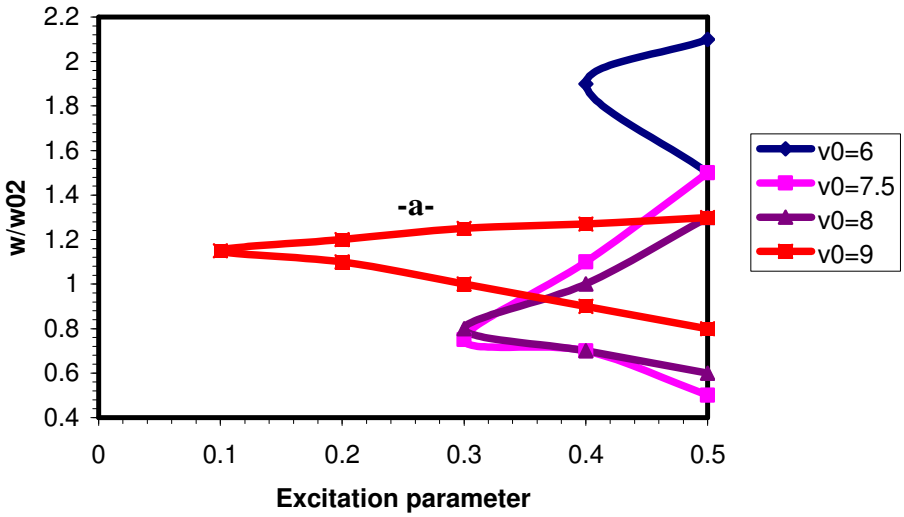

-b Fig. (6) Parametric instability boundaries for a clamped-pinned welded pipe
a- Primary instability regions b- Secondary instability regions

CONCLUSIONS

Analytical and finite element analyses are used to determine the regions of instability of a welded pipe conveying pulsatile flow with clamped-clamped and clamped-pinned boundary conditions. It was shown that these welded pipes are subjected to a multitude of parametric instabilities in all their modes. It was shown also that the pulsating flow in a welded pipe can cause parametric resonance, resembling a column subjected to periodic axial loads. The onset of instability in engineering systems, such as welded pipes could be catastrophic. The most important consideration from a practical point of view is to avoid the onset of parametric resonance.

REFERENCES

Bolotin V. V., "The Dynamic Stability of Elastic System", San Francisco Hoiden Day Inc. 1964.

Chen S. S., "Dynamic Stability of Tube Conveying Fluid", Journal of the Engineering Mechanics Division Proceeding of the American Society of Civil Engineering, pp. 1469-1485, 1971.

Kuiper G. L., and Metrikine A. V., " On Stability of a Clamped-Pinned Pipe Conveying Fluid", Heron, Vol. 49, No. 3, pp. 211-231, 2004.

Lee S. Y., and Mote C. D., "A Generalized Treatment of the Energetic of Translating Continua, Part I: Strings and Tensioned Pipes", Journal of Sound and Vibration 204, pp. 717-734, 1997.

Lee S. Y., and Mote C. D., "A Generalized Treatment of the Energetic of Translating Continua, Part II: Beams and Fluid Conveying Pipes", Journal of Sound and Vibration 204, pp. 735-753, 1997.

Paidoussis M. P., "Fluid-Structure Interactions: Slender Structures and Axial Flow", Vol.1, Academic Press, London, 1998.

Singh K., and Malik A. K., "Parametric Instabilities of Periodically Supported Pipe Conveying Fluid", Journal of Sound and Vibration, Vol.62, No. 3, pp. 379-397, 1979.

Wang X., and Bloom F., "Stability Issues of Concentric Pipes Containing Steady and Pulsatile Flows", Journal of Fluids and Structures< 15, 1137-1152, 2001.

Zsolt Szabó, Sinha S. C., and Gabor Stepan, "Dynamics of Pipes Containing Pulsative Flow", ASME Design Engineering Technical Conferences, September 14-17, Sacramento, California, 1997.

Zsolt Szabó, "Bifurcation Analysis of a Pipe Containing Pulsatile Flow", PERIODICA POLYTECHNICA SER. MECH.ENG. VOL.44, NO.1, 149-160, 2000.

Zsolt Szabó, " Nonlinear Analysis of a Cantilever Pipe Containing Pulsatile Flow", Journal of Meccanica, Springer Netherlands, Volume 38, Number 1,pp. 163-174, January, 2003.

STUDY OF PERFORMANCE OF S.I.E. FUELED WITH SUPPLEMENTARY HYDROGEN TO GASOLINE

Miqdam T. Chaichan

Asst.Lecturer, Mechanical Eng. Dep., University of Technology, Baghdad, Iraq
E-mail: Miqdam_tc@hotmail.com

ABSTRACT

This paper includes study of performance of single cylinder, 4-stroke spark ignition engine Ricardo E6, with variable compression ratio, spark timing and equivalence ratio, fueled with supplementary hydrogen to gasoline.

The speed of 25 rps and higher useful compression ratio were chosen in studying the effect of wide range of equivalence ratios and spark timing.

The results showed that HUCR for mixture of two fuels was (9:1). The brake power when operated with gasoline was higher than when it was fueled with hydrogen alone, but when mixing two fuels the brake power increased and became higher than that when working with gasoline to a certain limit (the hydrogen volumetric ratio in the mixture reached 80%), after this limit the brake power reduced by increasing hydrogen volumetric ratio.

The equivalence ratio at which the brake power reach its highest value was between (Ø=1-1.1) when mixing the two fuels. The results showed that the engine can work with very lean equivalence ratios with supplementary hydrogen, the indicated thermal efficiency increased also, and the brake specific fuel consumption reduced when hydrogen volumetric ratio increased.

الخلاصة

تضمن هذا البحث دراسة أداء محرك أحادي الاسطوانة رباعي الأشواط يعمل بالشرارة، نوع (Ricardo E6)، ذي نسبة انضغاط وتوقيت شرر ونسبة مكافئة متغيرة عند عمله بإضافة الهيدروجين للجازولين.

تركزت الدراسة على بحث تأثير متغيرات رئيسية في أداء المحرك، وهي نسبة الانضغاط والنسبة المكافئة وتوقيت الشرر والسرعة، أظهرت النتائج أن نسبة الانضغاط النافعة العليا لخليط من الوقودين هي (1: 9)، وان القدرة المكبحية كانت تزداد بزيادة نسبة الانضغاط، كما ان القدرة المكبحية في حالة الجازولين تزيد عن تلك الناتجة باستخدام الهيدروجين، ولكن عند خلط الوقودين تزداد القدرة المكبحية عن حالة استخدام الجازولين الى حد معين، (نسبة الهيدروجين الحجمية في الخليط 80%) بعدها تقل بزيادة هذه النسبة.

وان النسبة المكافئة التي تم الحصول عندها على أعلى قدرة مكبحية تتراوح بين (Ø=1.0-1.1) عند خلط الوقودين، كما بينت الدراسة ان المحرك يمكن أن يعمل عند نسب مكافئة ضعيفة جدا" بإضافة الهيدروجين،

كما ان الكفاءة الحرارية البيانية تزداد بهذه الإضافة، ويقل معدل الاستهلاك النوعي المكبحي للوقود بزيـــادة النسبة الحجمية للهيدروجين المضاف.

KEY WORDS

Hydrogen, gasoline, equivalence ratio, compression ratio, spark timing, speed, brake power, specific fuel consumption, indicated thermal efficiency, exhuast gas temperature.

INTRODUCTION

There is no room for doubt that the world's convenantiol source of fossil fuel are being exhuasted at an alarming rate. The transportation sector is one of the most important areas which has been badly hit by the energy crisis, which is basicaly a fuel crisis. It is certain that the demand of indeividual transport will continue to grow despite the decline in petroleum production, because autimobiles have become an integral part of the present day life style. With the growing use of the individual transporttion system, the need for spark ignition engine is rapidly growing.

Internal combustion engines provide 85% of the energy needed by mankind, and it is supposed that in populated areas their shear of air pollution reaches up to 70%. It is supposed that for a period of 60 – 80 years thay will remain the basic converter of heat energy from the combustion of fuels in mechanical work **(Mathur and Das, 1991)**.

Compared to the fuels now in use or under considration, for future application, hydrogen offers many advantages. Its use in spark ignition engine will not only eliminate the present day proplem of dependence on petrolium fuel, but it will also reduce vehicular pollution as hydrogen is a clean burning fuel. It offers the unique advantage of being a fuel, the basic resourse of which is recycable in a short time cycle by completely normal means. It starts with the molecule of water being split and upon combustion produces water vapour as the prencipal exhuast. Water is available in plenty every where. So, looking at the future, hydrogen has a practically unlimited supply potential **(Chaichan, 1989).**

As a fuel gas, hydrogen possesses significant invironmantal advantages that compensate for preliminary reservation as asociated with the controversial issue of unproven safety. In comparission with natural gas, hydrogen possesses a higher burning velocity, greater flash back tendency, lower relative density, wider limits of flammability and lower ignition energies, selected combustion characteristics are reported in **Table (1) (Petkov and Parazev, 1987).**

There is general agreement that the hydrogen enrichment concept permets very lean combustion of hydrocarbon fuels with attendant increase in engine efficiency and reduction of engine emissions. It is an opportunity to achieve now adays standards of toxic components content in the exhaust gases of automobile engines, considerably lowering gasoline consumption.

Another advantage of this method is that it requires a smaller quantity of hydrogen to be fed to the engine which considerably lessens the problems connected with hydrogen storage in the automobile **(Frances, 1981).**

It has been well established that burning lean mixtures results in improved fuel economy and higher engine thermal efficiency. Moreover, the lean operation of gasoline fueled spark ignition engines can result in the reduction of exhaust emissions without the addition of emission control devices **(Hoen and Dowdy, 1973).**

Recently much attention has been focussed on the use of hydrogen as a supplementary fuel, to extend the engine operation in range to equivalence ratios beyound the lean operating limit of gasoline, as hydrogen exhibits a significantly lower flammability limit (around 0.1 equivalence ratio). Comparasion with other hydrocarbon fuels (around 0.6 equivalence ratio). However, no conventional engine system has been developed that can operate with gasoline at equivalence ratios leaner than 0.85 or so, while the lean limit of gasoline- air combustion is about 0.6. There are

several reasons for this but perhaps the two most important are non-homogenity of the mixture and poor cylinder to cylinder distribution **(Hoen and Baisly, 1973).**

The presence of hydrogen during the ignition and initial phases of the combustion process provides a source of enthalpy release and active species of equivalence ratio where gasoline fuel alone isn't readily reacted and for these reasons hydrogen is the prime candidate for gasoline supplementation to obtain ultralean burning. **Table (2) (Bansal and Mathur, 1980)** shows a comparison of flammability limit of hydrogen with other commenly used hydrocarbon fuels.

EXPERIMANTAL TECHNIQUE

Experiments were conducted on single cylinder, variable compression ratio Ricardo E6/US engine, to assess the effect of hydrogen supplemintation on the operation of SIE.

Tests were also conducted to determine the engine output and fuel economy with gasoline and with various degrees of hydrogen supplementation. Mixture equivalence ratios were varid over a wide range while hydrogen volumatric fraction (defined as the ratio of the hydrogen volume to the total volume of hydrogen and gasoline used, that's mean HVF= $V_{H2}/V_{H2}+V_{gasoline}$) varid from 20% to 100% hydrogen. HUCR and OST were used in studing wide range of equivalence ratios. All tests were carried out at wide open throttle and at engine speed 25 rps, except those for studying speed effect. In all experiments bottled hydrogen was used as a supplemantary fuel.

DISCUSSION

Compression ratio effect

Supplimentation of different volume fracters was studied, the different fractions were used to know which percentage was the best one to mix the two fuels, the CR was studied also to assess the HUCR. The experiments was started at CR= 6:1 untill CR=9.5:1.

Fig. (1) shows the relation between the brake power and equivalence ratio [$(A/F)_{stoichiometric}$ /$(A/F)_{actual}$] for different mixing volume fractions from 0 to 100% hydrogen at HUCR for each fuel, OST and 25 rps speed.

The experiment showed that brake power increased with HVF increase from 0 to 80% for compression ratios (6,7,8,8.5,9), and for volumatric fraction (0-60%) at CR=9.5, this increase in brake power was expected because hydrogen presence in combustion chamber gives significant improvment in energy release.

Also, it increase burning rate and gives better and more complete combustion. The brake power was reduced when HVR was increased above 80%, that's because a higher fraction of gasoline-air mixture was replaced with hydrogen that caused decreasing in combustion energy released, where hydrogen energy on volume basis is less than the gasoline heating value. This is obvious when hydrogen was used alone, it gave brake power less than that produced when using gasoline alone, as appear from the figure. The mixture behaviour at CR=9.5 was different from other compression ratios, because at this CR the combustion was rough and severe knock happened with increased load.

Fiq. (2) distincts realation between HVF and the highest brake power of the engine at different compression ratio in the experments done. **Fig.2** shows that HUCR for mixtures of hydrogen and gasoline is 9 while it was 8 only for gasoline-air mixture. The highest brake power happened at 80% mixture rate.

Fig. (3) shows the effect of different mixture rates and the studied CR on OST.

It appeared that ther OST retarted with HVF and compression ratio increase. This is because of high hydrogen burning velocity in comparable with gasoline, also burning velocity increase with CR increase, because the mixture temperature increased in combustion chamber.

Equivalencr ratio effect

From **Fig.1** the highest brake power when gasoline was used alone was at Ø=1.1, with hydrogen supplemintation it was approach to Ø=1.0. The hydrogen addition effect was bigger in the lean side, where the flammability limit for gasoline was at Ø=0.79 but with hydrogen addition it reached Ø=0.34 .

Fig. (4) shows the relation between brake power and HVR in mixture for five equivalence ratios at OST and 25 rps engine speed and HUCR for each fuel.

The figure shows that the brake power increased at Ø= 0.7 when HVF was increased from 0 to 80 is very large, the brake power was increased about 300 % compared with gasoline alone, the same thing can be said about Ø=0.8, where the brake power increased about 40%, this is because of three facters: precence of enough oxygen for reaction, precence of hydrogen which improves the combustion, and increase its burning velocity, and the precence of high heating value of gasoline.

The effect of addition of hydrogen at richer equivalence ratio is limited, because the intering air quantity decreased, while the intering hydrogen-gasoline mixtue removed developed volume from air. This is obvious at Ø=1.0, where brake power increased with 10% , also, at Ø=1.1 the increase was about 3.5%.

From the above it is appeared that hydrogen supplementation improves engine brake power for lean equivalence ratios in great manner.

The relation between equivalence ratio and OST is shown in **fig. (5)** for different mixing rates, at HUCR and 25 rps, where **fig. (6)** shows the effect of HVF on OST for difined equivalence ratios.

The OST retarted with hydrogen addition for all equivalence ratios, it was about 20 degree BTDC with 80% volume hydrogen , at stochiometric equivalence ratio about 10 degrees BTDC.

The effect of HVF addition to gasoline on bsfc was studied in **fig. (7)** for wide range of equivalence ratios at HUCR, 25 rps and OST.

From the figure, the bsfc decreased to a concedarable extent, especiely for lean equvilence ratios with hydrogen supplemintation, for example, at Ø=0.7 with HVF=80%, bsfc reduction was about 67%, and at Ø=1.0 for the same HVF the reduction was 17%.

Fig. (8) shows the effect of hydrogen addition on indicated thermal efficiencyat HUCR and OST, for three chosen HV fractions.

The indicated thermal efficiency increased highly with hydrogen supplementation at lean side to reach its highest value at this side, then it decreased quickly with mixture enrichment, the rise of indicated thermal efficiency in the lean side presents important and obvious improvement in combustion at this side with hydrogen adittion. The high reduction in indicated thermal efficiency at rich equivalence ratios after it reached its highest value is because of combustion difficulties in this side, so, the hydrogen supplementation in the rich side didn't improve the combustion nor the indicated thermal efficiency.

The highest value of indicated thermal efficiency was at lean equivalence ratios, this ratio decreased with hydrogen addition to gasoline-air mixture, as an example, the highest indicated thermal efficiency was at Ø= 0.9 when using gasoline, then it became at equivalence ratios (Ø= 0.83,0.8,0.77) for supplying ratios (HVF=0.3,0.6,0.8) respectively, also, when using hydrogen it was at Ø=0.4.

Fig. (9) indicates the relation between exhuast gas temperatures and equivalence ratio, when adding different hydrogen volumatric fractions (HVF=0.3,06,0.8), engine was operated at HUCR and 25rps.

Hydrogen supplimantation decreases exhaust gas temperature for all equivalence ratios, and we got the minimum exhust gas for the whole range of equivalence ratios temperature when hydrogen was used. This was explained by (Al-Alousi, 1982), that the hydrogen heating value on volume basis is low, so it cuases this reduction in temperature, also it can be explained in another way, where the burning velocity for hydrogen is fast, and the mixture combusted in very high speed, especialy when engine operated at OST, so when expansion stroke takes place the whole mixture will be burned and became combusted gases, and it will be cooled in this stroke, and when exhuast

valve opened these gases will get out cooler than any hydrocarbon fuels may be used, also the heat transfer from cylinder wall increased because of the reduction of unburned gases in the inner film thickness, which are near the cylinder walls as sugested by (Chaichan, 1989).

SPEED EFFECT

Fig. (10) represents the relation between the highest engine brake power and HVF in mixture, to obtain different speed effects at HUCR and OST.

It is appeared that the effect of engine speed is invariable when using any fuel alone. The brake power increased with speed increase, for all experiment speeds, although the increase rate is different this increase was too large when engine speed accelerate from low to meduim speeds, then this rate lessened when engine run from meduim to high speeds. This is because of the inlarged friction power with engine speed.

Fig. (11) shows the effect of supplementary hydrogen on OST when the engine run at different speeds. Hydrogen supplementation caused retarding OST about 20 degrees BTDC, for all experiment speeds. Also, the speed increase cuased advancing of OST, as it is familiar when working with any fuel alone, and the optimum spark timing at any speed and equivalence ratio is the resultant of these two parameters.

SPARK TIMING EFFECT

Figs. (12 to 14) represent the relation between engine brake power and equivalence ratio for three different spark timings (10,15,20) degree BTDC, with hydrogen addition to gasoline in three different volumatric percentage (HVF=.3,.6,.8), the engine operated at HUCR and 25 rps.

Spark timing 10 degrees BTDC is very late for gasoline as appears from **Fig. (12)**, where engine brake power went down, but with hydrogen supplementation the brake power became larger in very obvious manner, especiely for equivalence ratios from Ø=0.7 to Ø=1.1, where this timing is neer the OST.

Spark timing 15 degrees BTDC is a better timing for gasoline, so the brake power increased for all equivalence ratios as appears in **Fiq. (13)**, also brake power increased clearly with hydrogen added to mixturs at 30% volumatric fraction for equivalence ratios from Ø=0.7 to Ø=1.3. The brake power increased also with hydrogen supplied to system at 60% by volume, but a smaller increase for the same equivalence ratios mitioned above, that is because the timing is advanced compared with OST for these equivalence ratios, but when hydrogen was supplied to system in 80% volume, the brake power increased in lean side, and decreased for equivalence ratios between (Ø=0.75-1.3), and the curves take another figures. This was expected because this timing is highly advanced timing from OST for these equivalence ratois.

Brake power figures take another style from their relatives in **Fig. (14)**. Gasoline brake power became better, that's because the timing (20 degrees BTDC) close to OST, and the equivalence ratios which gave the highest brake power were between Ø=1.0-1.15. Brake power decreased with hydrogen addition in 30, 60% by volume for range of (Ø=0.85-1.35), and engine operation was not available for HVF=80, at this fraction and for this spark timing, because it considerd very advanced from OST for these equivalence ratios, so it caused reduction in brake power for HVF= 0.3-0.6, and caused the phenomenant of the high pressure rate before top dead centre to occur, which cause negative work on engine.

CONCLUSIONS

1-The HUCR for a mixture of gasoline and hydrogen is 9:1.
2-The OST retards with hydrogen supplementation for all equivalence ratios.
3-The OST retards with CR increase for all kind of fuels.
4-The OST advanced with speed increase for all kinds of fuels.

5-With hydrogen supplied in volumatric fractions to gasoline-air mixture the brake power increased to extend limit (HVF=80%) then it started to fall down if HVF continue increasing above this percentage.
6-With hydrogen supplementation engine can operate with very lean equivalence ratios, can't be reached with gsoline operation.
7-Indicated thermal efficiency increased with hydrogen supplementation, it's highest value when using hydrogen alone, at very lean equivalence ratio.
8-Exhaust gas temperature reduced with hydrogen supplementation.
9-Brake specific fuel consumption reduced with hydrogen supplimantation to gasoline.

REFRENCES

Al-alousi,Y.H., (1982), Examination of combustion processes and performance of S.I. Engine using a data acquisition system, Ph.D. thesis, Calgary, Canada.

Bansal, B.B. and Mathur, H.B., (1980), Performance studies of a S.I. engine using hydrogen as a supplimantary fuel, 3rd world hydrogen energy progress conference, Tokyo, Japan.

Chaichan, M.T, (1989), Study of performanceand emissions of S.I.E. fueled wih different gases, M.Sc. thesis, Baghdad, Iraq.

Frances, D.H, (1981), Combustion charactristics of hydrogen, Int. J. Hydrogen Energy, vol.5, pp. 369-374.

Hoen, F.W., Baisly, R.L. and Dowdy, M.W., (1973), Advanced in altra lean combustion technology using hydrogen enrich gasoline, SAE paper No. 759173.

Hoen, F.W., and Dowdy, M.W., (1974), Feasibility demonstration of road vehicle fueled with hydrogen – enriched gasoline, SAE paper No. 749105.

Petkov, T.J and Brazev, K.N, (1987), Some aspects of hydrogen application as a supplementary fuel to the fuel – air mixture for internal combustion engine, Int. J. Hydrogen Energy, vol. 12, No.9, pp.633-638.

Mathur, H.B. and Das, L.M, (1991) Performance charactristics of hydrogen fueled S.I. engine using time manifold injection, Int. J. hydrogen Energy, Vol.16, No.2,pp.115-127.

NOMENCLATURE

TDC	top dead centre
BDC	bottom dead centre
BMEP	brake mean effictive pressure
BSFC	brake specific fuel consumption
BTE	brake thermal efficiency
CA	crank angle
CR	compression ratio
HUCR	higher usful compression ratio
OST	optimum spark timing
SIE	spark ignition engine

Table (1)
Combustion characteristics for gasous hydrogen

Ignition energies (at 1 atm and 298 K)	
$E_{min\ at\ stoicheometric}$	0.019MJ
Critical E_{min}	0.0185MJ
Auto-ignition temperature (at 1 atm and room temperature)	847-864 K
Quinching distance (at 1 atm and 298K)	
Critical port at stoichiometric	0.64mm
Slotted point at stoichiometric	0.81mm
Limit of flammability (at 1 atm and 298K)	
Lower limit	4.0%
Upper limit in air	75.0%
Upper limit in oxygen	94.0%
Limit of detonability (at 1 atm and room temperature)	
In air	18.3-59.0%
In oxygen	15.0-90.0%
Detonation velocity (at 1 atm and 291K)	
In air	2055 m/s
In oxygen	2819 m/s
Maximum flame temperature (at 1 atm and room temp)	
In air	2318 K
In oxygen	2933 K

Table (2)
Lean flammability limits for gases and vapors in air

Compound	formula	Lean flammibality limit	
		Vol%	Ø
Paraffins			
Methane	CH_4	5.3	0.53
Propane	C_3H_8	2.2	0.54
Pentane	C_5H_{12}	1.5	0.58
octane	C_8H_{18}	1.0	0.60
Aromatics			
Benzene	C_6H_6	1.4	0.51
Alcohols			
Meathanol	CH_3OH	7.3	0.56
Inorganic			
$CO+H_2O$ vapor at 18^oC	$CO+H_2O$	12.5	0.54
Hydrogen	H_2	4.0	0.10
Indoline 30 gasoline	$C_7H_{13.02}$		0.57

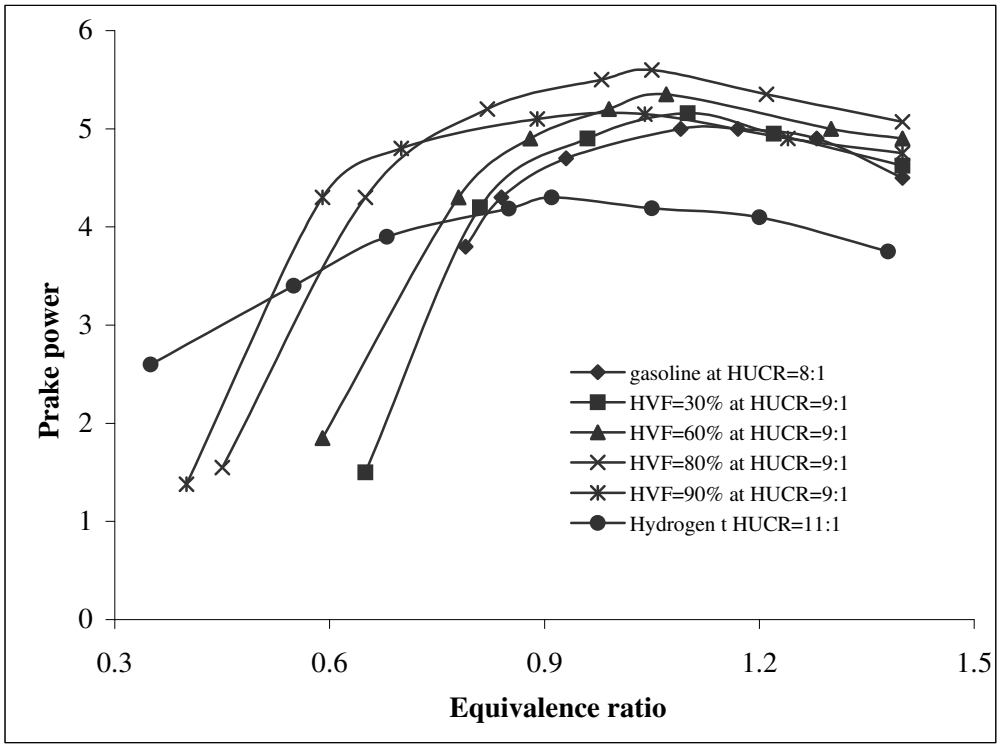

Fig. (1). The relation between the brake power and equivalence ratio for different mixing volume fractions from 0 to 100% hydrogen at OST and 25 rps speed

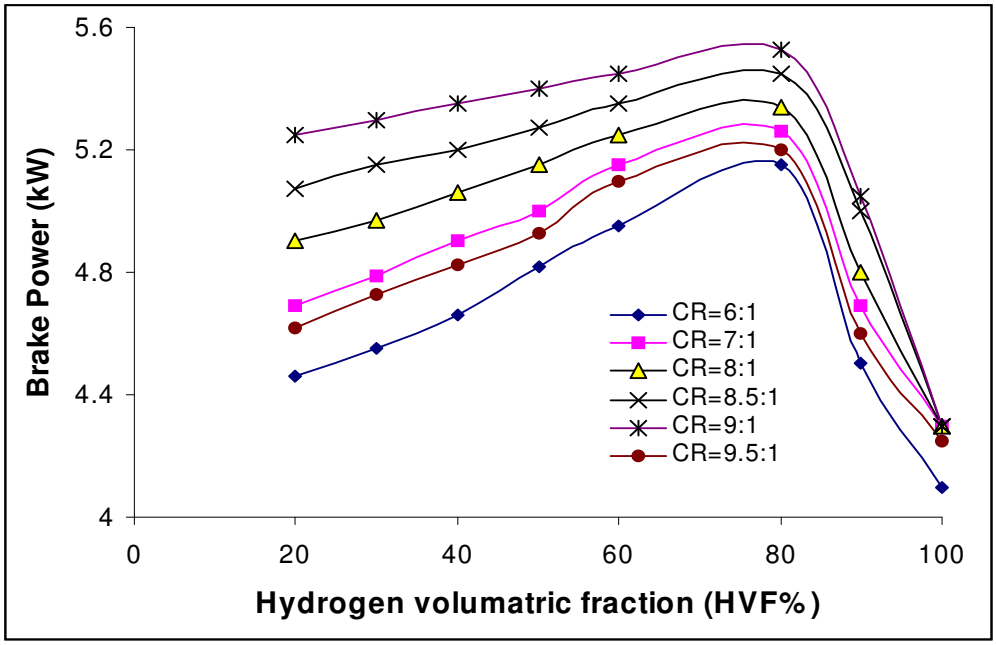

Fig. (2). The realation between HVF and the highest brake power of the engine at every compression ratio in the experments done

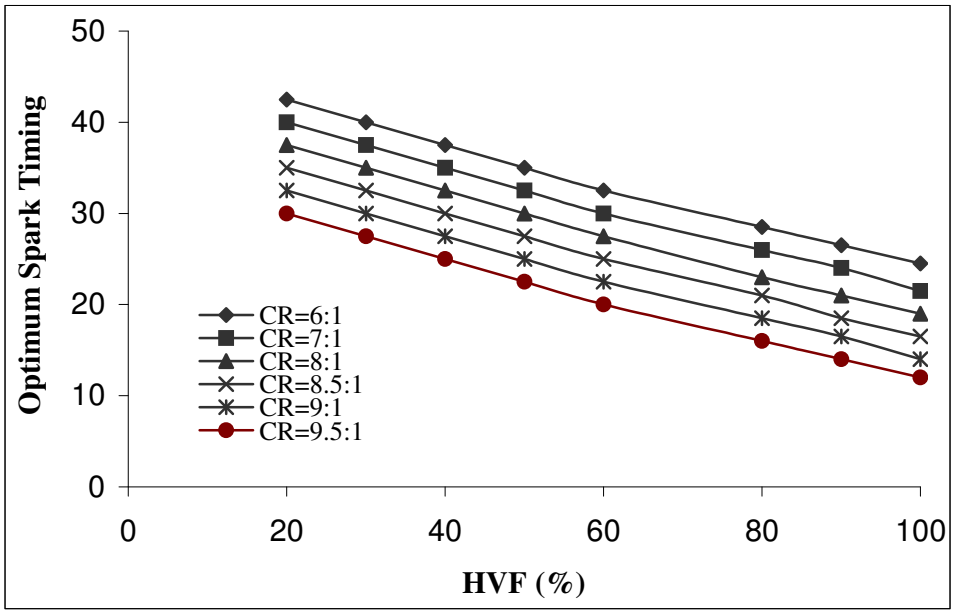

Fig. (3).The effect of different mixture rates and the satudied CR on OST

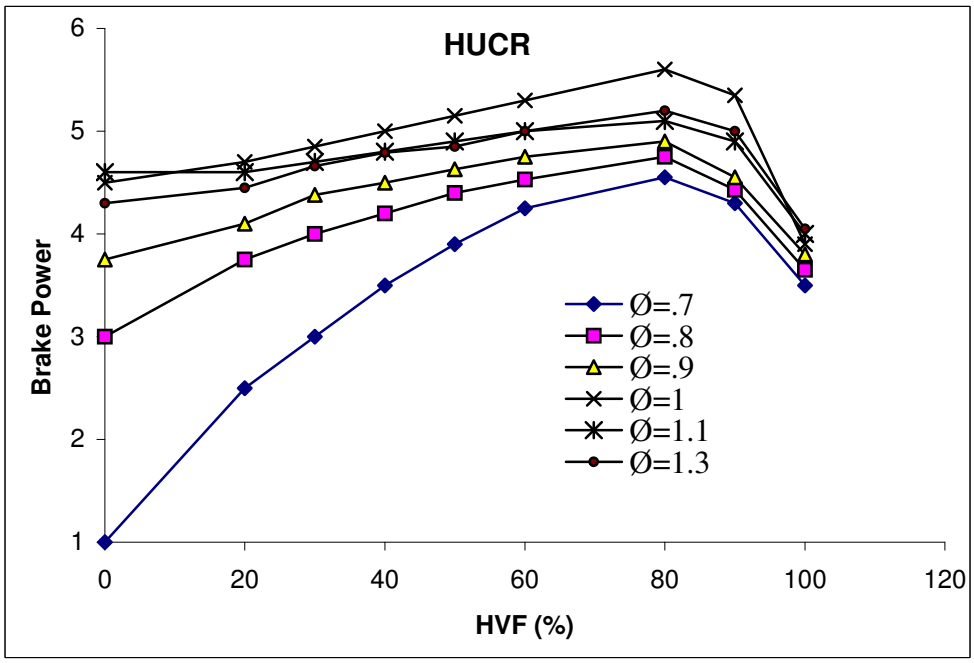

Fig. (4). The relation between brake power and HVR in mixture, for five different equivalence ratios at OST and 25 rps engine speed, and HUCR for each fuel

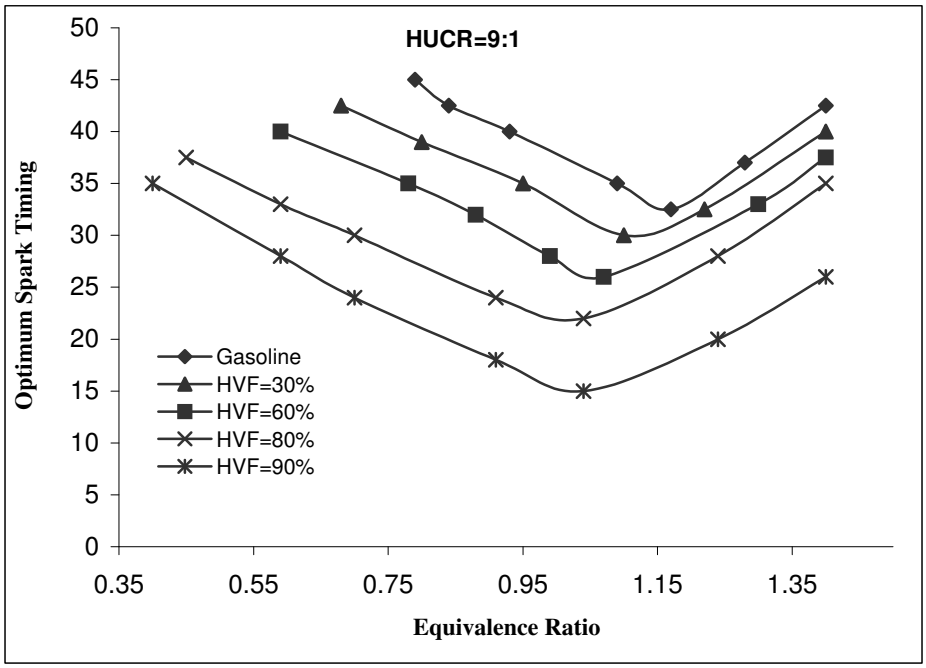

Fig. (5). The relation between equivalence ratio and OST, for different mixing rates, at HUCR and 25 rps

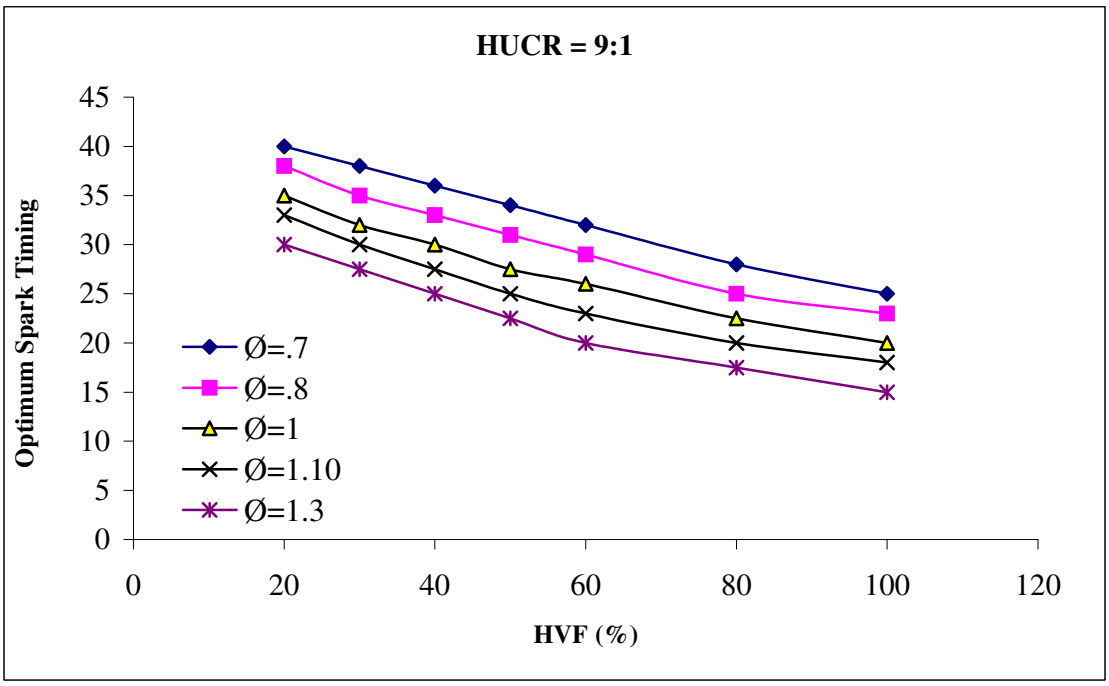

Fig. (6). The effect of HVF on OST for difined equivalence ratios

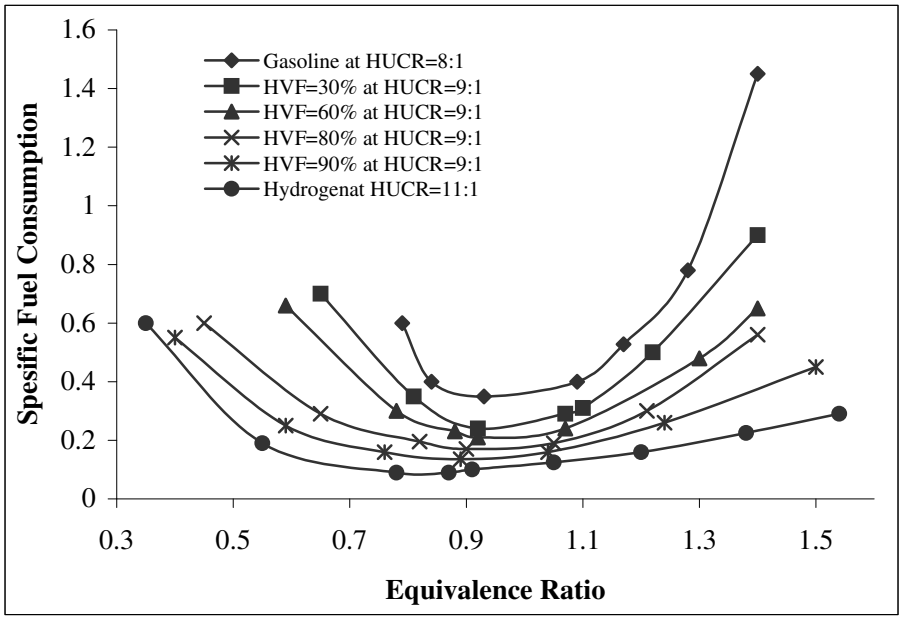

Fig. (7). The effect of HVF addition to gasoline on bsfc was studied for wide range of equivalence ratios at HUCR, 25 rps and OST

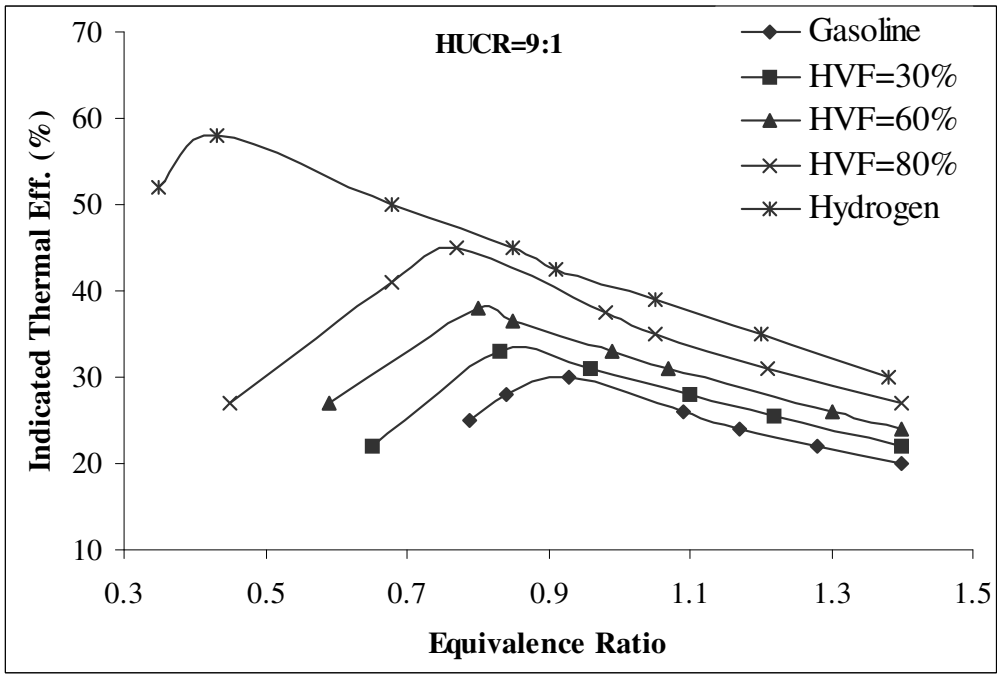

Fig. (8). The effect of hydrogen addition on indicated thermal efficiency, at HUCR and OST, for three chosen HV fractions

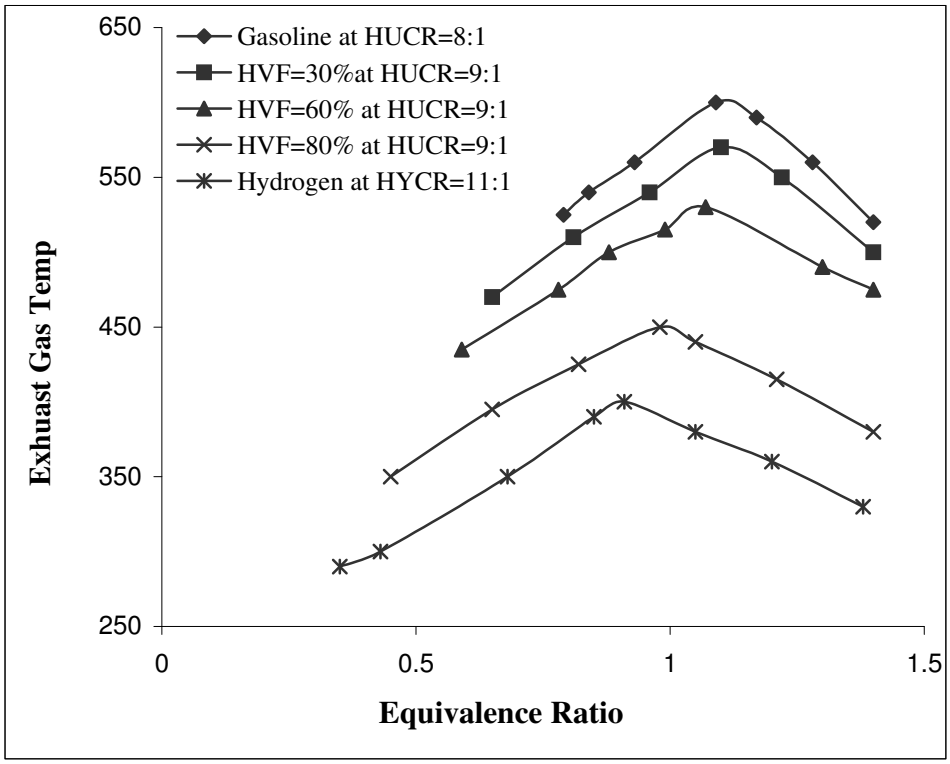

Fig. (9).The relation between exhuast gas temperature and equivalence ratio when adding different hydrogen volumatric fractions (HVF=0.3,06,0.8)

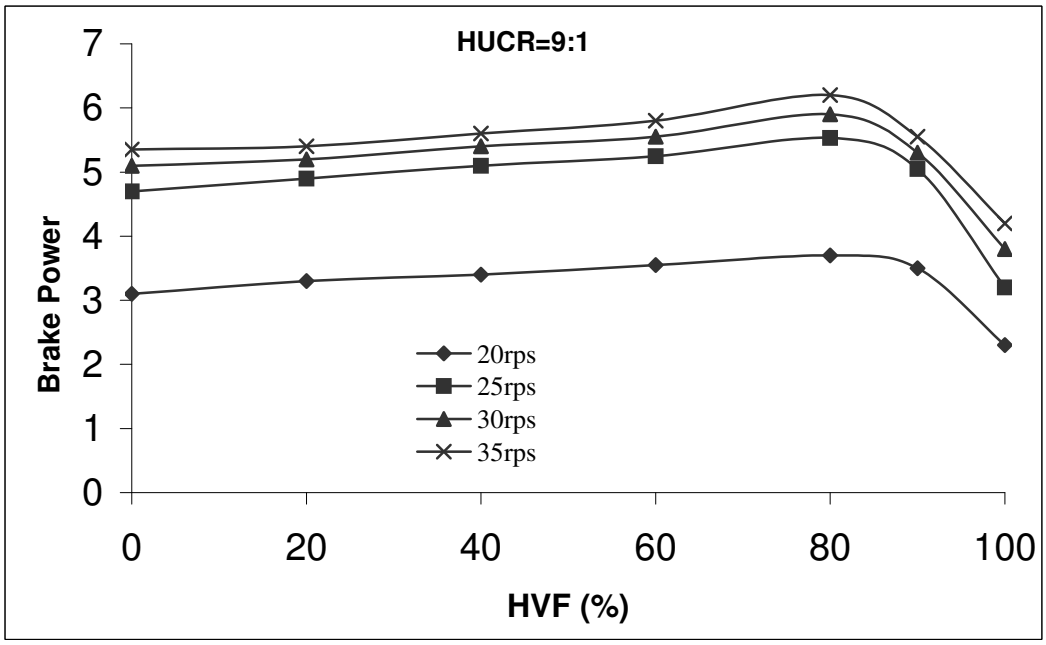

Fig. (10). The relation between the highest engine brake power and HVF in mixture, to obtain different speed effects at HUCR and OST

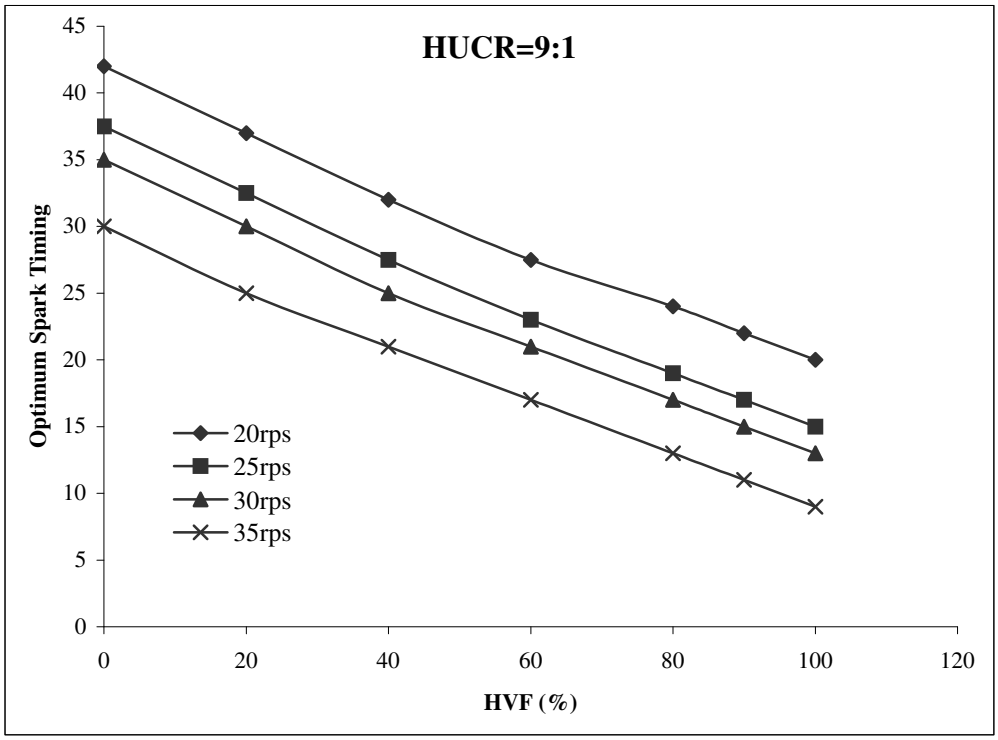

Fig. (11). The effect of supplementary hydrogen on OST, when the engine run at different speeds

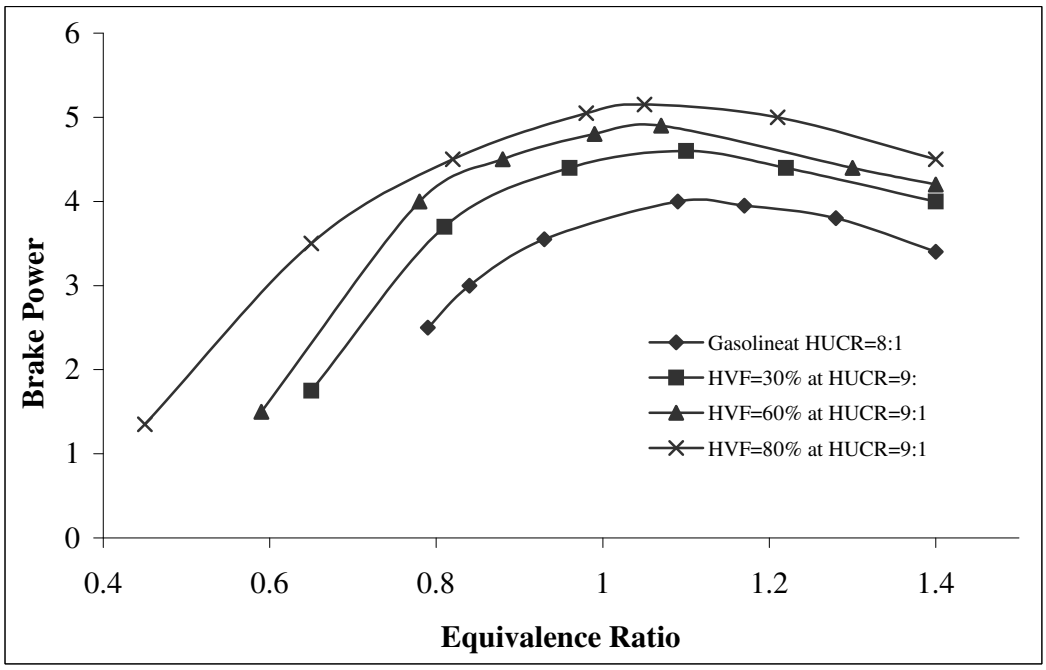

Fig. (12). The relation between engine brake power and equivalence ratio for spark timing 10 degrees BTDC

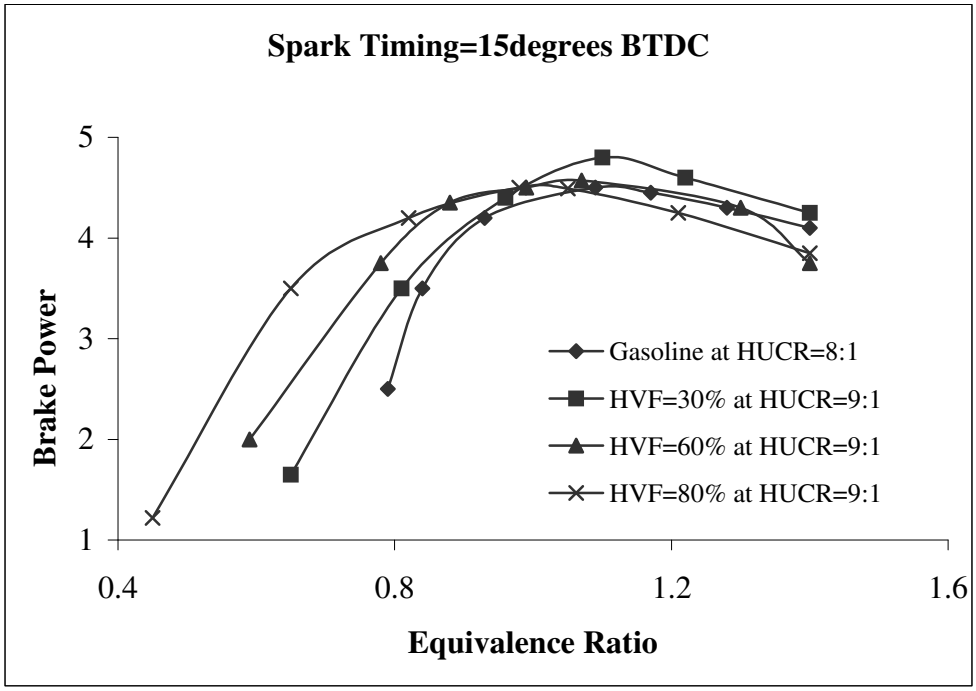

Fig. (13). The relation between engine brake power and equivalence ratio for spark timing 15 degrees BTDC

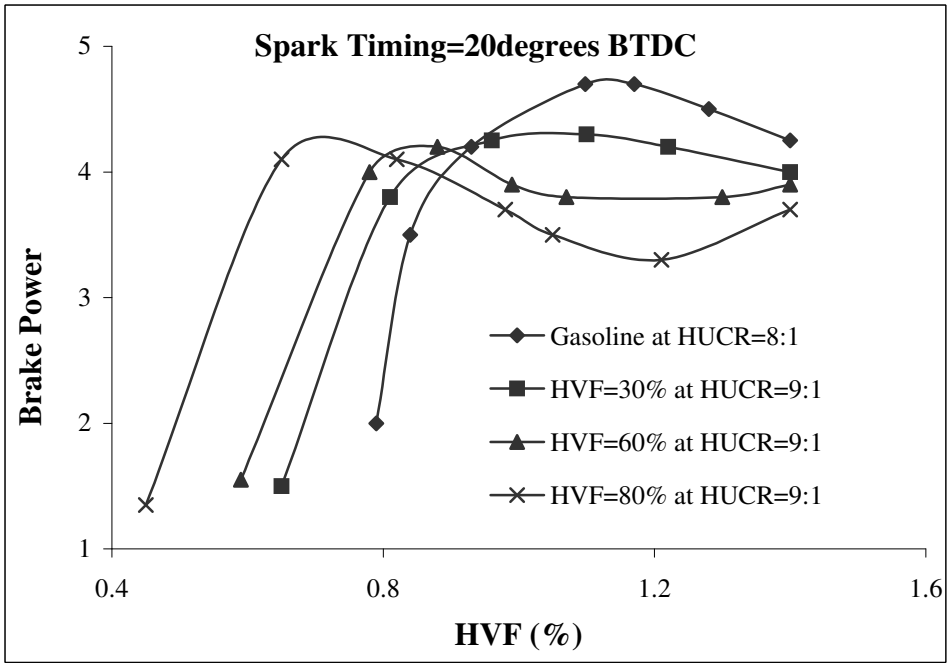

Fig. (14), The relation between engine brake power and equivalence ratio for spark timing 20 degrees BTDC

FRICTION AND WORN SURFACE TOPOGRAPHICAL FEATURES OF AS-CAST, MODIFIED AND HOMOGENIZED ALUMINUM-SILICON ALLOYS

Dr. Akeel Dhahir Subhi
Department of Production Engineering and Metallurgy
University of Technology
Baghdad-Iraq

ABSTRACT

The coefficient of friction was experimentally calculated for aluminum-silicon alloys by connecting a strain gauge to the arm of pin-on-disc wear machine in order to take microstrain readings from the strain-meter. As-cast and modified aluminum-silicon alloys were thermally homogenized for long periods of time (1-40hr) in order to study the effect of homogenization on friction. Scanning electron microscopy was successfully used to build up the mechanism of surface damage during sliding. The results showed that the coefficient of friction was increased with increasing bearing pressure for as-cast, modified and homogenized aluminum-silicon alloys. Thermal homogenization led clearly to remarkable changes in the frictional behavior of as-cast and modified aluminum-silicon alloys. Many mechanisms were responsible for aluminum-silicon alloys surface damage during sliding.

الخلاصة

تم حساب معامل الاحتكاك عمليا لسبائك الالمنيوم–سليكون من خلال ربط مقياس الانفعال بجهاز البلى الالتصاقي لغرض تسجيل قراءات الانفعال المايكروية . اجريت المجانسة الحرارية لسبائك الالمنيوم–سليكون المصبوبة والمحورة لفترات زمنية طويلة (1-40 ساعة) لغرض دراسة تاثيرها على الاحتكاك. استخدم المجهر الالكتروني الماسح بنجاح لغرض دراسة تضرر المنطقة السطحية اثناء الانزلاق. اوضحت النتائج زيادة معامل احتكاك بزيادة ضغط التحميل لجميع السبائك المصبوبة والمحورة والمجانسة. ادت المجانسة الحرارية الى تغيرات واضحة في السلوك الاحتكاكي لسبائك الالمنيوم–سليكون المصبوبة والمحورة. اسهمت العديد من الاليات في تضرر سطح سبائك الالمنيوم–سليكون اثناء الانزلاق.

Key Words: **Friction and Worn Surfaces, Al-Si Alloy, Topographical Features, As-Cast**

INTRODUCTION

Friction can be defined as a resistance to motion occurring during tangential displacement of contact surfaces in the real area of contact under applied force **(Halling 1979 and Rigney 1981)**. Components used in tribological applications are exposed to friction during their work **(Nayak 2004 and Zhang 2004)**. One of the mostly used alloys in tribological applications is aluminum-silicon because of its good wear resistance, high strength to weight ratio, good corrosion resistance

and good castability and machinability **(Granger 1988 and Polmear 1989)**. Many investigators studied the friction property not only for aluminum-silicon alloys but also for other materials. **(Sarkar and Clarke 1980 and 1982)** found that the frictional resistance fluctuated violently for most as-cast and age hardened aluminum-silicon alloys, indicated stick-slip and suggested plastic interaction but correlation between surface damage and magnitude of friction could not be found. **(Sakamoto and Tsukizoe 1978)** found that the metal transfer from the soft metal to hard asperities in contact with it caused significant changes in the shape, size and height distribution of the asperities which led to reduce the effect of the initial surface roughness of the hard metal during friction. Consequently the friction force became less dependent on the surface roughness than it did when no metal transfer occur. **(Mahdavian and Mai 1984)** studied the variation in friction coefficient with sliding distance for similar and dissimilar metals. They found that for similar metals sliding on each other there was a significant contribution to friction owing to severe ploughing while for dissimilar metal, the coefficient of fiction was determined primarily by the way metal transfer occurred between sliding surfaces. **(Prasad and Mecklenburg 1993)** found that no significant differences in the friction behavior of the $Al_2O_3.SiO_2$ and Al_2O_3 fiber-reinforced aluminum metal-matrix composite (MMC) and unreinforced alloy when metallugraphically polished samples were used. They also found that when the surface of the MMC was etched, the friction coefficient dropped to a low value of 0.18 and the stick-slip type behavior disappeared. The addition effect of different lead percentages to aluminum-silicon alloys on friction properties was studied by **(Pathak et al. 1997)**. They found that the addition of lead was reduced the interfacial friction and improved the ability of aluminum-silicon alloys to resist seizure. A lower friction coefficient and higher seizure load were obtained for Al-Si-Pb alloys bearing in semi-dry sliding conditions compared with those observed for dry conditions.

The aim of this work is to study the frictional behavior of as-cast and modified aluminum-silicon alloys with titanium. The effect of thermal homogenization with different time periods for aluminum-silicon alloys on frictional behavior is also studied.

MATERIALS AND METHODS

Binary Al-12%Si alloy was prepared by adding small quantity of pure aluminum to Al-13%Si master alloy. Titanium was added to Al-12%Si alloy in different percentages (0.05 and 0.1%Ti) after putting it in an aluminum foil and inserting it to the molten Al-12%Si alloy with good mixing (10 min in time) to ensure solubility and distribution of titanium in the alloy matrix. All alloys were melted in an alumina crucible by using a gas fired furnace. Then these alloys were poured in a preheated carbon steel die (300 C°) to ensure no chilling occurring to these alloys after solidification. The ingots samples produced from casting process have 15 mm diameter and 100 mm length. The chemical composition of pure aluminum, master alloy and prepared aluminum-silicon alloys are illustrated in **Table 1**. All alloys were thermally homogenized at 525 C° with different time periods (1-40 hr) to increase the coherency between silicon particles and aluminum matrix.

Coefficient of friction was measured by taking the microstrain readings from the strain-meter. The strain-meter was connected to the arm of pin-on-disc wear machine through a strain gauge, in which the specimen has been supported. The time of each test was 30 min, in in which the coefficient of friction for each test represents the average value during the test. All specimens were dry slided on a 45 HRC carbon steel disc to make contact with other material.

RESULTS AND DISCUSSION

The frictional behavior of as-cast and modified Al-Si alloys

The relationship between bearing pressure and coefficient of friction (μ) **Fig.1** reveals that the coefficient of friction increases with increasing bearing pressure due to increased interaction and

cold welding between the asperities of pin surface and counterface. This means that the surface damage is greater due to tangential traction. Since, strong welds and interaction between the asperities should also mean a high value of friction coefficient because the shear force required to distangle the interaction and cold welding between these asperities is greater in order to make sliding continuous. **Fig.1** also shows that Al-12%Si alloy has a lower coefficient of friction in comparison with the other alloys containing titanium, while the coefficient of friction of the alloy containing 0.1%Ti approached the coefficient of friction of Al-12%Si at high bearing pressure. This approach relies on the wear rate, in which the coefficient of friction increases linearly with wear rate **(Mitchell 1976)**. The wear rate of Al-12%Si alloy is lower in comparison with the other alloys containing titanium **(Subhi 2000)**., therefore Al-12%Si alloy has a lower coefficient of friction. **Fig.2** shows the relationship between sliding distance and coefficient of friction of aluminum-silicon alloys. The figure shows that all alloys have two types of friction coefficient. The first is static and the other is dynamic coefficient of friction. Generally, the static coefficient of friction was greater than the dynamic coefficient of friction for all aluminum-silicon alloys. This is because the asperities are interacted before sliding under applied bearing pressure, and when sliding begins, they need high shear forces to distangle them to make sliding continuous. After increasing the coefficient of friction in the early stage of sliding, its magnitude gradually decreases due mainly to reduction in ploughing action by transfer of material from the aluminum-silicon alloy pin surface to the counter asperities, leading to an increase in the tip angle of the asperities. Under steady state sliding, the dynamic coefficient of friction becomes approximately constant with fluctuation in its magnitude. **(Mitchell and Osgood 1976)** found that this fluctuation depends on the fluctuation in friction force resulted from changes in the number of contacts as well as from changes in the proportion of the welded contacts. **(While Blau 1981)** introduced a comprehensive picture to this fluctuation in which it coincides with the present work. Blau found that the friction depends on many processes as (1) metal transfer (2) film formation and removal (3) debris generation and (4) cyclic surface deterioration. It has bean also shown from **Fig.2** that Al-12%Si alloy has a lower static and dynamic coefficient of friction compared with other alloys containing titanium. This is because the coefficient of friction depends on the wear rate **(Mitchell 1976).**

The frictional behavior of homogenized Al-Si alloys

Thermal homogenization affected the magnitude of friction coefficient and this effect is dependent on the thermal homogenization time. The relationship between bearing pressure and coefficient of friction of homogenized aluminum-silicon alloys **Figs.3-5** showed that the homogenization for 1 hr led to increasing the coefficient of friction for all homogenized aluminum-silicon alloys in comparison with its magnitude in the as-cast and modified aluminum-silicon alloys. This is because the ductility of homogenized aluminum-silicon alloys for 1 hr was increased as a result of internal stresses relief, led to increase the interaction and cold welding between the asperities of pin surface and counterface. Since, the wear mechanism appeared with increasing bearing pressure as interaction between the asperities, and galling as a result of incomplete cold welding during sliding [Subhi 2000]. This demonstrates our explanation in which the increasing coefficient of friction accompany with increasing bearing pressure. With increasing thermal homogenization greater than 1 hr (5-40 hr), the coefficient of friction decreased. This is because the coefficient of friction depends on the wear rate **(Mitchell 1976)**. Decreasing in the wear rate occurred with increasing thermal homogenization time greater than 1 hr **(Subhi 2000)**, therefore, coefficient of friction decreases with increasing thermal homogenization time in comparison with its magnitude at 1 hr. The frictional behavior of homogenized alloys was similar to that of as-cast and modified aluminum-silicon alloys in which the two types of friction coefficient were present regardless of its magnitude, therefore, there is no need to re-explain the frictional behavior during sliding of homogenized alloys at constant bearing pressure.

The study of worn surface

Fig.6 shows the worn surface of as-cast and modified aluminum-silicon alloys where different mechanisms contributed in surface damage during sliding. The predominant mechanism is dependent on the alloy composition and bearing pressure. The worn surface of Al-12%Si alloy revealed that there were many mechanisms responsible for material removal. It has been shown that there was spalling in the worn surface, leading to a large pit formation, as well as there were many subsurface cracks sheared to the surface which were responsible for wear particles formation. These wear particles can be recognized clearly in the worn surface of the alloy containing 0.05%Ti. It has been shown that there were many wear small particles on the surface removed from the surface during sliding. The same wear particles can be shown in the worn surface of the alloy containing 0.1%Ti. These small particles were removed by secondary delamination. Secondary delamination is distinguished by craze cracking. (**Clarke and Sarkar 1981**) found that this secondary delamination may be a function of surface forces only and may have nothing to do with probable subsurface cracking responsible for primary delamination.

The wear mechanisms remained the same for homogenized aluminum-silicon alloys, but in different degrees. The worn surface of homogenized Al-12%Si alloy **Fig.7** shows that there were many surface cracks due to surface traction. These surface cracks were responsible for material removal by secondary delamination. The worn surface of homogenized alloy containing 0.05%Ti shows advanced stage in subsurface crack growth sheared to the surface. There are many surface cracks in the worn surface of homogenized alloy containing 0.1%Ti, as well as many small particles compacted on the surface due to the action of bearing pressure in which these small particles delaminated by secondary delamination.

CONCLUDING REMARKS

1-The coefficient of friction was increased with increasing bearing pressure for as-cast, modified and homogenized aluminum-silicon alloys.

2-Two types of friction coefficient were present, static and dynamic regardless of the magnitudes of these two coefficient types.

3-Thermal homogenization at 1 hr led to an increase in the coefficient of friction in comparison with its magnitude for as-cast and modified aluminum-silicon alloys, while increasing thermal homogenization time greater than 1 hr (5-40 hr) led to a decrease in the coefficient of friction in comparison with its magnitude at 1 hr.

4-Many mechanisms were responsible for surface damage during sliding. The predominant mechanism was dependent on the alloy composition, bearing pressure and thermal homogenization time.

REFERENCES

Blau P.J., “Mechanisms for Transitional Friction and Wear Behavior of Sliding Metals”, Wear, 72 (1981) 55.

Clarke J. and Sarkar A.D., “Topographical Features Observed in a Scanning Electron Microscopy Study of Aluminum Alloy Surfaces in Sliding Wear”, Wear, 69 (1981) 1.

Granger D.A., Elliott R., "Solidification of Eutectic Alloys", Metals Handbook, Vol. 15, “Casting”, American Society for Metals, Metals Park, Ohio, 1988.

Halling J., “Principle of Tribology”, Macmillan Pres Ltd. (London) 1979

Mahdavian S.M. and Mai Y.W., “Further Study in Friction, Metallic Transfer and Wear Debris of Sliding Surfaces”, Wear, 95 (1984) 35.

Mitchell L.A. and Osgood C., “A Theory of Friction and Wear Based on a New Characterization of Asperity Interactions”, Wear, 40 (1976) 203.

Nayak S. and Dahotre N.B., "Surface Engineering of Aluminum Alloys for Automotive Engine Applications", JOM, Jan. (2004) 46.

Pathak J.P., Torabian H. and Tiwari S.N., "Antiseizure and Antifriction Characteristics of Al-Si-Pb Alloys", Wear, 202 (1997) 134.

Polmear I.J., “Light Metals”, Edward Arnold (London) 1989.

Prasad S.V. and Mecklenburg K.R., "Friction Behavior of Ceramic Fiber-Reinforced Aluminum Metal-Matrix Composite Against a 440C Steel Counterface", Wear, 162-164 (1993) 47.

Rigney D.A., “Fundamentals of Friction and Wear of Materials”, American Society for Metals, Metals Park, Ohio, 1981.

Sakamoto T. and Tsukizoe T., “Metal Transfer in the Frictional Contact of a Rough Hard Surface”, Wear, 47 (1978) 301.

Sarkar A.D. and Clarke J., “Friction and Wear of Aluminum –Silicon Alloys”, Wear, 61 (1980) 157.

Sarkar A.D. and Clarke J., "Wear Characteristics, Friction and Surface Topography Observed in the Dry Sliding of As-Cast and Age-Hardening Al-Si Alloys”, Wear, 75 (1982) 71.

Subhi A.D., “Study of Microstructure and Wear of As-Cast and Modified Aluminum-Silicon Alloys with Titanium”, M.Sc. Thesis, School of Production Engineering and Metallurgy, University of Technology, Baghdad, Iraq, 2000 (In Arabic).

Zhang C., Cheng H.S. and Wang Q.J., "Scuffing Behavior of Piston-Pin/Bore Bearing in Mixed Lubrication-Part II: Scuffing Mechanism and Failure Criterion", Trib. Trans., 47 (2004) 1.

Table.1 Chemical composition of pure aluminum, master alloy and prepared aluminum-silicon alloys.

Materials	*Composition (%)*				
	Si	Cu	Mg	Ti	A1
A1	0.113	0.008	0.008	0.008	Remainder
A1-13%Si	13.00	0.02	0.007	0.004	Remainder
A1-12% Si	12.23	0.02	0.005	0.035	Remainder
A1-12% Si-0.05% Ti	12.10	0.02	0.007	0.045	Remainder
A1-12% Si-0.1% Ti	13.33	0.02	0.007	0.108	Remainder

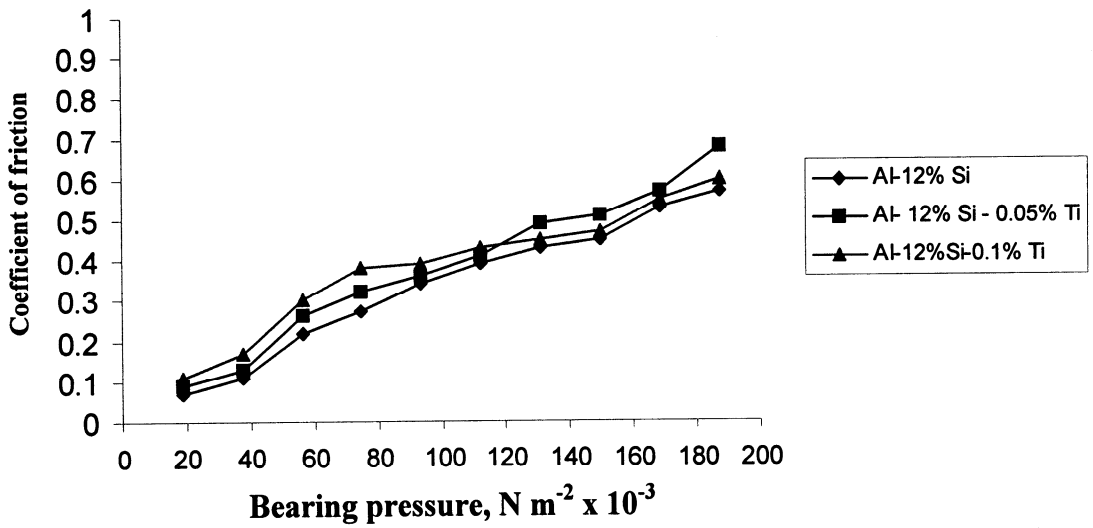

Fig.(1). The relationship between bearing pressure and coefficient of friction of as-cast and modified aluminum-silicon alloys.

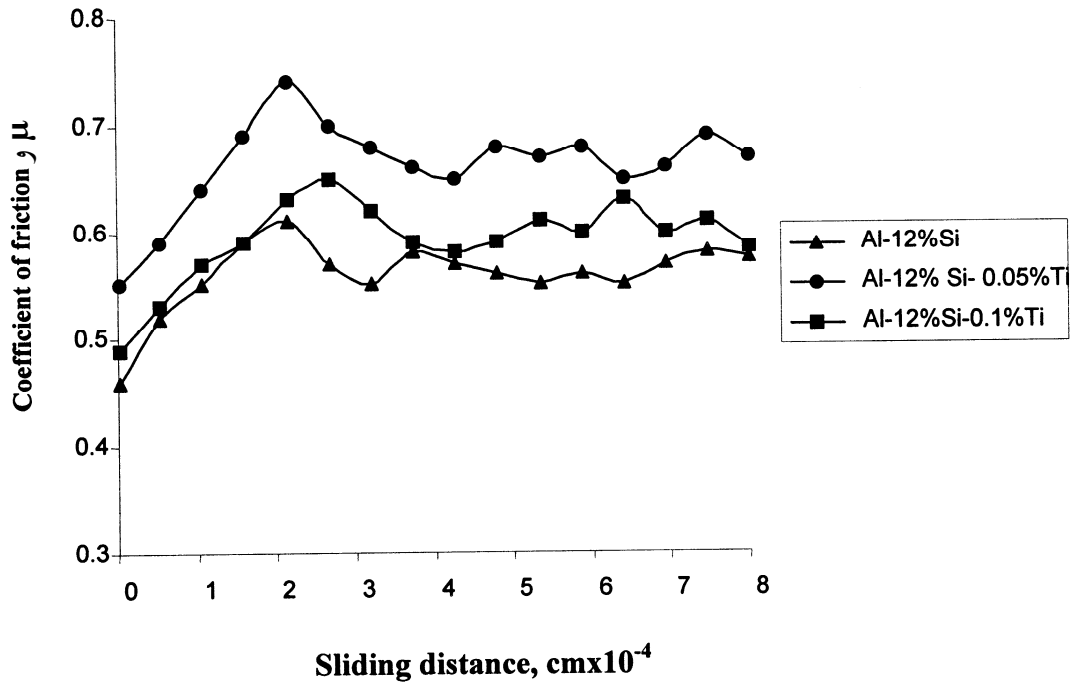

`Fig.2 The relationship between sliding distance and coefficient of friction of as-cast and modified aluminum-silicon alloys.

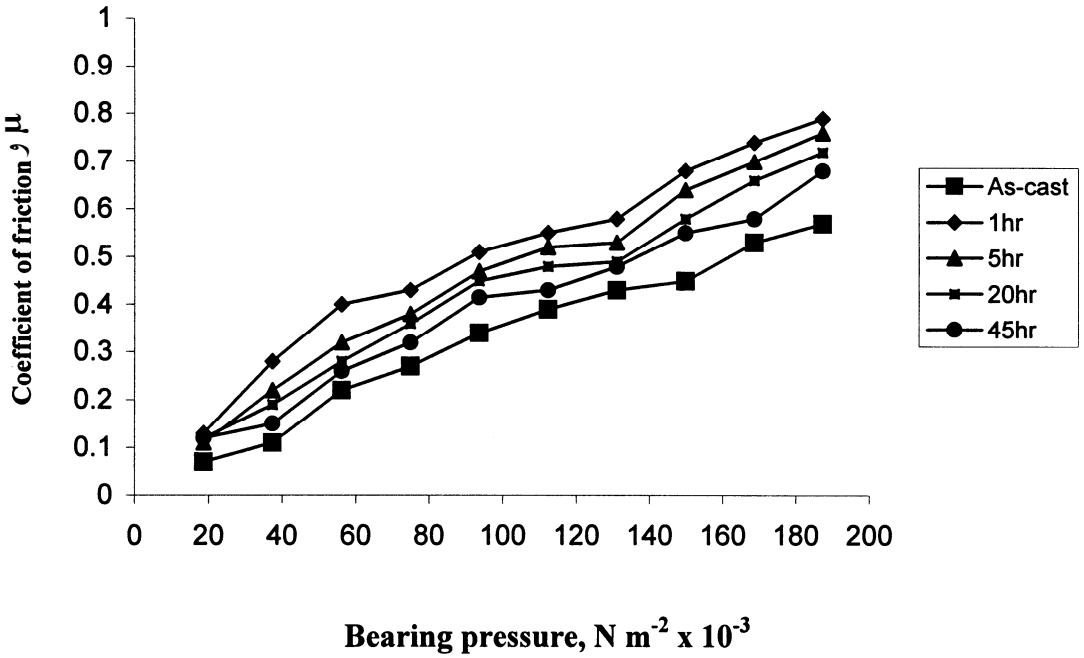

Fig.3 The relationship between bearing pressure and coefficient of friction of homogenized Al-12%Si alloy.

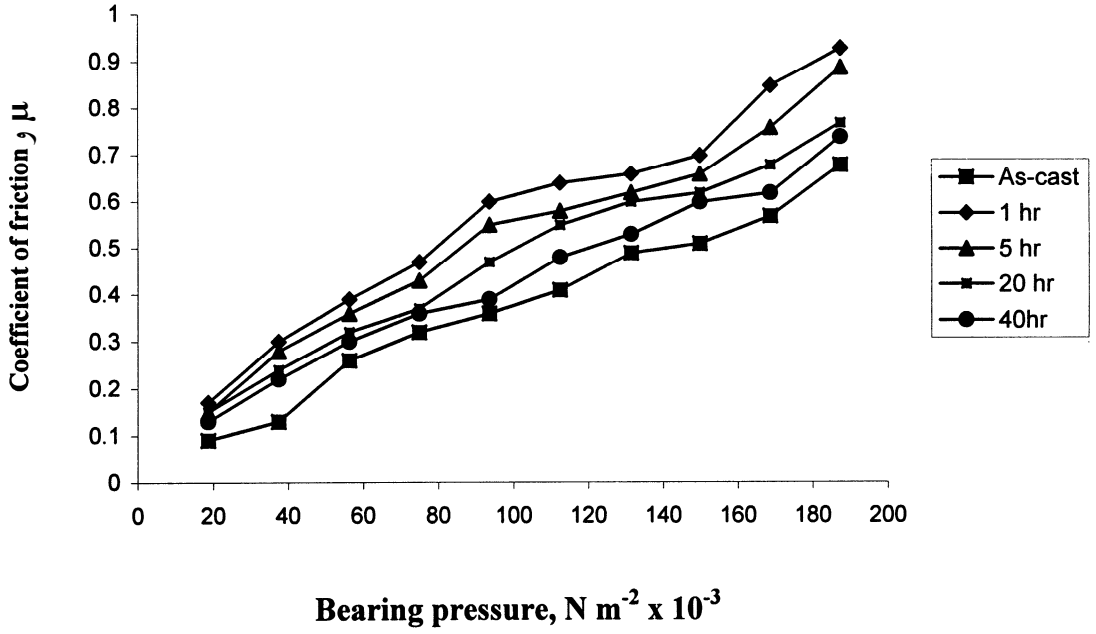

Fig.4 The relationship between bearing pressure and coefficient of friction of homogenized Al-12%Si-0.05%Ti alloy.

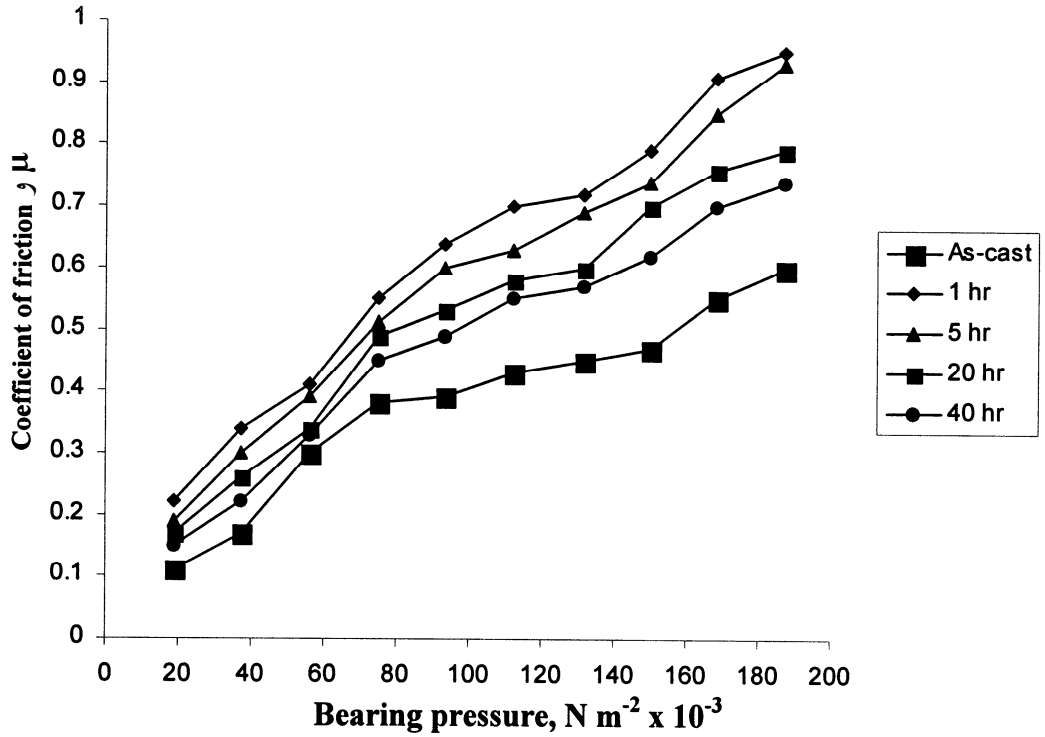

Fig.5 The relationship between bearing pressure and coefficient of friction of homogenized Al-12%Si-0.1%Ti alloy.

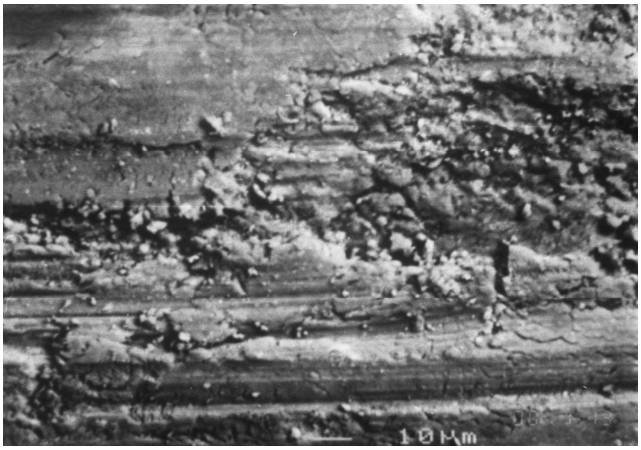

Al-12%Si

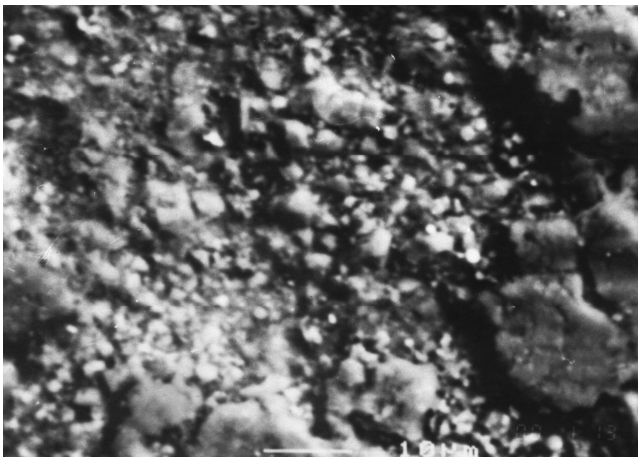

Al-12%Si-0.05%Ti

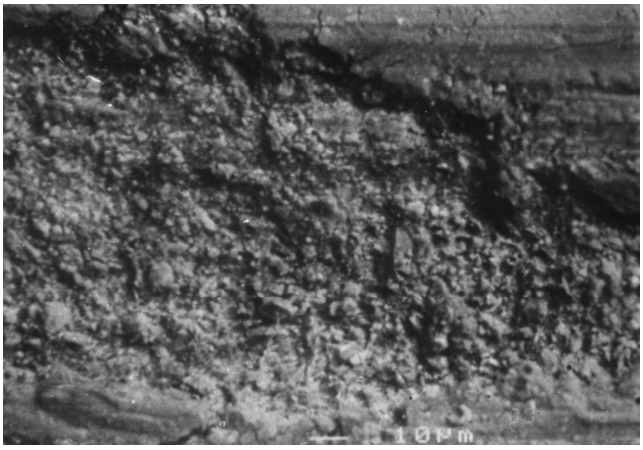

Al-12%Si-0.1%Ti

Fig.(6). Secondary electron images of freshly worn surfaces of as-cast and modified aluminum-silicon alloys. Bearing pressure, 168.6 kPa; sliding speed, 160.2 m min^{-1}. Arrow indicates sliding direction.

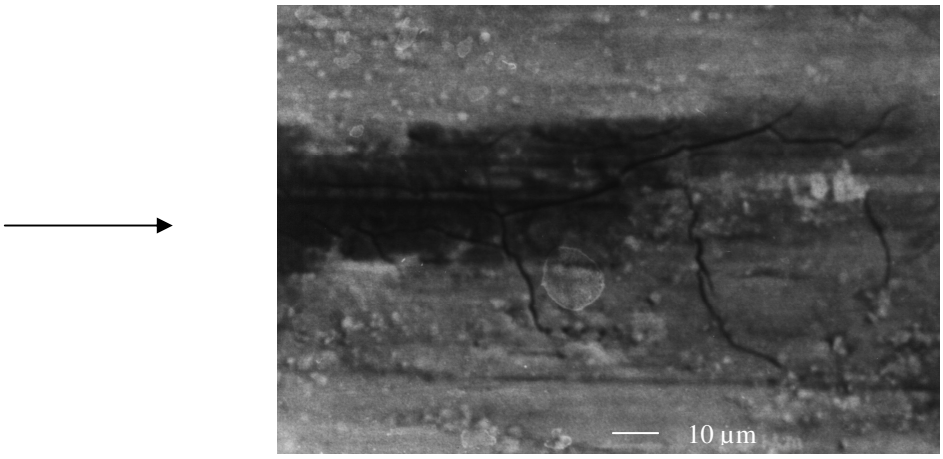

Al-12%Si

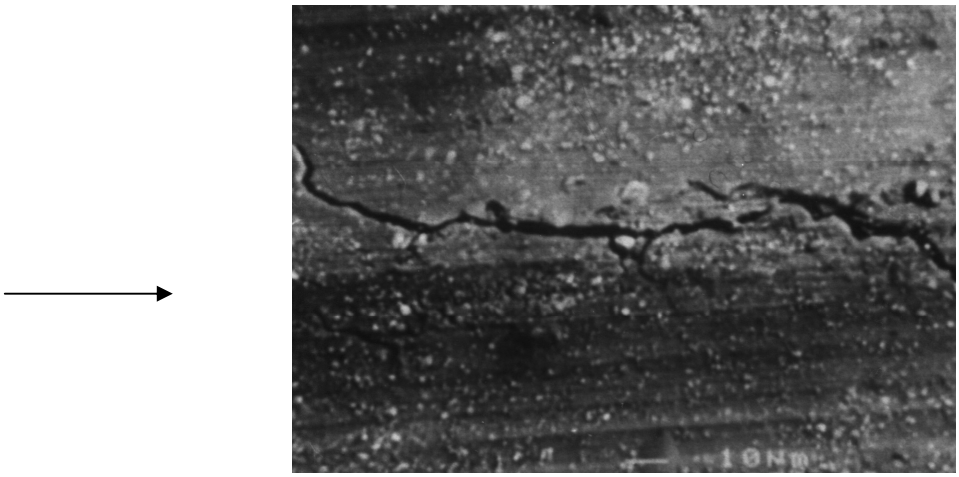

Al-12%Si-0.05%Ti

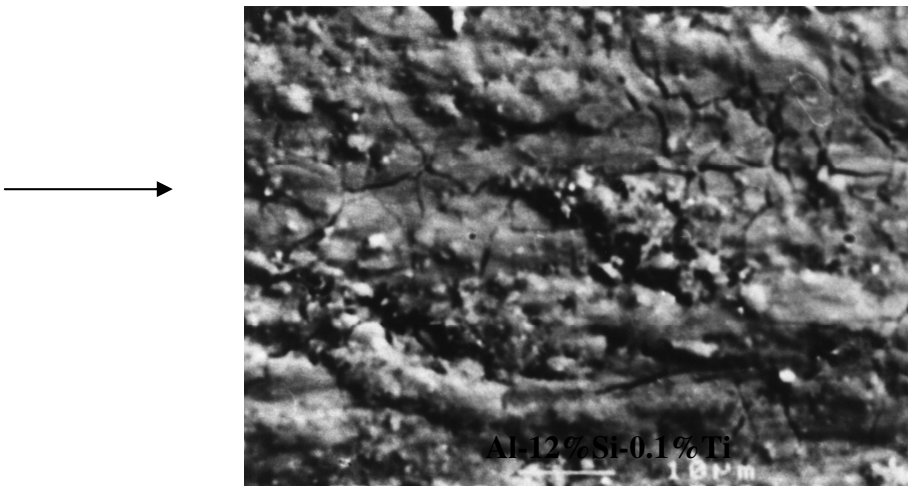

Fig.(7). Secondary electron images of freshly worn surfaces of homogenized aluminum-silicon alloys at 40 hr. Bearing pressure, 168.6 kPa; sliding speed, 160.2 m min^{-1}. Arrow indicates sliding direction.

STRATIFIED WATER-OIL-GAS FLOW THROUGH HORIZONTAL PIPES

Prof. Dr. Zeiad A. R. Aswad **Dr. Sameera M. Hamad-Allah** **M Sc. Faaiz H. R. Alzubaidi**
Baghdad University
Engineering Collage
Petroleum Engineering Department

ABSTRACT

Stratified three-phase flow through horizontal pipe has been studied experimentally. The fluids used in the system are water, kerosene, and air. A closed loop flow system, which composed of 0.051 m inside diameter and 4 m length test pipe, is designed with facilities for measuring flow rate, pressure drop and thickness of each phase.

The effects of gas, liquid flow rates and water liquid ratio (WLR) have been experimentally observed. It was found that liquid (water, and oil) thickness decreased when the gas flow rate is increased with constant liquid flow rate, and increased when the liquid flow rate is increased at constant gas flow rate. Pressure drop increased when the gas and/or liquid flow rate is increased.

Three equations have been formulated, using the experimental data of the present work, to predict liquid, water thickness and system pressure drop in stratified three-phase flow in horizontal pipe. High correlation coefficients are obtained for these equations.

The experimental results are compared with the results obtained from three-phase model of Taital, Barnea, & Brill (1995). The comparison showed that the predicted data which obtained from three-phase flow model Taital et al. (1995) is in good agreement with experimental data.

الجريان الطباقي للماء والنفط والغاز خلال الانابيب الافقية

الاستاذ الدكتور زياد عبد الرزاق اسود **الدكتورة سميرة محمد حمد الله**
السيد فائز هادي رشيد الزبيدي

الخلاصة

تمت دراسة الجريان الطبقي ثلاثي الأطوار خلال الأنابيب الأفقية مختبريا. الموائع المستخدمة في المنظومة هي : الماء, النفط الأبيض و الهواء وباستخدام أنبوب فحص قطره 0.05 م وطوله 4 م ليتم حساب: معدل جريان الموائع , هبوط الضغط في المنظومة , و سمك كل طور .

تأثيرات معدل جريان الغاز و السائل هي المدروسة لمعرفة تأثيرها على سمك الأطوار السائلة حيث وجد أن سمك أي طور من الأطوار السائلة (ماء – نفط) يقل عند زيادة معدل جريان الغاز عند ثبوت جريان السائل ,و يزداد السمك عندما يزداد معدل جريان السائل عند ثبوت معدل جريان الغاز . و وجد أن هبوط الضغط يزداد عندما يزداد معدل جريان الغاز و/ أو يزداد معدل جريان السائل.

تم صياغة ثلاثة معادلات لتمثيل النتائج المختبرية : معادلة تقوم بحساب سمك السائل الكلي ومعادلة لحساب سمك الماء و معادلة لحساب هبوط الضغط للجريان الطبقي ثلاثي الأطوار في الأنابيب الأفقية و هذه المعادلات أظهرت تمثيلا جيدا للنتائج المختبرية .

و قد تم مقارنة النتائج المختبرية مع النتائج المستحصلة من موديل ميكانيكي و هو :تايتل , بارنيه و بريل 1995 و هذ المقارنة اظهرت بان القيم المستحصلة من الموديل الثلاثي الطور جيدة في تمثيل النتائج المختبرية .

INTRODUCTION

Three-phase gas-oil-water flow commonly occurs in the petroleum industry. Perhaps the most relevant practice is the transportation of natural gas-oil-water mixtures through pipelines. Three-phase flow may also be encountered in pumping system, especially in surface gathering lines, and in well-bores and gas lift wells which produce water along with oil and gas. In off-shore and remote well sites, it is often intractable to separate oil and gas there. The transportation of oil and gas in multiphase pipelines is therefore becoming more common. The oil-water-gas mixtures produced are transported many kilometers to platform or central gathering stations where the fluids are separated.

Water production often increases significantly during the latter stage of a well and use of the conventional approximations of a two-phase oil-gas system neglecting the water, or combining the oil and water into a liquid phase, often becomes inaccurate.

There have been numerous investigations of two-phase flow regimes; in contrast, three-phase flow regimes have not been studied thoroughly. Because of the abundance of three-phase flow applications in the petroleum and chemical industries, a better understanding of this complex flow phenomenon is needed.

PURPOSE OF STUDY

The main purpose of this study is to investigate the pressure drop of the system and the levels of the liquid layers (water and oil) and the gas layer experimentally. Flow pattern map have been constructed for 50% water liquid ratio (WLR). Three empirical correlations have been developed for predicting liquid, and water thicknesses and pressure drop in three-phase stratified flow in horizontal pipes. The experimental data have been compared with the theoretical data of three-phase model of Taital et al. (1995).

FLUID PHYSICAL PROPERTIES

The physical properties of the liquid and gas phases are determined from laboratory measurements at atmospheric pressure and temperature of $12^{o}C$. These properties are shown in Table (1): -

Table (1): physical properties of water, oil, and gas

	Water	Oil (kerosene)	Gas (air)
Density $\rho\left(\frac{Kg}{m^3}\right)$	1000	775	1.22
Viscosity $\mu(Pa.s)$	0.001141	0.00127875	0.000018

EXPERIMENTAL FACILITIES AND TEST PROCEDURE

The experiments were conducted in horizontal three-phase flow loop as shown in Fig (1). Three kinds of phases are used in this study (water, kerosene and air). The individual phase of oil and water are pumped from their individual tank ($0.15m^3$) into 1 inch ID pipe. A two centrifugal pumps with maximum flow of ($4m^3/hr.$) is used to pump the two immiscible liquid (oil and water) to the mixing tee (mixing tank) at the up stream of test section. The water and oil flow rate are measured by flow meter. The gas from compressor with maximum flow rate of ($16m^3/hr.$) is also passed into the mixing tank. Its flow rate is measured by flow meter.

The gas-oil-water mixture from the mixing tank flow into a (0.051mm) internal diameter, and (4 m) long Plexiglas pipeline (transparent pipe), where the flow patterns are observed visually. The water and oil film thickness are measured by using a rule which was parallel with vertical diameter. The multiphase mixture is discharged into a ($0.768m^3$) separator. The gas is discharged from the top to the atmosphere. The oil-water mixtures settle and separate into individual phases and return to their respective tank. The majority of the experiments were carried out in the system which operated at atmospheric pressure and temperature of ($12^o C$). It should be noted that because of the waves at the gas-oil interface, the measurements obtained from these experiments did not provide a precise estimate of the film thickness. Only a range for the film thickness could be determined.

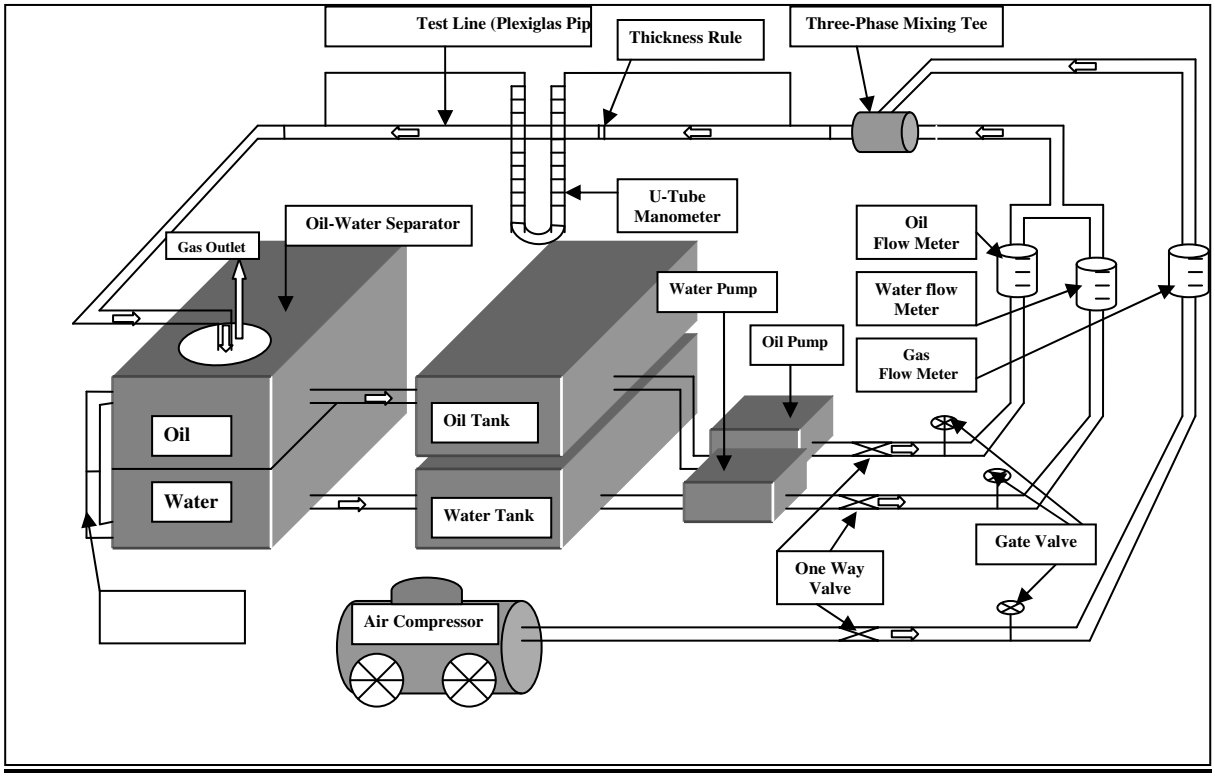

Fig.(1) Three-Phase Flow Loop

RESULTS

In this study, the effect of liquid (oil & water) and gas flow rates, and pressure drop have been studied experimentally. Flow pattern maps have been constructed for 50% WLR. Then experimental results are compared with Three-phase mechanistic model of Taital et al. (1995) for predicting liquid, water, and oil thickness and system pressure drop.

The Effect of Gas Flow Rate on Dimensionless Thickness

Figure (2) show the effect of liquid and gas flow rates on dimensionless liquid thickness (h_L / D). For constant liquid flow rate there is an inversely proportional relationship between dimensionless liquid thickness (h_L / D) and gas flow rate (vsg). A proportional relationship is observed between (h_L / D) and liquid flow rate (vsl) for constant gas flow rate.

The same results are obtained when plotting (h_w / D) or (h_o / D) instead of (h_L / D) as shone in Figs. (3) and (4) respectively.

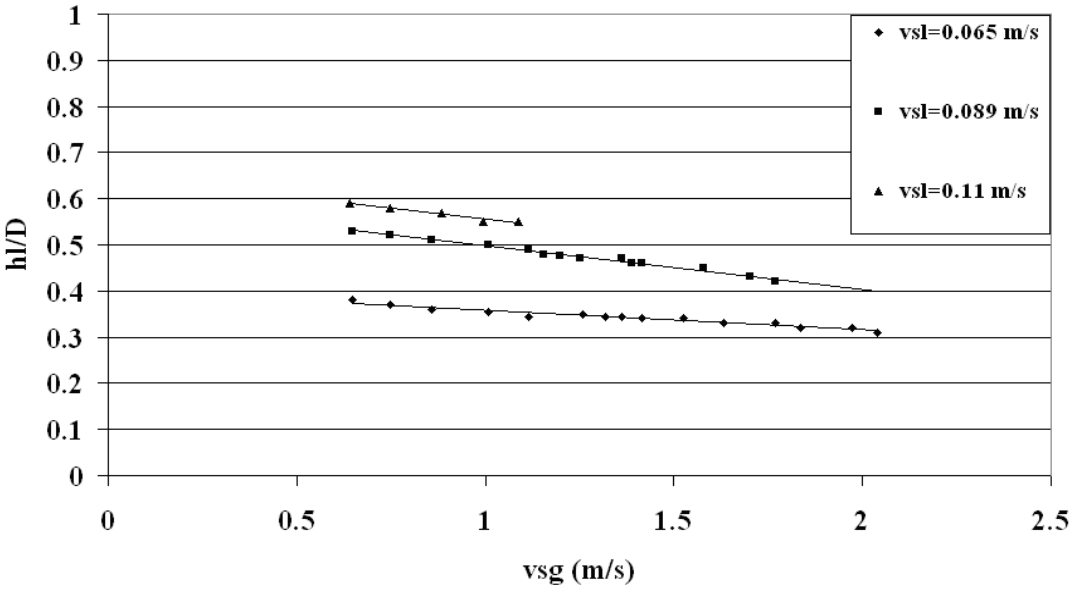

Fig .2 Relationship between vsg and hl/D for different vsl {WLR=50%}

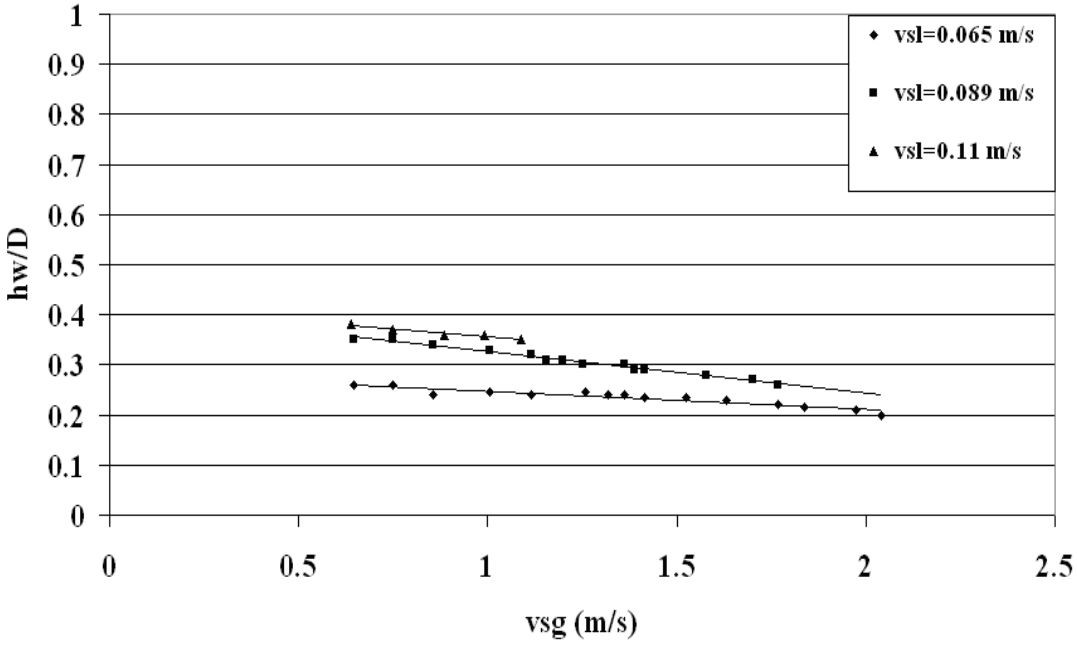

Fig.3 Relationship between vsg and hw/D for different vsl {WLR=50%}

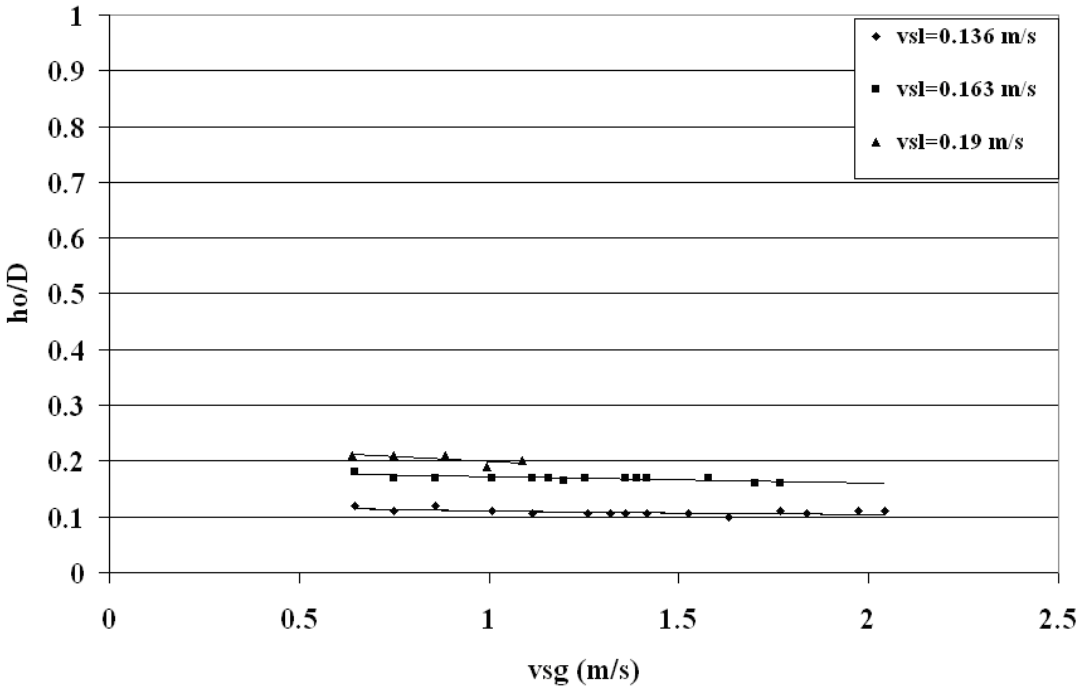

Fig.4 Relationship between vsg and ho/D for different vsl {WLR=50%}

The values of (h_L / D), (h_w / D), (h_o / D) are plotted on the same figure versus (vsg) for a constant (vsl). Several figures are obtained for different velocities (Fig.5 for vsl= 0.065, Fig.6 for vsl=0.089, Fig.7 for vsl=0.11. The water level is usually quit high and the liquid consists mostly of water. This is logical since the oil being closer to the fast moving gas, i.e., the oil is dragged by the gas at higher velocities compared with the water layer at bottom.

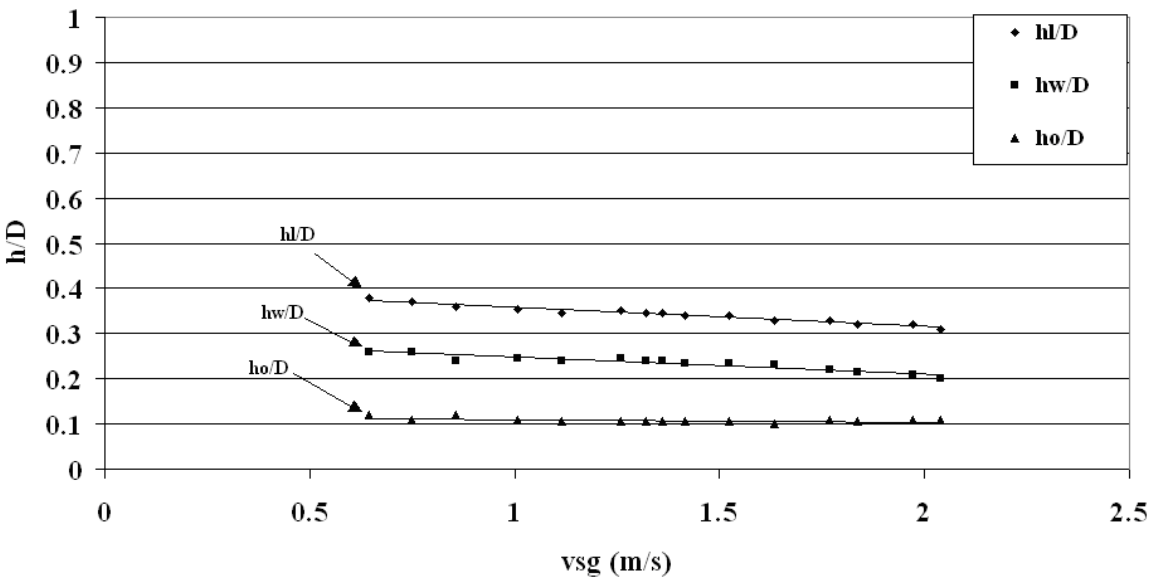

Fig.5 Relationship between vsg and h/D (vsl=0.065 m/s) {WLR=50%}

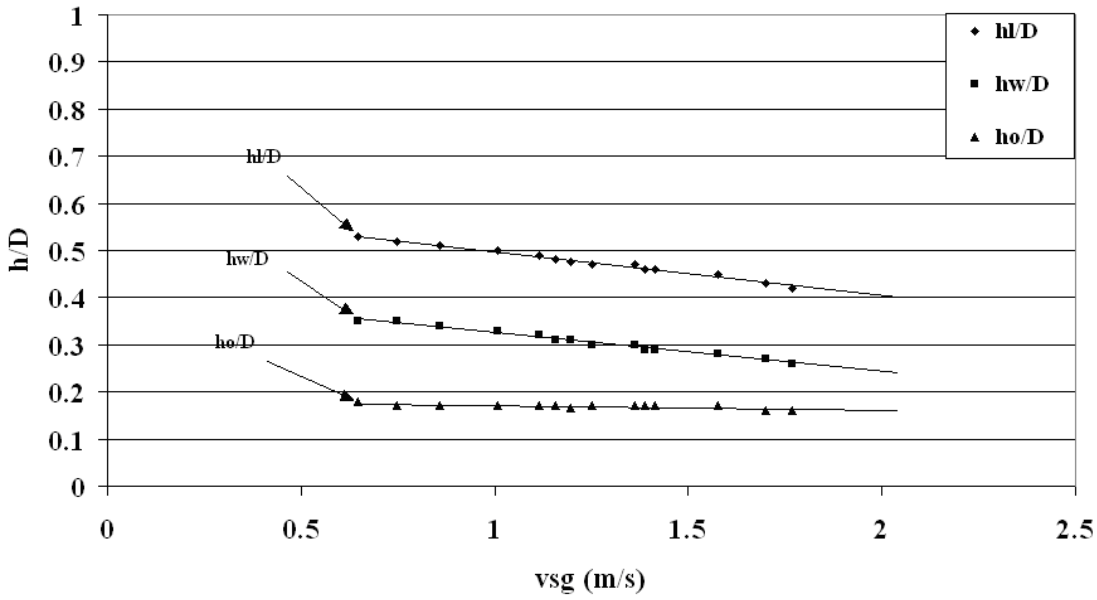

Fig. 6 Relatioship between vsg and h/D (vsl=0.089 m/s) {WLR=50%}

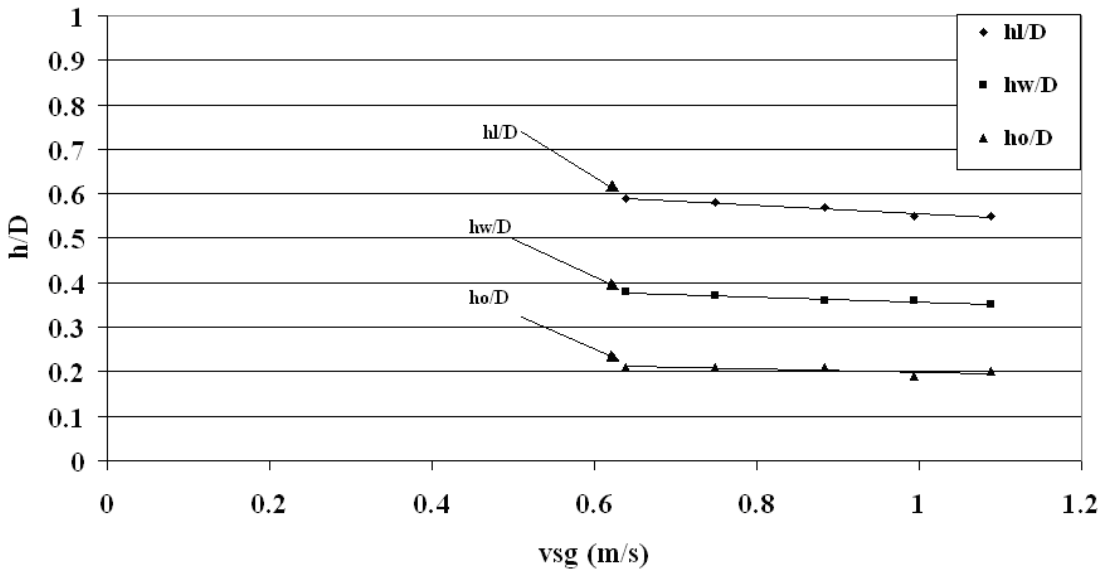

Fig.7 Relationship between vsg and h/D (vsl=0.11 m/s) {WLR=50%}

The Effect of Gas Flow Rate on Pressure Drop

The effects of liquid and gas flow rate on pressure drop are presented in Fig.8. In general the pressure drop increased when the gas and/or liquid flow rate increased.

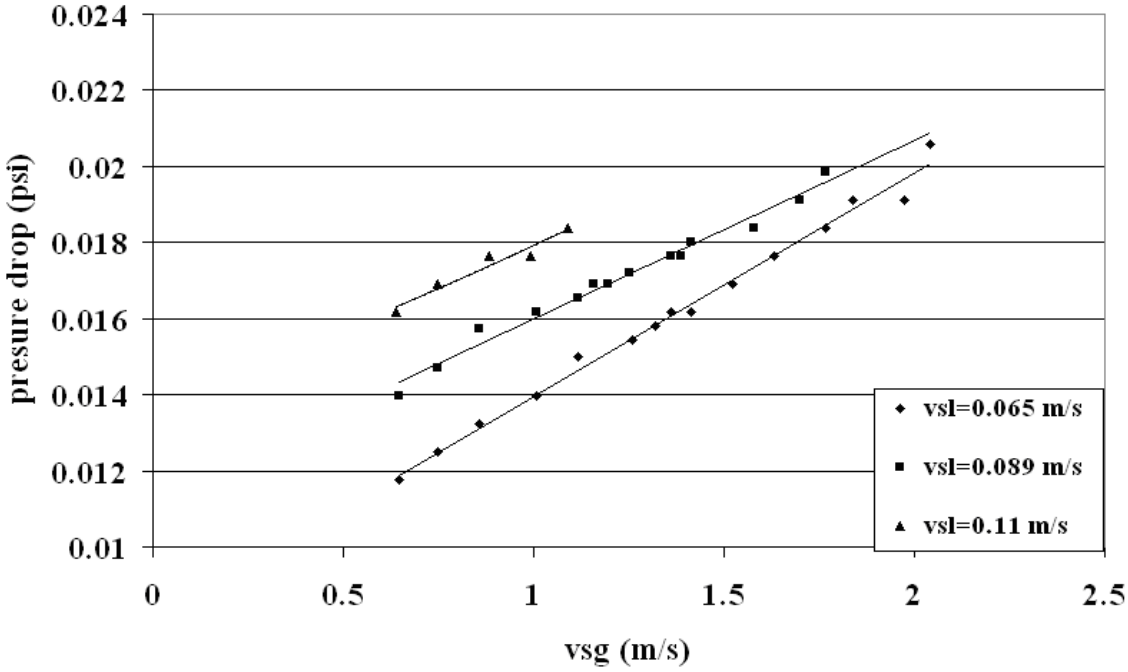

Fig. 8 Relationship between vsg and pressure drop for different vsl {WLR=50%}

Flow Pattern Maps

Fig.9 depict the flow pattern map for the stratified three-phase flow through horizontal pipes

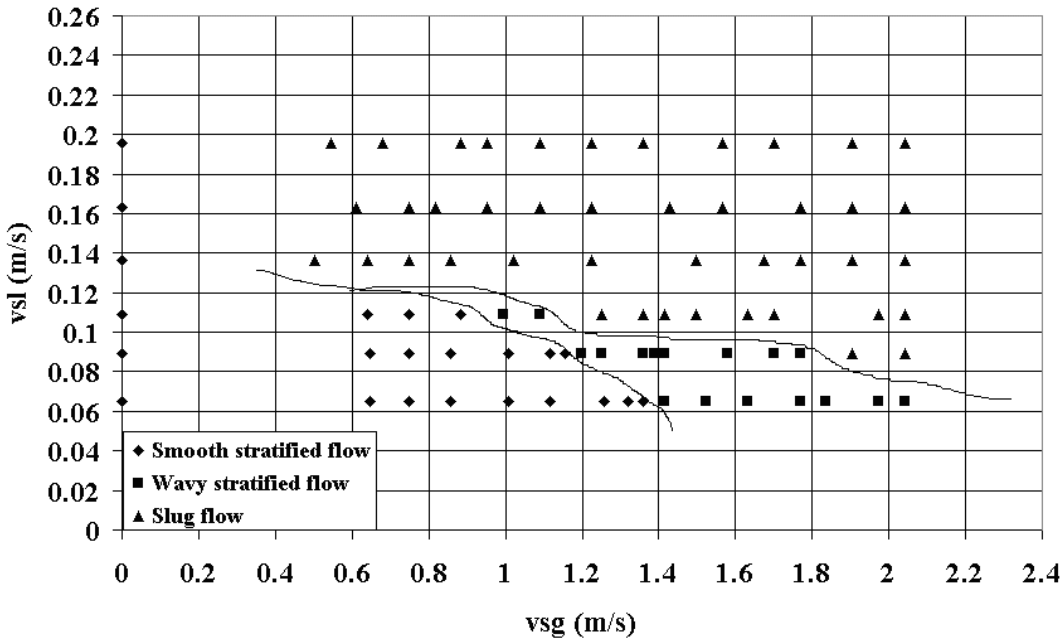

Fig .9 Relationship between vsg and vsl {WLR=50%}

THE FORMELATED EQUATIONS

Three empirical correlations for estimating dimensionless liquid, and water thicknesses and system pressure drop in three-phase stratified flow in horizontal pipe are developed. The diameter of the pipe used is 0.051 m and the length is 4 m. Constant fluid physical properties (table.1) are used in these correlations. As shown below the dimensionless thickness and pressure drop are correlated as a function of liquid flow rate, gas flow rate, and water liquid ratio (WLR):-

The correlated dimensionless liquid film thickness equation is: -

$$\frac{h_L}{D} = a_1 + a_2 * (WLR * Q_L)^{a_3} + a_4 * ((1 - WLR) * Q_L)^{a_5} + a_6 * Q_G^{\ a_7} \quad (1)$$

Where,

$a_1 = -0.116227$ $a_2 = 0.451614$ $a_3 = 0.850409$ $a_4 = 0.48286$

$a_5 = 0.981403$ $a_6 = 0.364976$ $a_7 = -0.193155$

$Q_L \,\&\, Q_G : m^3 / hr.$

$WLR : fraction$

The correlation coefficient for Eq. (5-1) is 0.96

The formulated dimensionless water film thickness equation is shown below: -

$$\frac{h_w}{D} = b_1 + b_2 * (WLR * Q_L)^{b_3} + b_4 * ((1 - WLR) * Q_L)^{b_5} + b_6 * Q_G^{\ b_7} \quad (2)$$

Where,

$b_1 = -0.117454$ $b_2 = 0.620129$ $b_3 = 0.590837$ $b_4 = 0.047055$

$b_5 = 0.805945$ $b_6 = 0.173923$ $b_7 = -0.375791$

Here, the correlation coefficient equal to 0.99

The pressure drop equation is formulated as follows: -

$$\Delta P = c_1 * ((WLR * Q_L + (1 - WLR) * Q_L) * Q_G)^{c_2} \quad (3)$$

Where,

$c_1 = 0.000863$ $c_2 = 0.409815$

The correlation coefficient for the above Eq. is 0.91

Figs.10, 11, and 12 show that there is a good agreement between experimental and predicted data obtained from Eqs.1, 2, and 3 for dimensionless liquid, and water thickness and pressure drop respectively.

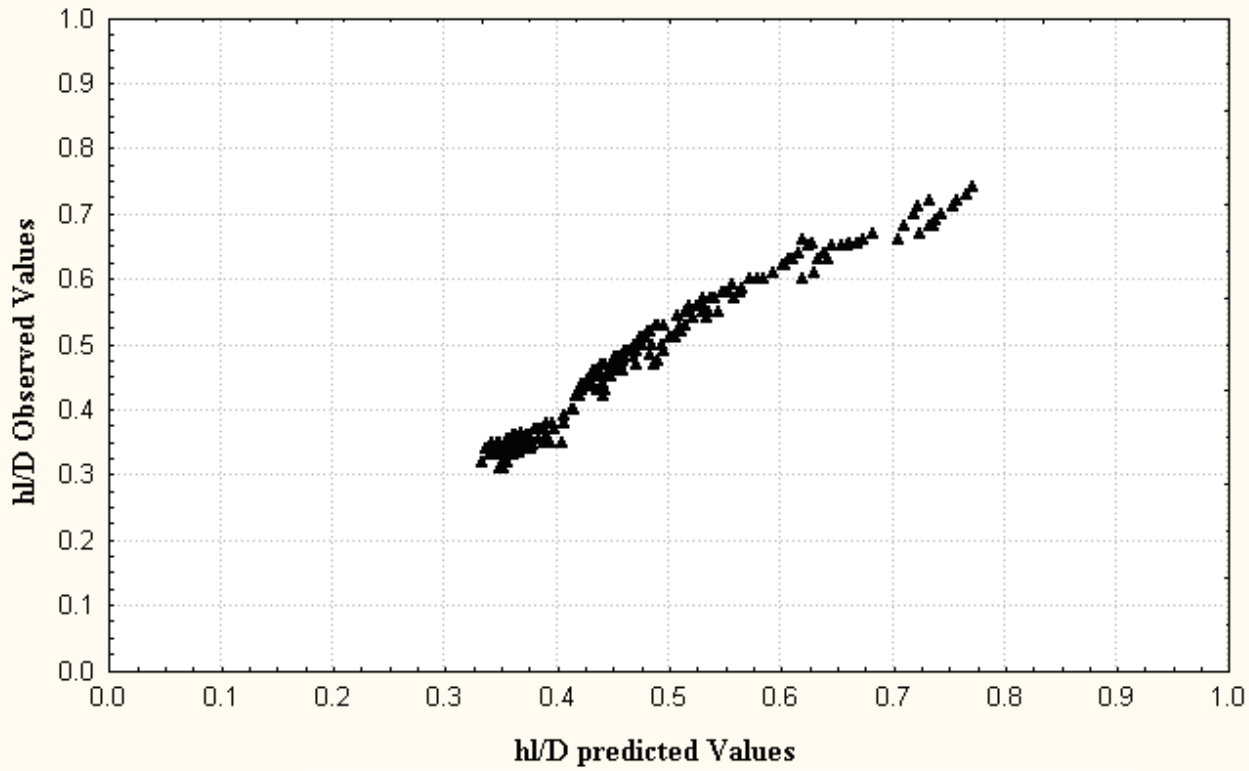

Fiq.10 Relationship between hl/D predicted vs. hl/D observed Values

.

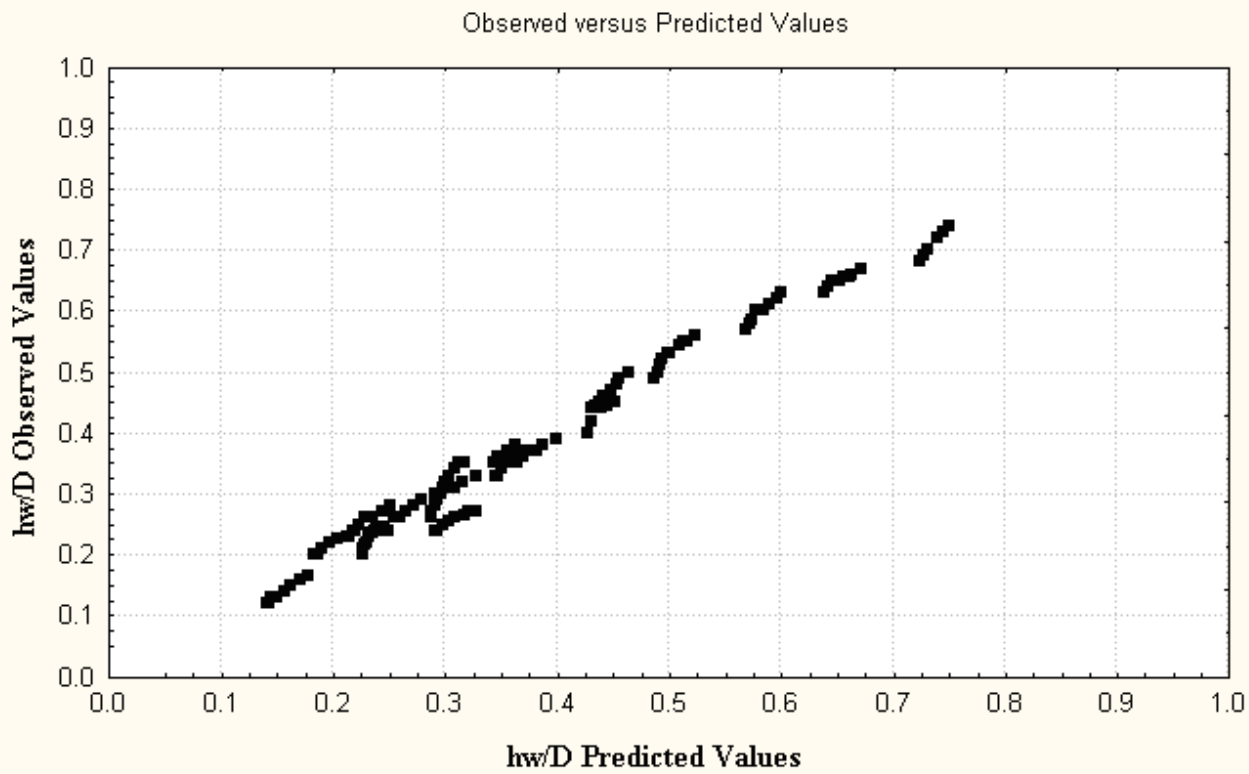

Fiq.11 Relationship between hw/D predicted ve. hw/D observed Values

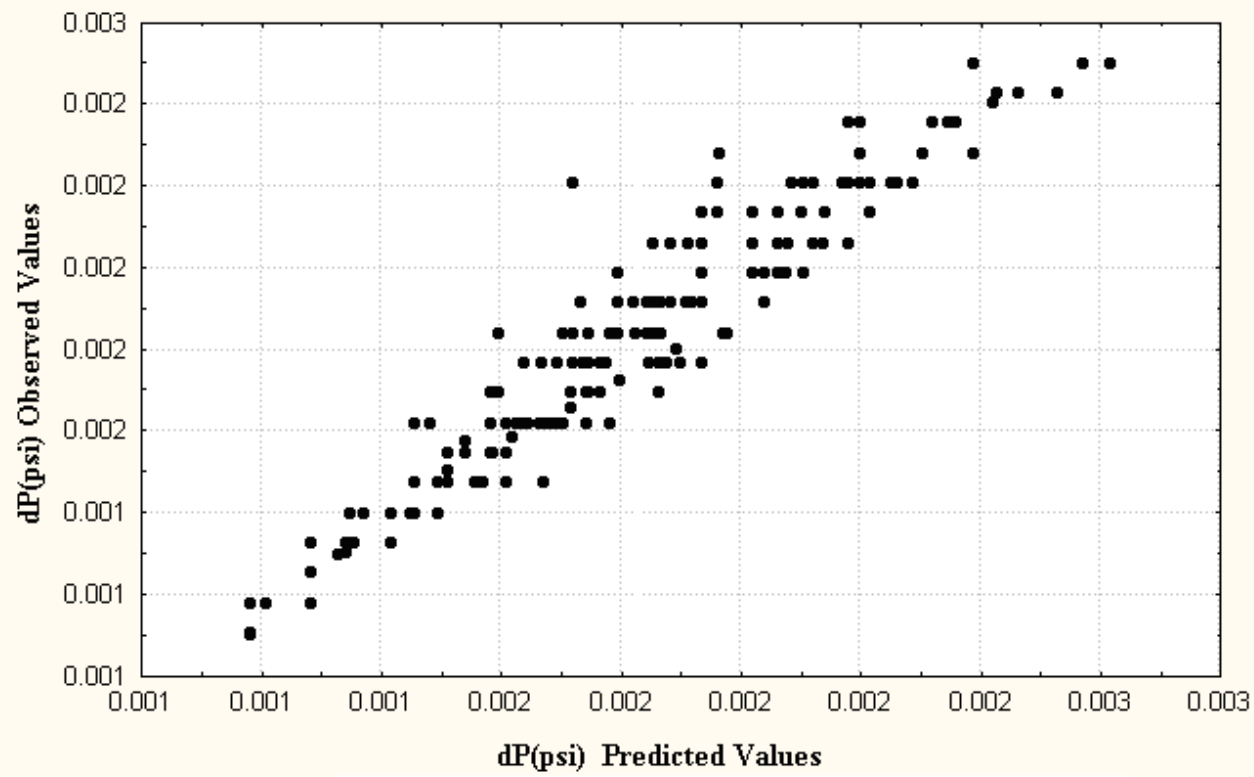

Fig.12 Relationship between dp predicted vs. dp observed values

THREE-PHASE FLOW MECHANISTIC MODEL

Several three-phase flow models were found. All of the models are developed from the three-phase momentum equations with few changes from one to the other.

Taital et al. (1995) developed a three-phase model for horizontal and near-horizontal three-phase flow. The model starts with the momentum balance equatins for each phase.

$$-A_W\left(\frac{dp}{dx}\right)-\tau_W\,S_W+\tau_i\,S_i-\rho_W\,A_W\,g\,\sin\beta=0 \tag{4}$$

$$-A_O\left(\frac{dp}{dx}\right)-\tau_O\,S_O-\tau_i\,S_i+\tau_j\,S_j-\rho_O\,A_O\,g\sin\beta=0 \tag{5}$$

$$-A_G\left(\frac{dp}{dx}\right)-\tau_G\,S_G-\tau_j\,S_j-\rho_G\,A_G\,g\sin\beta=0 \tag{6}$$

Summing Eqs.4 and 5 yields:

$$-\left(\frac{dp}{dx}\right)-\frac{\tau_L\,S_L}{A_L}+\frac{\tau_i\,S_i}{A_L}-\rho_L\,g\sin\beta=0 \tag{7}$$

Where;

$$\tau_L S_L = \tau_W S_W + \tau_O S_O \tag{8}$$

$$\rho_L = \frac{\rho_W A_W + \rho_O A_O}{A_L} \tag{9}$$

And;

$$A_L = A_W + A_O \tag{10}$$

Note that Eq.7 is the combined momentum equation for the liquid phase, which composed, of water and oil layers. Therefore, Eqs.8 and 9, have the same form as two-layer momentum equations for liquid and gas as derived by classical Taital and Dukler model (1976).

The pressure drop can be eliminated by adding Eqs.6 to 7 to yield:

$$-\frac{\tau_L S_L}{A_L} + \frac{\tau_G S_G}{A_G} + \tau_j S_j \left(\frac{1}{A_L} + \frac{1}{A_G} \right) - (\rho_O - \rho_G) g \sin\beta = 0 \tag{11}$$

In the same way the pressure drop is eliminated from Eqs.4 and 5 to yield:

$$-\frac{\tau_W S_W}{A_W} + \frac{\tau_O S_O}{A_O} - \frac{\tau_j S_j}{A_O} + \tau_i S_i \left(\frac{1}{A_W} + \frac{1}{A_O} \right) - (\rho_W - \rho_O) g \sin\beta = 0 \tag{12}$$

Eqs.11and 12 must be solved simultaneously to yield the liquid level (h_L), and the water level, (h_W).

In this study, Taitel et al (1995) model is used for comparison with the experimental data of this study.

Comparison with Mechanistic Model

The results of the Three-phase mechanistic model of Taital et al. (1995) are plotted against the experimental data ($\frac{h_L}{D}, \frac{h_W}{D}, \frac{h_O}{D}, \& \Delta P$) as shown in Fiqs.13 through 16.

It is clear that the good agreement is obtained between the experimental results of the presented study and that of Taital et al. (1995) model.

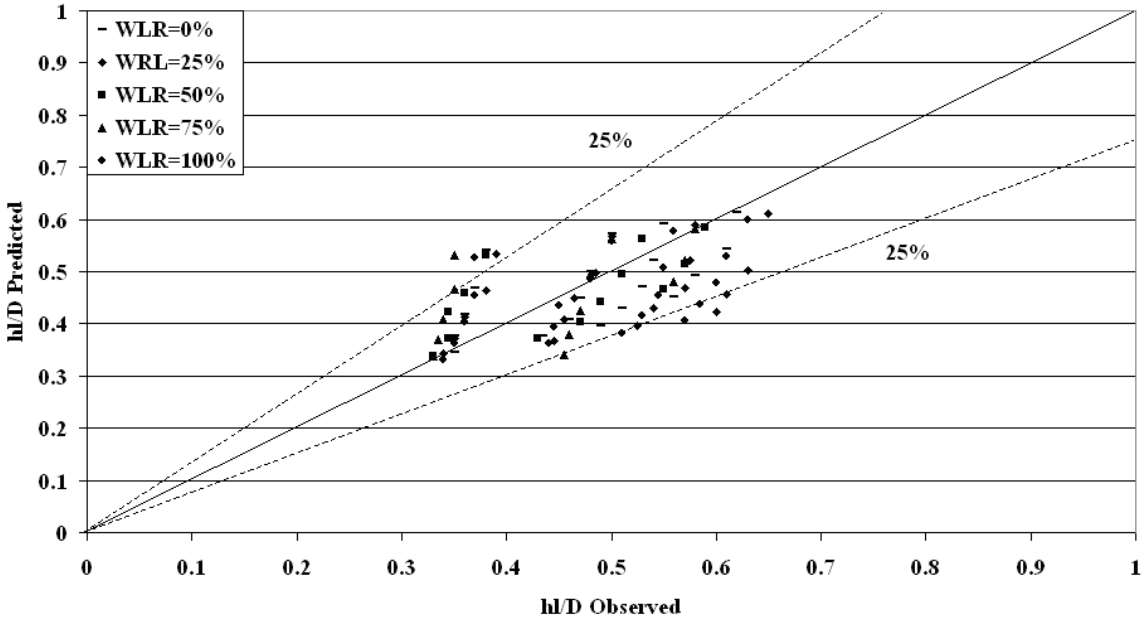

Fiq. 13 Relationship between hl/D Observed vs. hl/D Predicted {by Taital et al. model (1995)}

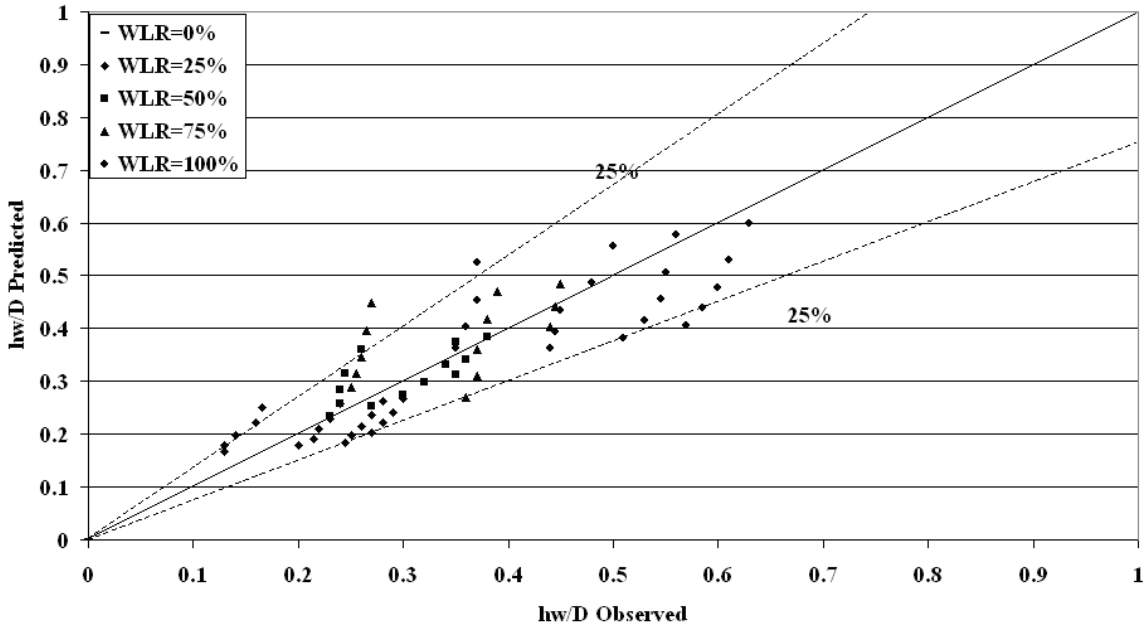

Fiq.14 Relationship between hw/D Observed vs. hw/D Predicted {by Taital et al. model (1995)}

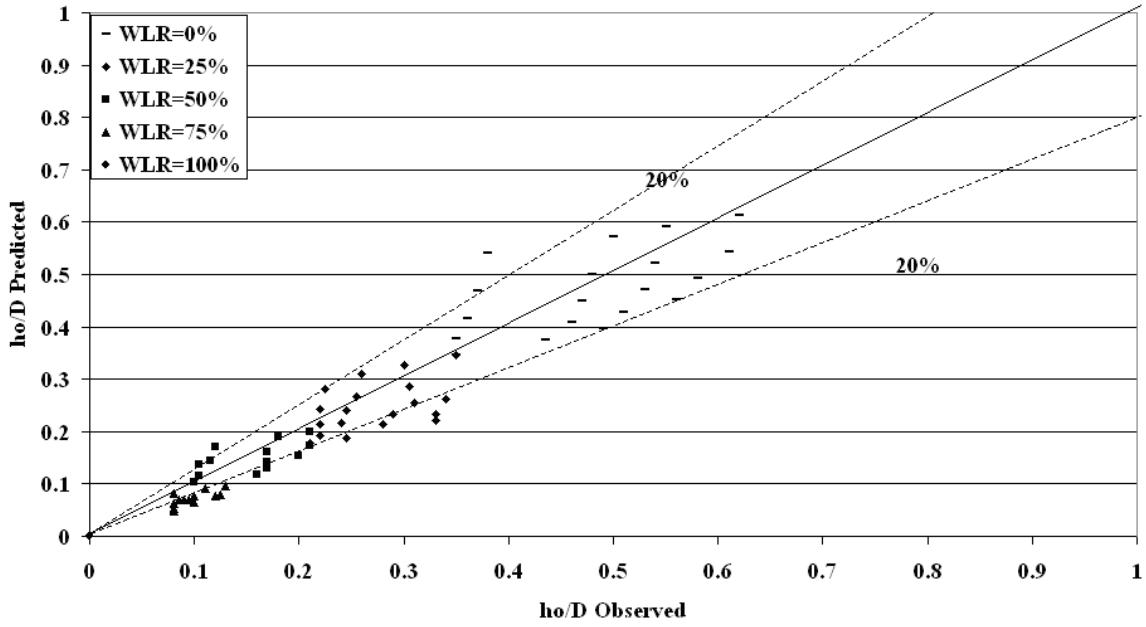

Fiq.15 Relationship between ho/D Observed vs. ho/D Predicted {by Taital et al. model (1995) }

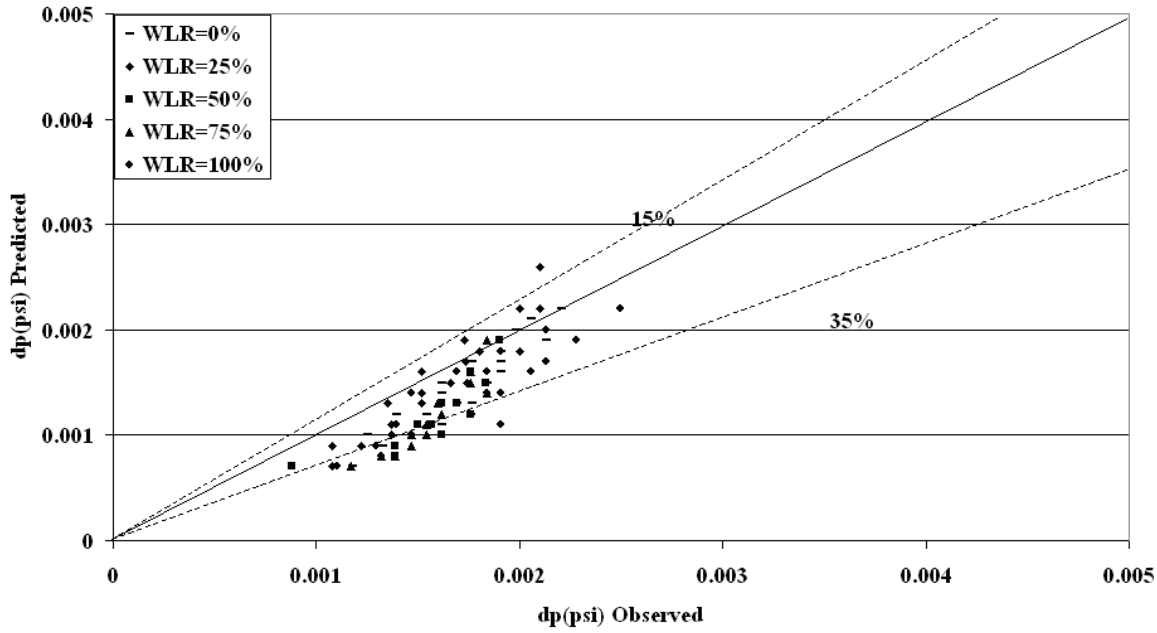

Fiq.16 Relationship between dP Observed vs. dP Predicted {by Taital et al. model (1995) }

Conclusions

1. Three equations have been developed by correlating the experimental data. These equations can be used to predict liquid, and water thicknesses and system pressure drop for the conditions specified in the present work.
2. Three-phase flow model Taital et al. (1995) gave good prediction for liquid, water thicknesses, and pressure drop.
3. In three-phase flow (water, oil, and gas) the water level is usually quit high and the liquid consists mostly of water for equal rate of water and oil (WLR=50%).

SYMMOLS AND ABBREVIATIONS

Symbol	Definition	Unit
A	Pipe area	m^2
h	Film thickness	m
P	Pressure	Pa
Q	Flow rate	m^3/s
S	Perimeter	m
V_S	Superficial velocity	m/s
β	Inclination of pipe	deg.
ρ	Density	kg/m^3
τ	Shear stress	Pa

Subscript	Definition
W	Water
O	Oil
G	Gas
L	Liquid
i	interface between oil and water
j	interface between gas and oil
K	Water, Oil, or Gas

Abbreviation	Definition
WLR	water liquid ratio
Exp.	Experimental
Pre.	Predicted
SS	smooth stratified flow
SW	wavy stratified flow

References

1. Taitel, Y. and Dukler, A. E.: "A Model for Predicting Flow Transition in Horizontal and Near Horizontal Gas-Liquid Flow," AIChE Journal, 22, (1976) p47.
2. Taital, Y., Barnea, D., and Brill, J. P.: "Stratified Three Phase Flow in Pipes," Int. J. Multiphase Flow Vol. 21. No. 1. pp. 53-60. (1995).
3. Faaiz H. R. Alzubaidi.: "Experimental Study of Stratified Three-Phase Flow Through Horizontal Pipes" MS thesis, Baghdad University (2005).

OPTIMUM SATELLITE LAUNCHER TRAJECTORY GUIDED WITH PROPORTIONAL NAVIGATION PLUS GRAVITY COMPENSATION GUIDANCE

Asst. Lecturer Waleed Kh. Al-Ashtari
Mech.Eng.Dept.
College of Engineering
University of Baghdad
Baghdad-Iraq

ABSTRACT

The optimum trajectory of a single or multi-stage satellite launcher guided with proportional navigation guidance (PNG) is addressed. The PNG is extended to compensate for the gravity effect. For the trajectory optimization problem, the launcher is modeled as a mass point flying around the center of the Earth. To provide a completely valid analysis, all known influences on the launcher trajectory have been considered; Empirical equations have been used in order to model the Earth standard atmosphere in SI units. A computer program had been constructed in order to simulate the trajectory of such launcher from the available initial conditions. Pegasus launcher is used as a hypothetical example. The simulator results show that the proportional navigation plus gravity compensation guidance gives fairly accurate results.

الخلاصة

في هذا البحث, تمت دراسة المسار الأمثل لناقل أقمار صناعية (مرحلة واحدة أو متعدد المراحل) موجه بطريقة الملاحة التناسبية وتم تطوير قانون الملاحة التناسبية للتعويض عن تأثير الجاذبية الأرضية على مسار الناقل. لغرض ايجاد المسار الامثل, تم فرض الناقل كجزيئة تطير حول مركز الكرة الارضية. ولغرض توفير تحليل رصين, تم اعتبار كل العوامل المؤثرة على مسار الناقل بما فيها تأثير دوران الكرة الأرضية ، وكذلك تم وضع معادلات تجريبية عالية الدقة لوصف تغير خصائص الغلاف الجوي للأرض مع ارتفاع الناقل بالوحدات العالمية الموحدة. لقد تم أعداد برنامج لمحاكاة مسار هكذا ناقل من خلال توفير المعلومات الأوليةلاطلاق الناقل ، وقد تم استخدام بيغاسوس كمثال لتطبيق موضوع البحث. وقد اضهرت النتائج آن استخدام طريقة الملاحة التناسبية مع التعويض عن الجاذبية الأرضية يعطي نتائج مقبولة الدقة.

KEYWORDS

Modeling of Flight System, Proportional Navigation Guidance Law, Gravity Compensation, Linearization, and Optimization.

INTRODUCTION

New concept for space transportation are proposed and investigated in various countries as a means for improving the space transportation capability and for reducing costs. The main task of guidance process is to determine the vehicle position and velocity, computation of control actions necessary to properly adjust position and velocity, and delivery of a suitable adjustments command to the vehicle control system to achieve the correct trajectory. **(Zarchan, 1990 and Bong Wie 1998).**

PNG is accepted as a celebrated guidance law for many guided missile applications like the surface-to-air, air-to-air, air-to-surface missile encounters, standoff weapon delivery, and space

rendezvous. The guided point (launcher) is assumed to move towards a target point in a plane containing the velocity vectors of the two points. The PNG technique is defined such that the

velocity vector (heading) of the launcher is turned at a rate proportional to the rotation rate of the line joining the launcher and the target, which is the line of sight (LOS). The PNG principle helps to estimate the magnitude of the lateral acceleration that is perpendicular to LOS as a function of LOS turn rate **(Zarchan, 1990 and Asher & Yaesh 1998).**

The trajectories of rocket vehicle have three successive phases. In the first phase, which is called the boost phase (initial phase), the rocket engine (or engines if the rocket is multi-stage) provide the precise amount of propulsion required to place the rocket on a specific trajectory. Then the engine quits, and the final stage of the rocket (payload) coasts in the second phase that is called midcourse phase, and finally the terminal phase (or gravity turn trajectory)

Guidance operations may occur in the initial, midcourse, or terminal phase of flight. Ballistic missiles are commonly guided only during the initial flight phase, while the rocket engines are burning. A cruise type of missile, such as the Shark or Matador, uses midcourse guidance, operating continuously during cruising flight. Air-to-air missile such as Sidewinder employ terminal guidance systems that lead the missile directly to the target on the basis of measurements on the target itself.

Errors in accuracy for rocket vehicles trajectories are generally expressed as launch point errors, guidance en-route errors or aim point error. Both launch and aim-point errors can be corrected by surveying the launch and the target areas more accurately. Aim errors on the other hand, must improve the rocket's design particularly its guidance systems. A missile's circular error probability (CEP) and bias usually measure aim errors. CEP uses the mean point of impact of missile test firings, usually taken at maximum range, to calculate the radius of a circle that would take in 50 percent of the impact points. Bias measures the deviation of the mean impact point from the actual aim point. An accurate missile has both a low CEP and low bias **(Encyclopedia Britannica, 2002).**

There are no single set of initial conditions required to arrive at a specified target, but rather there are an infinite number of possible free flight paths originating at points in space in the vicinity of some nominal starting point which terminate at the desired destination. For each such point there is a corresponding proper velocity. It is the task of the guidance system to cause the rocket to take up any one of these free flight paths.

LAUNCHER DYNAMIC MODEL

For the trajectory optimization problem the usual mass point modeling is applied for describing the flight system dynamics. With reference to the rotating spherical Earth, the equations of motion can be expressed as **Fig.(1) (Mayrhofer & Sachs 1997)**

$$\dot{V} = \left(\frac{T\cos(\alpha+\delta)-D}{m}\right) - g\sin\gamma + \omega_E^2(R_E+h)\cos\Phi(\sin\gamma\cos\Phi - \cos\gamma\sin\Phi\cos\psi) \tag{1}$$

$$\dot{\gamma} = \left(\frac{T\sin(\alpha+\delta)+L}{mV}\right)\cos\varphi + \left(\frac{V}{R_E+h} - \frac{g}{V}\right)\cos\gamma + 2\omega_E\cos\Phi\sin\psi + \frac{\omega_E^2(R_E+h)}{V}\cos\Phi \left(\cos\gamma\cos\Phi + \sin\gamma\sin\Phi\cos\psi\right) \tag{2}$$

$$\ddot{\psi} = \left(\frac{T\sin(\alpha+\delta)+L}{mV\cos\gamma}\right)\sin\varphi + \left(\frac{V}{R_E+h}\right)\cos\gamma\sin\psi\tan\Phi - 2\omega_E(\tan\gamma\cos\Phi\cos\psi - \sin\gamma) + \left(\frac{\omega_E^2(R_E+h)}{V\cos\gamma}\right)\sin\Phi\cos\Phi\sin\psi \tag{3}$$

$$\dot{\Phi} = \frac{V\cos\gamma\cos\psi}{(R_E + h)} \tag{4}$$

$$\dot{\Lambda} = \frac{V\cos\gamma\sin\psi}{(R_E + h)\cos\Phi} \tag{5}$$

$$\dot{h} = V\sin\gamma \tag{6}$$

The aerodynamic model can be described as:

$$L = C_L qS \tag{7}$$

$$D = C_D qS \tag{8}$$

Where C_L and C_D are function of α and M

The model of the main rocket propulsion is described as

$$T = \dot{m} g_0 I_{SP} \tag{9}$$

PROPORTIONAL NAVIGATION GUIDANCE LAW

This guidance method is based on the requirement **(Zarchan, 1990)**

$$\frac{d\gamma}{dt} = N'\frac{d\lambda}{dt} \tag{10}$$

And the command acceleration will be

$$a_c = V_c\dot{\gamma} = V_c N'\dot{\lambda} \tag{11}$$

Guidance Equations

According to (**Asher & Yaesh 1998).**

$$\dot{r}_{TM} = V_c = V_T\cos\varepsilon_T - V\cos\varepsilon \tag{12}$$

$$\dot{\lambda} = \frac{1}{r_{TM}}(V_T\sin\varepsilon_T - V\sin\varepsilon) \tag{13}$$

$$\dot{\gamma} = N'\dot{\lambda} \tag{14}$$

But for satellite launcher, the target is a fixed point in the space, so $(V_T = 0)$. Therefore, command acceleration expressed as

$$a_c = \frac{N'V^2}{2r_{TM}}\sin 2\varepsilon = \frac{N'V^2}{2r_{TM}}\sin 2(\lambda - \gamma) \tag{15}$$

The target can be defined as a fixed point in the missile local plane (ρ, z) as shown in **Fig.(2)** measured from the launcher , then the calculations of related quantities gives

$$\rho_M = \int_{t_0}^{t_f} V\cos\gamma dt \tag{16}$$

$$z_M = \int_{t_0}^{t_f} V\sin\gamma dt \tag{17}$$

$$\rho_{TM} = \rho_T - \rho_M \tag{18}$$

$$z_{TM} = z_T - z_M \tag{19}$$

$$r_{TM} = \sqrt{\rho_{TM}^2 + z_{TM}^2} \tag{20}$$

$$\lambda = \tan^{-1}\left(\frac{z_{TM}}{\rho_{TM}}\right) \tag{21}$$

LINEARIZATION

In order to allow better ways of analyses and optimization of the guidance command acceleration it is important to leave the non-linear missile target simulation and find a simpler model, as it is usual in engineering practice. We are going to linearize the acceleration command equations allowing the application of powerful analytical techniques **(Zarchan, 1990).**

As defined previously z_{TM} is the relative separation between the rocket and the target in local vertical plane, then the relative acceleration can be expressed as

$$\ddot{z}_{TM} = -a_c \cos\lambda \tag{22}$$

And the expression for the LOS angle will be

$$\sin\lambda = \frac{z_{TM}}{r_{TM}} \tag{23}$$

If we assume that the LOS angle is small, then **eq.(22)** and **eq.(23)**

$$\ddot{z}_{TM} - a_c \tag{24}$$

$$\lambda = \frac{z_{TM}}{r_{TM}} \tag{25}$$

In linearized analyses we treat the closing velocity as a positive constant and equal to the missile velocity. Since closing velocity has also been previously defined as the negative derivative of the range from the missile to target, and since the missile-target separation distance must go to zero at the flight, we can also linearized the range equation with the time varying relationship **(Zarchan, 1990 and Asher & Yaesh 1998).**

$$r_{TM} = V_c\left(t_f - t\right) \tag{26}$$

Since the missile-target separation distance goes to zero at the end of flight by definition, the linearized miss distance is taken to be the relative separation between missile and target z_{TM}, at the end of flight:

$$Miss = z_{TM}\left(t_f\right) \tag{27}$$

This linearized model will give very high accuracy, where its results are the same as those obtained from the non-linear model for fixed or non-maneuvering targets (the case of our search), and for heading error case, and will give overestimations from the non-linear model in the case of maneuvering targets **(Zarchan, 1990).**

Linearization of PNG Law

Substituting **eq.(26)**, into **eq.(24)** we get

$$\lambda = \frac{z_{TM}}{V_c\left(t_f - t\right)} \tag{28}$$

The derivative of **eq.(28)** will give the LOS rate by

$$\dot{\lambda} = \frac{z_{TM} + \dot{z}_{TM}\left(t_f - t\right)}{V_c\left(t_f - t\right)^2} = \frac{z_{TM} + \dot{z}_{TM} t_{go}}{V_c t_{go}^2} \tag{29}$$

Thus we can express the PNG law as

$$a_c = N' V_c \dot{\lambda} = \frac{N'\left(z_{TM} + \dot{z}_{TM} t_{go}\right)}{t_{go}^2} \tag{30}$$

The expression in the parentheses of **eq.(30)** represents the future separation between missile and target. More simply, the expression in parentheses is the miss distance that would result if the missile made no further corrective acceleration and the target did not maneuver. This expression is referred to as the zero effort miss (ZEM). Therefore, we can also think of PN as a

guidance law in which commands acceleration are issued inversely proportional to the square of time to go and directly proportional to the ZEM **(Zarchan, 1990 and Asher & Yaesh 1998).**

OTMIZATION OF PNG LAW

We seek to find a guidance law that is a function of the system states. There are an infinite number of possible guidance laws; thus, it is necessary to state in mathematical terms what the guidance law should do. Certainly we would like to hit the target; therefore, one feature of the guidance law should be a zero miss distance requirement. In addition, we would like to hit the target in an efficient manner. In other words, we desire to use minimal total acceleration. A poplar and mathematically convenient way of stating the guidance problem to be solved is that we desire to achieve zero miss distance and to minimize the integral of the square of the command acceleration **(Zarchan, 1990 and Asher & Yaesh 1998)** i.e.

$$z_{TM}(t_f) = 0 \tag{31}$$

Subject to minimizing

$$\int_0^{t_f} a_c^2(t)dt \tag{32}$$

Unfortunately, if we minimize a more meaningful performance index such as the integral of the absolute value of a_c, the solution would be mathematically intractable. Typically this type of problem with a quadratic performance index is solved using techniques from optimal control theory. However, this class of problems can be solved more easily using Schwartz inequality **(Zarchan, 1990).**

Now, we will construct from the previous equations the satellite launcher flight in state space form as

$$\begin{bmatrix} \dot{\mathbf{z}}_{\mathbf{TM}} \\ \ddot{\mathbf{z}}_{\mathbf{TM}} \end{bmatrix} = \begin{bmatrix} \mathbf{0} & \mathbf{1} \\ \mathbf{0} & \mathbf{0} \end{bmatrix} \begin{Bmatrix} \mathbf{z}_{\mathbf{TM}} \\ \dot{\mathbf{z}}_{\mathbf{TM}} \end{Bmatrix} + \begin{bmatrix} \mathbf{0} \\ -\mathbf{1} \end{bmatrix} \mathbf{a_c} \tag{33}$$

Before going in any further analyses, we must first check the controllability of the state space that we had performed. The general state space form

$$\dot{\mathbf{x}} = \mathbf{Ax} + \mathbf{Bu} \tag{34}$$

by comparing **eq.(33)** and **eq.(34)** we find that

$$\mathbf{A} = \begin{bmatrix} \mathbf{0} & \mathbf{1} \\ \mathbf{0} & \mathbf{0} \end{bmatrix}$$

$$\mathbf{B} = \begin{bmatrix} \mathbf{0} \\ -\mathbf{1} \end{bmatrix}$$

We must find the matrix $[\mathbf{B} \vdots \mathbf{AB}]$

$$[\mathbf{B} \vdots \mathbf{AB}] = \begin{bmatrix} 0 & -1 \\ -1 & 0 \end{bmatrix} = \text{nonsigular}$$

The system is therefore completely state variable **(Ogata, 2002).**

The solution of the state space vector deferential equation is given at the final time t_f by the vector relationship **(Zarchan, 1990).**

$$\mathbf{x}(\mathbf{t}) = \mathbf{\Phi}(\mathbf{t_f} - \mathbf{t})\mathbf{x}(\mathbf{t}) + \int \mathbf{\Phi}(\mathbf{t_f} - \boldsymbol{\tau})\mathbf{Bu}(\boldsymbol{\tau})\mathbf{d}\boldsymbol{\tau} \tag{35}$$

Where $\mathbf{\Phi}(\mathbf{t}) = \begin{bmatrix} \mathbf{1} & \mathbf{t} \\ \mathbf{0} & \mathbf{1} \end{bmatrix}$

Using the above fundamental matrix in the solution for the state space vector deferential equation and only looking at the first state, we get

$$z_{TM}(t_f) = z_{TM}(t) + \dot{z}_{TM}(t)(t_f - t) - \int_t^{t_f} (t_f - \tau) a_c(\tau) d\tau \tag{36}$$

For convenience, let us define the terms

$$f_1(t_f - t) = z_{TM}(t) + \dot{z}_{TM}(t)(t_f - t) \tag{37}$$

$$h_1(t_f - \tau) = t_f - \tau \tag{38}$$

Then we can say that

$$z_{TM}(t_f) = f_1(t_f t) - \int_t^{t_f} h_1(t_f - \tau) a_c(\tau) d\tau \tag{39}$$

For the conditions in which we have zero miss distance $z_{TM}(t_f) = 0$, we can rewrite **eq.(39)**

$$f_1(t_f - t) = \int_t^{t_f} h_1(t_f - \tau) a_c(\tau) d\tau \tag{40}$$

If we apply the Schwartz inequality to **eq.(40)** we get the relationship **(Zarchan, 1990).**

$$f_1^2(t_f - t) \le \int_t^{t_f} h_1^2(t_f - \tau) d\tau \int_t^{t_f} a_c^2(\tau) d\tau \tag{41}$$

Then $$\int_t^{t_f} a_c^2(\tau) d\tau \ge \frac{f_1^2(t_f - t)}{\int_t^{t_f} h_1^2(t_f - \tau) d\tau} \tag{41}$$

The integral of the square of the command acceleration will be minimized when the equality sign holds in the preceding inequality. According to the Schwartz inequality, the equality sign holds when

$$a_c(\tau) = k h_1(t_f - \tau) \tag{42}$$

This means that the integral of the squared acceleration is minimized when

$$k = \frac{f_1(t_f - t)}{\int_t^{t_f} h_1^2(t_f - \tau) d\tau} \tag{43}$$

Therefore, the command acceleration is given by

$$a_c = \left[\frac{f_1(t_f - t)}{\int_t^{t_f} h_1^2(t_f - \tau) d\tau} \right] h_1(t_f - t) \tag{44}$$

Substituting yields to the feedback control guidance law

$$a_c = \frac{3(z_{TM} + \dot{z}_{TM} t_{go})}{t_{go}^2} \tag{45}$$

By comparing **eq.(30)** with **eq.(45)** we find that the optimum value of effective navigation ratio for the satellite launcher is $N' = 3$.

PNG LAW WITH GRAVITY COMPENSATION

One of the major effects that prevent to obtain a straight-line missile's trajectory is the gravity effect. Changes in the missile velocity due to gravity caused the LOS to rotate. The PNG law responds to the apparent LOS rate with command acceleration. If we have knowledge of

gravitational acceleration, it seems reasonable that it might be possible to compensate for unnecessary acceleration via the guidance law. **(Zarchan, 1990).**
Fortunately in our particular case the target did not have gravitational acceleration. The launcher gravitational acceleration can be expressed as **(Meriam, & Kraige, 1998).**

$$g = \frac{Gm_o}{r^2} \tag{46}$$

The component of the gravity acceleration perpendicular to the LOS for the launcher is

$$g_{M_{PLOS}} = g\cos\lambda \tag{47}$$

And the component of the gravity acceleration perpendicular to the LOS for the target is zero.

The gravitational acceleration difference between the target and the missile can be treated as an additional terms in the ZEM. Therefore, we can modify the PNG law to account for gravity. The resultant law is **(Zarchan, 1990 and Asher & Yaesh 1998).**

$$a_c = N'V_c\dot{\lambda} + \frac{N'}{2}\left(g_{T_{PLOS}} - g_{M_{PLOS}}\right) \tag{48}$$

For the case of the satellite launcher, **eq.(48)** can be reduced to

$$a_c = N'V_c\dot{\lambda} - \frac{N'g\cos\lambda}{2} \tag{49}$$

HYPOTETICAL EXAMPLE

Pegasus is used for showing PNG and PN plus gravity compensation guidance. Pegasus is a small commercial launch vehicle developed by orbital science. It is provided with solid propellant booster and wings, and is lunched from an aircraft. Pegasus mission is to inject the satellite at altitude of (123 km), with velocity of (7790 m/sec), and zero flight path angle (FPA). Pegasus is released from its carrier with an initial velocity of about (0.8 Mach) and zero initial FPA with free flight duration of (5 sec). At the free flight, delta wing of the Pegasus is capable of achieving a zero FPA at the start of the first stage burning. **(Isakowitz, & Hopkins Jr, & Hopkins, 1999).**

RESULTS AND DISCUSSION

Three cases are simulated. The first case when Pegasus launched without guidance, the second when Pegasus guided with optimum PNG, and the third Pegasus guided with PN plus gravity compensation guidance. The altitude, velocity, and FPA are shown in **Figs.(3), Figs.(4),** and **Figs.(5)** respectively.

Pegasus without guidance is rapidly falling due to negative values of the FPA, which cause the thrust force to push down. This means that Pegasus cannot fly without guidance.
For the second case the large drop in altitude, and FPA during the second stage flight lead the rocket be unable to reach its target which is very far from the rocket, although the altitude and FPA increase, the velocity continue to decrease then starts to increase before the end of flight.
For the third case, the altitude of this case is highly accurate, and we can see from **Figs.(5)** that launcher is exceed the target and return to it because of the guidance, i.e. the launcher is reach to altitude of (136 km) at (267 sec) then return to attitude of (132 km) at the end of flight. At the end of flight for this case the launcher velocity about (5.62 %) less than the required velocity and the FPA is about (-3.9°).

From comparing the Pegasus trajectory and the final mission requirements as given in **(Isakowitz, & Hopkins Jr, & Hopkins, 1999),** and that obtained from the PN plus gravity compensation guidance, we can say that the PN plus gravity compensation guidance is fairly applicable for satellite launcher case.

CONCLUSION

The following concluding remarks are drawn from the present work:

1. The optimum value of the effective navigation ratio of the proportional navigation guidance for a satellite launcher application is $N' = 3$.
2. The proportional navigation plus gravity compensation guidance advised to use for the satellite launcher application.

REFERENCES

Bong Wie "Space Vehicle Dynamics and Control", AIAA, Inc., 1998.

Encyclopedia Britannica, 2002.

Joseph Asher, and Isaac Yaesh, "Advance in Missile Guidance Theory", Vol.180; 1998.

Katsuhiko Ogata, "Modern Control Engineering", 4th Edition, 2002.

Mayrhofer M, and. Sachs G, "Orbital Stage Abort Trajectories after Separation from Carrier", Proc-12th, International Symposium on Space Flight Dynamics, ESOC, Darmstadt, Germany, pp. 463-469, June 1997.

Meriam J.L., and Kraige L.G., "Dynamics"; Vol.2, 4th Edition, 1998.

Paul Zarchan ,"Tactical and Strategic Missile Guidance", Vol.124; 1990.

Steven J. Isakowitz, Joseph P. Hopkins Jr., and Joshua B. Hopkins: "Pegasus"; Space Launch System, International Reference Guide to Space Launch, AIAA, pp. 267-279; 1999.

NOMENCLATURE

(SI units are used, unless otherwise stated)

a_c	Command acceleration
C_D	Drag coefficient
C_L	Lift coefficient
D	Drag force
G	Universal constant
g	Local Earth gravitational acceleration
g_o	Earth gravitational acceleration at sea level
g_{PLOS}	Gravitational acceleration component perpendicular to LOS
h	Altitude of the launcher vehicle
I_{SP}	Specific impulse
L	Lift force
M	Mach number
m	Total launcher vehicle mass
$\dot{m}$	Fuel mass flow rate
m_o	Mass of the Earth
N'	Proportional navigation constant
q	Dynamic pressure
r	Radial distance between the center of the Earth and the launcher center
R_E	Mean radius of the Earth

r_{TM}	Target-Missile separation distance
S	Launcher reference area
T	Total thrust of the launcher
t_f	Final flight time
t_{go}	Time to go
t_0	Initial flight time
V	Launcher vehicle velocity
V_c	Closing velocity between the missile and the target
z_{TM}	Target-Missile separation distance in local z direction
α	Attack angle
ψ	Azimuth angle
ε	Launcher lead angle
Φ	Geocentric latitude angle
φ	Roll (Bank) angle
ϕ	Sight angle
γ	Flight path angle
Λ	Geographic longitude
λ	Local line of sight angle
ω_E	Angular velocity of the Earth rotation
(ρ, z)	Local coordinates of launcher vehicle
θ	Pitch or (Elevation) angle

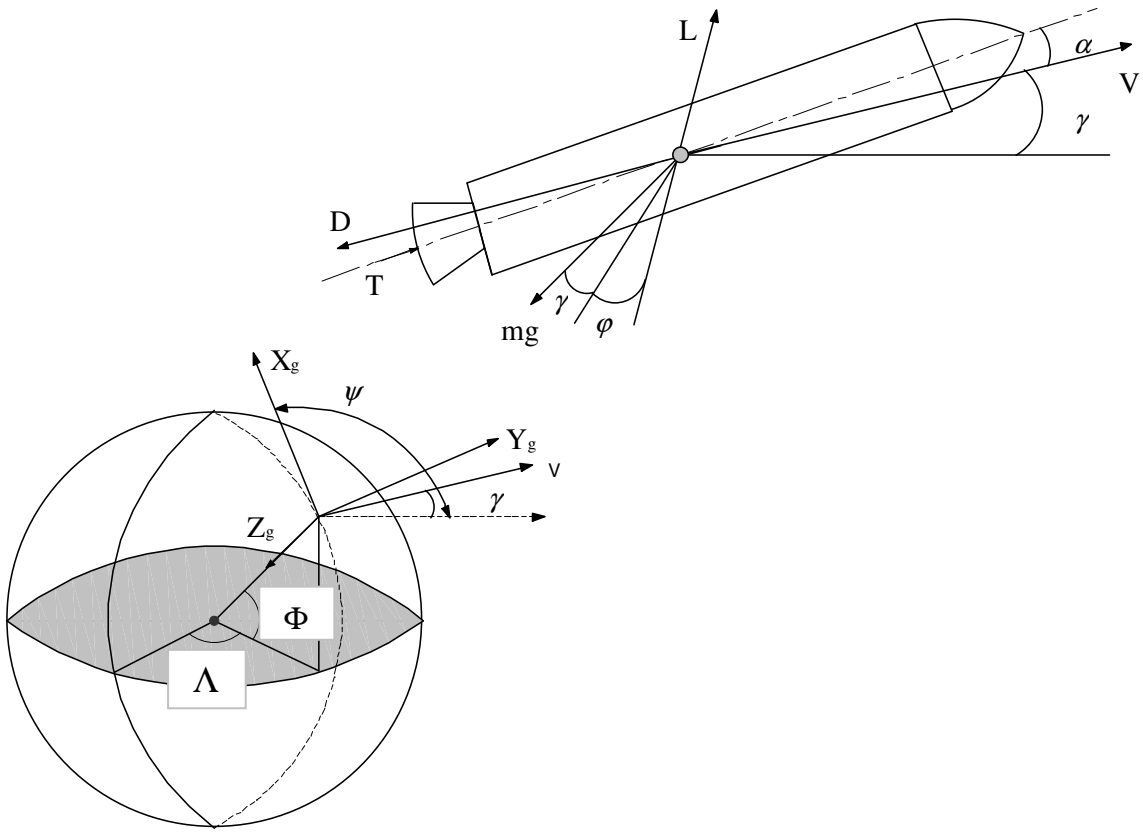

Fig.(1)

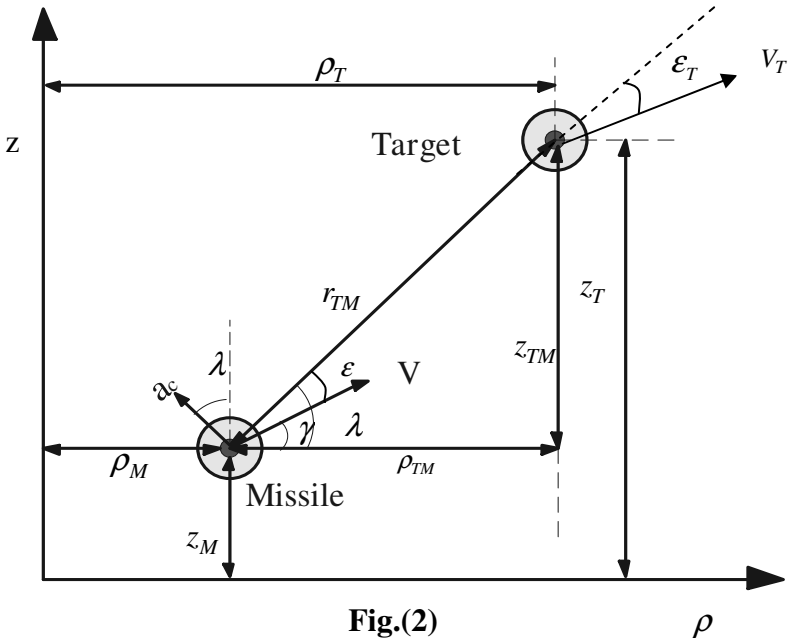
ρ_T
ε_T
V_T
z
Target
r_{TM}
z_T
z_{TM}
λ
ε
V
γ
λ
ρ_M
ρ_{TM}
Missile
z_M
ρ

Fig.(2)

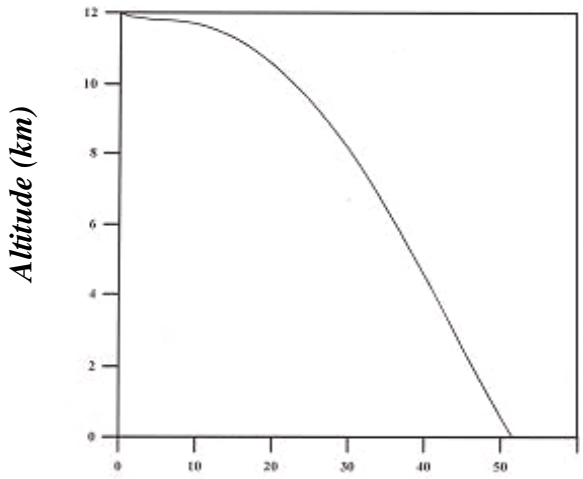
Altitude (km)
Time (sec.)

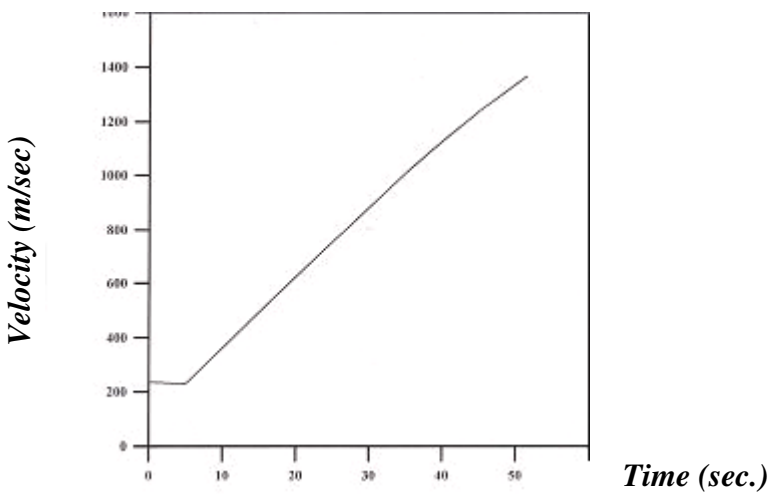
Velocity (m/sec)
Time (sec.)

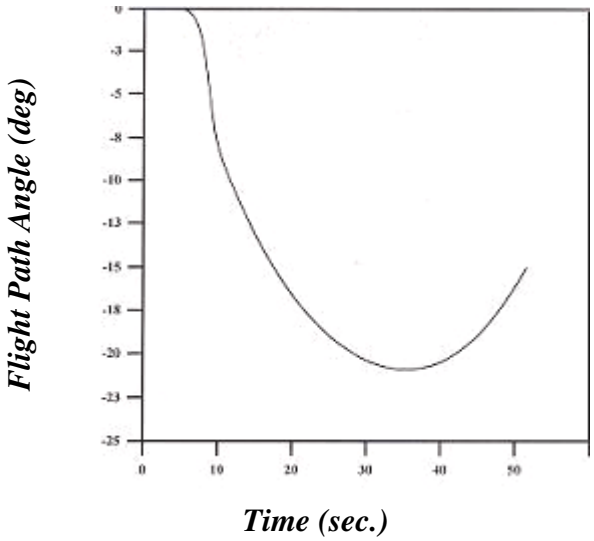

Figs.(3a,b,c) respectively
Launcher without guidance

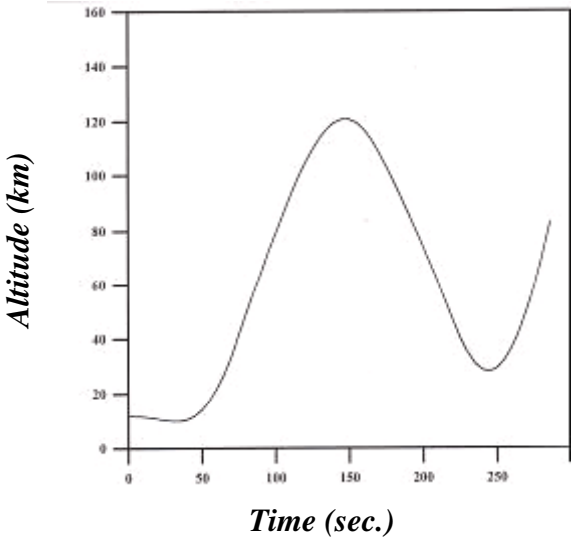

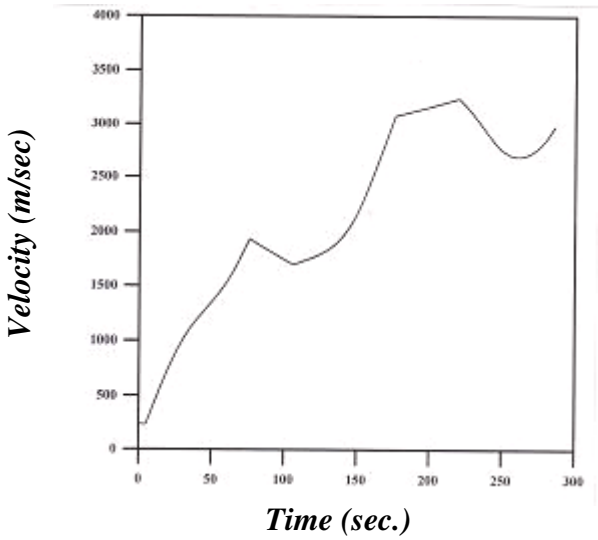

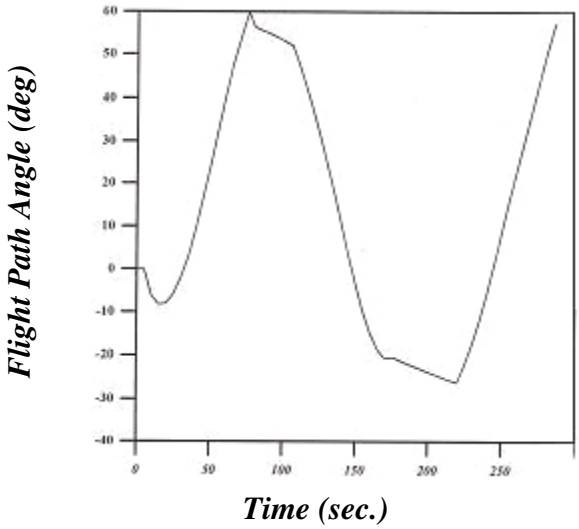

Figs.(4a,b,c) respectively
Launcher with PN guidance

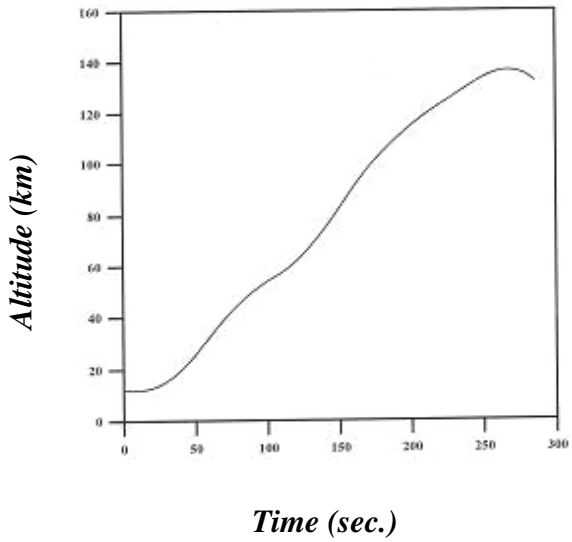

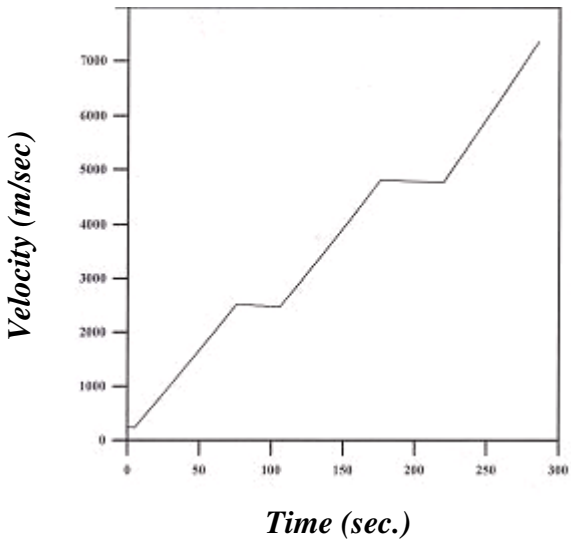

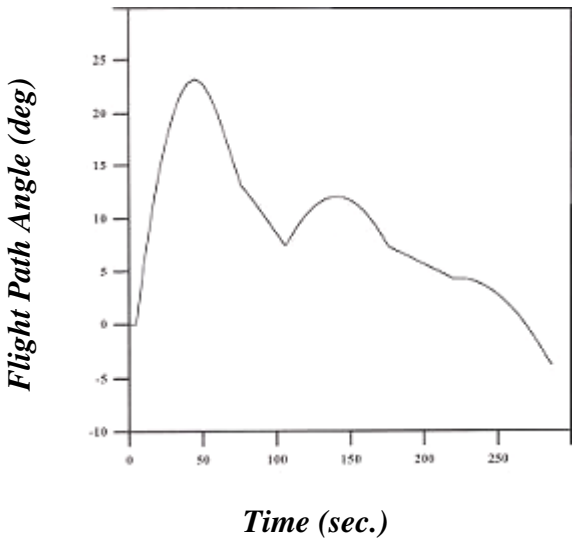

Figs.(5a,b,c) respectively
Launcher with PN plus gravity compensation guidance